PROCEEDINGS

OF THE

AMERICAN SOCIETY OF CIVIL ENGINEERS

VOL. 73 SEPTEMBER, 1947 No. 7

TECHNICAL PAPERS

AND

DISCUSSIONS

Published monthly, except July and August, at Prince and Lemon Streets, Lancaster, Pa., by the American Society of Civil Engineers. Editorial and General Offices at 33 West Thirty-ninth Street, New York 18, N. Y. Reprints from this publication may be made on condition that the full title of paper, name of author, page reference, and date of publication by the Society are given.

Entered as Second-Class Matter, September 23, 1937, at the Post Office at Lancaster, Pa., under the Act of March 3, 1879. Acceptance for mailing at special rate of postage provided for in Section 1103, Act of October 3, 1917, authorized on July 5, 1918.

Subscription (if entered before January 1) $8.00 per annum Price $1.00 per copy

Printed in the United States of America

Current Papers and Discussions

	Published	Discussion closes
Machis, Alfred. Experimental Observations on Grouting Sands and Gravels	Nov., 1946	
Discussion in Feb., Mar., June, 1947		Closed*
Symposium: Cleaning and Grouting of Limestone Foundations, Tennessee Valley Authority	Dec., 1946	
Discussion in Mar., May, June, 1947		Closed*
Matthes, Gerard A. Mississippi River Cutoffs	Jan., 1947	
Discussion in Mar., June, Sept., 1947		Closed*
Tan, Ek-Khoo. Stability of Soil Slopes	Jan., 1947	
Discussion in May, June, Sept., 1947		Closed*
Muldrow, W. C. Forecasting Productivity of Irrigable Lands	Feb., 1947	
Discussion in May, June, 1947		Nov. 1, 1947
Freudenthal, Alfred M. Reflections on Standard Specifications for Structural Design	Feb., 1947	
Discussion in June, 1947		Nov. 1, 1947
Blaisdell, Fred W. Development and Hydraulic Design, Saint Anthony Falls Stilling Basin	Feb., 1947	
Discussion in Sept., 1947		Nov. 1, 1947
DuVal, Miles P. The Marine Operating Problems, Panama Canal, and the Solution	Feb., 1947	
Discussion in Apr., 1947		Uncertain
Claybourn, J. G. Sea Level Plan for Panama Canal	Feb., 1947	
Discussion in Apr., 1947		Uncertain
Hrennikoff, Alexander. Theory of Inelastic Bending with Reference to Moment Design	Mar., 1947	
Discussion in June, 1947		Nov. 1, 1947
Hsu Shih-Chang. Beam Deflections by Second and Third Moments	Mar., 1947	
Discussion in Sept., 1947		Nov. 1, 1947
Ryder, Frederick L. A Rational Explanation of Column Behavior	Mar., 1947	
Discussion in May, June, Sept., 1947		Nov. 1, 1947
Rathbun, J. Charles, and Cunningham, C. W. Continuous Frame Analysis by Elastic Support Action	Apr., 1947	
Discussion in Sept., 1947		Nov. 1, 1947
Hickox, G. H., Peterka, A. J., and Elder, R. A. Friction Coefficients in a Large Tunnel	Apr., 1947	
Discussion in June, Sept., 1947		Nov. 1, 1947
Sturm, R. G. Stability of Thin Cylindrical Shells in Torsion	Apr., 1947	Nov. 1, 1947
Report: Water Supply Engineering: Report of the Committee of the Sanitary Engineering Division for the Two Years Ending December 31, 1946	Apr., 1947	
Committee of the San Francisco (Calif.) Section, ASCE, on Timber Test Program. Tests of Timber Structures from Golden Gate International Exposition	May, 1947	Nov. 1, 1947
Westergaard, H. M. New Formulas for Stresses in Concrete Pavements of Airfields	May, 1947	Nov. 1, 1947
Bergendoff, R. N., and Sorkin, Josef. Mississippi River Bridge at Dubuque, Iowa	June, 1947	
Discussion in Sept., 1947		Nov. 1, 1947
Casagrande, Arthur. Classification and Identification of Soils	June, 1947	
Discussion in Sept., 1947		Nov. 1, 1947
Barron, Reginald A. Consolidation of Fine-Grained Soils by Drain Wells	June, 1947	Nov. 1, 1947
Kazmann, Raphael G. River Infiltration as a Source of Ground Water Supply	June, 1947	Nov. 1, 1947
Spangler, M. G. Underground Conduits—An Appraisal of Modern Research	June, 1947	Nov. 1, 1947

Note.—The closing dates herein published are final except when names of prospective discussers are registered for special extension of time.

* Publication of closing discussion pending.

CONTENTS FOR SEPTEMBER, 1947

PAPERS

DISCUSSIONS

CONTENTS FOR SEPTEMBER, 1947 (*Continued*)

A list of "Current Papers and Discussions" may be found on the page preceding the table of contents

HINTS TO AUTHORS

Those who are planning papers for submission to PROCEEDINGS *will expedite Committee action measurably by first studying the standard instructions as to style, content, and format. For reprints, address the Manager, Technical Publications, 33 W. 39th St., New York 18, N. Y.*

AMERICAN SOCIETY OF CIVIL ENGINEERS
Founded November 5, 1852

PAPERS

DRAINAGE OF AIRPORT SURFACES—SOME BASIC DESIGN CONSIDERATIONS

By Stifel W. Jens,[1] M. ASCE

Synopsis

For determination of runoff from the flat turf surfaces encountered on the inter-runway areas of airports, a methodology is presented employing the newer knowledge concerning retention, infiltration, and overland flow. Since determination of supply rates is required, a detailed procedure is given that takes into account not only the fact that in nature antecedent precipitation within the storm reduces infiltration capacity values, but also the fact that in many storms rainfall rates are less at times than the related infiltration capacities.

Within most turfed areas a peak-reducing pondage is available and practical procedures are developed for obtaining the outflow rates from the ponded areas. Two examples of design are presented. These illustrate that, once pipe sizes are selected and a hydraulic balance is achieved for runoff from rainfall of a selected frequency and duration, the capacity of a system varies but little for other frequencies or durations due to the relation of large changes in mass pondage to very small changes in depths.

Introduction

To permit safe and satisfactory landing and take-off of airplanes, the removal of surface runoff is generally the primary problem in airport drainage. At properly selected airfields, only isolated and relatively small parts of the area ordinarily will require subdrainage. For scheduled airline operation or any other use that does not require all-over landing, a basic drainage requirement has been established by government regulatory authorities, airport managers, and engineers that surface runoff from rains occurring once in two years be removed to the extent necessary to prevent pondage on runways, taxiways, or aprons—or within about 50 ft of their edges. This requirement offers grading and drainage engineers a remarkable opportunity to minimize the cost of the drainage facilities.

Note.—Written comments are invited for immediate publication; to insure publication the last discussion should be submitted by **February 1, 1948.**

[1] Partner, Horner and Shifrin, St. Louis, Mo.

In setting the pavement and inter-runway grades, consideration should be given to the possibilities for providing maximum pondage capacity below a horizontal plane surface whose nearest edge approaches within 50 ft of the pavement edges. Thus, practically the entire field can be served by inlets at low points in turf areas surrounded by paved runways and taxiways. The dominant character of this type of drainage is illustrated by the fact that, for a major transport field, such as the Lambert-Municipal Airport at St. Louis, Mo. (Fig. 1),

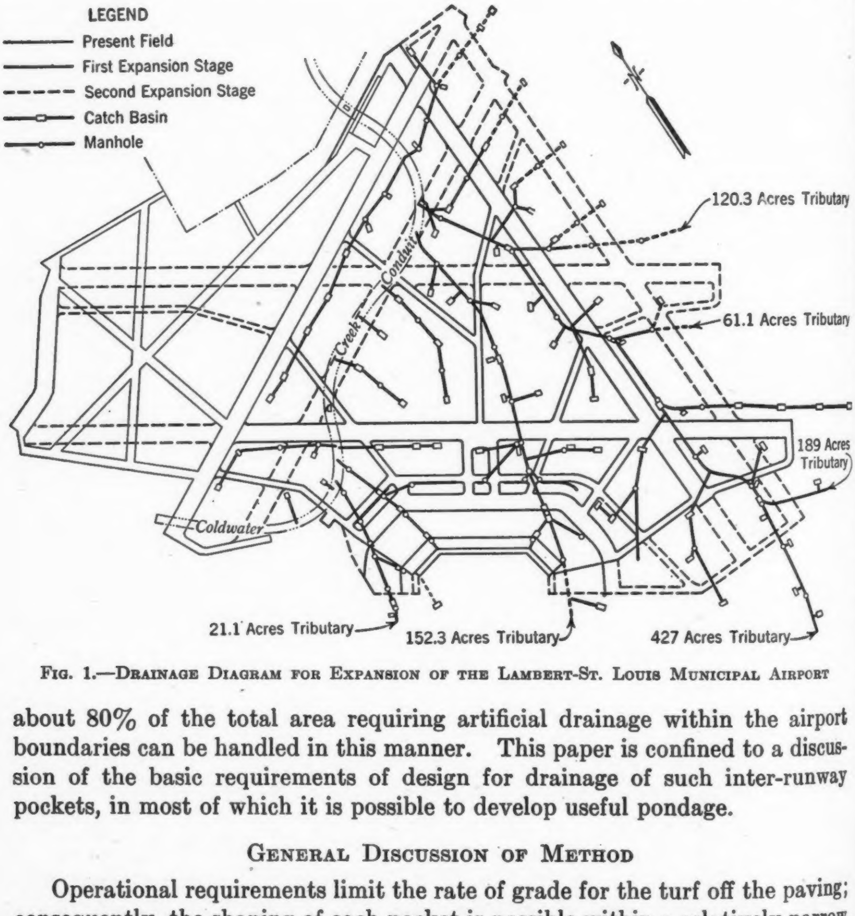

FIG. 1.—DRAINAGE DIAGRAM FOR EXPANSION OF THE LAMBERT-ST. LOUIS MUNICIPAL AIRPORT

about 80% of the total area requiring artificial drainage within the airport boundaries can be handled in this manner. This paper is confined to a discussion of the basic requirements of design for drainage of such inter-runway pockets, in most of which it is possible to develop useful pondage.

General Discussion of Method

Operational requirements limit the rate of grade for the turf off the paving; consequently, the shaping of each pocket is possible within a relatively narrow range of plane slopes. Thus, for each pocket the designer has a tributary area of accurately determinable drainage characteristics such as length and slope of sheet flow, and depth and extent of available pondage, as well as actual amounts of pervious and impervious areas. Determination of flow rates to and from each ponded area lends itself especially well to methods employing the newer knowledge concerning retention, infiltration, and overland flow.

The so-called rational method is inapplicable in view of the availability of

better hydrologic knowledge and the lack of data or experience on which to base selection of the runoff coefficient C of the rational formula—

$$Q = C\,I\,A \qquad (1)$$

—in which Q is the rate of runoff, in cubic feet per second; I is the intensity of rainfall, in inches per hour; and A is the drainage area, in acres.

Using only accepted hydrologic engineering principles and generally available data, it is possible to develop a procedure whereby values of q, the discharge per unit width, may be directly determined. Such procedures involve: (1) Choice of gross rainfall patterns or critical rates for various durations for the agreed frequency (in this case two years); (2) selection of an infiltration capacity curve representative of soil and cover conditions under average antecedent circumstances; (3) correlation of the infiltration capacity curve with the gross rainfall, to secure a net supply pattern; (4) further correction of the net supply pattern by abstraction of retention from the first excess rainfall; (5) determination of the effect of surface detention in altering the shape and peak of the net supply pattern through the requirements of overland or sheet flow; and (6) determinations, required for the ponded areas in the airport, of the effects of pond storage on the shape and peak of the inflow hydrograph in its translation to an outflow hydrograph. For urban areas, similar procedures have been developed as in Los Angeles,[2] Calif., and St. Louis.[3] Also, the United States Engineer Department has adopted a general procedure for the design of airport drainage,[4] and is making systematic observations of rainfall and runoff at selected military airports for the purpose of checking and improving design procedure.

Organization of Basic Rainfall Data

The customary rainfall-duration curve for any specific frequency, such as is shown in Fig. 2, gives only the average precipitation intensity for any particular duration and supplies no information as to how the intensity varies from the average during the duration period—and the intensity practically always does vary in nature. Neither does the curve suggest how these isolated periods are involved in storms as a whole.

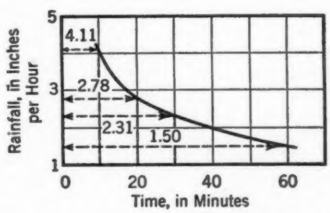

Fig. 2.—Rainfall-Duration Relation for Two-Year Frequency in the St. Louis Area

Since detailed knowledge of both these matters is necessary to the methodology presented, a special analysis is carried out in the following manner: For the St. Louis area,[5] detailed rainfall data forming the basis of the statistical studies for the development of the two-year frequency rainfall curve shown in Fig. 2 are available. For each duration a sample of about twelve

[2] "A Method of Computing Urban Runoff," by W. I. Hicks, *Transactions*, ASCE, Vol. 109, 1944, p. 1217.

[3] "Surface Runoff Determination from Rainfall Without Using Coefficients," by W. W. Horner and S. W. Jens, *ibid.*, Vol. 107, 1942, p. 1039.

[4] "Design of Drainage Facilities," by Gail A. Hathaway, in "Military Airfields: A Symposium," *ibid.*, Vol. 110, 1945, p. 697.

[5] "Relation Between Rainfall and Run-Off from Small Urban Areas," by W. W. Horner and F. L. Flynt, *ibid.*, Vol. 101, 1936, p. 140.

individual storms was chosen, well distributed throughout the series, with the same average precipitation rate for the critical period as that shown on the two-year frequency curve.

Table 1 tabulates these storms for the maximum 20-min intensities. For

TABLE 1.—DEVELOPMENT OF NET RAINFALL PATTERN, INCLUDING IMPERVIOUS AREA AND

Line No.	Date of storm	Item	Preceding 10-Min Periods						
			First	Second	Third	Fourth	Fifth	Sixth	Seventh
(1)	(2)	(3)	(4)	(5)	(6)	(7)	(8)	(9)	(10)
1	8- 2-15...	Rain	....	....	....	....	....	....	....
2		Infiltration	....	....	....	....	....	....	....
3		Net rain	....	....	....	....	....	....	....
4	8-12-16...	Rain	....	....	....	....	....	....	0.26
5		Infiltration	....	....	....	....	....	....	2.94
6		Net rain	....	....	....	....	....	....	0
7	4-25-21...	Rain	....	....	....	....	....	....	....
8		Infiltration	....	....	....	....	....	....	....
9		Net rain	....	....	....	....	....	....	....
10	8-27-21...	Rain	....	....	....	....	....	0.42	1.82
11		Infiltration	....	....	....	....	....	2.92	2.34
12		Net rain	....	....	....	....	....	0	0
13	8-22-22...	Rain	....	....	....	....	....	....	....
14		Infiltration	....	....	....	....	....	....	....
15		Net rain	....	....	....	....	....	....	....
16	8- 8-23...	Rain	....	....	....	....	....	....	....
17		Infiltration	....	....	....	....	....	....	....
18		Net rain	....	....	....	....	....	....	....
19	8-11-25...	Rain	....	....	....	....	....	....	2.36
20		Infiltration	....	....	....	....	....	....	2.38
21		Net rain	....	....	....	....	....	....	0
22	9-12-25...	Rain	....	....	....	0.71	0.72	2.64	1.52
23		Infiltration	....	....	....	2.84	2.44	1.66	1.04
24		Net rain	....	....	....	0	0	0.38	0.48
25	8-23-26...	Rain	....	....	....	....	....	....	0.09
26		Infiltration	....	....	....	....	....	....	2.98
27		Net rain	....	....	....	....	....	....	0
28	9- 8-26...	Rain	....	....	....	....	....	....	....
29		Infiltration	....	....	....	....	....	....	....
30		Net rain	....	....	....	....	....	....	....
31	6-19-28...	Rain	1.14	2.20	0.76	0.55	0.25	0.23	0.62
32		Infiltration	2.72	1.91	1.17	0.93	0.83	0.78	0.72
33		Net rain	0	0	0	0	0	0	0
34	7- 5-28...	Rain	....	....	....	....	....	....	0.43
35		Infiltration	....	....	....	....	....	....	2.91
36		Net rain	....	....	....	....	....	....	0
37	Average...	Rainfall	(0.08)	(0.18)	(0.12)	(0.11)	(0.08)	(0.27)	(0.059)
38	Average...	Supply rate	(0)	(0)	(0)	(0)	(0)	(0.03)	(0.04)

each storm the rainfall rate in each 5-min or 10-min period is so arranged that the critical 20-min values are entered one below the other. In Table 1, Col. 4 denotes the 10-min period beginning 70 min before start of the maximum 20-min period; Col. 10, that 10-min period immediately preceding the maximum period. From Table 1 and similar tables, the average precipitation in each 10 min was determined and the resulting patterns appear in Fig. 3 for the critical

two-year, 10-min, 20-min, 30-min, and 60-min duration periods. For each of these average storm patterns, there was appreciable precipitation both before and after the critical period. Study of these patterns shows clearly that the idea of isolated critical periods is quite unrealistic.

THE MAXIMUM 20-MIN RAIN, IN INCHES PER HOUR, FOR 0% TWO-YEAR FREQUENCY

Maximum 20 Min				Ensuing 10-Min Periods				Line No.
5 Min	5 Min	10 Min	Total	First	Second	Third	Fourth	
(11)	(12)	(13)	(14)	(15)	(16)	(17)	(18)	(19)
1.20	5.16	1.49	2.33	0.06	....	....	....	1
2.86	2.42	1.62	1.94	1.05	0.80	0.68	0.61	2
0	1.54	0	0.39	−0.99	−0.80	−0.68	−0.61	3
1.44	2.41	2.28	2.10	0.82	0.35	0.12	....	4
2.70	2.24	1.32	1.87	0.92	0.74	0.67	0.60	5
0	0.00	0.45	0.23	−0.10	−0.39	−0.55	−0.60	6
1.80	2.34	2.61	2.34	1.04	0.84	0.35	0.02	7
2.77	2.27	1.54	2.09	0.98	0.78	0.68	0.61	8
0	0	0.50	0.25	0.06	0.06	−0.33	−0.59	9
2.64	3.04	4.35	3.59	0.01	....	....	....	10
1.66	1.26	0.96	1.50	0.77	0.68	0.61	0.56	11
0	1.56	3.39	2.09	−0.76	−0.68	−0.61	−0.56	12
3.34	5.40	0.30	2.34	0	....	....	....	13
2.65	2.06	1.20	1.63	0.89	0.73	0.66	0.59	14
0	2.83	0	0.71	−0.89	−0.73	−0.66	−0.59	15
3.72	7.23	4.33	4.90	3.80	0.74	0.65	0.45	16
2.65	2.06	1.20	2.07	0.89	0.73	0.66	0.59	17
0	5.04	3.13	2.83	2.91	0.01	−0.01	−0.14	18
0.44	0.20	2.48	1.40	0.06	....	....	....	19
1.79	1.68	1.26	1.09	0.90	0.74	0.66	0.60	20
0	0	0.62	0.31	−0.84	−0.74	−0.66	−0.60	21
2.52	3.72	1.68	2.40	0.49	0.03	....	....	22
0.86	0.77	0.69	0.75	0.63	0.57	0.53	0.52	23
1.66	2.95	0.99	1.65	−0.14	−0.54	−0.53	−0.52	24
1.26	2.26	4.32	3.04	0.36	....	....	....	25
2.81	2.40	1.62	1.99	1.02	0.80	0.69	0.62	26
0	0	2.10	1.05	−0.66	−0.80	−0.69	−0.62	27
5.89	2.90	1.80	3.09	1.55	1.12	0.63	....	28
2.65	2.06	1.20	2.07	0.89	0.73	0.66	0.59	29
2.04	0.84	0.60	1.02	0.66	0.39	−0.03	−0.59	30
1.44	3.00	2.52	2.37	0.99	0.45	....	....	31
0.68	0.65	0.60	0.79	0.55	0.52	0.51	0.51	32
0.14	2.35	1.92	1.58	0.44	−0.07	−0.51	−0.51	33
4.38	4.68	2.31	3.42	0.74	1.40	0.07	....	34
2.50	1.94	1.27	2.04	0.92	0.74	0.66	0.60	35
0.68	2.74	1.04	1.38	−0.18	0.66	−0.59	−0.60	36
(2.506)	(3.529)	(2.539)	(2.778)	(0.827)	(0.411)	(0.152)	(0.039)	37
(0.377)	(1.654)	(1.228)	(1.122)	(−0.041)	(−0.304)	(−0.488)	(−0.544)	38

INFILTRATION CAPACITY OF TURFED AREAS

The United States Department of Agriculture, through measurements of flow from small watersheds and from infiltrometer applications, has produced a large number of infiltration capacity curves for various soils with grass cover, generally for agricultural areas used as meadow or pasture. At least two studies have been made of the infiltration capacity of such turfed areas as would

be normal for airfields. These areas would be similar in surface condition to city lawns. One such series was carried out at St. Louis for lawn grass on a yellow clay subsoil; the other in Anacostia Park, at Washington, D. C., for lawn grass on hydraulic fill subsoil consisting of mud dredged from the Potomac River. For similar antecedent conditions the values for these two areas are very nearly identical. Curve (*a*), Fig. 4, is representative of the values at either

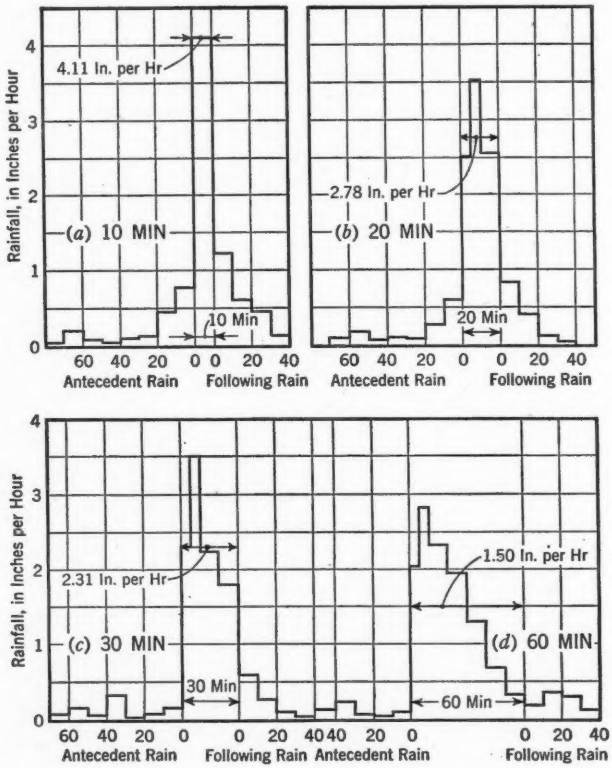

FIG. 3.—AVERAGE RAINFALL PATTERNS FOR STORMS OF VARIOUS DURATION PERIODS IN THE TWO-YEAR FREQUENCY SERIES

location for generally wet seasonal conditions and heavy rainfall within the preceding 24 hours. Curve (*b*) is representative of St. Louis conditions under average summer monthly rainfall with no considerable application of precipitation for the preceding three days. Undoubtedly, for very dry summer conditions with considerable soil checking, a much higher series of values would prevail.

Infiltration capacity values shown in Fig. 4 may be accepted as reasonably representative of the values for a turfed cover for a rather wide range of soils. There is little artificial compaction such as would occur from trampling of the surface under intensive recreational use or from walking over city lawns. In

all probability, representative curves for city lawns would be slightly lower than those shown. For sandy loams or sands, values would be materially higher.

Relating Infiltration Capacity to Rainfall Occurrence

Since the objective is to develop runoff values which on the average will be equaled or exceeded once in two years, the sample critical rainfalls previously discussed should be matched by an infiltration capacity curve which is normal for the turf areas at the time of occurrence. Also, the curves should be properly related on the basis of the rainfall preceding the critical period. For the sample rains, the average elapsed time to the preceding rain was 3 days, and the average

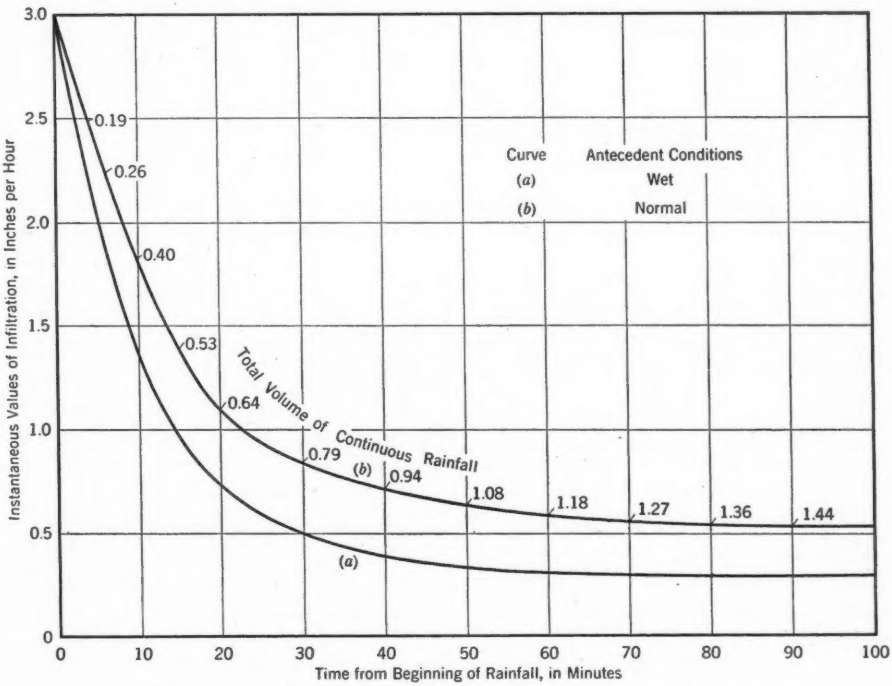

Fig. 4.—Infiltration Capacity Curves for Wet and Normal Antecedent Conditions of Turf Areas

mass of the preceding rain was about 0.4 in. These conditions compare closely to normal summer conditions for the area and result in the conclusion that, on the average, curve (*b*), Fig. 4, is properly applicable during the occurrence of these storms. Applying an initial value of 3 in. per hr as the probable infiltration capacity rate at the beginning of rainfall, curve (*b*), Fig. 4, was matched to the rainfall pattern in each of the representative sample storms.

To obtain infiltration values (such as are given in Table 1) that would apply to each 5-min or 10-min rainfall period, the following principle was used: On curve (*b*), Fig. 4, are indorsed, at various points, the mass infiltration that could occur up to each time if the rainfall at all times until then equaled or exceeded

the rates shown on the infiltration capacity curve. For example, at capacity rates, the total possible mass infiltration between 15 min (0.53 in.) and 20 min (0.64 in.) is 0.11 in. Whenever the rainfall rate exceeds the infiltration capacity rates throughout any one time period, the drop in average infiltration capacity from one period to another follows curve (*b*), Fig. 4. Whenever the rainfall rate falls below the infiltration capacity values for normal antecedent conditions, the position of the actual infiltration rate at the end of such a time period is assumed to be at the value shown by the infiltration capacity curve corresponding to the same actual incremental mass infiltration interpolated on the curve. This relationship between infiltration capacity, actual rate, and mass is only approximate, but it is sufficiently well indicated to justify its use in positioning the infiltration capacity curve.

Table 1 shows the related infiltration and rainfall rates for each 5-min or 10-min period of each of the representative sample storms for the 20-min duration period.

Net Surface Runoff for 100% Pervious Areas

For each 5-min or 10-min period of the rains in Table 1, the net surface runoff is obtained by direct subtraction of the infiltration rates from the related rainfall rates. These rates represent production of surface runoff at the ground and are further adjusted by deducting from the first excess rainfall the value of 0.1 in. to allow for surface retention. The results so secured represent the series of surface supply rates produced on the average by the rains which give the two-year frequency critical 20-min period. More particularly, values are determined rain by rain and no averaging is done until the net supply values in each 5-min or 10-min period have been calculated. Satisfactory values could not have been calculated from the average rainfall for each 10-min period for the whole sample and from the average infiltration rate.

These values of supply rates result from a procedure that takes full account of both the effect of antecedent rainfall in reducing infiltration capacity values, and the fact that for many storms rainfall rates are sometimes less than the related infiltration capacity values. The adjustment for retention recognizes the existence of very shallow saucer-like depressions which must be filled before surface runoff proceeds and in which a small amount of water is retained at the end of surface runoff. The procedure also makes evident the infiltration capacity rates that will exist after the end of production of net supply, and therefore permits evaluation of the additional infiltration that will result from overland flow during the recession of the hydrograph.

Runoff from Partly Impervious Airport Areas

The procedure thus far gives fully realistic values of runoff from wholly pervious surfaces where infiltration is proceeding throughout. However, in the majority of the ponded interpavement areas, water is discharged from half-runways or half-taxiways on to the turf. These mixed areas are designated by the percentage of impervious surface.

It should be possible to evaluate such mixed areas satisfactorily by assuming that the discharge from the pavement, after a slight deduction (0.05 in.) for

retention on the pavement, can be considered as resulting from a proportionate increase of rainfall on the turfed area. For example, for a 30% impervious area, the impervious part is three sevenths of the turfed part, and the rainfall pattern accordingly can be increased item by item to ten sevenths of the original value. This procedure has been followed for each of the selected sample rains in each of the duration series and for imperviousnesses of 10%, 30%, and 50%—the range of values encountered in airport drainage.

With these modified rainfall patterns, infiltration capacities were recomputed for each successive time period for each sample rain, and new patterns of supply were prepared in the same manner as in Table 1. When the antecedent rainfall on the turf is assumed increased in this manner, infiltration capacities at the beginning of the critical duration are successively reduced below

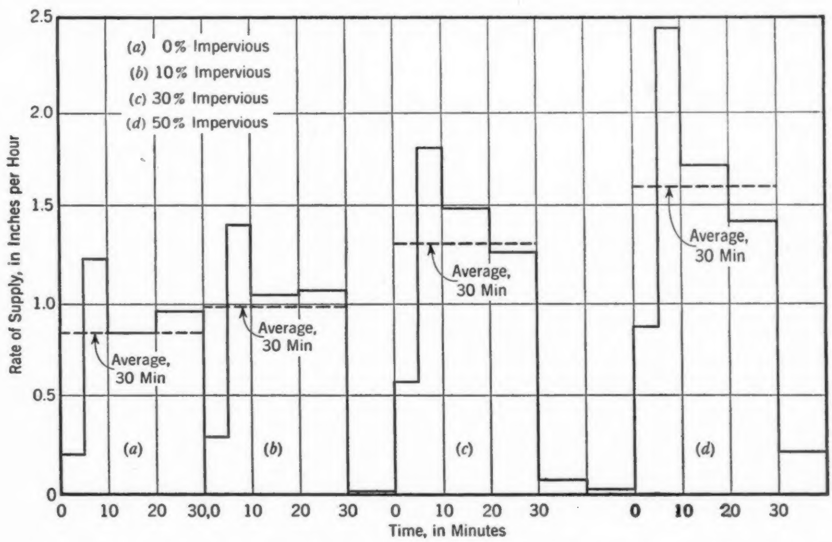

FIG. 5.—PATTERNS OF SURFACE RUNOFF SUPPLY RATES FOR 30-MIN RAINFALL PERIOD AND VARIOUS PERCENTAGES OF IMPERVIOUSNESS

those originally computed, and hence the resulting supply rate patterns are increased not only by higher rainfall rates but also by reduction of infiltration capacity. Fig. 5 shows patterns for one rainfall duration and four percentages of imperviousness.

The question naturally arises as to the physical propriety of treating water poured on the upper margin of the turf from the pavement as the equivalent of additional distributed rainfall over the turf. This matter has been subjected to rough analytical checks. Generally the velocities of flow over the turf are sufficiently high so that some of the water entering the upper margin near the beginning of the rain will arrive at the outlet by the end of the critical period. The water from the pavement should become distributed over the turf strip within a critical duration. No doubt, the actual distribution is not the same as that resulting from the assumption, but this difference does not seem great

enough to alter either the average detention on the turf or the critical rate of outflow from the lower margin of the turf.

Fig. 6 shows the entire series of supply rates for the various durations and percentages of imperviousness considered. These two-year frequency values are related to an all-turf area and must be adjusted by multiplying by 0.5, 0.7,

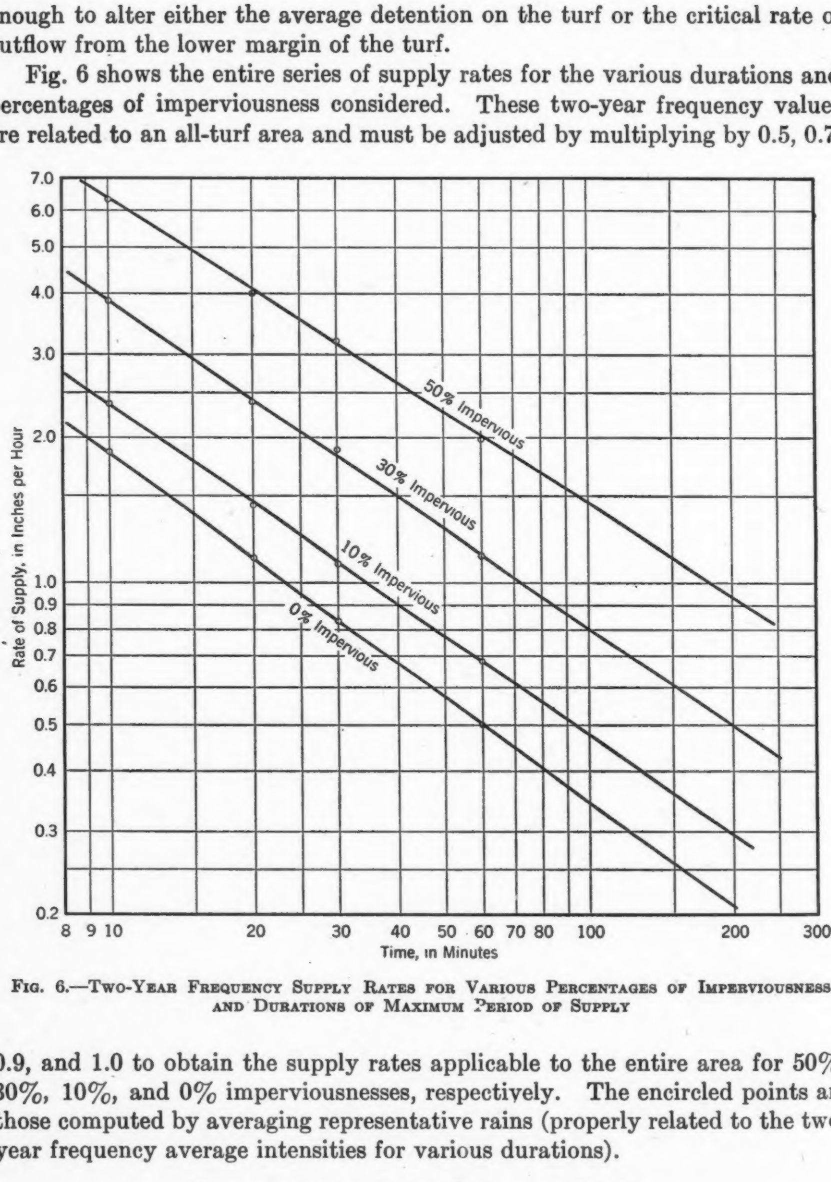

FIG. 6.—TWO-YEAR FREQUENCY SUPPLY RATES FOR VARIOUS PERCENTAGES OF IMPERVIOUSNESS AND DURATIONS OF MAXIMUM PERIOD OF SUPPLY

0.9, and 1.0 to obtain the supply rates applicable to the entire area for 50%, 30%, 10%, and 0% imperviousnesses, respectively. The encircled points are those computed by averaging representative rains (properly related to the two-year frequency average intensities for various durations).

RATES OF INFLOW TO PONDS OR INLETS

With the supply patterns available for various durations and various percentages of impervious area, it becomes necessary to determine the hydrographs of inflow to the ponds or inlets. Thus, an evaluation of the effects of overland flow is required.

On the impervious areas, the supply for surface runoff quickly develops a

thin film through which flow takes place down the slope to the upper edge of the adjacent turf. For the lengths and slopes involved in half-runways and half-taxiways, flow is quite rapid and reaches equilibrium in from about 2 min to 5 min; thereafter, for a constant supply rate, discharge from the pavement on to the turf continues equal to the supply rate. As discussed previously, the assumption is made that the effects of runoff from the pavement may be treated by adjustment of the rainfall on the turf.

Characteristics of flow over turf are quite different. As the rainfall builds up supply within the grass, flow takes place down the slope between the grass blades at comparatively low velocities. For determining the outflow rate at the lower margin of a turf strip and the related depth of surface detention on the turf, the following formula developed by the late R. E. Horton,[6] M. ASCE, have been used:

$$q = \sigma \tanh^2 \left(\frac{K \sqrt{3,520}\, S^{0.25} \sigma^{0.50} t}{60\, l^{0.50}} \right) \ldots\ldots\ldots\ldots (2)$$

and

$$\delta = \frac{l^{0.5} \sigma^{0.5}}{S^{0.25} \sqrt{3,520}} \tanh \left(\frac{K \sqrt{3,520}\, \sigma^{0.5} S^{0.25} t}{60\, l^{0.5}} \right) \ldots\ldots\ldots\ldots (3)$$

in which q is the outflow rate, in inches per hour, at the lower margin of a turf strip; σ is the supply rate, in inches per hour; tanh is the hyperbolic tangent; t is the time of supply, in minutes; δ is the depth of flow, in inches, at the lower margin of the turf; l is the length of overland flow, in feet; S is the absolute slope of the turf strip; and K is the reciprocal of the ratio of the average depth to that at the margin. The numerical coefficient 3,520 was selected from pertinent experimental data for good bluegrass turf—closely checking the n-value of 0.400 used by the United States Army Engineers.[7] This n-value is not strictly comparable to the Manning n. An average overland flow slope of 1.75% has been used for all pervious areas.

Mr. Horton found that, for overland flow over turf, the profile is essentially parabolic with an average depth two thirds of that at the margin. Where additional supply is poured on to the upper margin from pavement, the profile will involve greater depths in the upper part of the turf strip and the average depth will be somewhat greater than two thirds. For 50% impervious areas the average depth has been assumed as fourth fifths and intermediate values were used for the lesser amounts of imperviousness.

Eqs. 2 and 3 are for strips of uniform width and are, therefore, rigorously applicable only to a rectangular area where the flow arrives along one margin. In practically all airfield grading, the pockets are essentially inverted pyramids with the flow converging toward a central inlet. The flow, therefore, may be visualized as occurring on triangular strips with an average width of 1 ft. For this situation, the overland flow hydrograph is so complex that it cannot be reduced to usable mathematical equations. A rough analysis indicates that the total detention on the triangular strip may be slightly less than that of the

[6] "The Interpretation and Application of Runoff Plat Experiments," by R. E. Horton, *Proceedings*, Soils Science Soc. of America, Vol. 3, 1938, p. 340.

[7] "Design of Drainage Facilities for Airfields," *Engineering Manual*, Office of the Chf. of Engrs., War Dept., Washington, D. C., September 1942, Chapter XXI.

equivalent rectangular strip, and the discharge at the lower margin may be slightly greater. The differences, however, are not great and the basic formulas have been used to determine the rates of flow into the pond or inlet.

Table 2 and Fig. 7 illustrate application of Eqs. 2 and 3 to the supply rates. For the actual varying supply rates the rising side of the hydrograph of flow to the inlet is shown as curve A; the corresponding curve B arises out of the aver-

TABLE 2.—COMPUTATION OF OVERLAND FLOW PEAKS AND NET MASS RUNOFFS FOR TURF AREAS 1 FT WIDE, 100 FT LONG, AND 0% AND 30% IMPERVIOUS

Impervious area (%)	Time period (min)	σ (in. per hr)	Discharge, q[a] (in. per hr)	Mass rain (in.)	Hydrograph Component[b]: Estimate of base (min)	Rising side (min)	Estimate of recession (min)	Recession mass infiltration (in.)	Net Mass Runoff (in.): On all-pervious area	On actual area	Corrected hydrograph base (min)
(1)	(2)	(3)	(4)	(5)	(6)	(7)	(8)	(9)	(10)	(11)	(12)
0	10	0.08	0.00159	0.013	....	....	....	....	....	....	....
	10	0.10	0.00823	0.017	....	....	....	....	....	....	....
	10[c]	1.88	0.835	0.314	51.9	11.0	40.9	0.069	0.292	0.292	42.0
	10	0.10	....	0.017	....	....	....	....	....	....	....
	Total	....	....	0.361	....	....	....	....	....	....	....
	10	0.03	0.000276	0.005	....	....	....	....	....	....	....
	10	0.04	0.001384	0.007	....	....	....	....	....	....	....
	20[c]	1.12	0.762	0.373	60.6	20.6	40.0	0.050	0.335	0.335	52.7
	Total	....	....	0.385	....	....	....	....	....	....	....
	30[c]	0.848	0.690	0.425	73.3	30.0	43.3	0.071	0.354	0.354	61.6
	45[c]	0.622	0.571	0.467	98.1	45.0	53.1	0.082	0.385	0.385	81.0
	60[c]	0.503	0.483	0.503	125.0	60.0	65.0	0.086	0.417	0.417	103.8
	90[c]	0.378	0.374	0.566	181.5	90.0	91.5	0.115	0.451	0.451	145.0
30	10	0.22	0.0108	0.037	....	....	....	....	....	....	....
	10	0.46	0.0922	0.077	....	....	....	....	....	....	....
	10[c]	3.84	2.465	0.640	42.7	11.8	30.9	0.060	0.818	0.572	38.4
	10	0.67	(1.727)	0.112	....	....	....	....	....	....	....
	10	0.07	....	0.012	....	....	....	....	....	....	....
	Total	....	....	0.878	....	....	....	....	....	....	....
	10	0.16	0.00577	0.027	....	....	....	....	....	....	....
	10	0.18	0.0240	0.030	....	....	....	....	....	....	....
	20[c]	2.388	2.035	0.796	53.6	21.4	32.2	0.065	0.845	0.59	49.9
	10	0.34	(1.424)	0.057	....	....	....	....	....	....	....
	Total	....	....	0.910	....	....	....	....	....	....	....
	10	0.02	....[d]	0.003	....	....	....	....	....	....	....
	30[c]	1.888	1.745	0.944	66.4	30	36.4	0.071	0.894	0.626	61.5
	10	0.11	(1.222)	0.018	....	....	....	....	....	....	....
	Total	....	....	0.965	....	....	....	....	....	....	....
	45[c]	1.375	{1.343 (0.941)}	1.031	92.3	45	47.3	0.088	0.943	0.66	84.0
	60[c]	1.13	{1.12 (0.774)}	1.13	121.0	60	61.0	0.071	1.049	0.733	112.5
	90[c]	0.86	{0.86 (0.602)}	1.29	180.0	90	90	0.122	1.168	0.819	163.0

[a] Col. 4 based on Eq. 2, with $K=1.5$ for 0% imperviousness and 1.35 for 30% imperviousness. In Col. 4, for 30% impervious, numerals in parentheses are 0.7 of the discharge immediately above and hence represent actual runoffs from areas of 30% imperviousness. [b] Cols. 6 through 12 based on Eqs. 4 and 5; f taken from tables similar to Table 1. [c] Maximum. [d] Negligible.

age supply rate for the critical period. The differences are not great and, in all computations for peak rate to the inlet, the average supply rate has been used. Examination of a number of such hydrographs indicates that a straight line, C, can be adopted without appreciable error, with the shaded area repre-

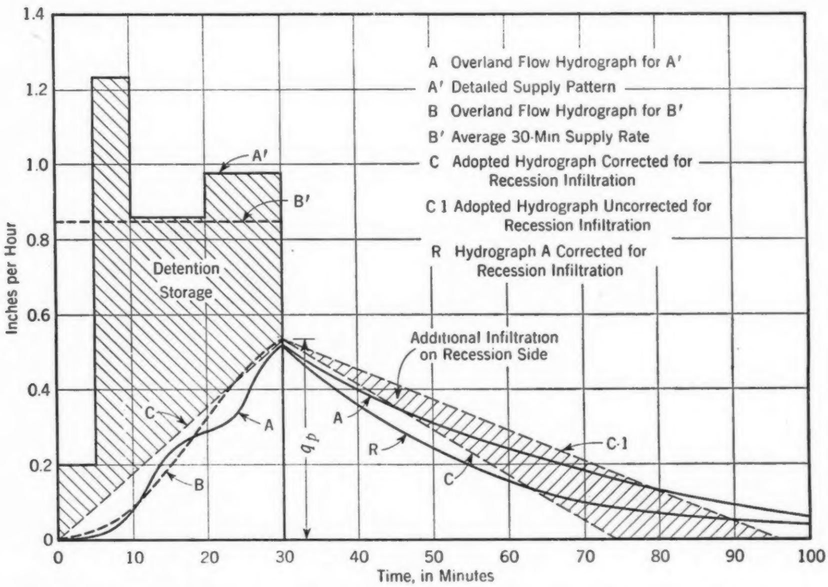

FIG. 7.—SUPPLY AND RUNOFF CURVES FOR 30-MIN SUPPLY ON 0% IMPERVIOUS AREA WITH OVERLAND FLOW LENGTH OF 185 FT AND SLOPE OF 1.75%

senting water in detention storage at the end of the critical period. This water, reduced by some further infiltration, supplies the recession side of the hydrograph marked A before correction for additional infiltration and, after such correction, hydrograph R. A number of recession curves indicate again the propriety of a straight line for design purposes and in all cases the overland flow hydrograph has been assumed to be a triangle as shown in Fig. 7, with the peak rate q_p constituting the altitude and with the area of the triangle equal to the mass runoff, m.

Likewise, the method of correcting for recession infiltration is shown in Fig. 8 and Table 2. In Fig. 8, area ABC represents the corrected mass runoff, m (Col. 10, Table 2); area A'BC' represents p, the available mass pondage; and area CBD represents F, the mass infiltration, on the recession side of the hydrograph. All mass units are in inches of depth over the entire tributary area. In these determinations it has been assumed that the average infiltration capacity rate f is fully effective during only one third of the entire recession time. This assumption is necessary because the receding sheet of overland flow after cessation of supply covers a diminishing part of the total area and consequently the infiltration opportunity progressively becomes less. Thus,

$$F = \frac{q_p X}{2 \times 60} = \frac{(t_r - X) f}{3 \times 60} \qquad (4)$$

and

$$X = \frac{t_r f}{1.5\, q_p + f} \qquad (5)$$

Also, from similar triangles,

$$q_o = q_p \left(1 - \sqrt{\frac{p}{m}}\right) \qquad (6)$$

While this study was in progress, results began to be available from actual investigations on the character of overland flow which have been conducted largely by the United States Public Roads Administration. Some of these have been presented in papers[8,9,10] by Carl F. Izzard, Assoc. M. ASCE. Although

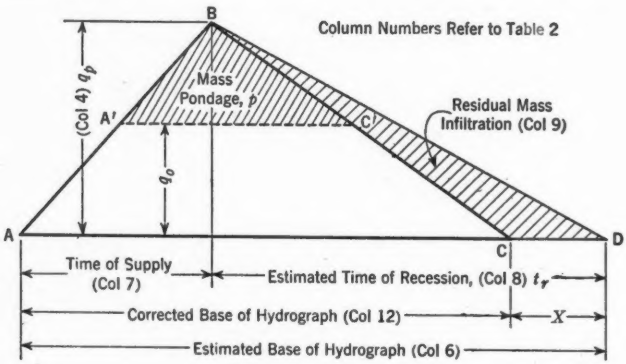

FIG. 8.—SCHEMATIC REPRESENTATION OF TRIANGULAR HYDROGRAPH SHOWING ADJUSTMENT FOR INFILTRATION ON RECESSION SIDE

the studies were primarily on pavement surfaces, including aprons and runways, a number of runs were made on turfed surfaces.

Several comparisons have been made between the data developed by Mr. Izzard and those computed by the Horton formulas. For 30-min rains and overland flow lengths of from 150 ft to 200 ft, the two sets of values are very closely in accord. However, on 10-min rains, Mr. Izzard's values are only about two thirds of those computed by the Horton equation. There is a question, therefore, whether the application of the Horton equation to periods of short duration may not indicate excessive values of inflow to the ponds.

In Tables 3 and 4, design values are prepared for a three-inlet system for duration periods of from 10 min to 60 min. If Mr. Izzard's data are applicable, the 10-min flows to the ponds will be reduced to about two thirds of those shown and the 20-min inflow rates will be slightly reduced. Thus, for this particular system, the 20-min or 30-min rain would be critical and the correct design rate for the outlet pipe would be about 12 cu ft per sec instead of 14 cu ft per sec. If the outlet were actually designed for a flow of 14 cu ft per sec, there would

[8] "Runoff from Flight Strips," by Carl F. Izzard, *Proceedings*, Highway Research Board, National Research Council, Vol. 22, 1942, p. 94.

[9] "Preliminary Report on Analysis of Runoff Resulting from Simulated Rainfall on a Paved Plot," by C. F. Izzard and M. T. Augustine, *Transactions*, Am. Geophysical Union, 1943, Pt. II, pp. 500–511.

[10] "The Surface Profile of Overland Flow," by C. F. Izzard, *ibid.*, 1944, Pt. VI, pp. 959–968.

be less utilization of storage in the ponds, so that the ponds would stand at slightly lower levels than those indicated in Table 3 and Fig. 9.

Since the overdesign is apparently not great (in fact in this instance it would have been impossible to use a smaller commercial pipe size), and since all the

TABLE 3.—COMPUTATION OF OUTFLOW RATES FROM PONDS, AND PRELIMINARY PIPE SIZE SELECTION, THREE-POND SYSTEM

Pond or pipe No.	Flow quantity, (cu ft per sec)	DURATION (MIN)					Preliminary slope[a] (ft per ft)	Diameter (in.)	Preliminary velocity (ft per sec)	$1.5 \frac{V^2}{2g}$	Adjusted slope (ft per ft)
		10	20	30	45	60					
(1)	(2)	(3)	(4)	(5)	(6)	(7)	(8)	(9)	(10)	(11)	(12)
1......	Q_o	7.1	6.1	5.4	4.3	3.0	....	....	....	....	....
1-2......	Q_o	7.1	6.1	5.4	4.3	3.0	0.0039	19	3.9	0.35	0.0044
2......	Q_o	1.7	1.7	1.7	1.6	1.5	....	....	....	....	....
2-3......	Q_o	8.8	7.8	7.1	5.9	4.5	0.0071	18	5.0	0.58	0.0104
3......	q_p[b]	1.16	1.11	1.04	0.86	0.75	....	....	....	....	....
	m[c]	0.54	0.57	0.61	0.67	0.73	....	....	....	....	....
	Q_p	8.0	7.7	7.2	5.9	5.2	....	....	....	....	....
	Q_o	5.2	5.0	4.8	4.1	3.6	....	....	....	....	....
3-outlet..	Q_o	14.0	12.8	11.9	10.0	8.1	0.0256	17	9.0	1.89	0.020

[a] Cols. 8 through 12 based on quantities of Col. 3. [b] Inches per hour. [c] Inches.

basic design data are predicated upon the Horton equations, the illustrative examples will be calculated from those data.

BASIC DESIGN DATA

For the two-year frequency rainfall, the values of the peak rate of runoff, q_p, in inches per hour or in cubic feet per second per acre, and the values of the related mass runoff m, in inches, have been determined. These values have been calculated directly from the supply rates for the 10-min, 20-min, 30-min, and 60-min durations; for other durations, such as 45 min and 90 min, corresponding supply rates have been extrapolated from Fig. 6. The values have been determined separately for areas of 0%, 10%, 30%, and 50% imperviousnesses, and for turf lengths of overland flow of from 100 ft to 500 ft. Different plottings have been prepared to make available the best facility for interpolation. Figs. 10 and 11 show typical sheets relating q_p and m to length of overland flow for 1% imperviousness and for various times of supply.

TABLE 4.—CHARACTERISTICS OF PONDS IN THREE-POND SYSTEM

Pond No.	Area (acres)	Imperviousness (%)	Flow length (ft)	Pondage (in.)
1......	4.04	50	150	0.0082
2......	5.84	30	200	0.31
3......	6.90	30	200	0.068

USE OF HYDROGRAPHS IN DESIGN

Where no deliberate storage ponding is possible, the inflow hydrograph to the inlet may be assumed to be triangular with its peak flow rate and mass runoff determined by selection from the basic design data. Such hydrographs may be offset by the time of flow from one inlet to another, and the peak rate of flow below any inlet may be determined by the addition of ordinates.

Where pondage is practicable, the triangular hydrograph represents inflow to the pond from which a simple determination can be made for the outflow rate as reduced by detention storage in the pond. In Fig. 8, from the properties of a triangle, the relation between inflow, outflow, pondage, and mass runoff

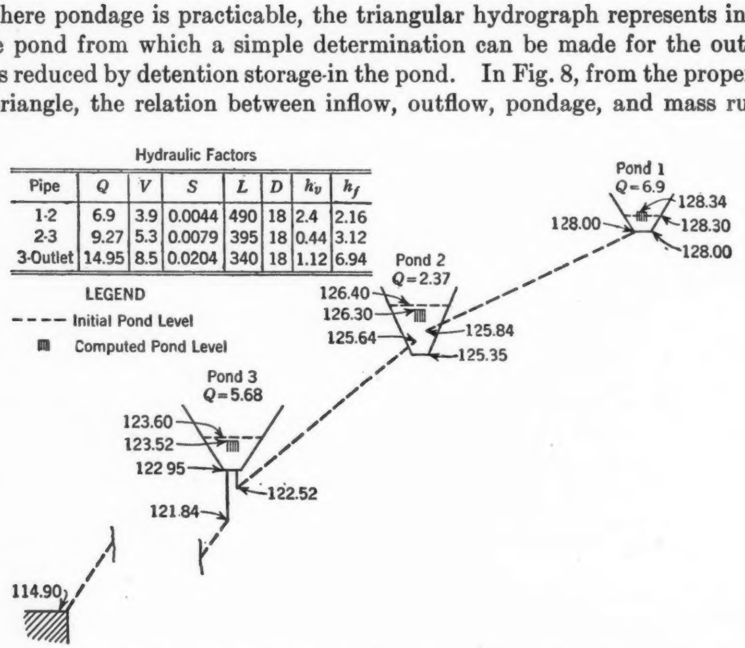

Hydraulic Factors

Pipe	Q	V	S	L	D	h_v	h_f
1-2	6.9	3.9	0.0044	490	18	2.4	2.16
2-3	9.27	5.3	0.0079	395	18	0.44	3.12
3-Outlet	14.95	8.5	0.0204	340	18	1.12	6.94

FIG. 9.—PROFILE AND HYDRAULIC FACTORS FOR THREE-POND SYSTEM

can be expressed as Q_o (in cubic feet per second) $= Q_p$ (in cubic feet per second) $\times \left(1 - \sqrt{\frac{p}{m}}\right)$, with both p, the mass pondage, and m, the mass runoff, in inches of depth over the entire tributary area. For any particular inlet area, the values of Q_p (q_p from design graphs times the total area), m (from the design diagrams), and p (the permissible pondage developed from the field grading plans) are available. Then Q_o is the minimum outflow capacity that must be provided if the pondage is not to exceed that computed as the desirable maximum. However, it should be remembered that the pyramidal shape of the ponds permits an appreciable change in volume without any large change either in depth, or in the distance from margin of pond to pavement. To accommodate commercial pipe sizes, the initial or optimum values of p obtained from the grading plan may, therefore, be varied somewhat in the course of design. Changes in pond depths are assumed to vary with the cube roots of the related pond volumes.

APPLICATION OF BASIC DATA AND HYDROGRAPHS IN ACTUAL DESIGN

The principle of designing the field drainage system, which takes advantage of permissible ponding in the intra-runway pockets, requires that the outlet capacity from any one pocket be the same as the calculated outflow rate from that pocket when the inflow to it has been reduced by the available detention storage. Thus, the objective of the design of the pipe system is to develop

pipe capacities which will throttle the outflow from the ponds to such an extent that the permissible pondage will be utilized.

If the grading plan provides a series of pockets with the water surface elevations descending in order toward the outlet of the system, it is entirely feasible to provide pipes of such capacity that the ponds will "float on the line." Where this can be done, inlet manholes with adequate gratings can be placed at the low point in each pond. In actual operation a water column will be descending through the manholes and the acceleration of the water from zero velocity in the pond to the velocity in the outgoing pipe will utilize a velocity head equal to $\frac{V^2}{2g}$. In addition, there will be entrance losses through the grating and at the bottom of the manhole; and, to provide for this, the total entrance head including velocity head and entrance losses has been treated as $1.5 \frac{V^2}{2g}$. Thus, the hydraulic gradient in the pipe line at any particular inlet manhole must be lower than the level of the pond in the amount indicated by this expression, and pipe capacities must be based on the hydraulic gradient so determined.

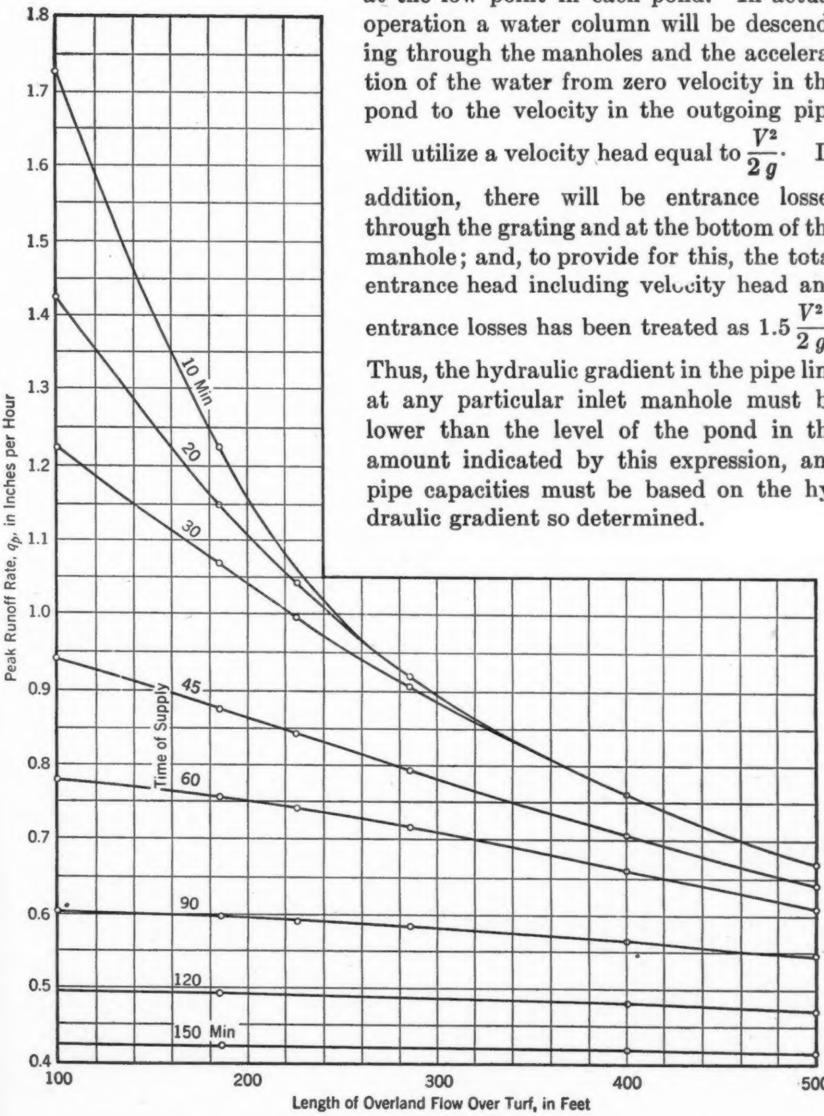

FIG. 10.—PEAK RUNOFF RATES FOR VARIOUS DURATIONS OF RAINFALL IN TWO-YEAR FREQUENCY CYCLE ON TURF AREA WITH 30% IMPERVIOUSNESS

Obviously, when the nearest commercial size pipes have been selected, both the flow rates in the pipes and the concordant surface elevations of the ponds will, in the state of equilibrium, become stabilized with slightly different values than those indicated by permissible storage from the ponds alone. Actual

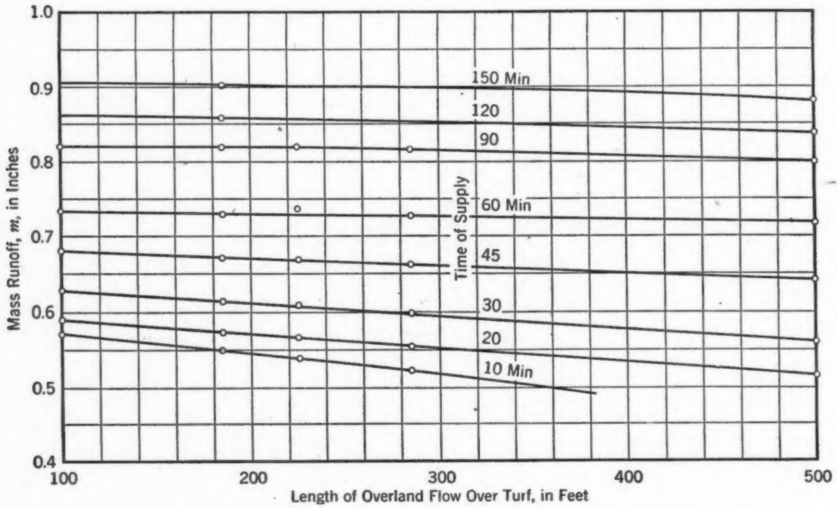

FIG. 11.—MASS RUNOFF FOR VARIOUS STORM DURATIONS IN TWO-YEAR FREQUENCY CYCLE ON TURF AREA WITH 30% IMPERVIOUSNESS

examples of the design of two pipe systems are presented in the succeeding sections.

THREE-AREA PIPE SYSTEM WITH PONDS FLOATING ON THE LINE

In Fig. 9, the profile of a proposed sewer serving three-pond inlets is shown. Table 4 gives characteristics of each of the ponds and Table 3 tabulates the design computations. Table 3 shows in detail the computations for pond 3. Values of q_p and m, for various critical precipitation periods to 60 min, are taken from the basic design curves for the indicated 30% imperviousness and the 200-ft overland flow length. Of course, Q_p is the multiplication of q_p by the total acreage. Values of Q_o are computed as previously described and represent the outflow rates which would result if the permissible pondage of 0.068 in. was used. Similar values are shown for ponds 2 and 1, as are the accumulated indicated runoff rates for the three reaches of pipe.

The latter accumulated values show that, for this system, a 10-min supply is critical and therefore the capacities of the pipes should approximate them. If the 20-min values were used and smaller pipe capacities were furnished, when the 10-min rain occurs, the restricted capacities would result in greater storage requirements and consequent slightly higher pond levels.

Using the 10-min runoffs an initial selection of pipe sizes can be made based on differences in permissible pond levels. This procedure gives the hydraulic

grades shown in Col. 8, Table 3; and, for $n = 0.013$, pipe sizes of 19 in., 18 in., and 17 in. shown in Col. 9; obviously the commercial 18-in. pipe is indicated.

As will be noted later, design is practically complete. The pipes may be laid at satisfactory construction grades and will operate under pressure with the ponds floating on the system at slightly different elevations than those originally chosen. However, the actual outlet discharge rate must be accurately checked; and it is also desirable to demonstrate as a matter of experience just how the ponds will adjust themselves.

Accordingly, the chosen pipe system is re-analyzed in detail. The first step involves recognition of the entrance head and other minor losses required for the individual ponds. Col. 11, Table 3, shows the approximate values of $1.5 \frac{V^2}{2g}$, which, when plotted down from the chosen pond levels, give the revised hydraulic grades shown in Col. 12. At this point it is possible to visualize very nearly the values that will enter into an equilibrium condition in the system. For line 1–2, the final grade will probably be a little greater and the quantity a little smaller, since an 18-in. pipe is being used instead of the 19-in. pipe ideally indicated. Line 2–3 will involve a somewhat greater quantity because of a slightly higher gradient. Since the quantity coming in from line 1–2 will be somewhat less than the original value, it is clear that the discharge from pond 2 will be appreciably more than it was originally.

The 18-in. pipe is somewhat large for the line 3-outlet. However, some of this disadvantage is offset by the lower available grade; and, consequently, there should be a slight increase in discharge to the outlet.

From the foregoing it seems probable that the equilibrium flow rates with ponds floating on the line would be about as shown in Fig. 9. The equilibrium conditions determined from the use of these revised discharges are also shown in Fig. 9 and indicate that pond 3 will stand 0.08 ft below the originally chosen value; pond 2, 0.10 ft below; and pond 1, 0.04 ft above. Ponds 2 and 3 are now in exact balance and pond 1 is within 0.01 ft of an exact balance.

Any check to within about 0.02 ft is considered satisfactory since the theoretical changes in pipe flows and pond levels accompanying such very small corrections would not affect the design in a practical way.

Three-Pond System Under 30-Min, Two-Year Frequency Supply

Since the critical storm for the main trunk sewer into which the three-pond system discharges will be much longer than 10 min, it is necessary to investigate the rate of discharge that will occur for longer storms. Table 5 gives an analysis of the 30-min values for Q_p and m, with Q_o equal to the pipe capacities which were found to represent an equilibrium condition for the 10-min supply. The mass pondages and depths related to these outflow rates are given in Cols. 6 and 7.

From Table 5, it can be concluded, therefore, that, for storms of longer duration, the discharge from the chosen commercial-sized pipe system will be slightly less than the discharges for short storms, but less by so small an amount that the original value can be used in the design of the trunk system over a wide range of durations.

Three-Pond System Under 30-Min, Ten-Year Frequency Supply

Since the trunk sewer will carry an "off-field" flow based upon a ten-year frequency rainfall it is important to determine not only the rate of discharge from the three-pond system, but also the pond levels under the less frequent but greater rains. A preliminary calculation indicates that, for the higher supply rates of the ten-year rains, the 30-min duration produces the worst condition of ponding. This condition results because the longer rain permits overland flow more nearly to reach equilibrium, and the peak rates at the end of the rain are actually higher for the 30-min than for the 10-min duration. Also, the 30-min mass runoff is appreciably greater and hence uses more pondage volume.

TABLE 5.—Analysis of Three-Pond Line for 30-Min Rainfall of Two-Year Frequency

Pond No.	Inflow, Q_p (cu ft per sec)	Mass runoff, m (in.)	Outflow, Q_o (cu ft per sec)	Ratio, $\frac{Q_o}{Q_p}$	Mass pondage, p (in.)	Pond depth (ft)	Equilibrium outflow (cu ft per sec)	Outflow below pond (cu ft per sec)	Final pond depth (ft)
(1)	(2)	(3)	(4)	(5)	(6)	(7)	(8)	(9)	(10)
1......	6.1	0.83	6.90	1.13	0	0	6.0	6.0	0
2......	6.0	0.61	2.37	0.39	0.23	0.95	3.10	9.10	0.81
3......	7.2	0.61	5.68	0.79	0.027	0.477	5.80	14.90	0.45
Total..	19.2	....	14.95	....	....	....	14.90	....	....

The values in Table 6 are closely representative of an equilibrium condition under the occurrence of a ten-year frequency, 30-min rain, and it may be concluded that the discharge under the more severe conditions would increase a negligible amount (about 2%). Therefore, in the design of the main trunk sewers to carry the runoff from a ten-year frequency rain on the "off-field" area, the contributions of the ponded laterals can be taken to be the same as those obtained from the two-year frequency analysis.

TABLE 6.—Analysis of Three-Pond Line for 30-Min Rainfall of Ten-Year Frequency

Pond No.	Supply rate (in. per hr)	Area (acres)	Peak inflow, q_p (in. per hr)	Mass runoff, m (in.)	Peak inflow, Q_p (cu ft per sec)	Estimated outflow, Q_o (cu ft per sec)	Ratio, $\frac{Q_o}{Q_p}$	Pondage (in.)	Pond depth (ft)
(1)	(2)	(3)	(4)	(5)	(6)	(7)	(8)	(9)	(10)
1........	2.60	4.04	2.6	1.23	10.50	6.9	0.65	0.15	0.80
2....	2.25	5.84	2.05	1.09	11.97	2.4	0.20	0.70	1.38
3........	2.25	6.90	2.05	1.09	14.14	6.0	0.43	0.35	1.10
3-outlet...	....	....	....	....	36.61	15.30	....	....	....

For the half-foot higher pond elevations due to a ten-year storm, the edge of the ponds will be about 25 ft from the nearest pavement edges. Since this condition will occur on the average only once in ten years, and then will persist for only one or two hours, it is clear that no appreciable intrusion of soil moisture

under the pavement subgrade will result, and the condition is one which may be safely accepted.

SEVEN-POND SYSTEM WITH "NONFLOATING" PONDS

Fig. 12 is a condensed profile in which the upper five ponds descend in order of elevation, but ponds 6 and 7 ascend. Obviously, no hydraulic grade could

Hydraulic Factors

Pipe	Q	V	S	L	D	h_v	h_f
1-2	4.0	3.25	0.0038	280	15	0.16	1.07
2-3	6.47	2.7	0.00165	590	21	0.11	0.97
3-4	10.42	3.3	0.00215	440	24	0.17	0.95
4-5	14.58	3.6	0.00222	550	27	0.20	1.22
5-6	21.7	3.6	0.00167	370	33	0.20	0.62
6-7	23.2	3.26	0.0012	460	36	0.16	0.55
7-Outlet	25.5	3.6	0.00145	500	36	0.20	0.73

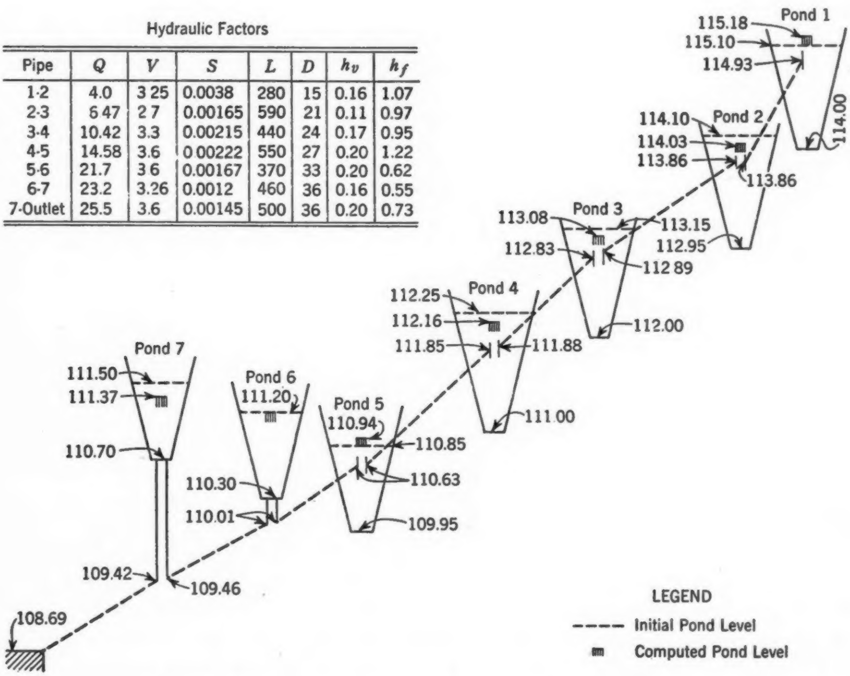

FIG. 12.—PROFILE AND HYDRAULIC FACTORS FOR SEVEN-POND SYSTEM

permit these two ponds to float on the line. In actual design the pipes connecting the upper five ponds are treated in the same manner as the previously discussed three-pond system; open grated manholes can be installed at the low points of these ponding areas.

For ponds 6 and 7, similar inlet manholes will be constructed but they will be connected to the main system by small laterals so chosen in size and length as satisfactorily to throttle discharge from the ponds. Discharge from the ponds will then be determined in no direct way by the capacity of the pipes in the main system.

Determination of outlet rates as related to the permissible pondage for each of the areas is given in Table 7. It is interesting to note that, for pond 7, Q_o is given as 0 for the 10-min time—because the permissible pondage is greater than the whole of the mass rainfall. However, an outlet pipe is required to drain the pond and a specific discharge rate will exist during the rain. In

Table 8, it will be noted that a nominal value of 1 cu ft per sec has been initially assumed.

The totals at the outlet as shown in Table 7 indicate that the 10-min critical rainfall produces the largest runoff, and the design of the pipe system is worked out to handle these rates adequately (Col. 8, Table 7) without appreciably exceeding the desirable pond depths.

Table 8 summarizes the design information. Final equilibrium gradients and pond levels are shown in Fig. 12.

It must be understood that equilibrium flow conditions require not only a balanced scheme of hydraulic gradients but also outflow rates from the ponds

TABLE 7.—REDUCTION OF DISCHARGE

Pond No.	Area (acres)	Impervious (%)	Flow length, L (ft)	Mass pondage, p (in.)	10-Min Supply			20-Min Supply		
					Inflow, Q_p (cu ft per sec)	Runoff, m (in.)	Outflow, Q_o (cu ft per sec)	Inflow, Q_p (cu ft per sec)	Runoff, m (in.)	Outflow, Q_o (cu ft per sec)
(1)	(2)	(3)	(4)	(5)	(6)	(7)	(8)	(9)	(10)	(11)
1......	7.51	46	180	0.27	12.5	0.73	4.9	11.3	0.75	4.5
2......	7.55	34	180	0.41	10.1	0.59	1.7	9.3	0.62	1.7
3......	9.42	32	220	0.28	11.0	0.57	3.2	10.3	0.59	3.2
4......	10.30	40	210	0.42	14.5	0.66	2.9	13.8	0.68	3.0
5......	5.60	60	100	0.15	13.5	0.89	8.0	12.0	0.91	7.1
6......	8.68	32	150	0.45	12.8	0.58	1.5	10.7	0.60	1.5
7......	11.2	27	265	0.51	10.3	0.50	0	10.0	0.53	0.2
Total..	....	....	....	....	84.7	....	22.2	77.4	....	21.2

(which make up the discharge values of the pipe system) resulting from the pondage depths which are in balance with the hydraulic grades of the pipe system. For example, at pond 5, the hydraulic grade of the outgoing pipe is 110.63, the velocity in the pipe is 3.6 ft per sec, and 1.5 times the velocity head is 0.31 ft. In other words, the elevation of the pond floating on the line at a static elevation which will provide the necessary velocity and entrance loss heads is 110.63 plus 0.31 or 110.94. From Table 7, it is noted that the peak flow rate to this pond is 13.5 cu ft per sec; and the outflow rate is 7.12 cu per sec (Table 8). For the pond to reduce the runoff rate by this amount, the volume of pondage must be 0.20 in., equivalent to a 0.99-ft depth. When this value is added to the elevation of the inlet grating, the surface of the pond checks the 110.94 elevation obtained, indicating that the pipe system and the detention pondage are in accord. As previously stated, any check to within about 0.02 ft is ordinarily considered satisfactory.

To complete the design of this system, the connecting pipes for ponds 6 and 7 must be selected. For pond 6, the desired outflow of 1.5 cu ft per sec occurs when the pond level is 111.20 and the available fall from this water surface to the hydraulic gradient of the pipe line is 1.19 ft. If an 8-in. pipe is used, the velocity head plus entrance loss is 0.42 ft. Thus, 0.77 ft is available for friction loss; and, since the 8-in. pipe requires a gradient of 0.0152, the necessary resistance would accordingly be provided by a pipe connection 50.6 ft long. A similar analysis for a flow of 2.3 cu ft per sec from pond 7 results in an 8-in.

pipe connection 26.5 ft long. The computed connection lengths are quite important and must actually be used in the plan if outflows from these ponds are to be throttled to the amounts indicated.

Relation of Flow Time Through Pipes to Outlet Discharge Rate

In the foregoing discussion the flow through any reach of pipe has been taken as the sum of the inflows at all points upstream. This procedure is correct since all hydrographs resulting from restricted pond outflow will have flat tops of such considerable duration as to overlap. Fig. 13 shows this characteristic of the outflow hydrographs for the seven-pond system.

BY PONDAGE IN SEVEN-POND SYSTEM

30-Min Supply			45-Min Supply			60-Min Supply		
Inflow, Q_p (cu ft per sec)	Runoff, m (in.)	Outflow, Q_o (cu ft per sec)	Inflow, Q_p (cu ft per sec)	Runoff, m (in.)	Outflow, Q_o (cu ft per sec)	Inflow, Q_p (cu ft per sec)	Runoff, m (in.)	Outflow, Q_o (cu ft per sec)
(12)	(13)	(14)	(15)	(16)	(17)	(18)	(19)	(20)
10.3	0.79	4.3	8.4	0.87	3.7	7.1	0.94	3.3
8.6	0.66	1.8	7.1	0.71	1.7	6.1	0.78	1.7
9.7	0.63	3.2	8.2	0.70	3.0	7.25	0.76	2.8
12.7	0.72	3.0	10.4	0.79	2.8	8.9	0.86	2.7
9.75	0.95	5.9	7.5	1.05	4.7	6.1	1.16	3.9
10.0	0.64	1.6	8.0	0.69	1.5	6.8	0.76	1.6
9.75	0.57	0.5	8.6	0.63	0.9	7.7	0.69	1.1
70.8	....	20.3	58.2	....	18.3	49.95	....	17.1

Table 9 gives pertinent data required for the preparation of the hydrographs. Cols. 2, 3, and 4 are taken from Tables 7 and 8. Col. 5 represents the time length of the rising side of the hydrograph, obtained by multiplying the 10-min time at which Q_p would have occurred if no pondage were available by the ratio of Q_o to Q_p. This relationship arises out of the properties of the assumed triangular hydrograph.

Col. 6 is the average time length of the hydrograph from the center of the rising side to the center of the recession. It is obtained by changing the values of m in Col. 4 to cubic feet and then dividing by Q_o. Col. 7 gives the times of flow in each reach of pipe. These times between ponds are based on length and average velocity as it is believed that for these small lines the higher flow rate of wave velocity can be ignored, particularly inasmuch as the summation would not be affected by the changes that refinement would produce.

Direct addition of the ordinates of all the hydrographs gives the hydrograph of discharge at the outlet for the system. The exact shape of the rising side is necessarily approximate since the discharges are based on the critical hydraulic grades for maximum discharge; and, during the rising side, partial flows, lower hydraulic grades, and somewhat different discharges from the ponds can take place. The error in ignoring this condition is quite small and affects only the shape of the rising side, not the peak values.

For this seven-pond system with a 16-min pipe flow time, under the application of the two-year, 10-min rain, the maximum discharge will be reached in

about 10 min and will persist for somewhat longer than 40 min from the beginning of the critical 10-min rain. Particularly noteworthy is the fact that for a period of more than 20 min all hydrographs are flat topped and their

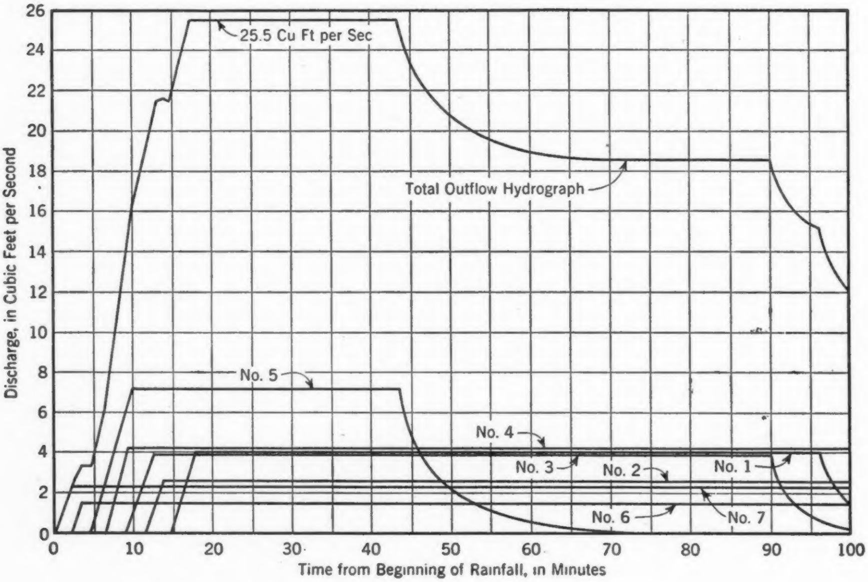

FIG. 13.—SUMMATION OF HYDROGRAPHS FOR SEVEN-POND SYSTEM

values can be added directly.

For the three-pond example, it was shown that there would be no appreciable difference in the discharge rate at the outlet under the occurrence of the

TABLE 8.—SUMMARY OF DESIGN DATA FOR SEVEN-POND SYSTEM

Pond or pipe No.	Initial pond elevation	Discharge (Cu Ft per Sec)		Length (ft)	Slope (ft per ft)	Pipe diameter (in.)	Discharge (Cu Ft per Sec)		Equilibrium pond elevation
		Initial	Total				Revised	Equilibrium	
(1)	(2)	(3)	(4)	(5)	(6)	(7)	(8)	(9)	(10)
1	115.10	4.9	....	....	....	....	3.8	4.0	115.18
1–2	....	....	4.9	280	0.0036	15	3.8	4.0	....
2	114.10	1.7	....	....	....	....	2.8	2.47	114.03
2–3	....	....	6.6	590	0.0016	21	6.6	6.47	....
3	113.15	3.2	....	....	....	....	3.0	3.95	113.08
3–4	....	....	9.8	440	0.0020	24	9.6	10.42	....
4	112.25	2.9	....	....	....	....	5.9	4.16	112.16
4–5	....	....	12.7	550	0.0025	27	15.5	14.58	....
5	110.85	8.0	....	....	....	....	5.5	7.12	110.94
5–6	....	....	20.7	370	0.0016[a]	33	21.0	21.70	....
6	111.20	1.5	....	....	....	....	....	1.50	111.20
6–7	....	....	22.2	460	0.0016[a]	36	27.0	23.2	....
7	111.50	1.0[b]	....	....	....	....	....	2.3	....
7-outlet	....	....	23.2	500	0.0016[a]	36	27.0	25.5	111.37
Outlet	108.7	....	....	....	....	....	....	....	....

[a] Average. [b] Actual value, 0.0.

two-year, 10-min rain, the two-year, 30-min rain, or the ten-year, 30-min rain. Plotting similar to that of Fig. 13 shows that both the first and last of these rains, which represent the most severe conditions, have long flat topped hydrographs extending for 20 min or more. The two-year, 30-min rain, because two

TABLE 9.—TIME CHARACTERISTICS OF OUTFLOW HYDROGRAPHS FOR SEVEN-POND SYSTEM

Pond No. (1)	Inflow, Q_p (cu ft per sec) (2)	Outflow, Q_o (cu ft per sec) (3)	Mass run-off, m (in.) (4)	Inflow time, t_2 (min) (5)	Average hydrograph time, t_{avg} (min) (6)	Flow time (min) (7)
1...........	12.5	4.0	0.73	3.2	83	1.4
2...........	10.1	2.47	0.59	2.4	109	3.6
3...........	11.0	3.95	0.57	3.6	82	2.2
4...........	14.5	4.16	0.66	2.9	99	2.5
5...........	13.5	7.12	0.89	5.3	42	1.7
6...........	12.8	1.5	0.58	1.2	203	2.4
7...........	10.3	2.3	0.50	2.2	147	2.3
Outlet......	84.7	25.5	....	....	....	16.1

of the inlets use very little pondage, comes almost to a peak, but still has a flat top of about 5-min duration.

SUMMARY

Where surface drainage of airports permits the development and utilization of pondage in the flat turfed areas, accepted hydrologic knowledge concerning retention, infiltration, and overland flow is directly applicable. The development of supply rates requires an analysis of actual storms and their related infiltration values so selected as to result in surface supply rates produced, on the average, by the rains which give the critical average rates of the desired frequency. For facility of design, hydrographs of inflow to ponds can be considered triangular in shape.

The pondage resulting from the very flat grades required in airports can be allowed to "float" on the line and has the fortuitous characteristic of very small depth changes (and consequent minor differences in actual hydraulic gradient between ponds) for relatively large pondage volume changes. Once commercial pipe sizes are chosen for a definite duration and frequency, their capacities vary insignificantly for rains of longer duration or greater frequency. Pondage so flattens the hydrograph that direct addition of pond outflow rates can be used, obviating the laborious offsetting of each outflow hydrograph.

ACKNOWLEDGMENTS

This paper resulted from studies initiated by W. W. Horner, Past-President, ASCE, and had the benefit of his collaboration and constructive criticism. The studies were part of a "Report on Basis of Design for Field and Off-Field Drainage Systems for Lambert-St. Louis Municipal Airport" submitted to Milton M. Kinsey, president of the Board of Public Service of St. Louis, and reviewed by Guy Brown, M. ASCE, chief engineer, and E. J. A. Gain, Assoc. M. ASCE, engineer, Division of Sewers and Paving, Board of Public Service of St. Louis.

A

br
fo
tic
sp
th
co
to
cu
st
be
ci
la
m
ti
w
li
p
de
a

cu

AMERICAN SOCIETY OF CIVIL ENGINEERS

Founded November 5, 1852

PAPERS

INFLUENCE LINES FOR CONTINUOUS STRUCTURES BY GEOMETRICAL COMPUTATION

By Dean F. Peterson, Jr.,[1] Assoc. M. ASCE

Synopsis

As the practical span length of continuous girder bridges and rigid frame bridges becomes progressively greater, the use of influence lines or coefficients, for the purpose of investigating the effect of more numerous possible combinations of loading, and for placing loads for maximum effect, becomes correspondingly important. Although such influence lines may be constructed in the usual manner by loading the structure at a number of different points and computing the resulting stress or moment, this is an arduous task and amounts to finding the desired load points by trial and error. The equality of the elastic curve of a structure loaded with a unit deformation at the point for which the stresses are desired, and the influence line for stress at that point, has long been used for determining the influence line for trussed structures. The principle was applied mechanically to all types of indeterminate structures by the late George Beggs,[2] M. ASCE, Otto Gottschalk,[3] and others. This relationship may easily be extended to the analytical computation of influence lines for continuous structures subjected principally to flexure, accomplishing analytically what the use of models accomplishes mechanically. Examples of influence lines for several types of continuous structures have been computed by this procedure using various types of statical analysis. Formulas have also been developed for locating the position and value of the maximum influence ordinate and for the area under the influence line for members of constant cross section.

Note.—Written comments are invited for immediate publication; to insure publication the last discussion should be submitted by **February 1, 1948.**

[1] Associate Prof. of Civ. Eng., Utah State Agri. College, Logan, Utah.

[2] *Transactions*, ASCE, Vol. 88, 1925, p. 1208.

[3] *Ibid.*, Vol. 103, 1938, p. 1019.

Basic Relationship

The basic relationship involved in the development of this paper—the Müller-Breslau relation— is well known. Its validity follows from a consideration of Maxwell's principle of reciprocal deflections, and the principle of superposition which is valid as long as the structures are built of materials that act elastically.

Fundamental Equations of Flexural Geometry

This paper is concerned with flexural equations both as a means of (1) producing a statical solution and (2) computing elastic curve ordinates. The fundamental differential equation of flexural geometry, $\frac{d^2y}{dx^2} = \frac{M}{E\,I}$ (neglecting the distortions due to shear and direct stresses), is a special case of the general equations of elasticity and has the following first and second integrals:

$$\left.\frac{dy}{dx}\right|_x = \int_0^x \frac{M_\xi}{E_\xi\, I_\xi}\, d\xi + C_1 \qquad \text{(1a)}$$

and

$$y\,\Big|_x = \int_0^x \frac{M_\xi}{E_\xi\, I_\xi}\,(x - \xi)\, d\xi + C_1\, x + C_2 \qquad \text{(1b)}$$

in which, in addition to the variable coordinates x and y, M_ξ is the bending moment at ξ; E_ξ is the modulus of elasticity at ξ; I_ξ is the moment of inertia at ξ; C_1 is a constant of integration; and C_2 is a constant of integration. Eqs. 1 may sometimes be solved by integral calculus, but are usually solved by finite integration. However, in the field of indeterminate structures, the imposition of more than the required boundary conditions makes necessary the solution of a set of simultaneous equations, or its mathematical equivalent. The many short cuts which the modern structural engineer uses in his analysis are simply means of setting up and solving Eqs. 1.

Procedure for Solution

Influence lines for moments, shears, thrusts, and reactions are obtained by determining the elastic curve of the structure when it is loaded with the corresponding unit axial rotation, transverse axial displacement, longitudinal axial displacement, or deflection in the direction of reaction. It is necessary first to make a statical analysis of the structure bearing only the required displacement loading using any method—moment distribution, slope deflection, elastic curve traverse, etc.—that the designer desires. In general, since all the members are unloaded (in the sense that they do not bear any gravity, wind, hydrostatic, or other usual load), the analysis is simpler than when conventional loads are involved.

After statical solution of the structure has been completed, the end rotations and deflections for each of the members are computed. Using some methods of analysis, such as slope deflection or elastic curve traverse, these will be known directly from the process of solution. Other methods of solution will require the use of the flexural-geometry equations, or some derivative of them (such as

the moment-area principle), to arrive at the required rotations and deflections. The elastic curve can be computed by solving Eq. 2, or by various modifications of Eq. 2.

Indirect Method

The statical solution for the structure loaded with the unit deflection or rotation may also be made using the method, developed in connection with moment distribution,[4] of (*a*) considering separately an unbalanced moment at each joint, (*b*) solving for the required moments in each case, and then (*c*) combining the result of the several fixed-end moments due to the loading in proportion to the original distributions. Instead of choosing fixed-end moments resulting from conventional loads, fixed-end moments compatible with the imposed displacement are proportioned and combined. This method is illustrated, subsequently, by Example 9 using moment distribution and may also be applied using the elastic curve traverse method.[5]

Calculating Elastic Curves of Members

Throughout the mathematical analysis the following sign convention will be adopted: Ordinate and abscissa as usual. Counterclockwise rotation in the direction of $+x$ will be plus and will produce a positive deflection from the tangent in the direction of $+x$. Moment causing concave bending upward will be considered positive. Positive moment will always give positive rotations and positive deflections in the direction of positive x-values. For a member whose axis can be considered straight, if y_A is the deflection from the original axis of point A and θ_A is the slope of the tangent to the elastic curve at point A, then, for any point, x_n:

$$y_n = y_A + \theta_A \, x_n + \sum_{\xi=1}^{\xi=n} (x_n - x_\xi) \frac{M_\xi}{E_\xi \, I_\xi} \Delta\xi \quad \text{.............} (2)$$

Generally, however, it is simpler to compute the slope and deflection point by point; thus:

$$y_n = y_{n-1} + \theta_{n-1} \frac{\Delta x_{n-1} + \Delta x_n}{2} \quad \text{................} (3a)$$

in which

$$\theta_n = \theta_{n-1} + \frac{M_n}{E \, I_n} (\Delta x_n) \quad \text{....................} (3b)$$

Analytical Solution.—Referring to the haunched beam in Fig. 1, suppose that:

$$\theta_A = -\frac{1{,}000}{E \, I_d}; \quad \theta_B = \frac{300}{E \, I_d} \quad \text{..................} (4)$$

$$y_A = \frac{20{,}000}{E \, I_d}; \quad y_B = 0 \quad \text{....................} (5)$$

[4] "Continuous Frames of Reinforced Concrete," by Hardy Cross and N. D. Morgan, John Wiley & Sons, Inc., New York, N. Y., 1932, p. 105.

[5] "Relative Flexure Factors for Analyzing Continuous Structures," by Ralph W. Stewart, *Transactions*, ASCE, Vol. 104, 1939, p. 521.

in which I_d equals the moment of inertia, in feet[4], at the center section of depth d; and E is the modulus of elasticity in kips per square foot.

The end moments may be obtained by any desired method. For purposes of generalization the basic formulas (Eqs. 1) will be applied; thus, after simpli-

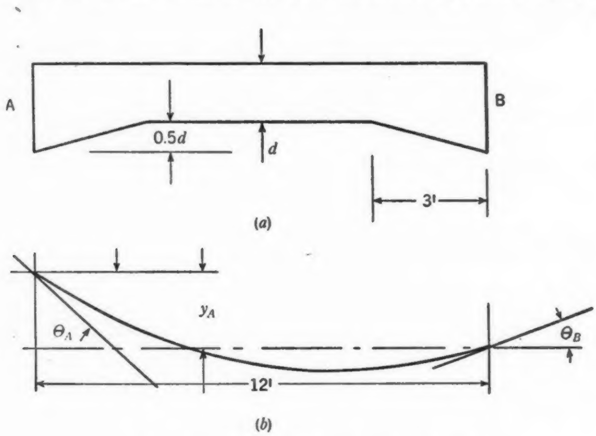

FIG. 1.—EXAMPLE OF A HAUNCHED BEAM

fying and substituting finite summation for the integrals:

$$1{,}300 = M_A \sum_1^n K_n \left(1 - \frac{x_n}{12}\right) \Delta x_n + M_B \sum_1^n K_n \frac{x_n}{12} \Delta x_n \qquad (6a)$$

and

$$-\,8{,}000 = M_A \sum_1^n K_n \left(1 - \frac{x_n}{12}\right) (12 - x_n)\,\Delta x_n$$
$$+ M_B \sum_1^n K_n \frac{x_n}{12} (12 - x_n)\,\Delta x_n \qquad (6b)$$

TABLE 1.—COMPUTATION OF M_A AND M_B IN THE SOLUTION OF EQS. 6

Segment	x_n (ft)	K_n (Eq. 7)	$\Delta x_n K_n$	$\frac{x_n}{12}$	$\frac{x_n}{12} \Delta x_n K_n$	$1-\frac{x_n}{12}$	$\left(1-\frac{x_n}{12}\right) \times \Delta x_n K_n$	$12-x_n$	$\frac{x_n}{12} (\Delta x_n K_n) \times (12-x_n)$	$\left(1-\frac{x_n}{12}\right) (\Delta x_n K_n) \times (12-x_n)$
(1)	(2)	(3)	(4)	(5)	(6)	(7)	(8)	(9)	(10)	(11)
1...	0.5	0.353	0.353	0.0416	0.0147	0.9583	0.338	11.5	0.169	3.885
2...	1.5	0.510	0.510	0.1250	0.0638	0.8750	0.446	10.5	0.670	4.480
3...	2.5	0.787	0.787	0.2083	0.1640	0.7916	0.623	9.5	1.557	5.920
4...	3.5	1.000	1.000	0.2916	0.2916	0.7083	0.7083	8.5	2.478	6.015
5...	4.5	1.000	1.000	0.3750	0.3750	0.6250	0.6250	7.5	2.815	4.685
6...	5.5	1.000	1.000	0.4583	0.4583	0.5416	0.5416	6.5	2.979	3.520
7...	6.5	1.000	1.000	0.5416	0.5416	0.4583	0.4583	5.5	2.975	2.520
8...	7.5	1.000	1.000	0.6250	0.6250	0.3750	0.3750	4.5	2.810	1.688
9...	8.5	1.000	1.000	0.7083	0.7083	0.2916	0.2916	3.5	2.480	1.020
10...	9.5	0.787	0.787	0.7916	0.623	0.2083	0.1640	2.5	1.558	0.410
11...	10.5	0.510	0.510	0.8750	0.446	0.1250	0.0638	1.5	0.669	0.096
12...	11.5	0.353	0.353	0.9583	0.338	0.0416	0.0147	0.5	0.169	0.007
Σ...	....	....	9.300	....	4.6493	....	4.6493	....	21.329	34.446

in which

$$K_n = \frac{E\, I_d}{E\, I_n} \qquad (7)$$

The coefficients under the sigma signs in Eqs. 6 are calculated by Table 1, and

TABLE 2.—COMPUTATION OF DEFLECTION CURVE FOR THE BEAM IN FIG. 1

x_n (ft)	$M_A\left(1-\frac{x_n}{12}\right)$	$M_B\,\frac{x_n}{12}$	M_n	$K_n\,M_n\,\Delta x_n$	θ_n	$\frac{\Delta x_{n-1}+\Delta x_n}{2}$	Δy	y_n
(1)	(2)	(3)	(4)	(5)	(6)	(7)	(8)	(9)
0.0....	−1,061	0	−1,061	....	−1,000	....	....	20,000
0.5....	−1,018	56	− 962	−340	−1,340	0.5	− 500	19,500
1.5....	− 930	168	− 762	−389	−1,729	1.0	−1,340	18,160
2.5....	− 841	279	− 562	−442	−2,171	1.0	−1,729	16,431
3.5....	− 752	391	− 361	−361	−2,532	1.0	−2,171	14,260
4.5....	− 664	503	− 161	−161	−2,693	1.0	−2,532	11,728
5.5....	− 576	614	38	38	−2,655	1.0	−2,693	9,035
6.5....	− 487	726	239	239	−2,416	1.0	−2,655	6,380
7.5....	− 398	839	440	440	−1,976	1.0	−2,416	3,964
8.5....	− 310	950	640	640	−1,336	1.0	−1,976	1,988
9.5....	− 221	1,060	839	660	− 676	1.0	−1,336	652
10.5....	− 134	1,173	1,039	529	− 147	1.0	− 676	− 24
11.5....	− 44	1,283	1,239	443	300	1.0	− 147	−171
12.0....	0	1,341	1,341	....	....	0.5	150	− 21
Total...	....	....	....	....	....	....	....	121,882

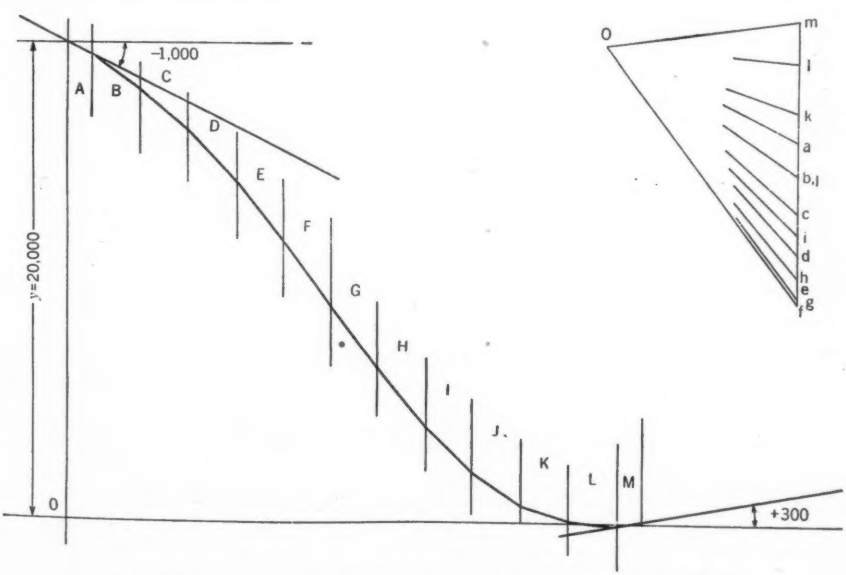

FIG. 2.—CONSTRUCTION OF DEFLECTION CURVE FOR THE BEAM IN FIG. 1

the equations thus solved yield: $M_A = -1{,}061$ ft-kips; and $M_B = 1{,}341$ ft-kips. Using Eqs. 3 the elastic curve is calculated by means of Table 2.

Graphical Solution.—Instead of using Table 2, Eq. 3*a* may be solved graphically by the use of the funicular polygon in Fig. 2. The chords passing through

the end points of the beam must have a slope equal to the known slope of the end tangents.

Prismatic Members.—Although beams of constant section may be handled by either the analytical or graphical method of finite integration, it is possible to pass to the integral in the summation of Eq. 2 and derive general equations for the elastic curves when the end rotations and deflections are known. Consider a length AB of a straight, unloaded member (Fig. 3). Let the rotation at

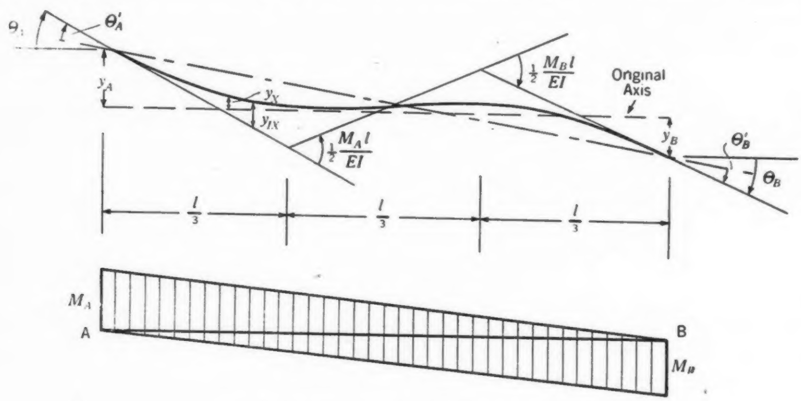

Fig. 3.—Example of a Prismatic Member

end A be equal to θ_A; and, at end B, to θ_B. Let y_A and y_B, respectively, represent the perpendicular displacement of points A and B from their original position. From the slope-deflection equations, or by geometry:

$$M_A = -\frac{2\,E\,I}{l}\left(2\,\theta_A + \theta_B - 3\,\frac{y_B - y_A}{l}\right) = \frac{-\,2\,E\,I}{l}\,(2\,\theta'_A + \theta'_B) \qquad (8a)$$

and

$$M_B = \frac{2\,E\,I}{l}\left(\theta_A + 2\,\theta_B - 3\,\frac{y_B - y_A}{l}\right) = \frac{2\,E\,I}{l}\,(\theta'_A + 2\,\theta'_B) \qquad (8b)$$

Since $M_\xi = M_A + (M_B - M_A)\,\frac{\xi}{l}$, Eq. 2 yields, by integration,

$$y_{1x} = \frac{1}{E\,I}\left[\,M_A\,\frac{x^2}{2} + (M_B - M_A)\,\frac{x^3}{6\,l}\,\right] \qquad (9a)$$

By geometry, however, Eq. 2 yields,

$$y_x = y_A + \frac{y_B - y_A}{l}\,x + \theta'_A\,x + y_{1x} \qquad (9b)$$

Substituting Eq. 9*a* in Eq. 9*b* as well as the values of M_A and M_B from Eqs. 8, simplifying and collecting terms:[6]

$$y_x = y_A + (y_B - y_A)(k_1)(1 - k^2{}_1 + k_1\,k_2) + l\,(\theta_A\,k_1\,k^2{}_2 - \theta'_B\,k^2{}_1\,k_2) \qquad (10)$$

[6] *Transactions*, ASCE, Vol. 104, 1939, Eq. 23, p. 555.

in which $k_1 = \frac{x}{l}$, and $k_2 = 1 - \frac{x}{l}$. If y_A and $y_B = 0$ this formula reduces to the equation developed elsewhere for a similar case by Ralph W. Stewart, M. ASCE.

Location of Maximum Load Point

When concentrated loads are being considered, it is important to know where the load should be placed to produce the maximum effect on the section being investigated. Eq. 10 may be rewritten since $k_2 = 1 - k_1$; thus:

$$y_x = y_A + [l\,\theta_A + l\,\theta_B - 2\,(y_B - y_A)]\,k^3{}_1 + [3\,(y_B - y_A) - 2\,l\,\theta_A - l\,\theta_B]\,k^2{}_1 + l\,\theta_A\,k_1 \qquad (11)$$

Differentiating with respect to k_1 and equating the result to zero a quadratic equation results, which may be solved to yield:

$$k_{1m} = \frac{1}{3\,[l\,(\theta_A + \theta_B) - 2\,(y_B - y_A)]}\,[l\,(2\,\theta_A + \theta_B) - 3(y_A - y_B) \pm \sqrt{9\,(y_B - y_A)^2 - 6\,l\,(y_B - y_A)(\theta_A + \theta_B) + (\theta^2{}_A + \theta_A\,\theta_B + \theta^2{}_B)\,l^2}] \qquad (12a)$$

If $y_B - y_A = 0$, then:

$$k_{1m} = \frac{1}{3\,(\theta_A + \theta_B)}\,[(2\,\theta_A + \theta_B) \pm \sqrt{\theta^2{}_A + \theta^2{}_B + \theta_A\,\theta_B}] \qquad (12b)$$

Value of Maximum Influence Ordinate

It is possible to derive an expression for the value of the maximum influence ordinate for a member of constant section when $y_B - y_A = 0$. Substituting the value of k_{1m} from Eq. 12*b* for k_1 in Eq. 11 and solving:

$$y_m = \frac{l}{27\,(\theta_A + \theta_B)^2}\,[(\theta^2{}_A + 4\,\theta_A\,\theta_B + \theta^2{}_B) \mp (\theta_A - \theta_B)\,\sqrt{\theta^2{}_A + \theta^2{}_B + \theta_A\,\theta_B}] \times [(\theta_A - \theta_B) \mp \sqrt{\theta^2{}_A + \theta^2{}_B + \theta_A\,\theta_B}] \qquad (13)$$

Area Under the Influence Line

An equation for the area under the influence line for a prismatic member may be obtained by integrating Eq. 11 between the limits $k_1 = 0$ and $k_1 = 1$. This operation yields:

$$Q = \frac{l}{2}\,(y_A + y_B) + \frac{1}{12}\,l^2\,(\theta_A - \theta_B) \qquad (14)$$

in which Q is the area under the influence line. Eq. 14 is of value when the entire span carries a uniformly distributed load. It cannot be used directly when the deflection curve is discontinuous or contains a slope discontinuity within the span. For members with varying cross section the area under the influence line may be determined by a summation of the influence line ordinates (see Col. 9, Table 2).

Examples

A fairly large number of examples have been included. This was done in order to furnish an illustration for each of several different methods of statical

analysis of the structure bearing the deformation load. Although fairly simple structures have been used in the examples, the principles can be extended easily to more complex structures.

Example 1. Draw the Influence Line for Moment at a Given Section of a Fixed-Ended Beam with Constant Cross Section.—The deflection y_B of point B in Fig. 4(a) can be determined by Mr. Stewart's traverse method,[7] imposing a rotation, θ, at that section. Designating the traverse angle associated with M_B as 4, the corresponding angle in length BC must be 5 since it also is associated with M_B. By equating the deflection at point B:

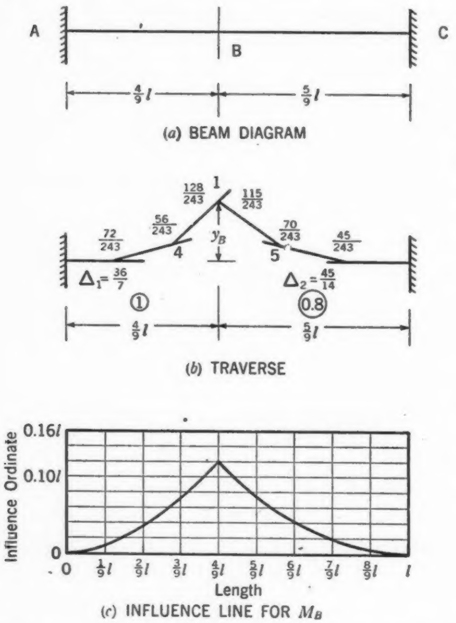

FIG. 4.—INFLUENCE LINE FOR MOMENT AT A GIVEN SECTION OF A FIXED-ENDED BEAM WITH CONSTANT CROSS SECTION

$$\Delta_1 = \frac{5}{4}\Delta_2 + \frac{9}{8} \ldots\ldots (15)$$

in which Δ (see Fig. 4(b)) is the relative curvature in the given length resulting from an end moment. From the moment diagram,

$$M_B = M_A + \frac{4}{9}(M_C - M_A) . (16)$$

but, in relative terms, $M_A = (1)\,\Delta_1 = \Delta_1$; $M_B = (1)\,4 = 4$; and $M_C = 0.8\,\Delta_2$. Substituting these values in Eq. 16 and solving simultaneously with Eq. 15, $\Delta_1 = \frac{36}{7}$; and $\Delta_2 = \frac{45}{14}$. Solving for θ, by summation of rotations from point A to point C, $\theta = -\frac{243}{4}$. For $\theta = 1$ the traverse angles must then be, in order, $\frac{72}{243}$, $\frac{56}{243}$, $\frac{70}{243}$, and $\frac{45}{243}$, respectively. From geometry, $y_B = \left(\frac{72}{243}\right) \times \left(\frac{8}{27}\,l\right) + \left(\frac{56}{243}\right)\left(\frac{4}{27}\,l\right) = 0.122\,l$. Other ordinates for the influence line (Fig. 4(c)) may be computed as desired using Eq. 10.

Example 2. Draw the Influence Line for the Fixed-End Moment at the Haunched End of a Fixed Beam.—Imposing the unit rotation at end A of the beam in Table 3 solve for the statical condition of the beam using column analogy.[8] With the results listed in Table 3, assuming a unit angle load at

[7] *Transactions*, ASCE, Vol. 101, 1936, p. 105.

[8] "Continuous Frames of Reinforced Concrete," by Hardy Cross and N. D. Morgan, John Wiley & Sons, Inc., New York, N. Y., 1932, Chapter III.

end A, the end moments are, respectively: $M_A = \frac{1}{26.15} + \frac{11.21 \times 11.21}{697.7} = + 0.2189$; and $M_B = \frac{1}{26.15} - \frac{11.21 \times 8.79}{697.7} = - 0.1031$. The final computations of influence ordinates are arranged in a manner similar to Table 2.

TABLE 3.—COMPUTATION OF END MOMENTS BY COLUMN ANALOGY[a]

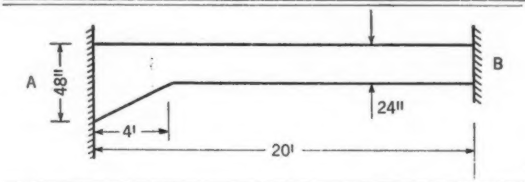

Section	L	d	x	a	$a\,x$	$a\,x^2 + i_x$
1	1	3.75	−9.5	0.228	−2.16	20.5
2	1	3.25	−8.5	0.349	−2.96	25.2
3	1	2.75	−7.5	0.574	−4.38	32.9
4	1	2.25	−6.5	1.050	−6.82	49.3
5	16	2.00	2.0	24.000	48.00	608.0
....	....	....	....	26.151	31.68	735.9
Correction.	($\bar{x} = +1.21$)		....	....	....	−38.2
Total......	....	....	....	....	....	697.7

[a] L = length AB; d = depth of the uniform section; x = distance from center of beam to centroid of each segment; $a = 12\, L/d^3$; and $i_x = 1/12\; a\, L^2$.

Example 3. Shear at the Support of a Fixed-Ended Beam.—Assume a beam of uniform cross section, fixed as shown in Fig. 5, with a unit deflection imposed at end A. In this instance the boundary conditions for the differential equations of flexure are: $y_A = 1$; $y_B = 0$; $\theta_A = 0$; and $\theta_B = 0$; and the general solution is to be found in Eq. 10 which reduces to

$$y_x = 1 - k_1 (1 - k^2_2 + k_1\, k_2) \qquad (17)$$

and which is used to compute the influence line (see Fig. 5(*b*)).

Example 4. Find the Maximum Value of M_C on the Frame of Uniform Cross Section in Fig. 6 Due to a Moving Load of 10 Kips. (Also Find the Moment at Joint C *Due to a Uniform*

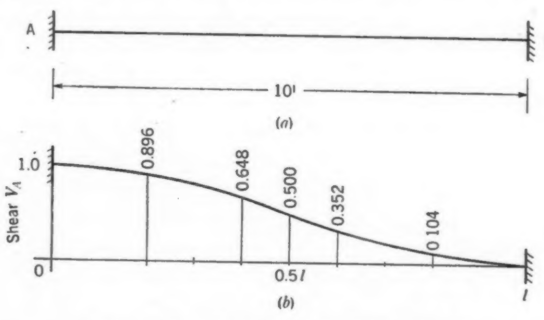

FIG. 5.—INFLUENCE LINE FOR SHEAR AT END A

Load of 1.5 Kips per Ft.)—From the slope-deflection equations,

$$\theta_{DC} = 0 = \frac{10\, M_{DC}}{3\, E\, I} + \frac{10\, M_{CD}}{6\, E\, I} + \frac{y}{10} \qquad (18a)$$

$$\theta_{CD} = - \frac{10\, M_{DC}}{6\, E\, I} - \frac{10\, M_{CD}}{3\, E\, I} + \frac{y}{10} \qquad (18b)$$

$$\theta_{CB} = \frac{10\ M_{BC}}{6\ E\ I} + \frac{10\ M_{CB}}{3\ E\ I} \qquad (18c)$$

$$\theta_{BC} = -\frac{10\ M_{BC}}{3\ E\ I} - \frac{10\ M_{CB}}{6\ E\ I} \qquad (18d)$$

$$\theta_{BA} = \frac{6\ M_{BA}}{3\ E\ I} + \frac{y}{6} \qquad (18e)$$

$$\theta_{AB} = -\frac{6\ M_{BA}}{6\ E\ I} + \frac{y}{6} \qquad (18f)$$

in which y equals the horizontal displacement of points B and C due to side lurch. From geometry, remembering that a unit rotation is imposed at joint C:

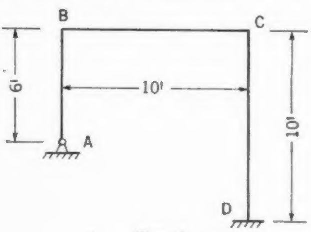

Fig. 6

$$\theta_{CD} - \theta_{CB} = 1;\quad \theta_{BC} - \theta_{BA} = 0 \qquad (19)$$

From statics,

$$M_{CD} = M_{CB};\quad M_{BC} = M_{BA} \qquad (20)$$

and if H and V are the horizontal and vertical components of the reaction at point A:

$$M_{DC} = 4\ H + 10\ V;\ M_{CD} = 10\ V - 6\ H;\ M_{BC} = 6\ H;$$
$$\text{and } M_{CD} - M_{BC} = 10\ V \qquad (21)$$

The simultaneous solution of Eqs. 18 to 21 yields: $M_{BA} = M_{BC} = -0.0444\ E\ I$; $M_{CD} = M_{CB} = 0.0972\ E\ I$; $\theta_{CD} = 0.603$; $\theta_{CB} = -0.398$; $\theta_{BC} = 0.310$; $\theta_{BA} = 0.311$; and $\theta_{AB} = 0.444$. From Eq. 12*b*: $k_{1m} = \frac{1}{3\ (0.310 - 0.398)}$ $(2 \times 0.310 - 0.398 \pm \sqrt{0.310^2 + 0.398^2 - 0.398 \times 0.310}) = 0.531$; and from Eq. 10: $y_m = 10\ [0.310 \times 0.531 \times 0.469^2 + 0.398 \times 0.531^2 \times 0.469] = 0.888$. Eq. 14 yields the area under the influence curve, thus: $\frac{1}{12}\ (10)^2(0.310 + 0.398) = 5.90$. The maximum moment at joint C due to a moving load of 10 kips,

TABLE 4.—Computation of Moments Corresponding to a Unit Rotation at Joint B, Fig. 6

Line	Description	M_B	M_C	M_D	Sidesway force
1	Moments from Fig. 7(*c*)	+2.50	−8.00	−4.50	....
2	Moments from Fig. 7(*d*) multiplied by 1.389	+9.72	−2.78	+1.39	....
3	Undistributed fixed-ended moment at point D	....	....	+17.00	....
4	....	+12.22	+10.78	13.89	4.504
5	Multiply line 4 by 1.467/4.504	+3.98	+3.51	+4.53	1.467
6	Moments Fig. 7(*a*)	−7.00	−2.00	−1.00	−1.467
7	Summation, lines 5 and 6	−3.02	+1.51	+3.53	0
8	Moment for unit rotation (divide line 7 by 6.8)	0.442	0.224	0.520	....

therefore, will be 8.88 ft-kips when the load is placed 5.31 ft from joint B (Fig. 5). The moment at joint C due to the uniform load will be 5.90 × 1.5, or 8.85 ft-kips.

Example 5. Find the Maximum Value of Moment at Joint B, Fig. 6, Using an Elastic Curve Traverse for Statical Analysis.—Impose the rotation θ at joint B. Beginning with a value of 1 for the lower elastic angle in column CD complete the traverse (Fig. 7), remembering that $M_{BC} = M_{BA}$. From Fig. 7(*a*), $\theta = 2.8 + 4.0 = 6.8$. Since sidesway has not been considered, these values must be corrected. The value of the unbalanced horizontal force is 1.467 $E\,I$. Assume the frame to be deflected sidewise without rotation of joints B and C (Fig. 7(*b*)). Assign the value Δ to the traverse angles and M to the end moments in CD. Since the "sidelurch" is equal for the vertical members the traverse angle in column AB must be 0.833 Δ and $M_{BA} = \frac{5}{6} \times \frac{5}{3} \times M = 1.389\,M$ (see line 2, Table 4).

Figs. 7(*c*) and 7(*d*) are solved for unbalanced moments at joints B and C. The unbalanced moment in each case is 17. If the value M in Fig. 7(*b*) is made equal to 17 then the moments for Fig. 7(*b*) may be computed and the sidesway correction made. The final moments must be divided by 6.8 to reduce to the condition of unit deflection at joint B. Starting at point D with these moments and changing to the equivalent angle units the corrected traverse may be constructed as shown in Fig. 7(*e*). From Eq. 12*b*, $k_{1m} = 0.474$ and, from Eq. 10, $y_m = 0.838$.

Example 6.—The influence line for vertical deflection at the center of span BC, Fig. 6, may be calculated by placing a unit vertical load at the center of the span and computing the resulting deflection curve. The values of M_B and M_C for this loading can be obtained from Eq. 10 using the values of θ_{BC} and θ_{CB} from Examples 4 and 5:

$$M_B = 10\,(0.369 \times 0.5^3 + 0.295 \times 0.5^3) = 0.830$$
$$M_C = 10\,(0.310 \times 0.5^3 + 0.398 \times 0.5^3) = 0.885$$

From statics, $V_B = 0.4945$, and $V_C = 0.5055$, and the moment diagram, Fig. 8(*a*) can be drawn. Applying Eq. 2 between points B and C, $\theta_{BC} = -\frac{2.02}{E\,I}$ and $\theta_{CB} = \frac{1.92}{E\,I}$ for the struc-

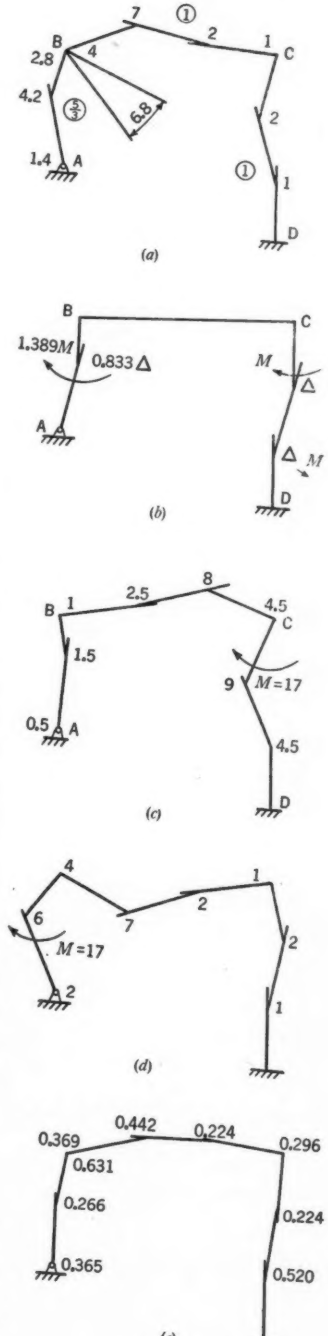

FIG. 7.—ANALYSIS OF AN UNSYMMETRICAL BENT

ture bearing the unit load at the center. The elastic curve (required influence line) may be computed by a tabulation using Eq. 3*a* (see Fig. 8(*b*)).

Example 7. Draw the Influence Line for M_{BC} for a Vertical Load on a Symmetrical Rigid Frame. (What Is the Moment at Joint B (Fig. 9) Due to a Horizontal, Uniformly Distributed Load of 500 Lb per Ft on Member AB?).—The method of moment distribution will be used in exploring this question. Impose a unit rotation at joint B. The fixed-end moments in member BC are then $M_{BC} = \frac{4\,E\,I}{l}$ and $M_{CB} = \frac{2\,E\,I}{l}$, respectively. The solution of Fig. 9(*a*) yields $M_B = -1.615\,\frac{E\,I}{l}$; $M_C = 0.461\,\frac{E\,I}{l}$; and

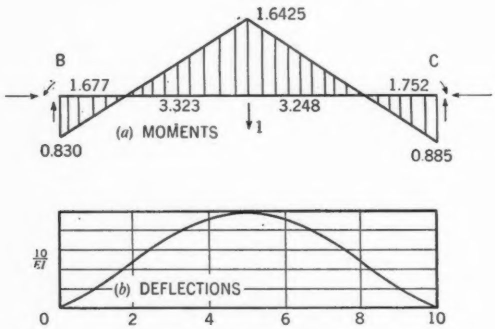

Fig. 8.—Influence Line for Deflection at the Center of the Span

$M_D = -0.230\,\frac{E\,I}{l}$. The unbalanced shear is $0.231\,\frac{E\,I}{l}$. Correction for sidesway is made by Fig. 9(*b*) and the corrected moments with sidesway allowed are encircled in Fig. 9(*a*). From the relation between end rotations and end moments, $\theta_{BC} = \frac{1.090}{3} + \frac{0.273}{6} = 0.409$; and $\theta_{CB} = \frac{-1.090}{6} - \frac{0.273}{3} =$

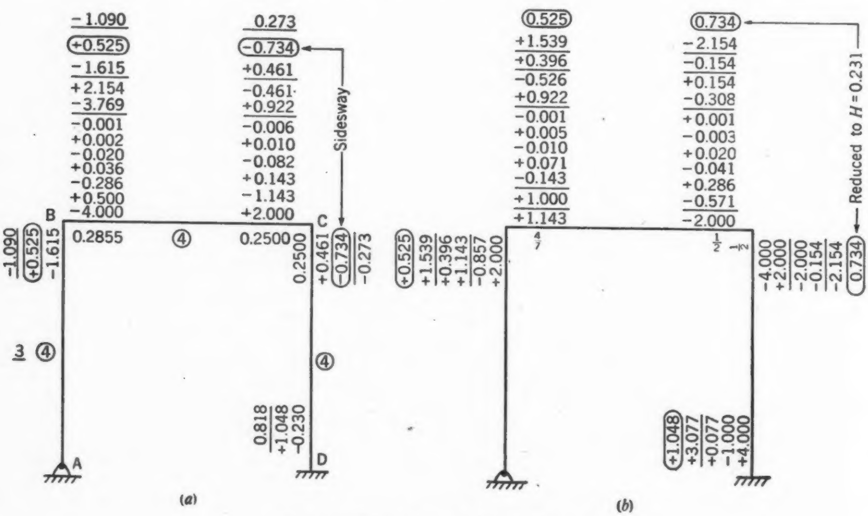

Fig. 9.—Symmetrical Rigid Frame

-0.273. Since $\theta_{BA} = \theta_{BC} - 1 = -0.591$, Eqs. 8 yield, for member AB:

$$M_{AB} = 0 = -2\left(2\,\theta_{AB} - 0.591 - \frac{3\,y}{l}\right) \ldots\ldots\ldots\ldots (22a)$$

and

$$M_{BA} = -1.090 = 2\left[\theta_{AB} - 2\,(0.591) - \frac{3\,y}{l}\right] \qquad (22b)$$

in which y is the displacement due to sidesway. Solving simultaneously, $\theta_{AB} = -0.046$ and $y = -2.277$. From Eq. 12*b* for member BC: k_{1m}

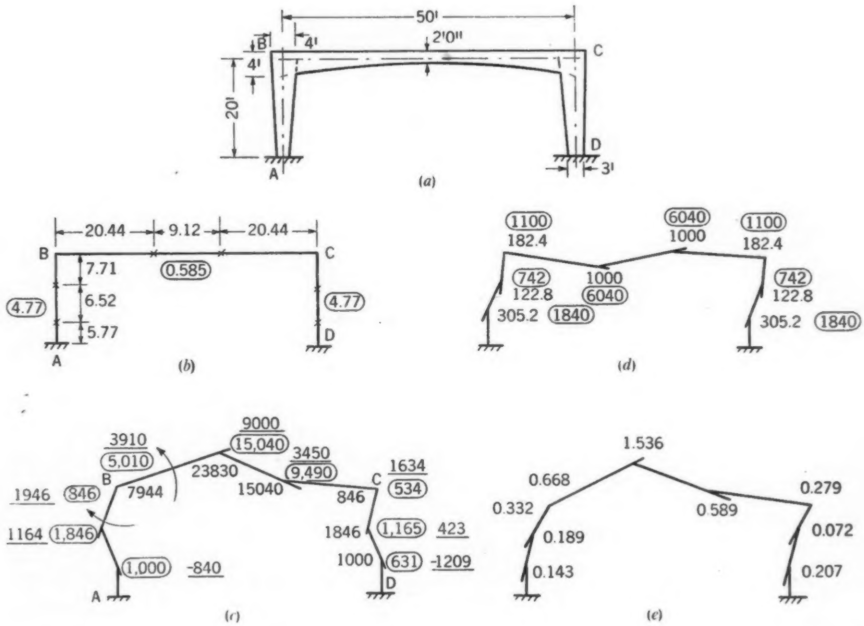

FIG. 10.—HAUNCHED RIGID FRAME

$= 0.456$ and, from Eq. 10, $y_m = 0.862$. From Eq. 14 for member AB: $Q = \frac{10}{2}(-2.277) + \frac{1}{12}10^2(-0.046 + 0.591) = 6.848$. Consequently, the moment at joint B due to a uniformly distributed horizontal load of 500 lb per ft on member AB is $M_B = 6.848 \times 500 = 3{,}424$ ft-lb.

Example 8. Haunched Rigid Frame.—Using the traverse method trace influence line for M_B for the frame of Fig. 10 due to vertical load on beam BC. What is the value of M_B for a uniform load of 1.5 kips per ft? Using this method, the traverse angle occurs at the center of gravity of the $\frac{M}{E\,I}$-diagram considering one end of the member to be loaded with a moment and the other end to be hinged. The distance to the center of gravity point is designated by $\bar{x}$. Solution procedures for these points and for the stiffnesses of members are demonstrated in Tables 5 and 6. In Table 5 a moment of $1{,}000\,\frac{E}{12}$ is applied

at joint B to member BC, Fig. 10. From this table, $\bar{x}_{BC} = \bar{x}_{CB} = \dfrac{\sum \frac{M}{E\,I}(\Delta x)(x_n)}{\sum \frac{M}{E\,I}(\Delta x)} = \dfrac{35{,}075.4}{1{,}711.18} = 20.44$ ft and the stiffness (the moment required to produce unit rotation in beam BC) is calculated by $\dfrac{1{,}000\,\frac{E}{12}}{1{,}711.18} = 0.585\,\dfrac{E}{12}\cdot$

From Table 6, $\bar{x}_{BA} = \dfrac{1{,}613.8}{209.8} = 7.71$ ft; $\bar{x}_{AB} = \dfrac{1{,}611.6}{279.6} = 5.77$; and

$$\text{Stiffness BA} = \frac{1{,}000\,\frac{E}{12}}{209.8} = 4.77\,\frac{E}{12}$$

$$\text{Stiffness AB} = \frac{1{,}000\,\frac{E}{12}}{279.6} = 3.58\,\frac{E}{12}$$

A rotation is imposed at joint B and the traverse, Fig. 10(*c*), is drawn ignoring sidesway. The traverse is started at point A and carried to point B, and independently at point D and carried to B. Since $M_{BA} = M_{BC}$, the right-hand side is correlated with the left-hand side by multiplying the right-hand side rotations by $\dfrac{15{,}040}{23{,}830}\cdot$ Corrected rotations are shown encircled.

The total unbalanced shear in the vertical members is $1{,}010\,\dfrac{E}{12}\cdot$ The solution procedure for an imposed horizontal force at joint B is demonstrated by Fig. 10(*d*). From symmetry, the traverse angles in beam BC are equal. Assuming them to be equal to 1,000 the traverse is completed as shown. The value of the horizontal force, Fig. 10(*d*) is $167.5\,\dfrac{E}{12}\cdot$ For a horizontal force corresponding to that of Fig. 10(*c*) the angles must be multiplied by $\dfrac{1{,}010}{167.5}\cdot$ Corrected angles are encircled in Fig. 10(*d*). These angles are then added algebraically to the corresponding angles of Fig. 10(*c*) to arrive at the correction

TABLE 5.—COMPUTATION OF PROPERTIES OF BEAM BC

Segment	x_n (ft)	d_x	d^3	$\frac{M}{E/12}$	$\frac{M}{E\,I}\Delta x$	$\frac{M}{E\,I}\Delta x\,x_n$
1......	1	3.84	56.7	980	34.56	34.6
2......	3	3.55	44.2	940	42.44	127.4
3......	5	3.28	35.1	900	51.24	256.2
4......	7	3.03	28.2	860	61.02	433.6
5......	9	2.82	22.3	820	73.50	663.0
6......	11	2.63	18.1	780	86.16	949.0
7......	13	2.46	14.8	740	99.90	1,297.0
8......	15	2.32	12.4	700	112.90	1,692.0
9......	17	2.20	10.6	660	124.50	2,116.0
10......	19	2.12	9.39	620	132.10	2,508.0
11......	21	2.05	8.59	580	135.10	2,838.0
12......	23	2.01	8.07	540	133.90	3,079.0
13......	25	2.00	8.00	500	125.00	3,125.0
14......	27	2.01	8.07	460	114.10	3,082.0
15......	29	2.05	8.59	420	96.80	2,808.0
16......	31	2.12	9.39	380	80.90	2,504.0
17......	33	2.20	10.6	340	64.10	2,016.0
18......	35	2.32	12.4	300	48.34	1,691.0
19......	37	2.46	14.8	260	35.12	1,301.0
20......	39	2.63	18.1	220	24.30	948.0
21......	41	2.82	22.3	180	16.14	662.0
22......	43	3.03	28.2	140	9.94	427.8
23......	45	3.28	35.1	100	5.70	254.6
24......	47	3.55	44.2	60	2.72	127.8
25......	49	3.84	56.7	20	0.70	34.4
Total...	..	....	....	....	1,711.18	35,075.4

due to sidesway. The resulting angles are shown underlined in Fig. 10(*c*). The value of the imposed rotation at joint B is 1,946 + 3,910 = 5,856. To reduce the rotation to unity it is necessary to multiply all the angles by $\frac{1}{5,856}$. These angles are shown in Fig. 10(*e*). Using Eq. 3*a* the elastic curve for beam

TABLE 6.—COMPUTATION OF PROPERTIES OF MEMBER AB

x_n (ft)	d_x	d^3_x	$\frac{M_B}{E/12}$	$\frac{M_B}{E\,I}\,\Delta x$	$\frac{M_B\,\Delta x}{E\,I}\,x_n$	$\frac{M_A}{E/12}$	$\frac{M_A}{E\,I}\,\Delta x$	$\frac{M_A\,\Delta x}{E\,I}\,(20-x_n)$
1.......	3.95	61.5	950	30.86	30.8	50	1.62	30.8
3.......	3.85	56.8	850	29.92	89.8	150	5.28	87.6
5.......	3.75	52.3	750	28.66	143.2	250	9.56	143.4
7.......	3.65	48.5	650	26.60	187.6	350	14.22	187.6
9.......	3.55	44.2	550	24.88	223.8	450	20.38	224.0
11.......	3.45	40.8	450	22.06	242.8	550	26.96	242.4
13.......	3.35	37.4	350	18.72	243.4	650	34.74	243.0
15.......	3.25	34.0	250	14.70	220.4	750	44.10	220.4
17.......	3.15	31.0	150	9.68	164.4	850	54.84	164.8
19.......	3.05	28.1	50	2.56	67.6	950	67.70	67.6
Σ.......	....	....	....	209.84	1,613.8	....	279.62	1,611.6

BC (influence line) is computed in Table 7. The area under the influence line is given by $\Sigma y_n\,\Delta x$ or 122.58 × 2 = 245.16 and the moment due to uniform load of 1.5 kips per ft is 367.74 kip-ft.

Example 9. Simply Supported Continuous Beam.—Using the indirect method and moment-distribution method draw influence lines for the continuous beam in Fig. 11. The analysis for the effect of undistributed moments of +100 at joint B and joint C is made in Fig. 11. (In this illustration the previous sign convention for moments has been temporarily discarded for convenience and moments acting clockwise on the joint are considered positive. For other computations involved in Example 9, the previous sign convention is used.)

For moment at support B a unit rotation is considered to be imposed at point B. Assuming this to be imposed on span AB alone the resulting fixed-end moment, M_{BA}, is $3\,E\,K$ and, since the stiffness, $E\,K$ is equal to 2, $M_{BA} = 3 \times 2 = 6$. Distributing this fixed-end moment in accordance with the distribution of Fig. 11 the moments are found to be $M_B = 4.120$, $M_C = -0.729$, and $M_D = 0.121$; and the end rotations are calculated as follows:

$$\theta_{AB} = -\frac{4.120}{6}\,\frac{1}{2} = -0.34$$

$$\theta_{BA} = +\frac{4.120}{3}\,\frac{1}{2} = +0.69$$

$$\theta_{BC} = -\frac{4.120}{3}\,\frac{1}{4} + \frac{0.729}{6}\,\frac{1}{4} = -0.31$$

$$\theta_{CB} = \theta_{CD} = \frac{4.120}{6}\,\frac{1}{4} - \frac{0.729}{3}\,\frac{1}{4} = +0.11$$

$$\theta_{DC} = \theta_{DE} = -\frac{0.121}{3}\,1 = -0.04$$

$$\theta_{ED} = +\frac{0.121}{6}\,1 = +0.02$$

For the reaction at support B a unit deflection is imposed at point B, Fig. 11. The corresponding fixed-end moments must be applied:

$$M_{BA} = \frac{3\,E\,K}{l} = +\,\frac{3 \times 2}{30} = +\,0.200$$

$$M_{BC} = \frac{6\,E\,K}{l} = +\,\frac{6 \times 4}{30} = +\,0.800$$

$$M_{CB} = \frac{6\,E\,K}{l} = -\,\frac{6 \times 4}{30} = -\,0.800$$

Using the distribution of Fig. 11 the resulting moments are computed to be

TABLE 7.—COMPUTATION OF DEFLECTION CURVE

x_n (ft)	$\dfrac{M_B\left(1-\frac{x_n}{50}\right)}{E/12}$	$\dfrac{M_c\left(1-\frac{x_n}{50}\right)}{E/12}$	$\dfrac{M_n}{E/12}$	$\dfrac{M_n\,\Delta x}{E\,I}$	θ_n	$\dfrac{\Delta x_{n-1}+x_n}{2}$	Δy	y_n
0.......	−0.899	0	−0.899	....	0.668	....	....	0.000
1.......	−0.881	0.007	−0.874	−0.031	0.637	1	0.668	0.668
3.......	−0.845	0.020	−0.825	−0.037	0.600	2	1.274	1.942
5.......	−0.809	0.304	−0.775	−0.044	0.556	2	1.200	3.142
7.......	−0.733	0.049	−0.724	−0.052	0.504	2	1.112	4.254
9.......	−0.737	0.062	−0.675	−0.060	0.444	2	1.008	5.262
11.......	−0.701	0.076	−0.625	−0.069	0.375	2	0.888	6.150
13.......	−0.665	0.089	−0.576	−0.078	0.297	2	0.750	6.900
15.......	−0.630	0.104	−0.526	−0.085	0.212	2	0.594	7.494
17.......	−0.594	0.117	−0.477	−0.090	0.122	2	0.424	7.918
19.......	−0.554	0.131	−0.426	−0.091	0.031	2	0.244	8.162
21.......	−0.521	0.145	−0.376	−0.089	−0.058	2	0.062	8.224
23.......	−0.486	0.159	−0.327	−0.081	−0.138	2	−0.116	8.108
25.......	−0.450	0.172	−0.278	−0.069	−0.208	2	−0.278	7.830
27.......	−0.414	0.186	−0.228	−0.057	−0.265	2	−0.416	7.414
29.......	−0.378	0.200	−0.178	−0.040	−0.305	2	−0.530	6.884
31.......	−0.342	0.213	−0.128	−0.027	−0.332	2	−0.610	6.274
33.......	−0.306	0.227	−0.078	−0.015	−0.347	2	−0.664	5.610
35.......	−0.270	0.241	−0.029	−0.006	−0.353	2	−0.694	4.916
37.......	−0.234	0.255	0.021	0.002	−0.351	2	−0.706	4.210
39.......	−0.198	0.268	0.070	0.008	−0.343	2	−0.702	3.508
41.......	−0.162	0.282	0.121	0.011	−0.332	2	−0.686	2.822
43.......	−0.126	0.296	0.170	0.012	−0.320	2	−0.664	2.158
45.......	−0.090	0.310	0.221	0.012	−0.308	2	−0.640	1.518
47.......	−0.054	0.324	0.270	0.013	−0.295	2	−0.616	0.902
49.......	−0.018	0.338	0.320	0.011	−0.284	2	−0.590	0.312
50.......	0	0.345	0.345	....	....	1	−0.284	0.000

$M_B = +\,0.298$, $M_C = -\,0.194$, and $M_D = 0.032$; and the corresponding rotations, remembering that $\delta_B = -\,1$, are:

$$\theta_{AB} = -\,\frac{1}{30} - \frac{1}{6} \times 0.298 \times \frac{1}{2} = -\,0.0583$$

$$\theta_{BA} = \theta_{BC} = -\,\frac{1}{30} + \frac{1}{3} \times 0.298 \times \frac{1}{2} = +\,0.0164$$

$$\theta_{CB} = \theta_{CD} = +\,\frac{1}{3} \times 0.194 \times \frac{1}{2} - \frac{1}{6} \times 0.032 \times \frac{1}{2} = +\,0.0296$$

$$\theta_{DC} = \theta_{DE} = -\,\frac{1}{3} \times 0.032 = -\,0.0107$$

$$\theta_{ED} = +\,\frac{1}{6} \times 0.032 = +\,0.0053$$

CONCLUSIONS

Influence lines may be computed exactly as the elastic curve due to a unit displacement corresponding to the "action" being studied and placed at the section under consideration. The computation of such an influence line in-

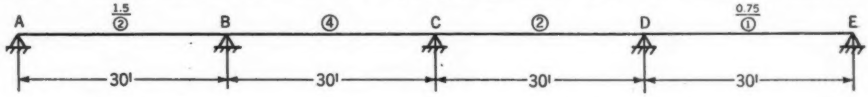

+100					
-27.25	-72.75	-36.38			
	+12.13	+24.26	+12.13	+6.06	
-3.31	-8.82	-4.41	-2.21	-4.41	-1.65
	+2.20	+4.41	+2.21	+1.10	
-0.60	-1.60	-0.80	-0.40	-0.80	-0.30
	+0.40	+0.80	+0.40	+0.20	
-0.11	-0.29	-0.14	-0.07	-0.15	-0.05
	+0.07	+0.14	+0.07	+0.03	
-0.02	-0.05	-0.02	-0.01	-0.02	-0.01
	+0.01	+0.02	+0.01		
-31.29	-68.70	-12.13	+12.13	+2.01	-2.01
		+100			
	-33.33	-66.67	-33.33	-16.67	
+9.07	+24.26	+12.13	+6.07	+12.13	+4.53
	-6.07	-12.13	-6.07	-3.03	
+1.67	+4.40	+2.20	+1.10	+2.20	+0.83
	+1.10	-2.20	-1.10	-0.55	
+0.30	+0.80	+0.40	+0.20	+0.40	+0.15
	-0.20	-0.40	-0.20	-0.10	
+0.05	+0.15	+0.07	+0.03	+0.07	+0.03
	-0.03	-0.07	-0.03	-0.01	
+0.01	+0.02				
+11.10	-11.10	-66.67	-33.33	-5.55	+5.55

FIG. 11.—SIMPLY SUPPORTED CONTINUOUS BEAM

volves (1) a statical analysis of the structure bearing only the displacement and (2) computation of as many points on the elastic curve as may be necessary. This is somewhat more work than a single statical analysis of the structure bearing a conventional load although the additional labor of calculating deflections is offset somewhat by the fact that the statical analysis is generally simplified since it involves only the unloaded structure. The statical analysis may be made using whatever method the designer prefers. It may be made indirectly by first distributing an unbalanced moment at each of the joints and then summing up proportionately a set of fixed-end moments corresponding to the required deflection. The elastic curve is calculated by geometry, or by equations or methods based on geometry. (Methods of analysis, as such, do not come within the scope of discussion.)

In many cases complete elastic curves are unnecessary. For prismatic members the location of the load for maximum effect, and the amount of the effect, are given by Eqs. 12. For uniform load on prismatic members the area under the influence line is given by Eq. 14.

A M

I

con
sen
slid
gat

cas
giv
lini
aux
tab
not
If
ma
of
in

on
co
te
th
en
of
we
cu

cu

AMERICAN SOCIETY OF CIVIL ENGINEERS

Founded November 5, 1852

PAPERS

ESTIMATING DATA FOR RESERVOIR GATES

BY FRANK L. BOISSONNAULT,[1] ESQ.

SYNOPSIS

Charts for the determination of weight and cost data on some of the most common forms of water control gates used in conjunction with dams are presented in this paper. The types included are: High-pressure hydraulic operated slide gates, radial crest gates, roller crest gates, drum crest gates, and Broome gates.

There are some published data on weights and costs of gates, but in most cases the exact items included are not known. Where tables of weights are given (in other publications), some gates may include much more conduit lining than others of the same type. Also, some may include considerable auxiliary equipment such as valves and piping, whereas others in the same table do not. In the case of radial gates, sometimes it is not clear whether or not the hoist or even the anchorages and other stationary parts are included. If adequate information is not given, no data are available for easily approximating the necessary addition for a complete estimate. Therefore, the utility of such data is limited, and it is believed that charts, such as those presented in this paper, fill a definite need.

INTRODUCTION

The charts in this paper were developed to assemble accurate information on weights and costs of existing gates in convenient graphic form so that they could be compared easily and so that the weight of any gate could be interpolated quickly from the nominal gate dimensions and maximum head on the gate center. The intent is to present all the pertinent data required to enable the engineer to use his own judgment in making an intelligent estimate of weight to fit the individual case, without the necessity of tedious research work each time an estimate is required. To accomplish these objectives with curves, in each chart an expression (involving only the nominal gate dimensions

NOTE.—Written comments are invited for immediate publication; to insure publication the last discussion should be submitted by **February 1, 1948.**

[1] Engr., U. S. Engr. Office, Los Angeles, Calif.

and maximum head as variables) is developed, some power of which will be as nearly as possible proportional to the weight of the gate. The weights and the costs (in some cases), were then plotted as ordinates against this expression as abscissas. Where the evaluation of the expression involves more than a simple slide rule operation, other curves are given to assist in the evaluation of this function.[1a] The dimensions are in feet in all cases.

The various dams mentioned in the text or noted in illustrations are further summarized and identified, as follows:

Dam	Location
Structures of the Bureau of Reclamation—	
Alamogordo	New Mexico
Alcova Tunnel	Wyoming
American Falls	Idaho
Black Canyon	Idaho
Boulder	Colorado River, Nevada
Caballo	New Mexico
Deadwood	Idaho
Easton	Yakima Project, Washington
Friant	Central California
Grand Coulee	Central Washington
Grassy Lake	Wyoming
Guernsey	Wyoming
Island Park	Idaho
Jackson Gulch	....
Madden	Panama Canal Zone
McKay	Northeastern Oregon
Norris	Tennessee
Owyhee	Oregon
Salinas	Southern California
Shoshone	Wyoming
Stony Gorge	Central California
Taylor Park	Colorado
Tieton	Yakima Project, Washington
Structures of the United States Engineer Department—	
Beach City	Ohio
Brea	Southern California
Caddoa	Arkansas River, Colorado
Conchas	New Mexico
Dover	Ohio
Fullerton	Southern California
Hansen	Southern California
Kanawha No. 1	West Virginia
Lytle Creek	Southern California

[1a] In this paper, presented expressly for purposes of discussion, the charts are necessarily condensed and can generally be used for broad illustrative purposes only. Those who have a practical need for full-scale charts of the figures in the paper, or for other charts not included, can secure photostats by addressing the author directly.—Ed.

Dam	Location
Structures of the United States Engineer Department (*Continued*)—	
Mississippi dams 5A, 9, 10, 11, 13, 14, 16, 18, 21, 22, 24, 25, and 26	Upper Mississippi River
Prado	Southern California
Santa Fe	Southern California
Sepulveda	Southern California
Wills Creek	Ohio
Wolf Creek	Cumberland River, Kentucky
Structures of the Appalachian Electric Power Company—	
Claytor Development	Radford, Va.
Structures of the Southern California Edison Company—	
Florence Lake	Southern California
Structures of the City of Pasadena—	
Morris	Southern California

MAJOR PARTS OF HIGH-PRESSURE SLIDE GATE SHOWN IN FIG. 1

Gate:
- Upstream frame.... 1
- Downstream frame.. 2
- Bonnet........... 3
- Leaf.............. 5
- Seats......6, 7, 8, 9, 10, 11
- Stuffing glands......31, 42
- Bonnet cover....... 4

Hoist:
- Cylinder Piston—
  - Stem extension. 19, 25, 41
  - Stem and stem nuts.......... 22, 23
  - Upper cylinder head.......... 20

Conduit:
- Lining........(not shown)
- Lining transition.... ....(not shown)

DESIGN DATA

Maximum Designed Head, for Gate Leafs, in Feet:
- Cast iron.......... 90
- Semisteel.......... 140
- Cast steel.......... 250

Pressure in Cylinder, in Pounds Per Square Inch:
- Working pressure... 750
- Designed pressure... 1,000

Coefficient of Friction at Starting:
- Bronze gate seat.... 0.6

The concrete surrounding conduit and bonnet castings are designed to carry all the load.

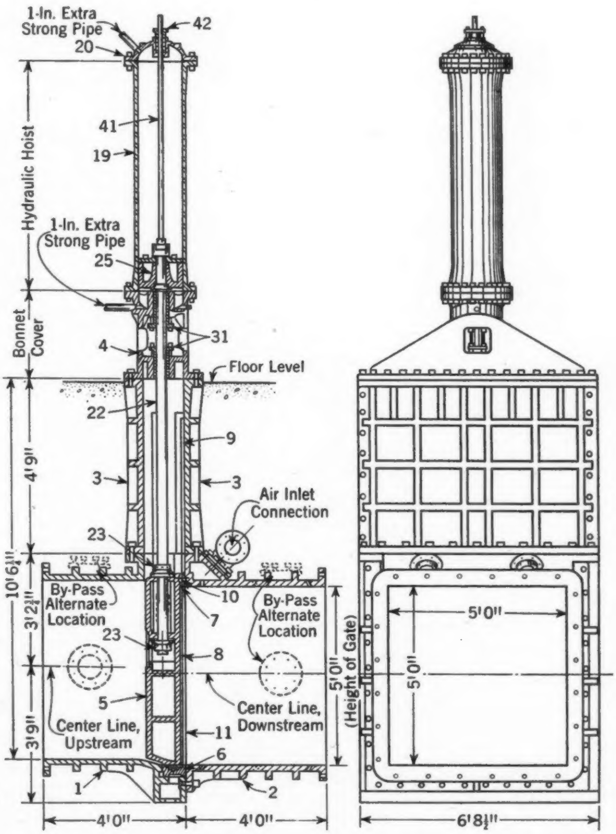

FIG. 1.—ASSEMBLY DRAWING OF A STANDARD HIGH-PRESSURE SLIDE GATE (5 FT BY 6 FT) AS BUILT BY THE BUREAU OF RECLAMATION (SEE ALSO TABLES 1 AND 2)

High-Pressure Slide Gates

Fig. 1 shows an assembly drawing of a typical high-pressure slide gate, so called because, in moving, the leaf slides on its sealing strips. The hoist is a hydraulic cylinder and the greatest part of its capacity is required for over-

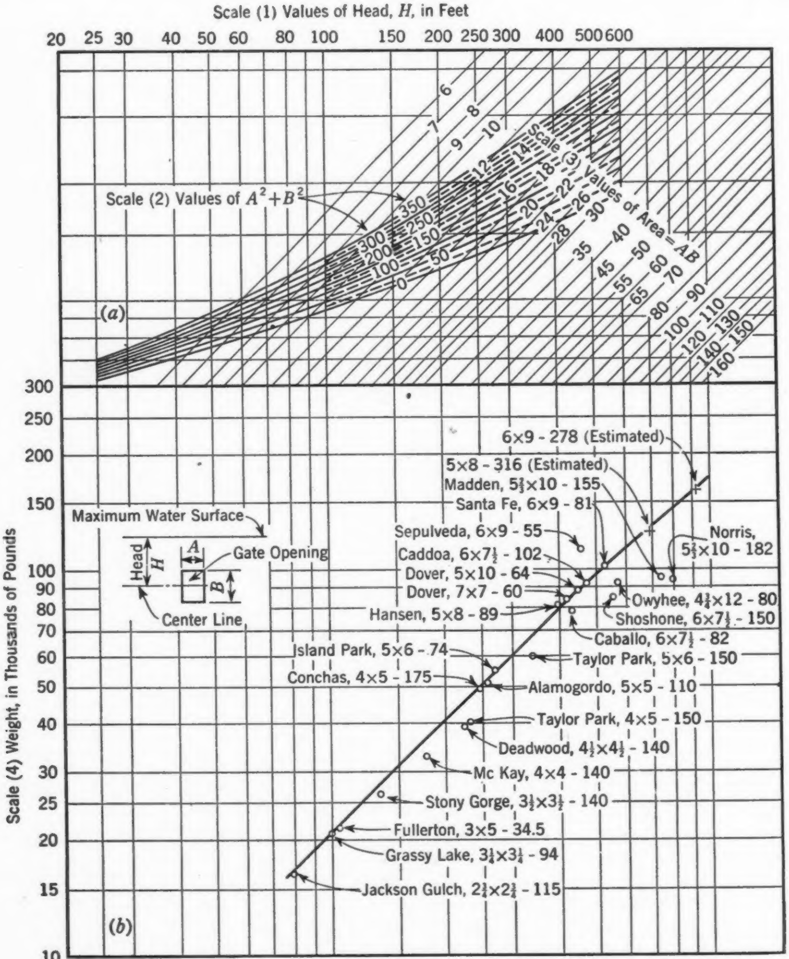

Fig. 2.—Weight of High-Pressure Slide Gates with Hydraulic Hoists

coming the seal friction created by the static pressure of the water against the upstream face of the leaf. The cast-iron conduit lining (not shown) is bolted to the flange on the body or "frame" of the gate and the entire assembly, including the bonnet, is embedded in the masonry structure up to the bonnet cover, which, with the hoist, projects into the gate chamber as shown.

The weight curve of Fig. 2 is plotted with the weight of the gate as ordinates and the expression—

$$F(W) = \frac{\text{(area)}}{10^5} (A^2 H + B^2 H + 6{,}420 \sqrt{H} + 30{,}000) \ldots\ldots\ldots (1)$$

—as abscissas. In Eq. 1, $F(W)$ is a function of the weight W; "(area)" is equal to $A\ B$ is equal to area of gate; A is the nominal breadth or width of gate; B is the nominal height of gate; and H is the maximum head to the gate center line. All dimensions are in feet. Eq. 1 is empirical, but it gives values that are practically proportional to the weights of gates with cast-iron leaves, as designed to United States Engineer Department (USED) standards for the particular application. The value of the abscissa $F(W)$ may be computed or it may be found graphically from the curves in Fig. 2(*a*). To solve graphically, compute values of $(A^2 + B^2)$ and $(A\ B)$. Enter Fig. 2(*a*) at maximum head H (scale (1)), and move vertically down to the curve for $A^2 + B^2$ (scale (2)). From this intersection, move horizontally to the value of $A\ B$ on the diagonal lines (scale (3)). The intersection gives the value of the abscissa for that particular gate. Hence, by moving vertically down on this abscissa value to the intersection with the weight curve (Fig. 2(*b*)), the corresponding weight ordinate is determined in scale (4).

To compare the weights of gates, it is necessary that the comparison be made on the same basis. In Fig. 2 the weights of all gates have been carefully checked and adjusted to include the leaf, frame, bonnet, bonnet cover, hydraulic hoist, and a 5-ft length of cast-iron conduit lining. No hanger, piping, or valves are included.

The curve in Fig. 2(*b*) is drawn through the average of points representing the weights of a range of sizes of gates designed by the USED offices for flood control projects. The notation "Conchas—4 × 5—175" denotes that the gates at Conchas Dam are 4 ft by 5 ft operating at a maximum head of 175 ft. All the gates, with the exception of the Conchas gates, have cast-iron leaves. The Conchas gate leaves are cast steel, but the weight shown has been adjusted to what it would be with a cast-iron leaf. The weight of the Fullerton gates (see Fig. 2(*b*)) was adjusted to the hydraulic type. The curve in Fig. 2(*b*) was produced through two estimated points with cast-iron leaves which are beyond the range of any gates that have been actually designed by the USED.

This curve, then, gives the weights of gates with cast-iron leaves designed by USED. Cast-iron leaves are used for heads to about 100 ft. For higher heads, cast-steel leaves would be used and the gates would be somewhat lighter. However, the unit cost of the steel casting is considerably more than that of cast iron, so that the over-all cost of the gate would be approximately the same as that for the cast-iron leaf gate shown. Therefore, Fig. 2(*b*) gives the weights, for cost purposes, of gates designed to USED specifications, although for heads greater than 100 ft, where the leaf is cast steel, the actual weight will be from 2% to 3% less.

The USED gates shown in Fig. 2 are those for Fullerton, Conchas, Hansen, Dover, Caddoa, Sepulveda, and Santa Fe dams. They were designed for each

job, on the basis of a coefficient of sliding friction of 1.00 as set up by the Office of the Chief of Engineers for flood control gates. This coefficient is probably higher than actually exists but, no doubt, was felt to be justified for flood control gates which may not operate under head for years, thus accumulating much corrosion on the sliding surfaces. However, when at last needed during a flood, they must not fail. The normal working pressure in the hoist cylinder is 750 lb per sq in. with a maximum of 1,000 lb per sq in. by the setting of a relief valve.

All other gates shown are designs of the Bureau of Reclamation (USBR). All except Madden, Norris, and Owyhee dams are part of a more or less standard line of slide gates, each size of which is used over the entire range of heads by changing the material in the leaf and applying the proper one of several sizes of hoist cylinders designed to fit mechanically. For heads to 90 ft, cast-iron leaves are used; for heads from 90 ft to 140 ft, semisteel leaves are substituted; and, for heads from 140 ft to 250 ft, cast steel is standard.

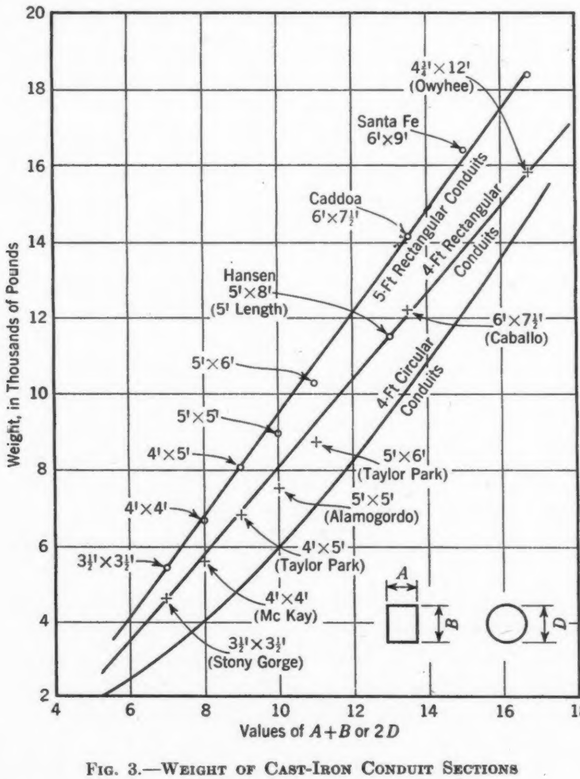

FIG. 3.—WEIGHT OF CAST-IRON CONDUIT SECTIONS

These standard gates are not closely designed for actual heads, therefore; and, when the actual head is used in plotting, they could not be expected to follow a smooth curve as well as if each was designed for an individual condition. Nevertheless, these USBR gates are generally lighter than the flood

control gates because the USBR uses a coefficient of sliding friction of 0.60—requiring a hoist and stem only 60% of the capacity of the USED hoists for the same standard working pressure of 750 lb per sq in. In addition, most of the USBR gates shown, have cast steel or semisteel leaves which still further reduce the weight in comparison to the flood control gates. However, the trend of weights in the standard line is roughly proportional to the function $F(W)$ as defined by Eq. 1, with an exponent slightly less than 1.00. On the other hand, the Norris and Madden gates are considerably lighter than would be expected from the trend of the other USBR dams. This deviation is explainable by the fact that the gates were of special size and shape and were specially designed so that the weights are very nearly the most economical for the particular conditions. Also, the normal working pressure on the hoists of these gates is increased to 1,000 lb per sq in., whereas the maximum pressure available for "cracking" the standing friction is at least 50% greater than that of the flood

TABLE 1.—UNIT COST OF SLIDE GATES, IN CENTS PER POUND

Dam	Location	Year	Number of gates	Size (ft)	Cost bid (¢ per lb)
Hansen	Los Angeles, Calif.	1939	8	5 by 8	14.3
Sepulveda	Los Angeles, Calif.	1940	4	6 by 9	13.4
Stony Gorge	Orleans, Calif.	1926	2	3.5 by 3.5	14
Conchas	New Mexico[a]	1936	12	4 by 5	17.55[b]
Conchas	New Mexico[a]	1939	4	6 by 7.5	12.2[c]
Deadwood	Idaho	1929	2	4.5 by 4.5	15
Alamogordo	New Mexico	1936	2	5 by 5	10
Grand Coulee	Los Angeles, Calif.	1939	..	8.5[d]	15.1
Santa Fe	Los Angeles, Calif.	1946	16	6 by 9	27.25
Bull Shoals	Arkansas	1946	32	5 by 9	31.4[e]

[a] The gates for Conchas Dam were built in Los Angeles. [b] After adjusting this unit cost to west coast delivery, the cost is 16.25¢. [c] This price was too low and should not be considered as a legitimate bid. [d] Ring seal gate, 102 in. in diameter; unit cost is F.O.B. the shop at Los Angeles. [e] After adjusting this unit cost to west coast delivery, the cost is 29¢.

control gates, thereby allowing a further saving in the weight of the hoist for this reason.

Conduit Lining.—It is anticipated that varying lengths of conduit lining will be required in some cases. Fig. 3 has been developed so that the weight of extra conduit lining can be found. This chart gives weights of 4-ft and 5-ft lengths of rectangular sections and also of 4-ft lengths of circular sections of cast-iron conduit lining. It should be understood that the unit cost used with extra conduit should be lower than the unit cost for the gate. Equations for the weights of conduit sections, in pounds (that is, the equations of the curves in Fig. 3), are: For the 4-ft length of rectangular conduit—

$$W = 1{,}151\,(A + B) - 3{,}445 \qquad (2a)$$

for the 5-ft length of rectangular conduit—

$$W = 1{,}338\,(A + B) - 3{,}943 \qquad (2b)$$

and, for the 4-ft length of circular conduit—

$$W = 370\,D^{1.731} \qquad (2c)$$

Costs.—The approximate shop cost of the gate can be estimated by multiplying the weight by a suitable unit cost for cast iron, machined and fabricated complete. This unit cost will vary with the general economic situation and with conditions in the particular shop. Some idea of the unit costs at which gates of this type have been sold or offered in the past is given in Table 1. The unit cost will also vary with the number of duplicate units involved. Table 2 gives an approximate idea of how the unit cost is thus affected. The table arbitrarily assumes 100% unit cost for the case of ten gates and shows the percentage unit costs for other gates. The data are based on a study of the fixed costs of eleven different jobs as bid by a large manufacturer in the Los Angeles (Calif.) area. This study showed a considerable range between the highest and lowest percentage of fixed costs to total costs when adjusted to a comparable number of gates. The table is arranged to show the effect of this range of variation from the average. In choosing the unit cost factor for a given number of gates, the following general principles should be used as a guide. The fixed costs tend to be higher than average if:

(*a*) The gates are small in size;

(*b*) The costs are quoted when pattern costs are relatively high compared to other costs, as in 1946 postwar conditions; and

(*c*) A large number of gates are involved.

TABLE 2.—VARIATION OF PERCENTAGE UNIT COST OF SLIDE GATES FOR DIFFERENT NUMBERS OF GATES IN CONTRACT

Number of gates involved	RELATIVE FIXED CHARGES IN THE STUDY		
	Lowest	Average	Highest
(1)	(2)	(3)	(4)
1	114	127	134
2	106.3	112	117
3	103.8	106.8	109.7
4	102.5	104.4	106.4
5	101.6	102.9	104.2
6	101	102	102.8
7	100.6	101.3	101.9
8	100.35	100.7	101.1
9	100.1	100.3	100.5
10	100	100	100
11	99.8	99.7	99.6
12	99.7	99.5	99.25
13	99.6	99.3	98.95
14	99.5	99.2	98.7
15	99.4	99	98.5
16	99.4	98.9	98.3
17	99.35	98.8	98.15
18	97.3	98.7	98
19	99.25	98.6	97.8
20	99.2	98.5	97.75
21	99.2	98.45	97.65
22	99.15	98.4	97.6
23	99.1	98.3	97.5
24	99.05	98.25	97.45
25	99.03	98.2	97.4
26	99	98.15	97.35
27	99	98.1	97.3
28	98.95	98.1	97.2
29	98.95	98.05	97.2
30	88.9	98.05	97.15

To obtain the installed cost, transportation cost to the site and erection cost must be added. Erection cost will vary with the location conditions. For average conditions before World War II it was between 3¢ and 4¢ per lb.

RADIAL CREST GATES

The radial or Tainter gate is quite often the most economical type of spillway gate, where it can be used. The length of Tainter gates is usually limited to from 50 ft or 60 ft by the expansion joint spacing in the dam, although gates 80 ft long are in operation at dam No. 24 on the Upper Mississippi project. A service bridge with sufficient headroom is required for the hoisting equipment. Fig. 4, with Tables 3 and 4, gives the weights (including the moving and stationary parts) of a number of radial gates plotted as ordinates against the

function:

$$F(W) = \frac{A^2 B H}{10^3} \qquad (3)$$

These weights do not include the hoist and chains. All gates are noncounterweighted for electric hoists except as noted.

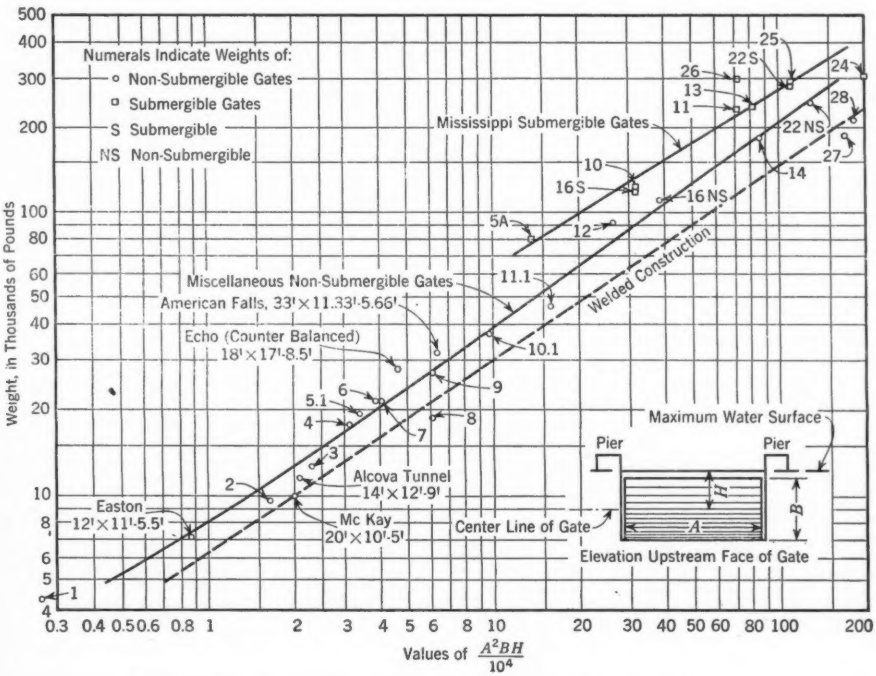

Fig. 4.—Weights of Radial Gates, Moving and Stationary Parts, Excluding Hoists and Chains

TABLE 3.—Unit Cost of Radial Gates, in Dollars Per Hundredweight, 1939 Data (Pacific Coast Delivery[a])

Gates[a]	Complete[b] Without Hoist and Chains		Complete[b] With Hoist and Chains	
	Range	Average	Range	Average
Mississippi gates[c]	\$ 8.70 to \$13.78	\$11.80	\$13.05 to \$17.55	\$13.65
Smaller gates	\$11.00 to \$16.37	\$13.40	\$11.60 to \$21.10[d]	\$16.12

[a] The unit costs in this table are for gates of the conventional riveted construction. The unit costs for welded construction are probably slightly higher. [b] The weights include all moving and stationary parts, with exceptions noted. [c] The freight allowance, on Mississippi gates, from the Mississippi River to the Pacific coast, is \$0.75 per hundredweight. [d] Higher figure due in part to high installation cost.

The information on the Mississippi gates was taken from the contract drawings and specifications and tabulated data made up by the designing offices of the USED. The first twelve items of Table 4 were taken from the

work of W. P. Creager and Joel D. Justin,[2] Members, ASCE. Other data were obtained from USBR Specifications 400 to 1,200 and from other publications of USBR.[3,4]

TABLE 4.—IDENTITY, DIMENSIONS, AND UNIT COSTS (DOLLARS PER HUNDREDWEIGHT, WITH HOIST) OF RADIAL GATES AT THE DAMS REPRESENTED BY THE PLOTTED POINTS IN FIG. 1

Point No. (Fig. 1)	Dam[a]	Dimensions (Feet)			Year	1939 unit cost
		A	*B*	*H*		
1	....[b]	6	12	6	....	....
8	....[b]	13	13	27.5	....	....
2	....[b]	15	12.2	6.1	....	....
7	....[b]	16	9.5	16.7	....	....
3	....[b]	18	12	6	....	....
5.1	....[b]	20	13.1	6.5	....	....
4	....[b]	25	10	5	....	....
9	....[b]	25	14	7	....	....
10.1	....[b]	25	14	11.3	....	....
6	....[b]	35	8	4	....	....
11.1	....[b]	20	20	20	....	....
12	....[b]	50	14.7	7.3	....	....
5A	5A	35	15	7.5	1935	14.08
16NS	16[a]	40	22	11	1934	12.09
16S	16	40	20	10	1934	....
10	10[c]	40	20	10	1935	12.59
14	14[a,c]	60	22	11	1937	12.3
11	11[c]	60	20	10	1935	13.3
26	26[c,d]	40	30	15	1935	13.65
22NS	22[a,c]	60	27	13.5	1936	16.75
22S	22[c]	60	25	12.5	1936	15.97
25	25[c]	60	25	12.5	1937	14.87
13	13[c]	64	20	10	1937	12.44
28	Caddoa[d,e]	64	30	15	1940	15.7
24	24[c,d]	80	25	12.5	1938	14
27	Wolf Creek[e]	50	37	18.5	1939	16.9

[a] All gates were submergible except 16NS, 14, and 22NS, which are nonsubmergible. [b] These data are from "Hydro-electric Handbook," by W. P. Creager and Joel D. Justin, John Wiley & Sons, Inc., New York, N. Y., 1927, p. 317. Identity of dams and other comparable information were not given. [c] Upper Mississippi River navigation dams. [d] Alloy steel. [e] Welded.

The Mississippi gates are designed for navigation control. For this reason, many of them are submergible—that is, they are arranged for lowering to allow ice and debris to go over the top. Consequently, the submergible gates are heavier than spillway gates, and are shown in a separate curve in Fig. 4.

Except at Caddoa and Wolf Creek dams, all the gates in Fig. 4 are of conventional riveted construction. In the most recent designs, substantial savings have been made in both weight and cost by the use of welded construction. The Caddoa and Wolf Creek gates are of this type. A chart prepared by A. E. Niederhoff,[5] Assoc. M. ASCE, gives the weights of radial gates representative of this type of construction. The dashed weight curve, designated "Welded Construction" in Fig. 4, is plotted to give weights in line with Mr. Niederhoff's chart. Not many gates of welded construction have been built, but the calculated weights of recent designs seem to show fairly close agreement with the "Welded Construction" curve (see Fig. 4). It is possible that better methods of analysis may effect further savings in the weights of this type of gate.

Cost.—The cost of the gate structure can be obtained by taking the weight from the appropriate weight curve and applying a suitable unit cost, estimated from the unit cost data given in Tables 3 and 4—with due regard for the type of construction to be used, location of the installation, and factors peculiar to that particular installation

[2] "Hydro-electric Handbook," by W. P. Creager and Joel D. Justin, John Wiley & Sons, Inc., New York, N. Y., 1927, p. 317.

[3] "Dams and Control Works," Bureau of Reclamation, U. S. Dept. of the Interior, Denver, Colo., 1st Ed., 1929.

[4] "Dams and Control Works," Bureau of Reclamation, U. S. Dept. of the Interior, Denver, Colo., 1938.

[5] "Selection of Tainter Gates," by A. E. Niederhoff, *Western Construction News*, December, 1943, p. 555.

that would affect shop costs or erection costs, or both. The cost of the hoist must be added to obtain the total cost of the gate.

The weight and cost of the hoist can be obtained from the chart in Fig. 5. Since the weight and cost of hoists are plotted against the hoist capacity, it is

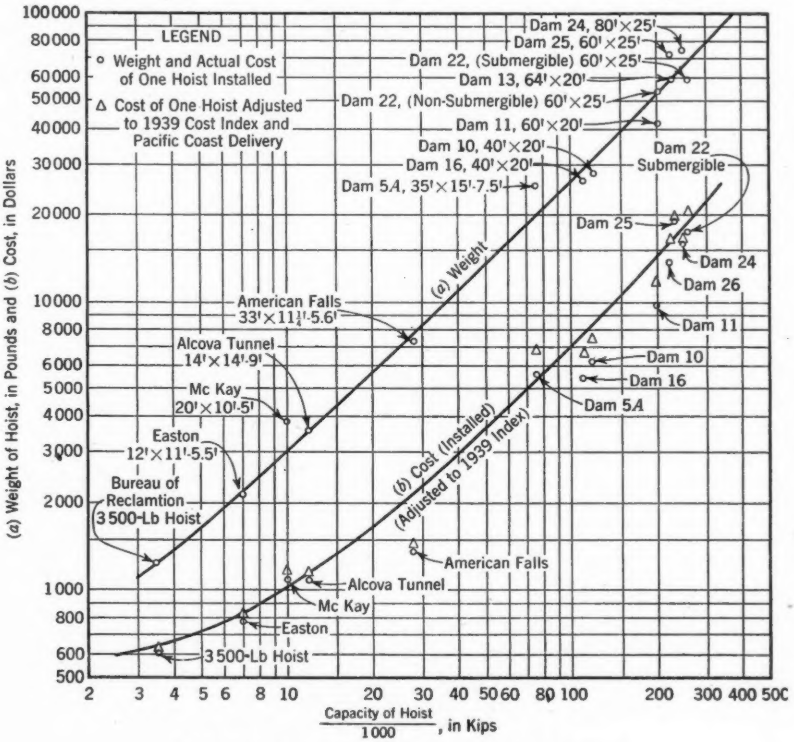

Fig. 5.—Weight and Cost of Radial Gate Hoists

first necessary to estimate the maximum hoist pull required. The hoist pull on the Mississippi gates varies considerably because of differences in ice and silt loading. The weight of the moving part of the leaf on these riveted gates averages about 77% of the total weight, whereas for welded construction the leaf may be nearer to 70% of the total weight as given in Fig. 4. To obtain a rough estimate of the required hoist capacity, it will be on the safe side to take the chain pull due to dead load of leaf, chain, and friction at the point of maximum pull as about equal to the weight of the leaf. To this estimate must be added the ice and silt loading allowed for the particular application. On the Upper Mississippi gates this allowance varies from 30% to 45% of the dead load. In many localities no allowance for ice load is required. The unit cost of the hoist may be taken from the auxiliary curve in Fig. 6.

Roller Gates

The roller gate (sometimes called rolling gate) consists of a steel cylinder with a large pinion at each end, which engages racks built into each abutting

pier, and the gate is raised by rolling up these inclined racks. Because of the high section modulus per unit weight, inherent in a cylinder, the roller gate can be built for long spans, thus making a saving in the number of piers required. Also, for the same reason, it is practicable to hoist the gate from one

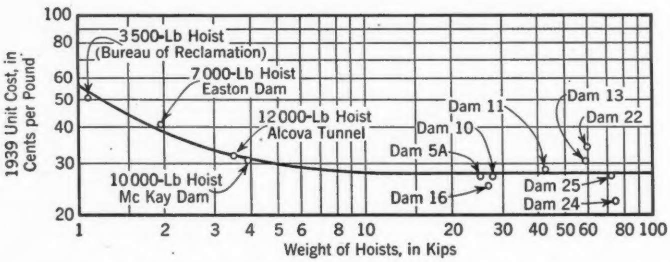

FIG. 6.—AUXILIARY CURVE SHOWING 1939 UNIT COSTS

end only. The piers and pier foundations, however, must be larger than those required for radial gates with shorter spans.

Although not many roller spillway gates are used, in a complete economic study on a project where a long spillway or wide channel is involved, it is usually

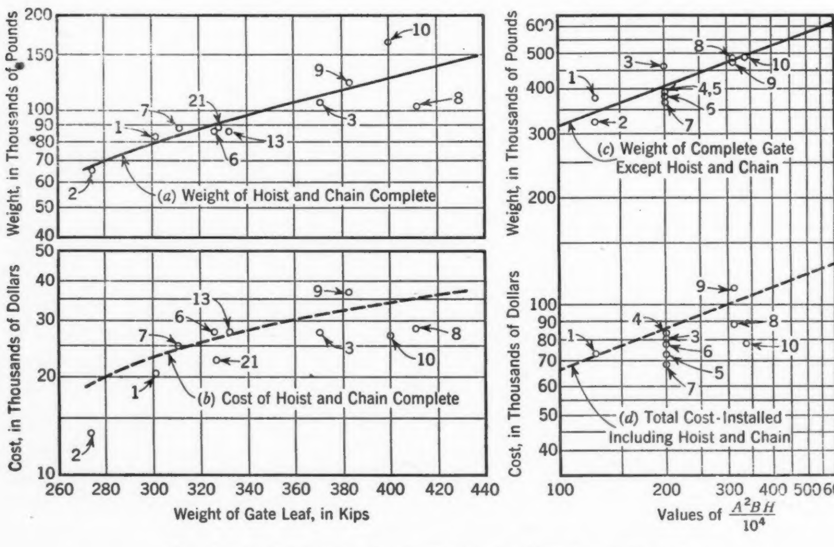

FIG. 7.—WEIGHTS AND COSTS OF ROLLER GATES AND HOISTS

necessary or desirable to consider this type of gate against a greater number of radial or other types of gate with much shorter spans. For this reason it is desirable to include weight and cost curves on the roller gate in this paper, although applications (and also available data) are somewhat limited.

Fig. 7 shows the weights and cost of roller gates and roller gate hoists. The weight and cost of the gates are plotted against the function $F(W)$ as de-

fined by Eq. 3. The identity of the plotted points in Fig. 7, including dimensions (in feet) and other data, are given in Table 5.

Except for one dam on the Kanawha River (point No. 10, Table 5) these gates are all on navigation dams on the Upper Mississippi River. They include the majority of gates of this type installed in the United States, with the exception of a number of similar gates on the Ohio River. Since only very large roller gates are built and the range of sizes is limited, it is difficult to draw trend curves. The "weight of gate" curve (Fig. 7(*c*)) does not include the hoist, whereas the cost curve (Fig. 7(*d*)) is for the gate and hoist complete. The plotted points show the actual cost.

TABLE 5.—IDENTITY OF PLOTTED POINTS IN FIG. 7.

Point (Fig. 7)	Dam No.[a]	B (ft)	H (ft)	Year
(*a*) WIDTH A = 80 FT				
1......	9	20	10	1936
2......	16	20	10	....
3......	26	25	12.5	1935
(*b*) WIDTH A = 100 FT				
4......	15	20	10	1938
5......	21	20	10	1936
6......	14	20	10	1938
7......	18	20	10	1935
8......	22	25	12.5	1936
9......	25	25	12.5	1937
10......	1	26	13	1935

[a] All Mississippi River dams except No. 10, which is on the Kanawha River.

The hoist curves show the weight (Fig. 7(*a*)) and cost (Fig. 7(*b*)) of the hoist and chain plotted against the weight of the moving part or leaf. The average weight of the moving parts may be estimated roughly as about 83% of the total structural weight, as given in the gate weight curve. The plotted points in the cost curves are actual costs. The dashed lines in each case are the average curves through the points after adjusting them to 1939 costs.

DRUM CREST GATES

Drum gates are watertight sector-shaped drums hinged on either the downstream or the upstream side, which, when lowered, rest in a pit in the spillway. They are designed so that the upper surface conforms to the contour of the spillway crest when the gates are in the lowered position. The pit is sealed so that, when water is admitted, the drum rises by flotation, the rate being regulated by the water level in the pit.

Although this type of gate is relatively heavy, it does not require any overhead structure other than piers between the gates where more than one gate is needed. These piers are merely for the purpose of carrying the seals and do not carry load. Also, like the roller gate, and for similar reasons, these gates can be built relatively long.

The weights and costs of representative medium and large-size drum crest gates are given in Fig. 8. The weight and costs are plotted as ordinates against the function $F(W)$ as defined by Eq. 3. Weights are for the complete gate including all anchorages, hinge castings, and other stationary parts as well as piping and apparatus for automatic control. The costs are for the complete gate installation, except in the case of Salinas gate. Adjusted unit costs (1939 basis) are as follows:

Dam (Fig. 8)	Cents per pound	Remarks
Tieton	13.2	....
Sepulveda	11.45	Hinged downstream
Florence Lake	25	Long truck haul into high mountains
Black Canyon	15.1	....
Guernsey	13.27	....
Easton	12.2	....
Boulder	10.91	....
Salinas	15.7	Includes 3.1¢ per pound for installation
Grand Coulee	11.78	....
Morris	....	Hinged downstream

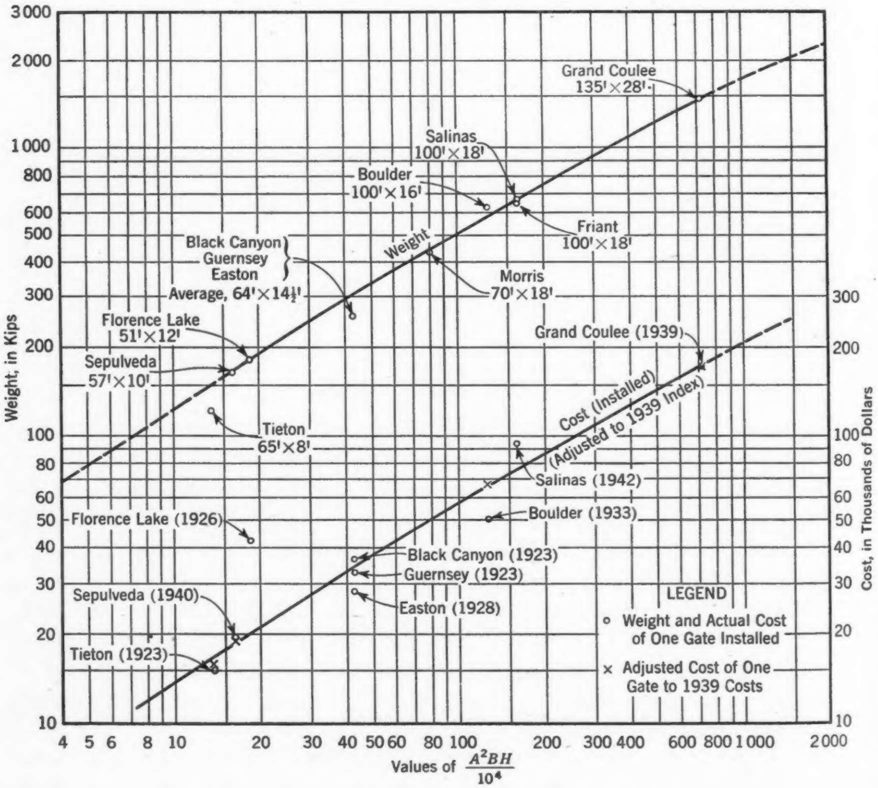

FIG. 8.—WEIGHTS AND COSTS OF DRUM CREST GATES

As indicated, all gates were hinged on the upstream side except those at Sepulveda and Morris dams.

Quite close estimates should be obtained from these data since all the points lie fairly close to the curves. Because of this it seemed justifiable to extrapolate

the weight curve at both ends, thus extending the range considerably. However, the extensions are shown by dashed lines to the limits of the page.

Broome-Type Caterpillar Gates

Under the heading, "High-Pressure Slide Gates," it was mentioned that hoisting capacities are required in the order of from 60% to 100% of the entire

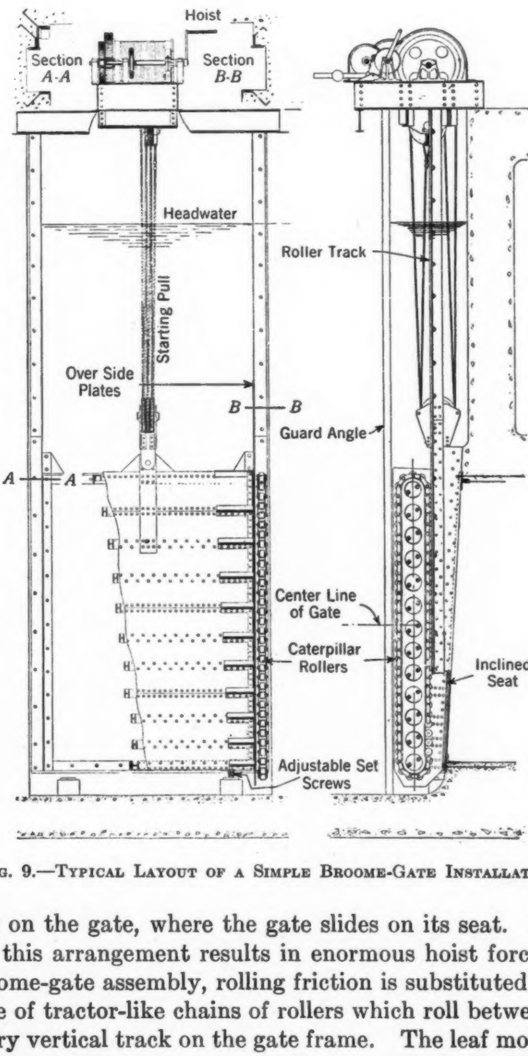

Fig. 9.—Typical Layout of a Simple Broome-Gate Installation

static pressure on the gate, where the gate slides on its seat. For large gates or high heads this arrangement results in enormous hoist force requirements.

In the Broome-gate assembly, rolling friction is substituted for sliding friction by the use of tractor-like chains of rollers which roll between the gate leaf and a stationary vertical track on the gate frame. The leaf moves in a vertical direction, therefore; but the seals are inclined at a slight angle from the direction of travel so that when the gate is closed the sealing surfaces at each side just touch. Any movement upward, in opening, lifts the leaf from the seals—eliminating sliding friction on the seal surfaces, with the result that the fric-

tion force is reduced to less than 5% of the static pressure. The gate is so designed that there is a sufficient downward component in the hydrostatic pressure on the gate at all times to insure closure, without requiring downward thrust from the hoist. This construction makes possible the use of simple drum hoists and sheaves. Fig. 9 shows a typical layout of the gate.

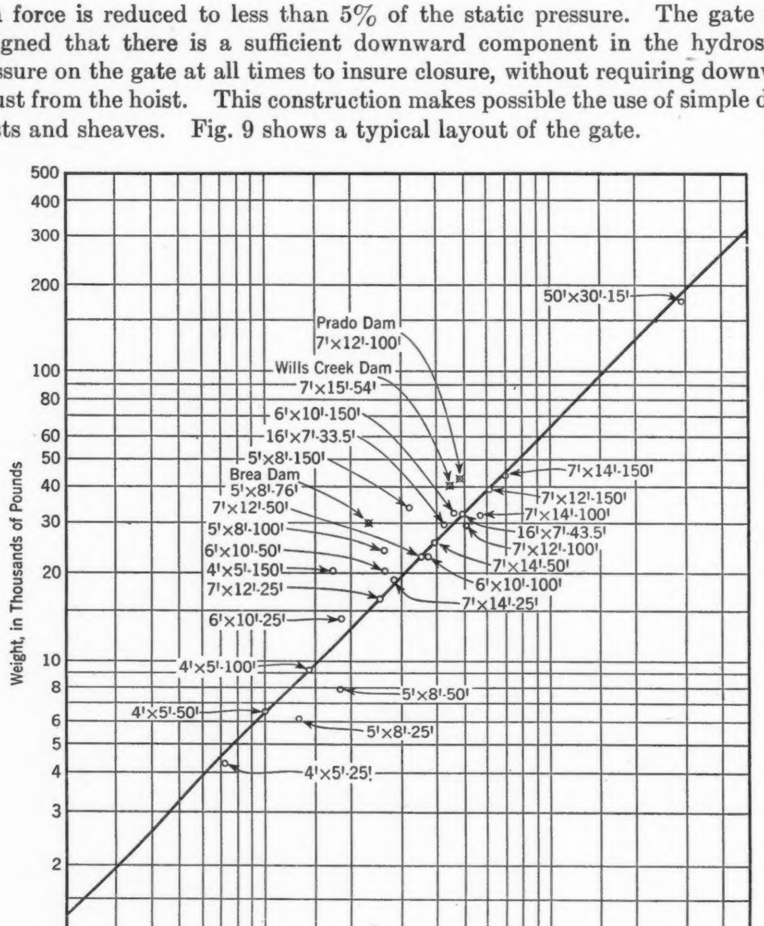

FIG. 10.—WEIGHTS OF BROOME GATES

To obtain an authoritative estimate of the price and weight of the gates made by any individual manufacturer, it is, of course, necessary to submit the requirements and some details of the installation to him before a quotation can be obtained. However, for rough preliminary studies, this is inconvenient and takes time. In Fig. 10 the available weights of a considerable range of this particular make of gates have been plotted as ordinates against the empirical function:

$$F(W) = A\ B^{0.8}\sqrt{H} \quad \text{(4)}$$

The auxiliary curve is also given (see Fig. 11) to evaluate $B^{0.8}$ quickly so that values of the abscissa can be obtained by a simple slide rule operation.

In Fig. 10, the points marked by the gate size only, represent a more or less standard line of gates which have been supplied to the hydroelectric industry for many years. The leaves of these gates, and in most cases the frames, are constructed of structural steel. The line drawn through the average of these points is a straight line with a slope of 45° which means that the ordinates are directly proportional to the first power of the weight as defined by Eq. 4.

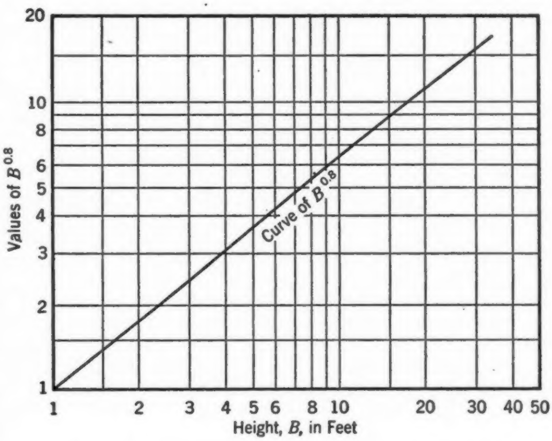

Fig. 11.—Auxiliary Curve for Evaluating $B^{0.8}$

Since 1935 the USED, in connection with its flood control projects, has exerted a considerable influence on Broome-gate design, in the direction of better construction, to give longer life and higher safety factors. This policy has resulted in heavier gates for government installations, particularly because of the substitution of cast frames. The specifications vary considerably with different USED offices and thus far it has not been possible to obtain accurate weight information on a sufficient range of sizes and heads to establish the trend of a curve for these cast frame gates as used in flood control work.

However, the actual weights of gates on Brea, Wills Creek, and Prado dams are plotted in Fig. 10 as guides for obtaining a rough estimate of the weight of other sizes of gates of this heavier construction.

All weights given in Fig. 10 include the leaf, frame, frame extensions, guides, and guide extensions, but do not include hoists or cables. These weights do not include conduit linings and none are used on any of these gates. If conduit lining is required for use with a Broome gate, its weight may be taken from the curves of Fig. 3.

Broome-Gate Hoists.—The required hoist capacity for a Broome gate depends, among other conditions, on the displaced volume of the leaf which, for preliminary estimates, is not known. Fig. 12 was developed from a study of the hoist requirements of existing gates. Hoist capacities are plotted against the empirical expression:

$$F(W) = A^{1.173}\, B^{0.82}\, H^{0.94} \qquad (5)$$

Auxiliary curves are given for the determination of the fractional powers of the variables (see Fig. 13). Curve No. 2, Fig. 12, shows approximate hoist capacities for the utility line of gates, whereas curve No. 1 is for use on the higher class of gates described. Knowing the required hoist capacity, the weight of the nearest standard hoist can be determined. Each hoist has a considerable range of capacity depending on the roping. The speed will vary inversely as the capacity for the same hoist with different roping.

Costs.—As a rough guide to obtain the cost of Broome gates for government projects, the following unit costs, adjusted to 1939 level, are given:

Gates installed at:	Cents per pound
Ohio Dams (1935)—	
Wills Creek	25.1
Beach City	25.1
Southern California Dams—	
Prado (1939)	20.2
Brea (1940)	23.7

These costs are for gates delivered complete at the site with hoists, but do not include installation. The weights of the gate and hoist should be added

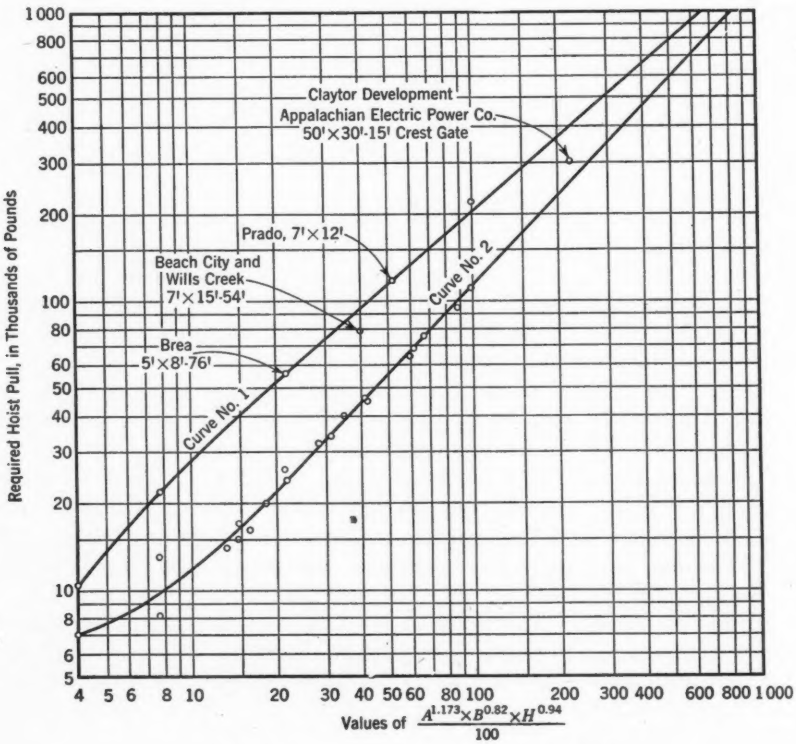

FIG. 12.—WEIGHTS OF HOISTS FOR BROOME GATES

together in applying these costs. The installation cost may be taken at from about 3¢ to 4¢ per lb for average conditions and locations close to centers of population.

Cost Index.—The cost level of 1939 has been taken as a representative level of prices before the inflation caused by World War II. For convenience in adjusting costs to this base, the curves in Fig. 14 have been plotted from the *Engineering News-Record* Construction and Building Cost Index of April, 1946.

The cost adjustments in Figs. 5 to 8 have been made in accordance with the yearly averages shown in the building cost index curve (Fig. 14(*b*)), since the

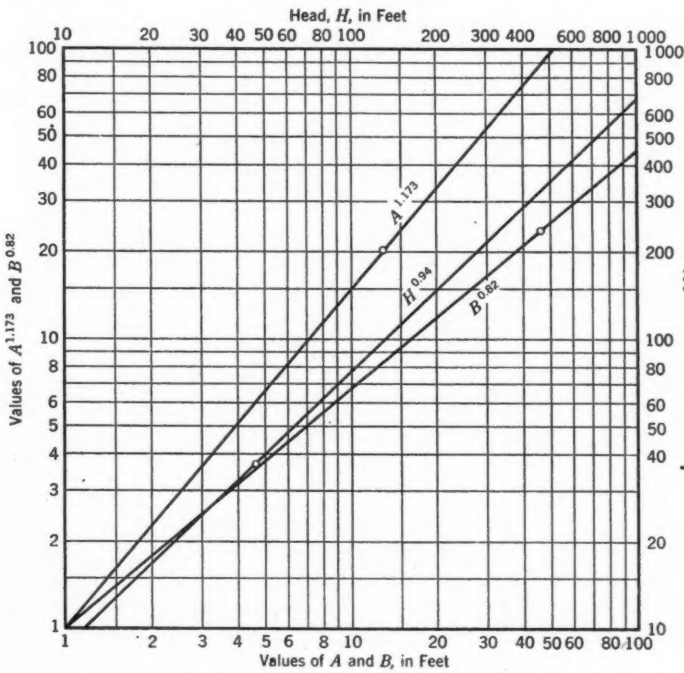

FIG. 13.—AUXILIARY CURVES FOR EVALUATING EQ. 5

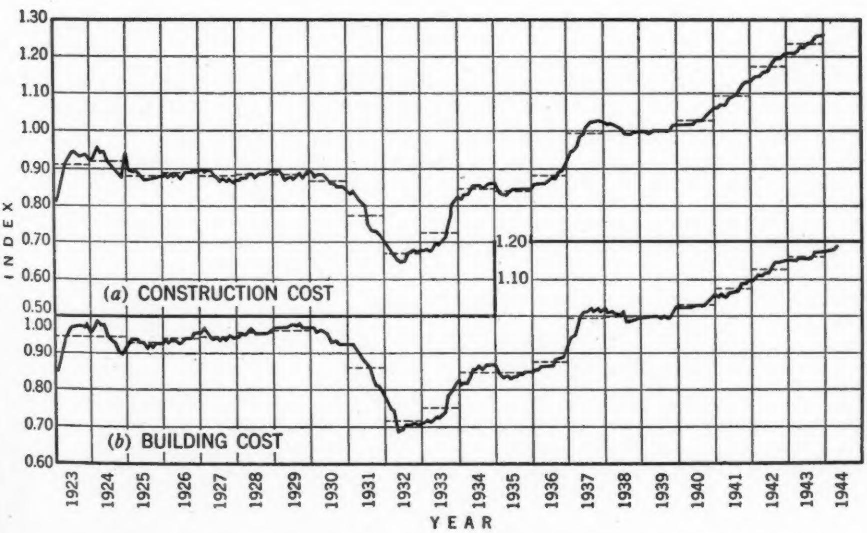

FIG. 14.—COST INDEX CURVES, ASSUMING THE 1939 AVERAGE COSTS EQUAL TO 1.00

best information obtainable seemed to indicate that this curve most nearly represented changes that occurred in shop cost previous to the war. However, a review of bids on both the cast-iron gates and fabricated steel gates received during 1946 definitely indicates that this curve does not reflect the true increase in gate costs for the postwar conditions. Unit costs in 1946 seem to be about double the 1939 costs.

Summary

The estimating charts in this paper can be utilized to advantage in three different ways:

a. As timesavers in preliminary studies to determine the most economic type of gates and the most economical over-all arrangement on the project;

b. As instruments for making consistent preliminary estimates of weights and costs for definite project reports before actual design of gates has been made; and

c. As checks to compare final designs with those compiled previously, to assure the designer that he is not wasting material on the one hand, and as checks against gross error or omission affecting the safety of the structure on the other.

Acknowledgment

Various offices of the United States Engineer Department furnished valuable data for this paper in connection with the radial and roller gates on the Upper Mississippi and Ohio rivers. The writer is also indebted to the Bureau of Reclamation, United States Department of the Interior, both for data furnished directly through the courtesy of the Chief Engineer's Office in Denver, Colo., and for data taken from its various publications and specifications. The courtesy of the Phillips and Davies Company, the Southern California Edison Company, and the Consolidated Steel Corporation in furnishing data on gates is also greatly appreciated.

In particular, the writer acknowledges the helpful suggestions and criticisms given by associates in the Los Angeles Office, USED, and the courtesy of that office in extending permission for publication of these data.

AMERICAN SOCIETY OF CIVIL ENGINEERS

Founded November 5, 1852

PAPERS

LEAST SQUARES ADJUSTMENT OF TRIANGULATION NET BETWEEN GEODETIC STATIONS

BY E. F. CODDINGTON [1] AND O. C. J. MARSHALL,[2] MEMBERS, ASCE

SYNOPSIS

Local triangulation nets, both urban and rural, can be precisely adjusted to large-scale geodetic triangulation control with comparatively little effort if all the angle, distance, and azimuth relations involved are reduced to simultaneous equations expressed in terms of direction corrections and then adjusted by least squares methods. The derivation of the correction equations is illustrated by a sample net containing three quadrilaterals. Application of the method is also illustrated by adjustment of a local net for Logan County, Ohio.

INTRODUCTION

The United States Coast and Geodetic Survey (U. S. C. and G. S.) triangulation system, which has 25-mile spacing of stations as its goal, has been adjusted to the local triangulation systems of at least two cities. As a result, Pittsburgh, Pa., and Columbus, Ohio, each have a triangulation system for local horizontal control to which the U. S. C. and G. S. has adjusted the overall net. The triangulation system for each of these cities was completed before geodetic control was available, but the U. S. C. and G. S. program has progressed to such an extent that it is available or can be made so for any future local requirement.

On several occasions, local cadastral surveys have been conducted without making a complete connection to available geodetic control. The objective of this paper, therefore, is to describe a method that will enable engineers in charge of supplementary triangulation projects to make full use of the control which the U. S. C. and G. S. has made available.

NOTE.—Written comments are invited for immediate publication; to insure publication the last discussion should be submitted by **February 1, 1948.**

[1] Prof. Emeritus of Geodetic Eng., Ohio State Univ., Columbus, Ohio.

[2] Prof. of Surveying and Geodesy, Ohio State Univ., Columbus, Ohio.

Sample Problems

To illustrate the problems involved, assume a system of three complete quadrilaterals connecting two fixed triangulation stations (1 and n in Fig. 1) of the type established by the U. S. C. and G. S. It is assumed that for the sample net all eight angles in each quadrilateral have been measured with the same relative accuracy consistent with the requirements of the project and that

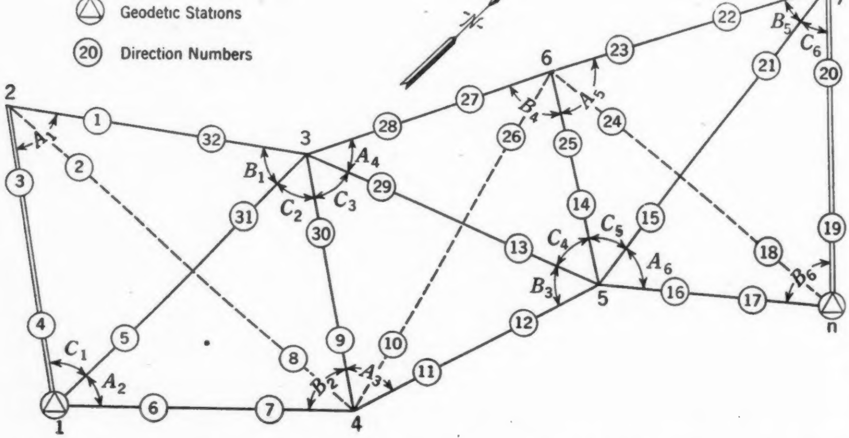

Fig. 1.—Triangulation Net of Three Complete Quadrilaterals Between Geodetic Stations

the azimuth and length of a starting base line (1–2 in Fig. 1) have been determined with adequate precision. In this example, the azimuth and length of a terminal base line, 7–n, are also assumed, for the purpose of illustrating the formation and use of the azimuth and length equations. In practice, a terminal base line would seldom be needed so close to the starting base line.

Several procedures are available for the preliminary adjustment, any of which will determine preliminary angles to be used in computing triangles from which the accumulated errors in latitude and departure between fixed stations can be found. In the first of these procedures the angle equations of each quadrilateral may be satisfied by the approximate method.[3,4] This is the equivalent of a rigid solution which disregards the relation of the sides, and is accomplished very rapidly where the figures are simple quadrilaterals or center point triangles with no overlapping figures involved. The preliminary solution also may be set up as a least squares solution involving the usual three angle equations and one side equation for each quadrilateral, leaving all tie equations for the final adjustment. Where there are no overlapping figures or other complications, these quadrilaterals may be adjusted separately. As a third possibility, the preliminary adjustment may also be made as a least squares solution including all condition equations involved in the net (angle, side,

[3] "The Principles and Practice of Surveying," by C. B. Breed and G. L. Hosmer, Vol. 2, "Higher Surveying," John Wiley & Sons, Inc., New York, N. Y., 5th Ed., 1938.

[4] "Least Squares in Engineering," by E. F. Coddington and O. J. Marshall, Ohio State Univ., Columbus, Ohio, 1941.

azimuth, and length equations) except the latitude and departure equations. When this solution is completed, the resulting latitude and departure closure is likely to be smaller than when any less inclusive preliminary adjustment is used.

In the example illustrated in this paper, the first of the foregoing methods is used. The first step is the preliminary computation of a selected set of triangles of the net, starting with the base line 1–2 and proceeding through the strongest pair of triangles of each quadrilateral to the final station, n. The triangles used in this example are those adjacent to the diagonal shown by a full line in each quadrilateral. The other diagonal in each case (not used in computation of triangles) is shown by a dashed line. The stronger set of triangles should be selected by the "strength of figure" theory, but use of triangles adjacent to the shorter diagonal in each quadrilateral will generally result in the selection of the stronger figure.

A selected traverse from station 1 to station n may then be computed along any of these calculated triangle sides by latitudes and departures. The distance by which this computed traverse fails to fit the gap between the original and the final fixed stations represents the closing error of the survey. Because the preliminary adjustment makes the triangles used geometrically consistent, the closing error will be independent of the traverse route selected between 1 and n. In practice it is advisable to close each quadrilateral by latitudes and departures, since this procedure provides a needed check on the computation of the triangles. For purposes of obtaining the relative closure, however, the computed straight-line distance from station 1 to station n should be used as the length of the survey.

The closing error of the connecting traverse is then used to make a combined readjustment of the entire triangulation net so as to obtain an exact fit between fixed stations. To make this readjustment, two equations—one for latitude and one for departure—are used in combination with the equations resulting from other geometrical conditions of the net. The constant terms for all equations in this final adjustment are based on the corrected angles resulting from any preliminary solution. Hence, those condition equations which are used in both preliminary and final adjustments will show zero for the constant term in the final adjustment. All equations are handled simultaneously in the final least squares adjustment of the net.

Derivation of Tie Equations

In deriving the previously mentioned equations, the measured base is considered as fixed in length and direction and as originating at one of the fixed coordinated points. The effect on the location of n, the end point of the connecting traverse line, caused by a change in each angle of the net is also considered.

Each triangle of the net is examined separately in deriving the relation between the angle changes and the change of the end point. Considering the triangle 123 (Fig. 1), the combined effect of its angle changes will be an expansion or contraction of the side 1–3, with point 1 remaining fixed, and a rotation of side 1–3 about point 1. The change of side 3–2 does not require consideration, because the rotation of side 1–3 will be due solely to the change in angle C,

and the expansion of side 1–3 will be due to the combined effects of the changes in angles A and B.

Expansion and Contraction of the Net

In triangle 123,

$$\frac{1\text{–}3}{2\text{–}1} = \frac{\sin A}{\sin B} \qquad (1a)$$

therefore,

$$1\text{–}3 = 2\text{–}1 \left(\frac{\sin A}{\sin B}\right) \qquad (1b)$$

and

$$\log (1\text{–}3) = \log (2\text{–}1) + \log \sin A - \log \sin B \qquad (1c)$$

If the changes in the angles of this triangle are assumed to be v_A, v_B, and v_C, the tabular differences for log sin A and log sin B are assumed as δ_A and δ_B, respectively, and the length of the variable side 1–3 is designated by L, then

$$d \log_{10} \sin A = \delta_A \, v_A \qquad (2a)$$

$$d \log_{10} \sin B = \delta_B \, v_B \qquad (2b)$$

$$d \log_{10} (2\text{–}1) = 0 \qquad (2c)$$

and

$$d \log_{10} L = \delta_A \, v_A - \delta_B \, v_B \qquad (2d)$$

If it is also assumed that

$$\log_{10} L = N \qquad (3a)$$

then

$$\frac{dL}{L} = \log_e 10 \, dN \qquad (3b)$$

However,

$$\log_e 10 = \frac{1}{\log_{10} e} \qquad (3c)$$

therefore,

$$\frac{dL}{L} = \frac{dN}{\log_{10} e} = \frac{dN}{0.434294} = \frac{d \log_{10} L}{0.434294} \qquad (3d)$$

Substitution of Eq. 2*d* in Eq. 3*d* gives

$$\frac{dL}{L} = \frac{\delta_A \, v_A - \delta_B \, v_B}{0.434294} \qquad (4a)$$

from which

$$dL = L \left(\frac{\delta_A \, v_A - \delta_B \, v_B}{0.434294}\right) \qquad (4b)$$

Numerical Illustration.—The validity of this formula may be demonstrated by assigning definite values to the angles of triangle 123 and a definite length to the base 2–1 in Fig. 1. From these original values the length 3–1 is first computed. Then, with changes to the three angles assumed as noted previously, the length 3–1 is recomputed. The difference, in these computed lengths, should correspond to the value of dL obtained by Eq. 4*b*. Thus, if it is

assumed that angles A, B, and C measure 68° 24′ 17.81″, 59° 47′ 36.45″, and 51° 48′ 05.74″, respectively (making a total of 180° 00′ 00.00″); that v_A, v_B, and v_C are +5″, −3″, and −2″, respectively; and that 2–1 = 13,672.64: Then $\delta_A = 0.83$, $\delta_B = 1.22$, and log (3–1) = log 13,672.64 + log sin 68° 24′ 17.81″ − log sin 59° 47′ 36.45″. Solution of this equation for 3–1 by seven-place log tables gives:

		Original angles	Corrected angles
log 13,672.64	=	4.1358523	4.1358523
log sin A	=	+9.9683934	+9.9683976
		4.1042457	4.1042499
log sin B	=	−9.9366229	−9.9366193
log (3–1)	=	4.1676228	4.1676306
3–1	=	14,710.34	14,710.61
Difference	=	....	0.27

Solving by Eq. 4*b*, $dL = L\left(\frac{\delta_A v_A - \delta_B v_B}{0.434294}\right) = \frac{14{,}710}{0.434294}(0.00000083 \times 5 + 0.00000122 \times 3) = 0.27$, which agrees with the difference previously found.

The values of δ_A and δ_B in this problem appear as eight places of decimals taken from a seven-place log table. This result is due to the fact that intervals in the table are for 10 sec of arc, whereas δ_A and δ_B are changes of log sin A and log sin B for a 1-sec change in the angle. Use of the sixth decimal place as the unit for the tabular differences δ_A and δ_B is also in accordance with the usual practice in setting up the side equation in adjustment of a quadrilateral.

General Application.—Returning to Eq. 4*a*, $\frac{dL}{L}$ is the relative change of the length of the side 3–1, due to the angle changes v_A and v_B. This ratio might be expressed as a percentage of change or rate of change. If no angle changes are made in the remainder of the net, all the remaining triangle sides will receive this same relative increase. Furthermore, all linear dimensions of the remainder of the net will receive this relative increase. The same may be stated concerning the line n–1 or any component of it, in which n is the designation of the end or final station.

Referring to Fig. 2, the x-component of n–1 is $x_n - x_1$. Let Δx be the change in the length of this component. Then $\frac{\Delta x}{x_n - x_1}$, the relative change in the length of this component, is

$$\frac{\Delta x}{x_n - x_1} = \frac{dL}{L} = \frac{\delta_A\, v_A - \delta_B\, v_B}{0.434294} \qquad (5a)$$

from which

$$\Delta x = (x_n - x_1)\,\frac{\delta_A\, v_A - \delta_B\, v_B}{0.434294} \qquad (5b)$$

which gives the amount the end point of the net is moved in an east-west

direction as a result of a definite change in angles A and B of the beginning triangle.

Similarly,

$$\Delta y = (y_n - y_1) \frac{\delta_A v_A - \delta_B v_B}{0.434294} \qquad (6)$$

Both Δx and Δy are obtained as a product of two factors, either of which may be plus or minus. When the latter factor $(\delta_A v_A - \delta_B v_B)$ is positive, the net is expanded by the changes v_A and v_B; when it is negative, the net is contracted.

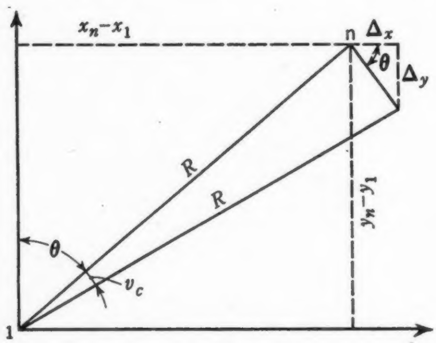

FIG. 2.—DISPLACEMENT FACTORS INVOLVED IN ANGULAR ROTATION ABOUT POINT 1

If an expanding net and positive $(x_n - x_1)$ are assumed, Δx is positive. If the end point falls west of the starting point, $x_n - x_1$ will be negative, which results in a negative Δx with an expanding net. A similar analysis also would apply to Δy. To derive Δx and Δy with proper signs, care must be taken to subtract the coordinate of the starting point from that of the end point. The computations indicated by these equations are accomplished in tabular form as illustrated by the numerical example to follow.

ROTATION DUE TO CHANGE OF ANGLE C

The effect of adding an increment to the C angle of the triangle under consideration is to produce a right-hand rotation of the line 3–1 about the fixed point 1, and such an angle increment is assumed as positive.

Any change in angle C produces a rotation of the whole net about the fixed point 1, so that the line n–1 rotates through the same angle increment as the line 3–1. Therefore, in Fig. 2, let v_C represent the increment to the angle C; let R be the distance n–1; and let θ be the bearing of line n–1. The length of the arc described by point n is $\frac{R\, v_C}{206{,}265}$, in which v_C is expressed in seconds. The east-west component of this arc is

$$\Delta x = \frac{R\, v_C}{206{,}265} \cos\theta = \frac{y_n - y_1}{206{,}265} v_C \qquad (7a)$$

Also, the north-south component is

$$\Delta y = -\frac{R\, v_C}{206{,}265} \sin\theta = -\frac{x_n - x_1}{206{,}265} v_C \qquad (7b)$$

Eq. 7*a* with Eq. 5*b*, and Eq. 7*b* with Eq. 6, give

$$\Delta x = \frac{x_n - x_1}{434{,}294} (\delta_A v_A - \delta_B v_B) + \frac{y_n - y_1}{206{,}265} v_C \qquad (8a)$$

and

$$\Delta y = \frac{y_n - y_1}{434{,}294}(\delta_A\, v_A - \delta_B\, v_B) - \frac{x_n - x_1}{206{,}265} v_C \qquad (8b)$$

In the triangle just completed A and B may be designated as expansion angles; and C, as the rotation angle. Line 3–1 may now be regarded as fixed and increments may be applied to the angles of triangle 134 to produce an expansion of line 4–3 and a rotation of this line about point 3, now also held fixed. Angle C is always at the intersection of the new fixed base and the next base to be established—in this case at point 3. Angle A must be opposite the next base or at point 1.

Expressions similar to Eqs. 8*a* and 8*b* can be derived to determine the components of motion Δx and Δy of the end point n caused by the application of increments to the angles of this second triangle, still holding the remaining angles of the net as fixed. With point 3 regarded as the initial point for this triangle, these equations become

$$\Delta x = \frac{x_n - x_3}{434{,}294}(\delta_A\, v_A - \delta_B\, v_B) - \frac{y_n - y_3}{206{,}265} v_C \qquad (9a)$$

$$\Delta y = \frac{y_n - y_3}{434{,}294}(\delta_A\, v_A - \delta_B\, v_B) + \frac{x_n - x_3}{206{,}265} v_C \qquad (9b)$$

It should be noted that the signs of the v_C-terms in Eqs. 9 are in opposition to those written for the first triangle—because the rotation point is at that end of the fixed line which gives a left-hand rotation when the angle at C is given a positive increment v_C.

In Fig. 1, triangle 345 has 3–4 as the fixed base with the point of rotation still at point 3. Thus, the signs in the equations for this triangle will be the same as in those for triangle 134. In this manner, all the triangles are used until the end point of the net is reached. The combined effect of the increments of the angles of each triangle applied in order is given by the expressions:

$$\Delta y = \sum \left[\frac{y_n - y_c}{434{,}294}(\delta_A\, v_A - \delta_B\, v_B) \mp \frac{x_n - x_c}{206{,}265} v_C\right] \qquad (10a)$$

$$\Delta x = \sum \left[\frac{x_n - x_c}{434{,}294}(\delta_A\, v_A - \delta_B\, v_B) \pm \frac{y_n - y_c}{206{,}265} v_C\right] \qquad (10b)$$

A sample numerical solution, based on the triangulation net of Fig. 1, is given in Fig. 3. Section (*a*) of these computations lists the fixed values of stations and bases; section (*b*), the angle adjustments for the entire net. Section (*c*) shows the preliminary angle adjustment for one quadrangle, on which the side equation, triangle computations, azimuths, and traverse computations of sections (*d*), (*e*), (*f*), and (*g*), respectively, are based. Together with similar computations for the remaining quadrangles of the net sections (*c*), (*d*), (*e*), (*f*), and (*g*) yield the preliminary coordinates shown in section (*h*) for all the stations in the net, as well as the y-component and x-component of the closure, as shown in section (*i*).

The side equation for one quadrangle, determined from section (*d*) of Fig. 3, is

$$
\begin{aligned}
&- 3.30\,(1) + 5.77\,(2) - 2.47\,(3) - 1.57\,(4) + 3.66\,(5) - 2.09\,(6) \\
&\quad - 2.43\,(7) + 5.06\,(8) - 2.63\,(9) - 1.47\,(30) + 3.02\,(31) \\
&\quad - 1.55\,(32) - 7.4 = 0 \qquad (11a)
\end{aligned}
$$

(*a*) Fixed Values

Station	Coordinates N	Coordinates E	Base	Length	Azimuth
1	20,000	20,000	1–2	14,352.09	124° 27′ 16.53″
n	50,615.79	41,078.07	n–7	15,009.58	132 08 04.58

(*b*) Angle Adjustment

Angle	Measured value	Preliminary adjustment	Correction	Final value
		Quadrilateral 1234		
− 1 + 2	32° 32′ 56.2″	56.46″	+1.19″	57.65″
− 2 + 3	40 28 47.8	47.59	+2.06	49.65
− 4 + 5	53 21 02.6	02.39	−0.85	01.54
− 5 + 6	45 12 16.7	16.41	−1.05	15.36
− 7 + 8	40 57 53.9	53.61	−0.16	53.45
− 8 + 9	38 44 11.8	11.99	−0.65	11.34
−30 +31	55 05 37.8	37.98	+1.86	39.84
−31 +32	53 37 13.3	13.57	−2.40	11.17
		Quadrilateral 3456		
− 9 +10	39° 55′ 29.4″	28.42″	+1.41″	29.83″
−10 +11	31 37 48.2	48.13	−2.47	45.66
−12 +13	51 49 15.9	15.84	−0.24	15.60
−13 +14	54 52 46.5	47.66	+0.89	48.55
−25 +26	41 40 07.2	08.36	+1.82	10.18
−26 +27	40 02 45.2	45.44	−0.86	44.58
−28 +29	43 24 18.3	18.54	−1.85	16.69
−29 +30	56 37 28.6	27.61	+1.30	28.91
		Quadrilateral 567n		
−14 +15	49° 29′ 07.7″	09.56″	+0.15″	09.71″
−15 +16	56 44 32.6	33.24	−1.83	31.41
−17 +18	35 13 57.2	57.84	+1.41	59.25
−18 +19	49 42 26.7	25.46	+0.90	26.36
−20 +21	38 19 04.7	03.47	−0.48	02.99
−21 +22	35 00 26.8	26.78	+1.75	28.53
−23 +24	56 58 04.3	04.29	−2.17	02.12
−24 +25	38 32 17.5	19.36	+0.27	19.63

(*c*) Preliminary Angle Adjustment—Quadrilateral 1234

	Angle	Measured value						Preliminary adjustment
	− 1 + 2	32° 32′ 56.2″	+ 0.22″	56.42″	+ 0.04″	....		56.46″
B_1	−31 +32	53 37 13.3	+ 0.23	13.53	+ 0.04	....		13.57
C_2	−30 +31	55 05 37.8	+ 0.22	....		38.02″	− 0.04″	37.98
	− 8 + 9	38 44 11.8	+ 0.23	....		12.03	− 0.04	11.99
		59.1						00.00
		+0.9						
	− 7 + 8	40° 57′ 53.9″	− 0.25″	....		53.65″	− 0.04″	53.61″
A_2	− 5 + 6	45 12 16.7	− 0.25	....		16.45	− 0.04	16.41
C_1	− 4 + 5	53 21 02.6	− 0.25	02.35″	+ 0.04″	....		02.39
	− 2 + 3	40 28 47.8	− 0.25	47.55	+ 0.04	....		47.59
		01.0		59.85		00.15		00.00
		−1.0		+0.15		−0.15		

Adjusted Angles

A_1	− 1 + 3	73° 01′ 44.05″
	− 4 + 6	98 33 18.80
B_2	− 7 + 9	79 42 05.60
	−30 +32	108 42 51.55
		360 00 00.00

Fig. 3.—Sample Numerical Solution of Triangulation Net Shown in Fig. 1 (See Text)

(*d*) SIDE EQUATION

Angle	Log sin	Angle	Log sin
− 1 + 2	9.7307992 + 3.30 (− 1 + 2)	− 2 + 3	9.8123659 + 2.47 (− 2 + 3)
−30 + 31	9.9138620 + 1.47 (−30 + 31)	−31 + 32	9.9058528 + 1.55 (−31 + 32)
− 7 + 8	9.8166366 + 2.43 (− 7 + 8)	− 8 + 9	9.7963953 + 2.63 (− 8 + 9)
− 4 + 5	9.9043388 + 1.57 (− 4 + 5)	− 5 + 6	9.8510300 + 2.09 (− 5 + 6)
	9.3656366		9.3656440
	6440		
	−7.4		

(*e*) TRIANGLE COMPUTATIONS, QUADRILATERAL 1234

1–2	14,352.09 ft	log = 4.1569145
B_1	53° 37′ 13.57″	colog sin = 0.0941472
A_1	73 01 44.05	log sin = 9.9806632
C_1	53 21 02.39	log sin = 9.9043388
1–3	17,050.03 ft	log = 4.2317252
2–3	14,302.12 ft	log = 4.1554005
1–3	17,050.03 ft	log = 4.2317252
B_2	79° 42′ 05.60″	colog sin = 0.0070535
A_2	45 12 16.41	log sin = 9.8510300
C_2	55 05 37.98	log sin = 9.9138620
3–4	12,297.27 ft	log = 4.0898087
1–4	14,211.52 ft	log = 4.1526407

(*f*) AZIMUTHS

1–2	124° 27′ 16.53″
A_1	73 01 44.05
2–3	231 25 32.48
$B_1 + C_2$	108 42 51.55
3–4	302 42 40.93
B_2	79 42 05.60
4–1	43 00 35.33
$C_1 + A_2$	98 33 18.80
1–2	124 27 16.53 (check)

(*g*) TRAVERSE COMPUTATIONS

Course	Bearing	Distance	Cosine	Sine	Latitude	Departure
1–2	N 55° 32′ 43.47″ W	14,352.09	0.5657529	0.8245755	8,119.73	−11,834.38
2–3	N 51 25 32.48 E	14,302.12	0.6235291	0.7818001	8,917.79	11,181.40
3–4	S 57 17 19.07 E	12,297.27	0.5404073	0.8414034	− 6,645.53	10,346.96
4–1	S 43 00 35.33 W	14,211.52	0.7312369	0.6821236	−10,391.99	− 9,694.01
					0.00	− 0.03

(*h*) PRELIMINARY COORDINATES

Station	N	E
1	20,000.00	20,000.00
2	28,119.73	8,165.63
3	31,037.52	19,347.03
4	30,391.99	29,694.00
5	43,052.89	32,913.22
6	48,355.23	24,077.12
7	60,685.70	29,947.68
n	50,615.18	41,078.47
Fixed n	50,615.79	41,078.07

(*i*) $\Delta y = -0.61$; $\Delta x = +0.40$

Let L = length of line (7–n)
Preliminary $\log L$ = 4.1763772
Fixed $\log L$ = 4.1763685
$\Delta \log L = +8.7$

FIG. 3.—(*Continued*)

or, dividing by 2.918, the average coefficient is

$$- 1.13\ (1) + 1.98\ (2) - 0.85\ (3) - 0.54\ (4) + 1.26\ (5) - 0.72\ (6) - 0.83\ (7) + 1.73\ (8) - 0.90\ (9) - 0.50\ (30) + 1.03\ (31) - 0.53\ (32) - 2.536 = 0 \quad (11b)$$

EXPLANATION OF TABLE 1

Table 1, which contains the data necessary to compute the coefficients of the unknown angle corrections, provides a column for each triangle used. The headings of these columns are the number designations of the stations at which the C angles are located. Stations 3 and 5 are repeated because two C angles are located at each of them and these stations are featured in determining the algebraic signs of the coefficients. Reference to Eqs. 10*a* and 10*b* will show the significance of the numbers in the body of the table.

Extreme care should be taken in respect to the algebraic signs of the coefficients, with due regard for the order of differences and also for the signs of the

products. These signs may be checked directly from Fig. 1. Considering the latitude coefficients, assume that all the A angles of the several triangles receive plus corrections, which will cause an expansion of each of the opposite triangle sides. This series of expansions indirectly will cause, for each triangle, an

TABLE 1.—DATA FOR LATITUDE AND DEPARTURE EQUATIONS OF SAMPLE NET

Item	Station at C Angle (Point of Rotation)					
	1	3	3	5	5	7
(1)	(2)	(3)	(4)	(5)	(6)	(7)
Coordinates[a] N	20,000.00	37,037.52	37,037.52	43,052.89	43,052.89	60,685.70
Coordinates[a] E	20,000.00	19,347.03	19,347.03	32,913.22	32,913.22	29,947.68
Angles A	73° 01′ 44.05″	45° 12′ 16.41″	71° 33′ 16.55″	43° 24′ 18.54″	95° 30′ 23.65″	56° 44′ 33.24″
Angles B	53° 37′ 13.57″	79° 42′ 05.60″	51° 49′ 15.84″	81° 42′ 53.80″	35° 00′ 26.78″	84° 56′ 23.30″
Angles C	53° 21′ 02.39″	55° 05′ 37.98″	56° 37′ 27.61″	54° 52′ 47.66″	49° 29′ 09.56″	38° 19′ 03.47″
δ_A	0.65	2.09	0.71	2.23	−0.20	1.38
δ_B	1.55	0.38	1.66	0.30	3.01	0.18
$y_n - y_c$	30,615	13,578	13,578	7,562	7,562	−10,071
$\frac{y_n - y_c}{434,294}$	0.0705	0.0313	0.0313	0.0174	0.0174	−0.0232
$x_n - x_c$	21,078	21,731	21,731	8,165	8,165	11,131
$\frac{x_n - x_c}{434,294}$	0.0485	0.0500	0.0500	0.0188	0.0188	0.0256
$\frac{y_n - y_c}{434,294}\delta_A$	0.0458	0.0654	0.0222	0.0388	−0.0035	−0.0320
$-\frac{y_n - y_c}{434,294}\delta_B$	−0.1093	−0.0119	−0.0520	−0.0052	−0.0524	+0.0042
$\mp\frac{x_n - x_c}{206,265}$	−0.1022	0.1054	0.1054	−0.0396	−0.0396	0.0540
$\frac{x_n - x_c}{434,294}\delta_A$	0.0315	0.1045	0.0355	0.0419	−0.0038	+0.0353
$-\frac{x_n - x_c}{434,294}\delta_B$	−0.0752	−0.0190	−0.0830	−0.0056	−0.0566	−0.0046
$\pm\frac{y_n - y_c}{206,265}$	0.1484	−0.0658	−0.0658	+0.0367	+0.0367	0.0488

[a] Coordinates of end station: N = 50,615.18; E = 41,078.47.

expansion of the line connecting the corresponding C angle station and the end station, n. When this expansion causes n to have a north component of motion, the corresponding sign of the coefficient will be plus. If the component of motion is south, the sign will be minus. Thus, if the C angle is south of n, the sign of the corresponding coefficient will be plus; if a C angle station lies north of n, the corresponding sign will be minus.

There is an occasional exception to this rule; for example, when the A angle in question is greater than 90°, an increase causes a contraction of the opposite side and the sign in question is reversed.

Since an increase in the magnitude of any B angle causes a contraction of the side opposite A, the sign of the corresponding coefficient will be the reverse of that derived from the A angle. As in the case of the A angle, if the B angle is more than 90°, the resulting sign is again reversed.

The signs of the latitude coefficients due to an assumed plus correction to

the C angles may now be considered. In this case, these displacements of n are due to a rotation of each of the lines connecting the C angle stations with station n. It must first be determined if the rotation is clockwise or counterclockwise about the C angle station in question, and then whether this rotation causes a north or south movement of n. The signs of the latitude coefficients in the problem under consideration may then be checked by Fig. 1.

Angle Change Coefficients.—Inspection of the A angles will show that the one in the second triangle at station 5 is greater than 90°, thus the sign of the v_A-coefficient will be reversed. Also, C angle stations 1, 3, and 5 are south of n, but station 7 lies north of n. Therefore, the first four are regular and plus, the fifth is minus because the angle is greater than 90°, and the last is minus because 7 lies north of n.

Since there are no angles greater than 90° among the B angles, all the v_B-coefficients will be minus except the last, which is plus because 7 lies north of n.

Determination of the v_c-coefficients for the various triangles gives the following: In triangle 1, the rotation is clockwise, and the displacement has

TABLE 2.—COMPUTATION OF COEFFICIENTS IN LATITUDE EQUATION OF SAMPLE NET (SEE TABLE 1)

Direction No.	TRIANGLE DESIGNATION						Final coefficients
	123	134	345	356	567	57n	
(1)	(2)	(3)	(4)	(5)	(6)	(7)	(8)
(1)	−0.0458	....	....	....	....	....	−0.0458
(2)	....	....	....	....	....	....	....
(3)	+0.0458	....	....	....	....	....	+0.0458
(4)	+0.1022	....	....	....	....	....	+0.1022
(5)	−0.1022	−0.0654	....	....	....	....	−0.1676
(6)	....	+0.0654	....	....	....	....	+0.0654
(7)	....	+0.0119	....	....	....	....	+0.0119
(8)	....	....	....	....	....	....	....
(9)	....	−0.0119	−0.0222	....	....	....	−0.0341
(10)	....	....	....	....	....	....	....
(11)	....	....	+0.0222	....	....	....	+0.0222
(12)	....	....	+0.0520	....	....	....	+0.0520
(13)	....	....	−0.0520	+0.0396	....	....	−0.0124
(14)	....	....	....	−0.0396	+0.0396	....	....
(15)	....	....	....	....	−0.0396	+0.0320	−0.0076
(16)	....	....	....	....	....	−0.0320	−0.0320
(17)	....	....	....	....	....	−0.0042	−0.0042
(18)	....	....	....	....	....	....	....
(19)	....	....	....	....	....	+0.0042	+0.0042
(20)	....	....	....	....	....	−0.0540	−0.0540
(21)	....	....	....	....	+0.0524	+0.0540	+0.1064
(22)	....	....	....	....	−0.0524	....	−0.0524
(23)	....	....	....	....	+0.0035	....	+0.0035
(24)	....	....	....	....	....	....	....
(25)	....	....	....	+0.0052	−0.0035	....	+0.0017
(26)	....	....	....	....	....	....	....
(27)	....	....	....	−0.0052	....	....	−0.0052
(28)	....	....	....	−0.0388	....	....	−0.0388
(29)	....	....	−0.1054	+0.0388	....	....	−0.0666
(30)	....	−0.1054	+0.1054	....	....	....	....
(31)	+0.1093	+0.1054	....	....	....	....	+0.2147
(32)	−0.1093	....	....	....	....	....	−0.1093

a south component. The sign is therefore minus; in triangles 2 and 3, C angle station 3, the rotation is counterclockwise, which produces a north displacement of n, so that these two signs are plus; in triangles 4 and 5, C angle station 5,

the rotation is clockwise and the displacements of n are south, producing minus coefficients; and in triangle 6, *C* angle station 7, the rotation is counterclockwise, producing a north displacement and plus coefficient.

The departure equation coefficients may be checked by a similar analysis, by considering the *A* angle changes as expansions, the *B* angle changes as contractions, and the *C* angle changes as rotations, clockwise or counterclockwise, and then determining whether the resulting displacements are east (+) or west (−).

Transformation to Directions

Corrections to the angles *A*, *B*, and *C* are designated by the symbols v_A, v_B, and v_C. However, the direction method is generally used in reduction of a triangulation net; and, since each angle is the difference of two directions, each angle correction will be the difference between corresponding direction corrections. As is customary, direction corrections are designated by numbers within parentheses.

It will be found convenient to use the form of Tables 2 and 3 to complete

TABLE 3.—Coefficients for Departure Equation of Sample Net (See Table 1)

Direction No.	Triangle Designation						Final coefficients
	123	134	345	356	567	57n	
(1)	(2)	(3)	(4)	(5)	(6)	(7)	(8)
(1)	−0.0315	....	....	....	....	....	−0.0315
(2)	....	....	....	....	....	....	....
(3)	+0.0315	....	....	....	....	....	+0.0315
(4)	−0.1484	....	....	....	....	....	−0.1484
(5)	+0.1484	−0.1045	....	....	....	....	+0.0439
(6)	....	+0.1045	....	....	....	....	+0.1045
(7)	....	+0.0190	....	....	....	....	+0.0190
(8)	....	....	....	....	....	....	....
(9)	....	−0.0190	−0.0355	....	....	....	−0.0545
(10)	....	....	....	....	....	....	....
(11)	....	....	+0.0355	....	....	....	+0.0355
(12)	....	....	+0.0830	....	....	....	+0.0830
(13)	....	....	−0.0830	−0.0367	....	....	−0.1197
(14)	....	....	....	+0.0367	−0.0367	....	....
(15)	....	....	....	....	+0.0367	−0.0353	+0.0014
(16)	....	....	....	....	....	+0.0353	+0.0353
(17)	....	....	....	....	....	+0.0046	+0.0046
(18)	....	....	....	....	....	....	....
(19)	....	....	....	....	....	−0.0046	−0.0046
(20)	....	....	....	....	....	−0.0488	−0.0488
(21)	....	....	....	....	+0.0566	+0.0488	+0.1054
(22)	....	....	....	....	−0.0566	....	−0.0566
(23)	....	....	....	....	+0.0038	....	+0.0038
(24)	....	....	....	....	....	....	....
(25)	....	....	....	+0.0056	−0.0038	....	+0.0018
(26)	....	....	....	....	....	....	....
(27)	....	....	....	−0.0056	....	....	−0.0056
(28)	....	....	....	−0.0419	....	....	−0.0419
(29)	....	....	+0.0658	+0.0419	....	....	+0.1077
(30)	....	+0.0658	−0.0658	....	....	....	....
(31)	+0.0752	−0.0658	....	....	....	....	+0.0094
(32)	−0.0752	....	....	....	....	....	−0.0752

the final latitude and departure equations, with a column allowed for each triangle. Since there are three angles in each triangle, three pairs of coefficients will appear in each column. For example, in triangle 123, Fig. 1, the

following relations for the latitude equation are found:

$$0.0458\, v_A = 0.0458\, [(3) - (1)] = -0.0458\,(1) + 0.0458\,(3) \quad \text{(12a)}$$

$$-0.1093\, v_B = -0.1093\, [(32) - (31)] = 0.1093\,(31) - 0.1093\,(32) \quad \text{(12b)}$$

$$-0.1022\, v_C = -0.1022\, [(6) - (5)] = 0.1022\,(5) - 0.1022\,(6) \quad \text{(12c)}$$

The final coefficient of each direction correction is found by adding the individual coefficients opposite that direction horizontally in each table.

Azimuth Equation

If the measured (field) angles are used in the derivation of equations for the final adjustment, the C angles, or corresponding directions, must be used in deriving the azimuth equation. However, if a preliminary adjustment of the angles in each quadrilateral is made, as in the sample net, the angles are consistent throughout the net and any chain of directions connecting the two fixed bases may be used. Reference to Fig. 1 shows that the simplest form of the azimuth equation is given by the following combination of directions:

$$-(4) + (6) - (7) + (11) - (12) + (16) - (17) + (19) + 2.50 = 0 \quad \text{(13)}$$

In Eq. 13, the constant term is found by the calculations shown in Table 4.

TABLE 4.—Determination of Constant Term in Eq. 13

Line or angle	Azimuth °	′	″
1−2	124	27	16.53
− 4 + 6	98	33	18.80
− 7 + 11	151	15	22.15
−12 + 16	212	55	46.30
−17 + 19	84	56	23.30
	672	08	07.08
3 × 180°	−540	00	00.00
n−7	132	08	07.08
n−7 (fixed)	132	08	04.58
$\Delta\alpha$			+02.50

The A and B angles are used to write an equation based on the length conditions connecting the two measured bases. Both of these distance measurements should be reduced to the standard elevation governing the coordinates of the two fixed (U. S. C. and G. S.) stations. If the net is to be computed on one of the state-wide systems of coordinates, the field measurement of each base must be reduced to sea level distance, and further corrected to the scale of the standard system.

A system of local coordinates is sometimes preferable for a small area such as a county or metropolitan district. For rural counties, it is customary to reduce all measured distances to sea level datum. In a large city, however, it may be desirable to make the published results of the control survey agree as nearly as possible with values which the local surveyor would find by accurate measurement on the ground. This can be accomplished by a system of local coordinates, reducing all distances (including distances between fixed stations) to a mean elevation selected for the district.

The distance equation for the sample net under consideration is derived from the computations shown in Table 5, and has the form:

$$\begin{aligned} -0.65\,(1) + 0.65\,(3) - 2.09\,(5) + 2.09\,(6) + 0.38\,(7) - 1.09\,(9) \\ + 0.71\,(11) + 1.66\,(12) - 1.66\,(13) - 2.23\,(28) + 2.23\,(29) \\ + 1.55\,(31) - 1.55\,(32) + 8.7 = 0 \quad \text{(14)} \end{aligned}$$

TABLE 5.—DETERMINATION OF COEFFICIENTS IN EQ. 14

Side or angle (1)	Value ° ′ ″ (2)	Log or log sin (3)	Side or angle (4)	Value ° ′ ″ (5)	Log or log sin (6)
1–2....	....	4.1569145	7–n....	....	4.1763685
A_1.....	73 01 44.07	9.9806632 +0.65 (− 1+ 3)	B_1....	53 37 13.57	9.9058528 +1.55 (−31 +32)
A_2.....	45 12 16.41	9.8510300 +2.09 (− 5+ 6)	B_2....	79 42 05.60	9.9929465 +0.38 (− 7+ 9)
A_3.....	71 33 16.55	9.9770948 +0.71 (− 9 +11)	B_3....	51 49 15.84	9.8954690 +1.66 (−12 +13)
A_4.....	43 24 18.54	9.8370533 +2.23 (−28 +29)	B_4....	81 42 53.80	9.9954436 +0.30 (−25 +27)
A_5.....	95 30 23.65	9.9979912 −0.20 (−23 +25)	B_5....	35 00 26.78	9.7586718 +3.01 (−21 +22)
A_6.....	56 44 33.24	9.9223180 +1.38 (−15 +16)	B_6....	84 56 23.30	9.9983041 +0.18 (−17 +19)
		3.7230650			3.7230563
		3.7230563			
log ΔL		+8.7			

A PRACTICAL APPLICATION

The principles and methods described in the preceding section were used to advantage on a triangulation project in Logan County, Ohio, where it was

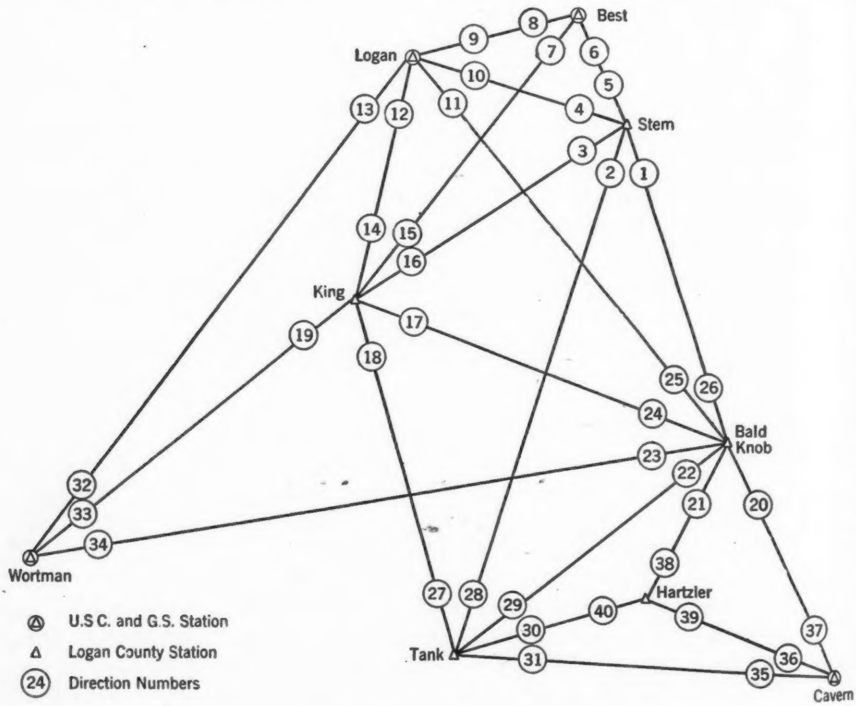

FIG. 4.—TRIANGULATION NET FOR PART OF LOGAN COUNTY, OHIO

decided to develop a sample area between four U. S. C. and G. S. triangulation stations to show some of the problems involved in extending geodetic control in a rural area. In addition, the completed project was intended to illustrate

some of the values of horizontal control for section, township, and other survey corners in such an area. Rolling terrain called for triangulation rather than traverse for the basic control, even considering the fact that triangulation alone does not tie in any section corners.

A reconnaissance party set out to establish a chain of quadrilaterals connecting U. S. C. and G. S. stations "Logan" and "Best" on the north with "Cavern" and "Wortman" on the south. The net shown in Fig. 4 was the result. It has several overlapping figures, a rather undesirable characteristic in a demonstration project, which should be kept as simple as possible. However, triangulation reconnaissance for daylight observation without the aid of towers is not always easy.

TABLE 6.—Coordinates of United States Coast and Geodetic Survey Stations in Logan County Net

Station	U. S. C. and G. S. Coordinates		Local Coordinates	
	Latitude ° ′ ″	Longitude ° ′ ″	North	East
(1)	(2)	(3)	(4)	(5)
Logan....	40 21 38.509	83 45 33.675	79,610.12	97,393.08
Best......	40 21 54.618	83 43 18.054	81,241.39	107,891.53
Cavern...	40 14 59.354	83 40 21.441	39,227.22	121,599.65
Wortman .	40 16 38.714	83 51 06.039	49,228.66	71,628.59
Origin....	40 25 00.000	83 45 00.000	100,000.00	100,000.00

The net shown is well controlled by the U. S. C. and G. S. stations at each of the four extreme corners. It was therefore considered complete in itself and adjusted for final coordinates. Since the project was intended to establish a local coordinate system for the county, the local coordinates of the four known stations were computed as shown in Table 6.

The angles were observed in daylight with a direction theodolite reading to single seconds. Special signals were constructed for the purpose, including two heliotropes for use on the longer lines. Triangle closures on the seventeen triangles averaged 2.23 sec, with a maximum of 5.80 sec.

Least Squares Adjustment

The first adjustment involving nineteen equations (thirteen angle equations and six side equations) was completed by least squares methods commonly used for this type of problem. A set of preliminary adjusted angles resulted which made all triangles in the net entirely consistent, but did not require that the total net fit between fixed triangulation stations in either latitude or departure.

Starting with the fixed line Logan-Wortman and using corrected angles from the first adjustment, the lengths and azimuths of lines Logan-Bald Knob and Bald Knob-Cavern were computed with the triangles shown in Fig. 5. By use of these two lines and the known coordinates of Logan, the local coordinates of Cavern were found to be N 39,228.14 and E 121,599.38, which, when compared with the known coordinates of Cavern given in Table 6, show a closing error of +0.92 ft in latitude and −0.27 ft in departure. This discrepancy cannot be adjusted satisfactorily by any simple arbitrary method such

as is commonly used for traverses, but should be eliminated by small changes in all the angles shown in Fig. 5. Corrections to other angles of the net also will be involved, since the triangle closures and side equation relations set up in the original least squares solution must not be disturbed. To accomplish this result, a complete new solution is needed using the former nineteen condi-

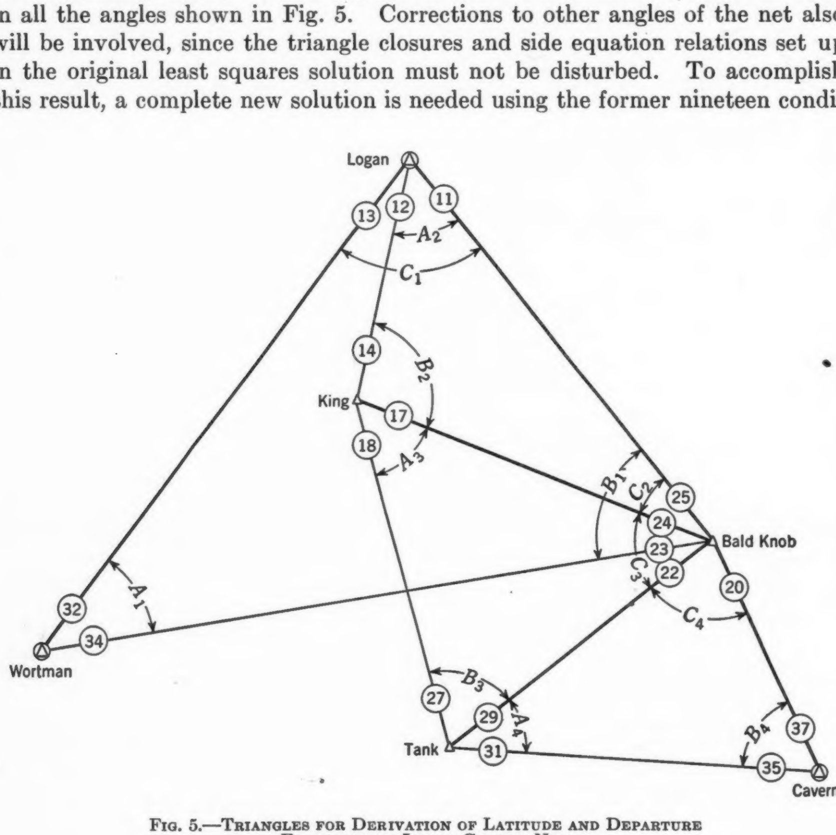

FIG. 5.—TRIANGLES FOR DERIVATION OF LATITUDE AND DEPARTURE EQUATIONS OF LOGAN COUNTY NET

tion equations based on corrected angles plus two additional equations to take out the errors in latitude and departure, respectively. The coefficients for the first nineteen equations will be the same as before, but the constant term will be zero in each case since the adjusted equations are based on corrected angles. The new solution is accomplished efficiently by adding the necessary columns to the tabular form of the preliminary solution.

FORMATION OF LATITUDE AND DEPARTURE EQUATIONS

The latitude and departure equations take the form of Eqs. 10*a* and 10*b*, in which x_n and y_n are the fixed coordinates of the end point, and x_c and y_c are the coordinates of the station at the C angle of each triangle used. Also, the constant terms are

$$\Delta y = y_n - y'_n \qquad (15a)$$

$$\Delta x = x_n - x'_n \qquad (15b)$$

in which x'_n and y'_n are preliminary coordinates of the end point as found from the first adjustment.

Derivation of the coefficients of the latitude and departure equations is greatly facilitated by the tabular arrangement shown in Tables 7 and 8. These tables are similar to Tables 1, 2, and 3 for the sample net of Fig. 1.

TABLE 7.—DATA FOR LATITUDE AND DEPARTURE EQUATIONS OF LOGAN COUNTY NET

Item	Station at *C* Angle (Point of Rotation)			
	Logan	Bald Knob	Bald Knob	Bald Knob
(1)	(2)	(3)	(4)	(5)
Triangle	1	2	3	4
Coordinates[a] N.	79,610.12	54,054.92	54,054.92	54,054.92
Coordinates[a] E.	97,393.08	115,295.23	115,295.23	115,295.23
Angles *A*	43° 24′ 57.0″	51° 23′ 40.2″	53° 31′ 29.4″	40° 45′ 38.0″
Angles *B*	61° 13′ 00.8″	98° 33′ 08.5″	66° 47′ 38.8″	60° 57′ 05.0″
Angles *C*	75° 22′ 02.2″	30° 03′ 11.3″	59° 40′ 51.9″	78° 17′ 17.0″
δ_A	2.22	1.69	1.56	2.44
δ_B	1.16	− 0.31	0.90	1.17
$y_n - y_c$	−40,383	−14,828	−14,828	−14.828
$\dfrac{y_n - y_c}{434{,}294}$	−0.0930	−0.0341	−0.0341	−0.0341
$x_n - x_c$	24,207	6,304	6,304	6,304
$\dfrac{x_n - x_c}{434{,}294}$	0.0557	0.0145	0.0145	0.0145
$\dfrac{y_n - y_c}{434{,}294}\,\delta_A$	− 0.2065	− 0.0576	− 0.0532	− 0.0832
$-\dfrac{y_n - y_c}{434{,}294}\,\delta_B$	0.1079	0.0106	0.0307	0.0399
$\mp\dfrac{x_n - x_c}{206{,}265}$	0.1174	0.0306	0.0306	0.0306
$\dfrac{x_n - x_c}{434{,}294}\,\delta_A$	0.1237	0.0245	0.0226	0.0354
$-\dfrac{x_n - x_c}{434{,}294}\,\delta_B$	− 0.0646	− 0.0045	− 0.0131	− 0.0170
$\pm\dfrac{y_n - y_c}{206{,}265}$	0.1958	0.0719	0.0719	0.0719

[a]Coordinates of end station: N = 39,227.22; E = 121,599.65.

The latitude equation is written by inserting the coefficients in Col. 6, Table 8, using the symbols (11), (12), ···, (37) to denote the unknown corrections. The constant term represents the fixed N-coordinate of the end point (Cavern) minus the computed coordinate of that point, in this case −0.92. Multiplication of the equation by 10 for more convenient use in the solution gives

$$\begin{aligned}&- 0.598\,(11) - 0.576\,(12) + 1.174\,(13) - 0.106\,(14) + 0.638\,(17)\\&- 0.532\,(18) - 0.306\,(20) - 1.079\,(23) + 1.385\,(25) - 0.307\,(27)\\&+ 1.139\,(29) - 0.832\,(31) + 2.065\,(32) - 2.065\,(34) - 0.399\,(35)\\&\qquad + 0.399\,(37) + 9.2 = 0 \quad\ldots\ldots\ldots\ldots\ldots\ldots (16a)\end{aligned}$$

By a corresponding procedure, the departure equation is written from

coefficients in Col. 11, Table 8, as follows:

$$
\begin{aligned}
&- 2.203\ (11) + 0.245\ (12) + 1.958\ (13) + 0.045\ (14) - 0.271\ (17) \\
&+ 0.226\ (18) - 0.719\ (20) + 0.646\ (23) + 0.073\ (25) + 0.131\ (27) \\
&- 0.485\ (29) + 0.354\ (31) - 1.237\ (32) + 1.237\ (34) + 0.170\ (35) \\
&\qquad - 0.170\ (37) - 2.7 = 0 \quad \ldots\ldots (16b)
\end{aligned}
$$

TABLE 8.—COMPUTATION OF COEFFICIENTS IN LATITUDE AND DEPARTURE EQUATIONS FOR LOGAN COUNTY NET

Direction No.	(a) Latitude Equation					(b) Departure Equation				
	Triangle				Final coefficient	Triangle				Final coefficient
	1	2	3	4		1	2	3	4	
(1)	(2)	(3)	(4)	(5)	(6)	(7)	(8)	(9)	(10)	(11)
(11)	−0.1174	+0.0576	....	....	−0.0598	−0.1958	−0.0245	....	....	−0.2203
(12)	....	−0.0576	....	....	−0.0576	....	+0.0245	....	....	+0.0245
(13)	+0.1174	....	....	....	+0.1174	+0.1958	....	....	....	+0.1958
(14)	....	−0.0106	....	....	−0.0106	....	+0.0045	....	....	+0.0045
(15)	....	....	....	....	....	....	....	....	....	....
(16)	....	....	....	....	....	....	....	....	....	....
(17)	....	+0.0106	+0.0532	....	+0.0638	....	−0.0045	−0.0226	....	−0.0271
(18)	....	....	−0.0532	....	−0.0532	....	....	+0.0226	....	+0.0226
(19)	....	....	....	....	....	....	....	....	....	....
(20)	....	....	....	−0.0306	−0.0306	....	....	....	−0.0719	−0.0719
(21)	....	....	....	....	....	....	....	....	....	....
(22)	....	....	−0.0306	+0.0306	....	....	....	−0.0719	+0.0719	....
(23)	−0.1079	....	....	....	−0.1079	+0.0646	....	....	....	+0.0646
(24)	....	−0.0306	+0.0306	....	....	....	−0.0719	+0.0719	....	....
(25)	+0.1079	+0.0306	....	....	+0.1385	−0.0646	+0.0719	....	....	+0.0073
(26)	....	....	....	....	....	....	....	....	....	....
(27)	....	....	−0.0307	....	−0.0307	....	....	+0.0131	....	+0.0131
(28)	....	....	....	....	....	....	....	....	....	....
(29)	....	....	+0.0307	+0.0832	+0.1139	....	....	−0.0131	−0.0354	−0.0485
(30)	....	....	....	....	....	....	....	....	....	....
(31)	....	....	....	−0.0832	−0.0832	....	....	....	+0.0354	+0.0354
(32)	+0.2065	....	....	....	+0.2065	−0.1237	....	....	....	−0.1237
(33)	....	....	....	....	....	....	....	....	....	....
(34)	−0.2065	....	....	....	−0.2065	+0.1237	....	....	....	+0.1237
(35)	....	....	....	−0.0399	−0.0399	....	....	....	+0.0170	+0.0170
(36)	....	....	....	....	....	....	....	....	....	....
(37)	....	....	....	+0.0399	+0.0399	....	....	....	−0.0170	−0.0170

Eqs. 16, when added to the preceding nineteen equations, gave final corrections to the angles, with the result that the position closure on the final station, Cavern, was 0.02 ft in latitude and 0.01 ft in departure. In this manner, the entire supplementary net was made consistent with U. S. C. and G. S. stations in the county. If it is assumed that U. S. C. and G. S. results are acceptable without local verification—certainly a logical assumption for a rural area—this method eliminates the need of measuring a base line or of determining a geodetic azimuth.

AMERICAN SOCIETY OF CIVIL ENGINEERS

Founded November 5, 1852

PAPERS

INVESTIGATION OF DRAINAGE RATES AFFECTING STABILITY OF EARTH DAMS

By F. H. Kellogg,[1] M. ASCE

Synopsis

The investigation described in this paper was undertaken for the purpose of studying the effects of increased rates of reservoir drawdown on the stability of an earth dam. Field observations of the rates of drainage of several dams were compared with rates computed from a method of analysis similar to procedures used in the theory of heat. Computed and observed rates agreed fairly well. To obtain a wider range of comparison, laboratory observations were made of models and sand samples under a variety of conditions. Both analytical and observed results indicated that the possibility of mass slides resulting from reservoir drawdown has been somewhat exaggerated, but that "sloughing" due to a process of flotation or "piping" induced by drawdown may deserve more attention than it has received. Limitations for the method of analysis are suggested.

Introduction

Anyone who has watched a spring during the dry part of the summer must have been impressed with the efficiency of nature's system of rationing, which continuously distributes water stored in some long-forgotten wet season at rates that instantly adjust themselves to the supply on hand. Engineers in many fields have endeavored to learn the mechanics of this system and to apply it to problems of water supply, land reclamation, and stabilization of foundations and subgrades, as well as to petroleum production and agriculture. They have been successful as long as water is constantly supplied to the ground from an external source. When underground pore spaces constitute the only source of outflowing water, engineers must either use empirical rules, with their numerous qualifications and local exceptions, or rely on flights into the realm of theory

Note.—Written comments are invited for immediate publication; to insure publication the last discussion should be submitted by **February 1, 1948.**

[1] Prof. of Civ. Eng., Univ. of Mississippi, University, Miss.

that often require a certain amount of "nature faking" to facilitate mathematical treatment.

It was necessary to choose between these alternatives in searching for a solution to a specific problem, relative to the effect of rate of reservoir drawdown on the stability of an old earth dam. Both were tried. The best results were obtained from an analytical method similar to that used in problems involving heat and consolidation. A description of that method, together with supporting data from field and laboratory observations and a discussion of the application of the results to estimates of slope stability, constitutes the principal part of the subject matter presented in this paper. Some suggestions as to the limitations of the methods used are offered in the hope that other engineers can supply a wider variety of data indicating the applicability of such analyses to drainage problems in general.

The term "steady state" is used to describe a condition of constant rate of seepage and a distribution of heads that does not vary with time. Seepage through a dam when the reservoir is held at constant level, so that all water escaping is replaced from the pool, is an example of this condition. The term "unsteady state" is used to represent a condition of variable rate of seepage and head distribution changing with time. Seepage from a dam during a drawdown, when all escaping water is not replaced, is an example of unsteady state flow. The scope of discussion is limited to those conditions under which Darcy's law is valid. No direct consideration is given to the related subject of consolidation.

Investigation

Specific Problem Involved.—The particular problem that led to the investigations was one of judging the maximum safe rate of drawdown of the reservoir impounded by the Blue Ridge Dam, a semihydraulic fill dam built about 1930, in northwest Georgia. Since 1939, Blue Ridge Dam has been operated as a part of a regional system of power plants.

An operating rule, inherited from the original owner, limited the rate of drawdown of the reservoir to 1 ft per day or 5 ft per week, to prevent "sloughing" of the dam. In 1943, during a period of unprecedented demand for power, this rule caused a bottleneck in the operation of the entire reservoir system. The question arose as to whether the rate of drawdown could safely be increased, and if so, how much.

The problem was attacked by trying to determine the rate of decrease of the hydrostatic pressures exerted by the water in the pores of the embankment, during a given drawdown, so that (*a*) stability against mass sliding could be estimated by "slip circle" analyses,[2] and (*b*) stability against flotation or "piping" could be estimated by analysis of the stresses at the upstream face.[3]

Published Data.—An analysis of seepage in the unsteady state similar to that used in problems of unsteady state heat flow has been applied to ground waters involving very low hydraulic gradients. The method and its fallacies were

[2] "Pendleton Levee Failure," by Kenneth E. Fields and William L. Wells, *Transactions*, ASCE, Vol. 109, 1944, pp. 1400–1429.

[3] "Uplift and Seepage Under Dams on Sand," by L. F. Harza, *ibid.*, Vol. 100, 1935, pp. 1354–1358.

discussed by Morris Muskat,[4] in 1937. Charles V. Theis[5] has used a thermodynamic analogy in computing the rates of drawdown of a pumped well. His computed data show a remarkably close agreement with observations under certain conditions. Mr. Muskat[6] has presented an analysis of steady state flow in which time enters as a boundary condition. This theory specifically applies to the rate of advancement of an oil-water interface. Karl Terzaghi,[7] M. ASCE, discusses the time rate of drainage of an ideal sand through its base. J. H. A. Brahtz[8] considers unsteady state drainage of an earth dam which involves three factors that must be determined in the laboratory—namely, permeability, percentage of air voids, and modulus of compressibility. Lacking the required facilities, the last of these factors could not be determined during this investigation, so no checks on this method could be made.

The various empirical rules generally applied to drainage involve grain size and plasticity. Their application would lead to the conclusion that clays cannot be treated by drainage. This conclusion is contrary to field experience, since many cuts in flocculent clays have been stabilized by drainage.

Since references to such literature as was available gave no procedure readily applicable to the problem at hand, it was decided to study observations of the rate of change of pore-water pressures in various earth dams in the hope of obtaining some empirical rule or of developing an analytical treatment with the aid of factual information not immediately available.

Notation.—The letter symbols in the paper are defined where they first appear, in the text or by illustration, and are assembled for convenience of reference in Appendix I.

Method of Investigation.—For the first stage of the investigation, the pore-water pressures were observed within several earth dams that had been in operation for two years or more. The initial observations were made while the elevations of the impounded reservoirs were held constant at high levels for prolonged periods. Thus, for each observation point, a pressure could eventually be read which would not change with time, indicating a steady state. Later, as the reservoir elevations were lowered, the rates of change of pore-water pressure at each point were compared with the rates of drawdown.

Obviously, any change in hydrostatic pressure indicated by sounding an open well involves a flow of water either into or out of the well. Unless this flow occurs in an infinitely short time, a sounding made during periods of changing water levels will merely represent the apex of a cone of depression or the top of a water cone. The height of such a cone will become progressively greater as the change continues.

Therefore, in this investigation, the same type of measuring devices were

---

[4] "The Flow of Homogeneous Fluids through Porous Media," by Morris Muskat, McGraw-Hill Book Co., Inc., New York, N. Y., 1st Ed., 1937, pp. 363–365.

[5] "The Relation Between the Lowering of the Piezometric Surface and the Rate and Duration of a Well Using Ground-Water Storage," by Charles V. Theis, *Transactions*, Am. Geophysical Union, Vol. 16, 1935, pp. 519–524.

[6] "The Flow of Homogeneous Fluids Through Porous Media," by Morris Muskat, McGraw-Hill Book Co., Inc., New York, N. Y., 1st Ed., 1937, p. 453 et seq.

[7] "Theoretical Soil Mechanics," by Karl Terzaghi, John Wiley & Sons, Inc., New York, N. Y., 1943.

[8] "Notes on Analytic Soil Mechanics," by J. R. Bruggeman, C. N. Zangar, and J. H. A. Brahtz, *Technical Memorandum No. 592*, Bureau of Reclamation, U. S. Dept. of the Interior, Denver, Colo., 1939, pp. 122–135.

used that are employed in reading pore-water pressures in silts and clays.[9] Special pressure cells, reading to 0.1 in. of hydrostatic head, were developed for use in studying model embankments. The purpose of these cells was to disturb the natural flow of pore water during drainage as little as possible by the pressure measurement.

Since pore pressures in an earth dam sometimes rise as the reservoir falls (for example, curve C, Fig. 1(*b*)), they have been converted to values that will be more sensitive indicators of response to reservoir fluctuations. These values are expressed in terms of "potential head." Potential head at a given point is defined as the sum of the pressure head at that point, $u_w \gamma$, plus the additional head between that point and the drain, $z_p - z_d$, or

$$h = z_p - z_d - \frac{u_w}{\gamma} \qquad (1)$$

in which h is potential head, at a given pore pressure cell; z_p is the elevation of that cell; z_d is the elevation of the drain or outlet; u_w is the pore pressure reading; and γ is the unit weight of water. Fig. 2(*a*) illustrates this conception. The dotted curves in Fig. 2(*a*) represent contours of potential head at zero time (initial steady state), and the curves marked by arrows represent lines of flow.

In Fig. 2(*b*), hydrographs have been plotted showing the variation in potential heads at various points within a sand model embankment during a drawdown of the pool impounded by that embankment. The potential heads (ordinates) were computed, from readings of pore pressure cells, by Eq. 1. Where observed values of head for zero time differed from those taken from the theoretical flow net of Fig. 2(*a*), the former were used in Fig. 2(*b*). The topmost curve of Fig. 2(*b*), marked "Pool," shows the time rate of drawdown of the pool. Comparing the hydrographs of the cells with the hydrograph of the reservoir, a functional relationship between the rate of change of reservoir level and the rate of change of potential head at each cell location is noted at once, whereas such a relationship is less readily apparent if only the rate of change of pore pressure is studied. (Compare Fig. 2(*b*) with Fig. 2(*c*).) Fig. 2(*b*) shows clearly how the rate of change of potential head during an unsteady state increases as the downstream toe or drain of the dam is approached.

A most important approximation revealed by such hydrographs was that, over most of the dam at least, all cells with a given potential head during periods of constant pool level would show the same hydrographs during periods of changing reservoir level, regardless of the locations of the cells. The hydrographs of cells 0 and 5, or of cells 2, 3, and 4 in Fig. 2(*b*), illustrate this. Such an observation does not hold in regions which, at the time of observation, are well above the level of the pool at that same time.

These properties of the hydrographs of pore pressure cells strongly invite the development of an empirical rule. In fact, one was formulated which expressed, quite closely, the rates of drainage for two particular dams. However, it indicated that rate of drainage is independent of permeability. Since these two dams involved extremely slow rates of drawdown, the effects of permeability

[9] "Measurement of Pore-Water Pressure in Silt and Clay," by K. Terzaghi, *Civil Engineering*, January, 1943, pp. 33–36.

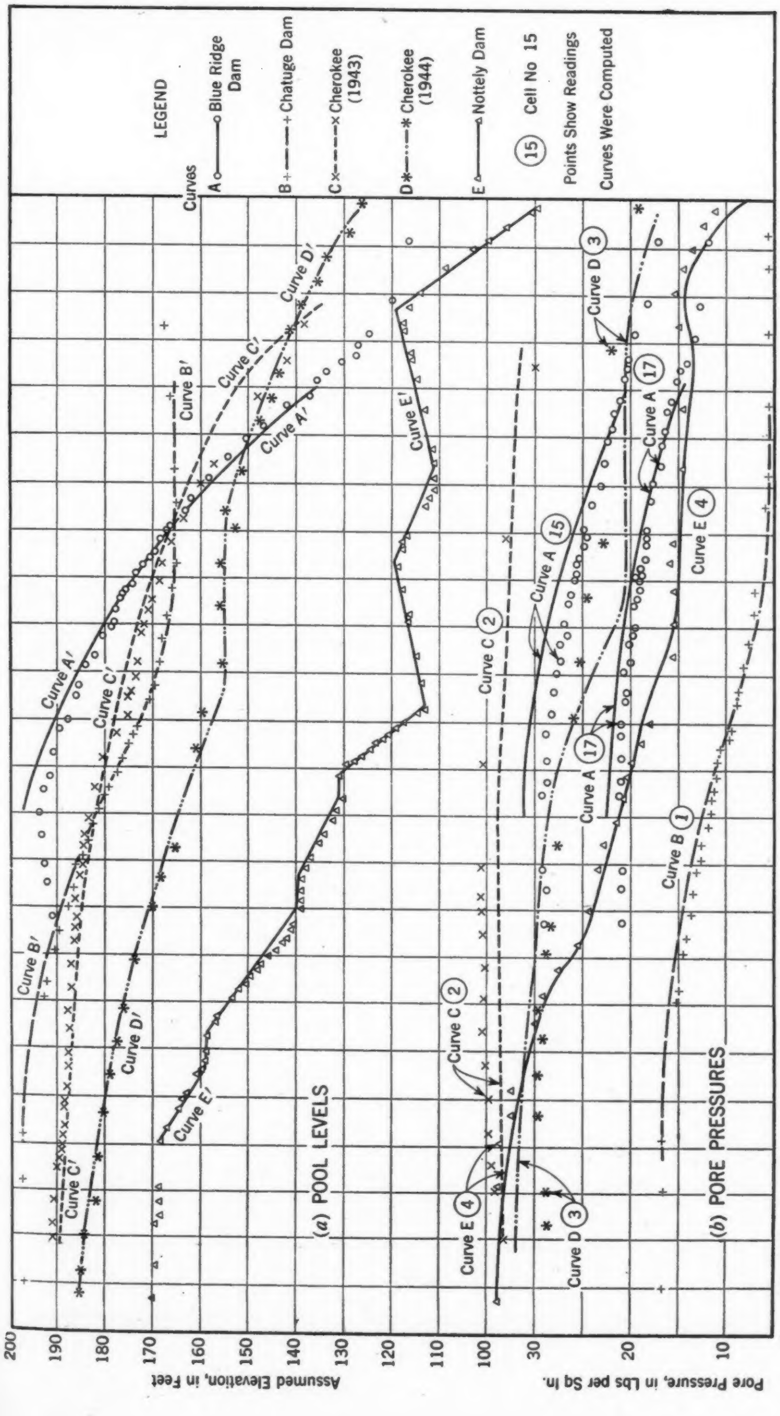

FIG. 1.—COMPARISON OF COMPUTED AND OBSERVED PORE PRESSURES

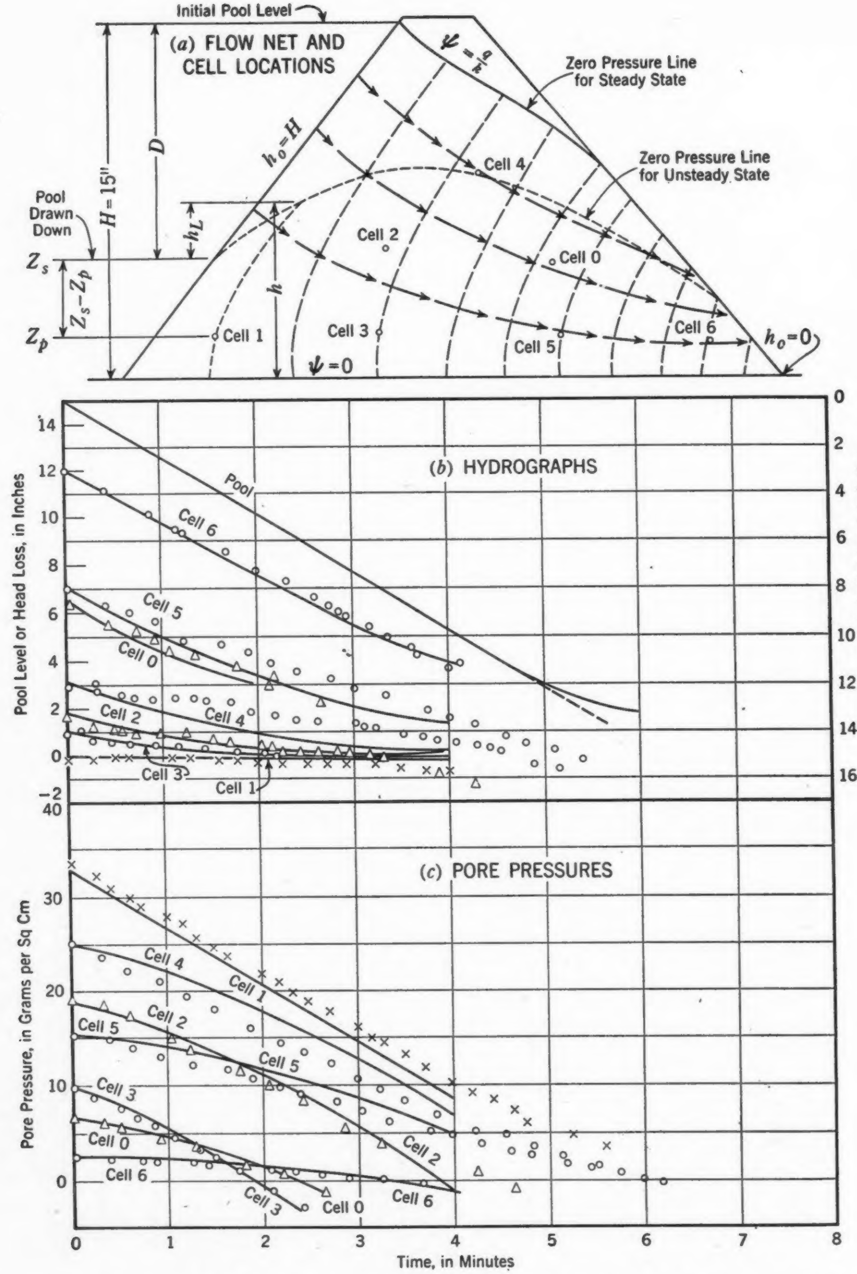

FIG. 2.—DRAINAGE OF SAND MODEL RESULTING FROM THE DRAWDOWN OF IMPOUNDED WATER

were so little as to be negligible, but the empirical rule holding for them could not be extended very far. After following various statistical studies "around a circle," such methods were abandoned in favor of a physical analysis of the problem.

Analogy Between Seepage and Heat Flow.—An analogy between unsteady state heat flow and flow of pore water squeezed from the pores of a clay during consolidation has been described in some detail by Professor Terzaghi and O. K. Froelich.[10]

In the structures involved in the present investigation, however, no definite evidences of consolidation were found, either from settlement measurements or from pore pressure observations. This section of the paper therefore refers to the problem of drainage from pore spaces, the volume of which is assumed to remain essentially constant. As one working hypothesis, the assumption has been made that under this condition analyses of drainage similar to those used in problems involving heat flow and consolidation can still be used, at least within limits.

In seepage, Darcy's law states that the average velocity is proportional to the hydraulic gradient, from which it follows, as shown in Appendix II, that the net quantity of water flowing in time dt out of an element of porous material having a volume $dx\,dy\,dz$ is $k\nabla^2 h\,dx\,dy\,dz\,dt$, in which h is the drop in head across the element and k is the permeability coefficient. In heat flow, the Biot-Fourier law states that quantity of heat per unit area is proportional to the temperature gradient, so that the net quantity of heat flowing out of an element in time dt is $k'\,\nabla^2\,T'\,dx\,dy\,dz\,dt$, in which k' is the coefficient of heat transmission and T' is the difference in temperature across the element. This quantity can also be expressed in another way: Specific heat is defined as the ratio $q_s:q_w$, in which q_s is the quantity of heat required to raise 1 g of transmitting substance 1° C and q_w is the quantity required to raise 1 g of water 1° C. Since this latter quantity may be considered as one calory, specific heat multiplied by unity gives the number of calories required to raise 1 g of conducting medium 1° C. In a volume $dx\,dy\,dz$, of this medium, there are $\rho\,dx\,dy\,dz$ grams, in which ρ is density in grams per cubic centimeter. Therefore, calling specific heat c', the quantity of heat required to raise an element of conducting medium dT' degrees is $c'\,\rho\,dx\,dy\,dz\,dT'$. If this quantity flows in time dt, then:

$$k'\,\nabla^2\,T'\,dx\,dy\,dz\,dt = c'\,\rho\,dx\,dy\,dz\,dT' \qquad (2)$$

or

$$\frac{k'}{c'\,\rho}\nabla^2\,T' = \frac{\delta T'}{\delta t} \qquad (3)$$

Eq. 3 is the basis of the classical analyses of heat flow in the unsteady state. The factor $\frac{k'}{c'\,\rho}$ is called the "diffusivity" of the conducting medium. If a relationship similar to Eq. 3 could be demonstrated for seepage, a wealth of analytical technique would be available for problems of drainage. For such

[10] "Theorie der Setzung von tonschichten," by K. Terzaghi and O. K. Froelich, F. Deuticke, Leipzig 1936.

an analogy to exist, there must be a constant w_d such that

$$\frac{k}{w_d} \nabla^2 h = \frac{\delta h}{\delta t} \qquad (4)$$

or

$$k \nabla^2 h \, dx \, dy \, dz \, dt = w_d \, dx \, dy \, dz \, dh \qquad (5)$$

The quantity $k/w_d = c_d$ would then be a constant characteristic of the porous medium in which drainage takes place, expressing potential speed of drainage. It will be designated as the "drainability" of the material, to emphasize the analogy with diffusivity in heat transmission.

Transposing Eq. 5,

$$\frac{k \nabla^2 h \, dx \, dy \, dz \, dt}{dx \, dy \, dz} = w_d \, dh \qquad (6)$$

If "yield" is defined as the volume of water drained without replacement from a unit volume of porous material, then the left-hand side of Eq. 6 represents the yield in time dt. Designating yield w_y, Eq. 6 may be written

$$\frac{dw_y}{dh} = w_d \qquad (7)$$

The constant w_d must therefore be defined as the volume of water that can be drained from a unit volume of porous material by a unit change in head. It will be designated as "specific drainage."

In Appendix II, various solutions of Eq. 4 are given. Values of pore pressures and yields computed from these solutions have been compared with field and laboratory observations. After these comparisons are summarized, the significance of the factors designated as drainability and specific drainage will be discussed further.

Procedure for Checking.—Observations of pore pressures were first made on earth dams that had been in operation for some time. Then, to check the conditions found and to extend them under controlled rates of drawdown, studies were made of model embankments in which a steady state was allowed to develop before applying drawdowns at uniform rates. Finally, to check the methods of computation against some factor other than pore-water pressure, sand samples were saturated and permitted to drain, the yield at various times being measured. In these samples, horizontal drainage and vertical drainage were observed separately. Also, both drainage under gravity alone and drainage under constant air pressure held at one end of the sample were studied.

For dams and model embankments, pore pressures were computed from Eq. 1, using Eqs. 30 in Appendix II to approximate values of potential head. Eqs. 30 are the result of a very crude analysis, but a rigorous solution of the problem could not be made, and the method used serves to give a fair estimate as long as points in the region of zero or negative hydrostatic pressure are not considered and as long as the drawdown is not so rapid as to leave the largest part of the region of positive hydrostatic pressure above the pool level at the time of computation.

The first steps in the computations were to take the observed pore pressure

for one cell and one time and to compute the drainability from Eqs. 30. Next, this value was inserted in Eqs. 30, and the pore pressure for this cell at other times was computed, for comparison with observed values. Finally, using the same value of drainability, the pore pressures at other cells at various times were computed. However, when laboratory tests indicated a considerable variation in materials at different cells, a new value of drainability was determined for each cell.

For sand samples, a drainage index was considered, defined as the yield at any given time divided by the total yield under the conditions considered. Eq. 24 in Appendix II was used for horizontal drainage; and Eqs. 25 and 26 were used for vertical drainage. The drainability was first computed from the drainage index observed at one time, and this value was used to compute the drainage indexes at other times for comparison with observations.

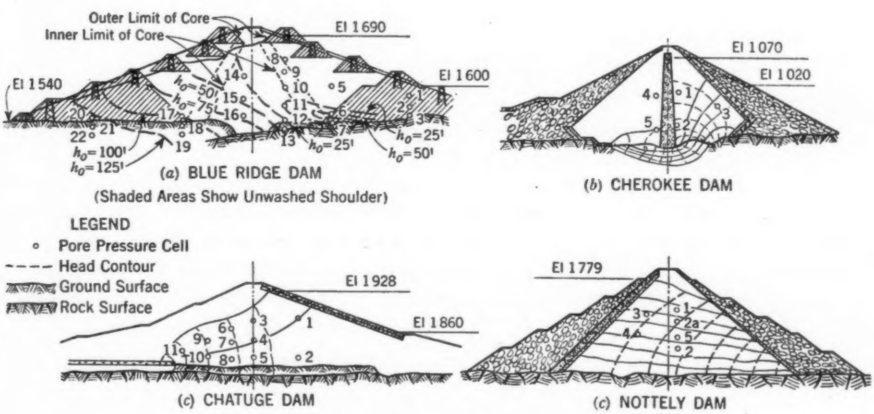

Fig. 3.—Typical Sections of Dams

Comparison of Computed and Observed Data.—The operation of the reservoirs impounded by four earth dams was such as to permit the attainment of a steady state of seepage, followed by an unsteady state induced by drawdown. Fig. 3 shows typical cross sections of these dams and the head contours during the initial steady state as determined from readings of pore pressure cells. Fig. 1(*a*) shows reservoir hydrographs for drawdown periods during which pore pressure readings were taken. Fig. 1(*b*) shows a few typical pore pressure-time curves. The curves were computed, whereas the points represent actual observations.

In general, computed pore pressures did not vary from those observed by more than 2 lb per sq in. In one case, where the cell reading was only 2 lb per sq in., and the cell was above pool level at the time of reading, a variation of 5 lb per sq in. was noted. However, since the analysis used becomes invalid at points within the embankment higher than pool level, a check could not be expected.

For Chatuge Dam, in southwestern North Carolina, and Cherokee Dam, in eastern Tennessee, a single value of drainability served to check all cells.

For Blue Ridge and Nottely dams both in northwestern Georgia, a value which would check observations at a given cell for one time would agree for other times, but not for other cells. A considerable variation in permeability was found in these two dams. Table 1 gives test data which serve to describe the materials in the various dams.

TABLE 1.—TEST VALUES FOR MATERIALS IN OBSERVED DAMS

Structure	Sand[a] (%)	Clay[a] (%)	Liquid limit	Plasticity index	Permeability coefficient[b]
Blue Ridge Dam (Georgia):					
Shoulder	73	5	....[c]	....[c]	0.3 to 3.0
Foundation	....	....	....[c]	....[c]	2.0 to 6.0
Core	52 to 73	5 to 17	30 to 42	2 to 9	0.003 to 0.007
Chatuge Dam (North Carolina)	64 to 76	4 to 8	45 to 47	4 to 15	0.0003 to 0.005
Cherokee Dam (Tennessee)	15 to 32	28 to 51	41 to 66	20 to 41	0.000008 to 0.00008
Nottely Dam (Georgia)	55 to 94	5 to 39	35 to 43	4 to 23	0.0003 to 0.2

[a] Percentage of the total sample, by dry weight. Particles with equivalent diameter greater than 0.05 mm are classified as sand and those with equivalent diameters less than 0.005 mm are classified as clay. [b] Feet per day. [c] Nonplastic.

Nine model embankments were studied, three of which were made of standard Ottawa sand, three of graded Ottawa sand, and three of a fine, micaceous sand. Four different linear rates of drawdown were used for each model. Fig. 2(*a*) shows a cross section of one of the models, with cell locations and a theoretical flow net. The material is assumed to be isotropic. Fig. 2(*b*) shows the typical hydrograph for one drawdown, and hydrographs for six pore pressure cells during that drawdown. The points represent observations. The curves are plotted from Eqs. 30, Appendix II, using the following data:

Specific drainage w_d	0.23
Permeability k, in inches per minute	0.8
Initial head H, in inches	15
Ratio of head loss to arc length $\Delta h_o/\Delta s_f$	0.6
Drainability, c_d	41.7
B	0.66

In the foregoing—

$$B = \frac{\pi^2 c_d}{H}\left(\frac{\Delta h_o}{\Delta s_f}\right)^2 \qquad (8a)$$

and

$$c_d = \frac{k}{w_d} \qquad (8b)$$

In Fig. 2(*b*) w_d is the specific drainage.

The value of the hydrograph of each cell at zero time represents the observed potential head during the initial steady state. Cells 2 and 3 show appreciably different initial values from those indicated by the theoretical flow net of Fig. 2(*a*). In Fig. 2(*c*), the hydrographs of the cells have been converted into pore pressure-time curves by Eq. 1. Results for other observations of model embankments are quite similar to those shown in Fig. 2, and to the results obtained from field observations on dams during drawdown.

The computed values shown in Figs. 1 and 2 have been obtained on the basis of steady state flow nets derived from readings of pore pressure cells. The question naturally arises as to how these computations would have checked had theoretical flow nets been used as a basis. The head distribution shown in Fig. 3 for Blue Ridge Dam is obviously unlike any that could be obtained theoretically. Since the dam is a semihydraulic fill with a fairly pervious foundation and considerable variation in the permeability of the flow system, this condition is not surprising. The flow nets for Chatuge, Cherokee, and Nottely dams are somewhat different from the corresponding theoretical flow nets for isotropic embankments. By assuming various values of anisotropy for each dam (calling "anisotropy" the ratio of permeability in a horizontal direction to that in a vertical direction), a fair agreement between observed and theoretical heads could be obtained for one particular value. The highest value of anisotropy that had to be used to obtain agreement between theoretical and observed flow nets was 50 at Guntersville Dam (in northern Alabama), but, usually, the value was between 1 and 4. Ordinarily, a theoretical flow net is made assuming an anisotropy of 1 or some other arbitrarily chosen value. Under such conditions, pore pressures computed for the unsteady state could be considerably in error.

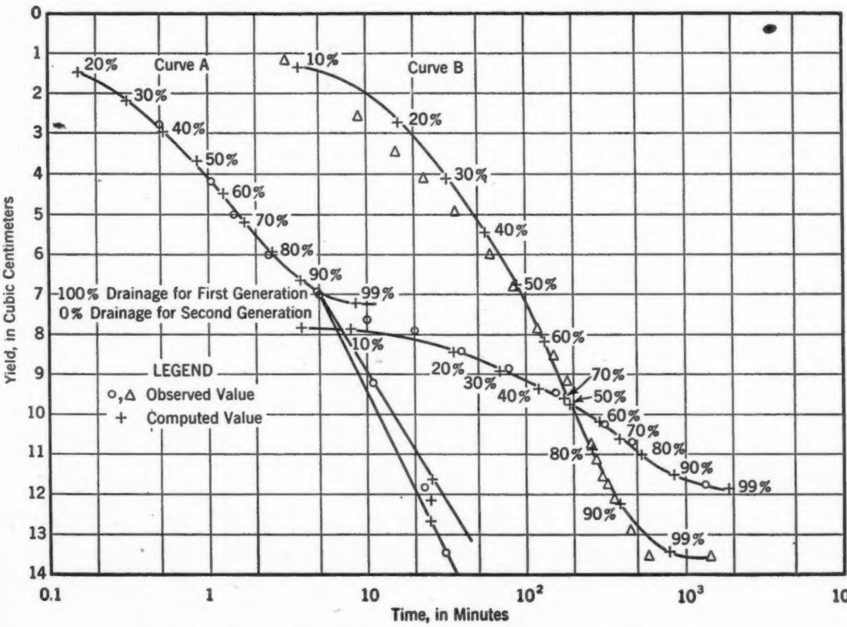

FIG. 4.—COMPARISON OF OBSERVED AND COMPUTED YIELDS

Fig. 4 shows the volume of water drained from a sand sample by gravity alone, plotted against time. Drainage occurred through vertical planes at each end of the sample. Curve A represents results for graded Ottawa sand, and curve B those for a micaceous sand, all of which passes United States

standard sieve No. 30, and is retained on a No. 200 sieve. The curves were computed by Eq. 24 in Appendix II, and the points represent actual observations. The two generations of drainage indicated by curve A seem to be characteristic of medium-grained to coarse-grained sands, and indicate that there may be several independent flow systems in a sand, of which the most permeable is the only one of practical significance.

Similar comparisons were obtained when all water flowed vertically, draining from the base of the sample. Drainage was induced in this case by gravity plus a constant external stress, maintained by applying a constant air pressure at the top of the sample. The curves were computed from Eqs. 24 and 25 applied to Eq. 26 in Appendix II.

Applications

Slope Stability.—The stability of a slope against mass sliding may be estimated by the "slip circle" method. Field evidence indicates this method is satisfactory for analyzing slope stability if the pore pressures are known.[2] In the case of an earth dam subjected to drawdown of its impounded reservoir, the pore-water pressures are frequently considered as those that would exist if no drainage whatsoever were to occur. Under such an assumption, the "factor of safety" for Blue Ridge Dam was computed as 0.95, indicating that the dam should not be standing. Using Eqs. 30 in Appendix II and Eqs. 1 in the text to estimate the pore pressures, and considering the maximum rate of drawdown due to water passing through the turbines in the powerhouse, the slip circle "factor of safety" was computed as 1.5.

Flotation Due to Drawdown.—Distinct from the question of mass sliding is the possibility of "sloughing" of the upstream slope during drawdown. This condition, frequently associated with a rapid lowering of reservoir levels, is distinguished from mass sliding in that it is local in extent, and would only lead to complete failure of the dam by progressive action over a period of time. It is suggested that such "sloughing" may be the result of a process of flotation or "piping," in which the seepage forces induced by drainage out of the upstream slope produce a quicksand. Since the hydraulic gradient at pool level during a drawdown may theoretically approach infinity, due to convergence of flow, a critical condition exists at this level when drawdown rates are rapid. A filter adequate to resist the seepage forces and to prevent washing of fill through its voids would obviously be a preventive measure. Usually, filters are not carried much below pool level at maximum drawdown.

Below pool level, there is still a possibility of flotation if the seepage forces, which are directed normal to the face of the dam, exceed the weight and frictional resistance of the embankment material. The inset in Fig. 5 shows a conception of the force polygon at the upstream face, in which F_i is the seepage force; F_ϕ is the frictional force; W is the buoyed weight; and ϕ is the angle of internal friction. The vector F_i represents the seepage force required for equilibrium. The actual seepage force at the end of a given period of drawdown may be expressed as $\gamma\, i$, in which γ is the unit weight of water and i is the hydraulic gradient at the upstream face at the time considered. Eq. 36 in Appendix II has been derived to express the approximate value of i for a

constant rate of drawdown. Knowing this value, a factor of safety against flotation can be expressed as

$$S = \frac{F_i}{\gamma\, i} \qquad (9)$$

For Blue Ridge Dam, such a factor of safety was computed for a drawdown of 90 ft at 2 ft per day as 2.23. Similar computations indicated that a quick

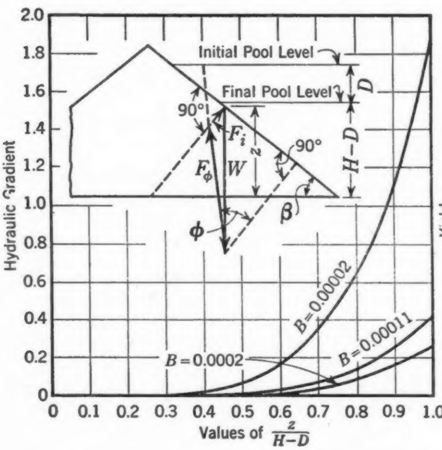

FIG. 5.—FACTORS THAT AFFECT THE PIPING RESULTING FROM DRAINAGE

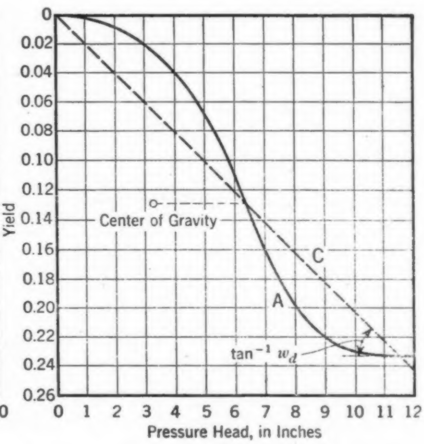

FIG. 6.—YIELD-PRESSURE CURVE (GRADED OTTAWA SAND)

condition would be imminent at the upstream face when the rate of drawdown increased to 5.3 ft per day. Actually, the rate has been increased from the old limit of 5 ft per week to 2 ft per day without harmful effects. The additional water supply made available by such an increase represents an appreciable monetary value.

The distribution of hydraulic gradient along the upstream face at points below minimum pool level is shown by the curves in Fig. 5 for materials of three different drainabilities. These curves suggest the desirability of filter protection below minimum pool level when the embankment material is not obviously free draining and the drawdown rate is appreciable.

SIGNIFICANCE OF DRAINAGE CONSTANTS

Pore Pressures in Media of Low Permeability.—Field observations of pore-water pressures in dams composed of relatively impervious materials indicate pressure drops quite similar to those that would be expected for nearly free draining media—contrary to the usual assumption that a relatively impervious material develops high excess hydrostatic pressures which dissipate very slowly. In this section, an effort will be made to explain such behavior.

Consider a porous body, such as an embankment, submerged in a pool of water so that its top is level with the water surface and imagine this body to be completely saturated. The body can be visualized as a plexus of intercom-

municating capillary channels of varying cross section. If the level of the pool is now lowered slightly, the water will remain in these capillary channels, and a meniscus will form at the top of each channel. The pore water is held above the surface of the pool by capillarity.[7] To idealize for a moment, if the channel were a circular cylinder, the upward force holding the water above pool level would be $2 \pi r \sigma_w \sin \beta$, in which r is the radius of the channel; σ_w is the surface tension of water; and β is the angle made by the meniscus with the horizontal. Resisting this force would be the weight of water above the pool, $\pi r^2 \gamma D$, in which D is the height of the meniscus above the pool. For equilibrium, $D = h_c$, the height of the capillary water column, and

$$2 \pi r \sigma_w \sin \beta = \pi r^2 \gamma h_c \qquad (10)$$

Solving for h_c:

$$h_c = \frac{2 \sigma_w \sin \beta}{r \gamma} \qquad (11)$$

Actually, the capillary channels are not cylindrical; they are not even uniform. However, the general relationship—

$$h_c = \text{constant} \times \frac{\sin \beta}{L} \qquad (12)$$

—may be considered to hold. In Eq. 12, L is the distance between the walls of the pore channel.

As the pool level drops further, more of the force of surface tension is mobilized to resist a drop of the water level in the pore channels by an increase in the curvature of the meniscus which increases the value of the angle β in Eqs. 11 and 12. The maximum value of $\sin \beta$ is unity, of course, and at this value the full force of surface tension is brought to resist a drop in pore-water level. In a relatively fine material, the pore width, L of Eq. 12, may be so small that a quite appreciable drawdown may occur with no drop in pore-water level ($D = h_c$). For example, in Cherokee Dam, at a distance of 70 ft above the free surface of the water, negative pore pressure and complete saturation (within the limits of accuracy of the tests used) were observed. Under such conditions (barring consolidation), the pore pressures vary from $-D$ at the top of the embankment, to zero at pool level, to $+h$ at a distance h below pool level (expressing pressure as equivalent head), and decrease as rapidly as the pool is drawn down. Thus, a relatively impervious embankment could show rates of decrease of hydrostatic pressure during drawdown similar to those exhibited by a free draining structure. In terms of Eq. 4, the permeability k is low and the yield per unit head w_d is zero; therefore, the drainability k/w_d is infinite.

Suggested Limitation of Analysis.—Eq. 12 represents a condition of equilibrium in which the pressure head created by the weight of water in the capillary channel h_c balances an equivalent force, expressed as head, which is created by surface tension. For equilibrium, the drawdown D is equal to the capillary head h_c, and the maximum value of D or h_c for this equilibrium in a channel of given width occurs when $\sin \beta = 1$. When $D > h_c$, Eq. 12 may be expressed as

$$D - \frac{\text{constant}}{L} = D - h_c = h \qquad (13)$$

in which h is the head available to produce flow in the capillary channel. The value of L is obviously not constant, but varies over a wide range, possibly similar to the variation in sizes of grains. Therefore, during a drainage due to drawdown, the largest pore channels will drain first whereas, in the smaller channels, there will simply be increases in curvatures of the menisci without appreciable loss of water. Thus, each increment of drawdown will drain water from successively smaller channels.

To illustrate these relationships, a cylinder of sand, 4 in. in diameter and 5 in. high, open at the top and base, was saturated and its base submerged. The air pressure at the top was adjusted so that the sand would remain saturated without flow. Then the pressure at the top was increased by an equivalent of 2 in. of hydrostatic head and the sand was allowed to drain until no additional water was added to the yield during a 24-hour period. This procedure was repeated at 2-in. head increments until no more water could be forced out of the sand. The total yield at the end of each pressure increment was plotted against the pressure head as shown in Fig. 6.

Although the equilibrium conditions in this experiment are different from those expressed in Eqs. 10 to 13, the principle that there is a capillary head, varying inversely as the width (or "diameter") of the capillary channel at the air-water interface (which head must be overcome by a greater force to produce drainage) holds in either case. In either case, when the pressure head is zero, there is no yield. Furthermore, the yield approaches a maximum value, beyond which there is no additional drainage. This value is called "specific yield" in ground-water hydrology;[11] and the test for specific yield is similar to that for the centrifuge moisture equivalent of a soil. Moreover, since pressure is a function of pore size, and yield, of pore diameter, the yield-pressure curve can be considered as a rough example of a pore-size distribution curve. Then, if there is any truth in the assumption that grain size is an index of pore size (as implied in the "effective size" hypothesis), the yield-pressure curve should have the same general characteristic shape as does a grain-size distribution curve—that is, it should suggest a probability curve, as does the curve in Fig. 6.

To apply the concept of the yield-pressure curve to the analyses in this paper, it is necessary to consider the draining mass as homogeneous, or better, as uniformly heterogeneous. In any element, the grain-size distribution and the pore-size distribution must be considered the same as in any other element. Consider an element at the top of the draining medium, containing pore spaces of every size in the range of the material. In any one of these pore channels, if there is a force F_d promoting drainage, and an equal capillary force, h_c, resisting drainage, there is no flow. If the force F_d is increased by an infinitesimal amount, dF_d, there is an increase in capillary resistance to $h_c + dh$ in those channels too small to permit flow, and seepage under a head not greater than $dh = dF_d$ in the larger channels. The yield increases by an amount dw_y. This increase eventually becomes smaller as successively smaller pore spaces are drained by additional increments of drawdown. Eventually, as the total yield approaches the value of specific yield, dw_y approaches zero. Therefore,

[11] "The Occurrence of Ground Water in the United States," by O. E. Meinzer, *Water-Supply Paper No. 489*, U.S.G.S., U. S. Govt. Printing Office, Washington, D. C., 1923.

the relationship in Eq. 7 ($dw_y/dh = w_d$) can at best be only an approximation. At the value of the specific yield, $dw_y/dh = w_d = 0$, and Eq. 4 becomes

$$\nabla^2 h = 0 \qquad (14)$$

which is the differential equation for steady state flow.

Since, as a material becomes finer, the specific yield becomes less and the pressure at which the value of specific yield is approached becomes greater, the curve is better approximated by a straight line, $dw_y/dh = w_d$, as indicated by the dashed line in Fig. 6. As the value of specific yield is exceeded, the straight line approximation becomes untenable. It is concluded, therefore, that analysis of drainage problems by methods analogous to those used for determining the unsteady state of heat flow is an approximation that can hold only as long as drainage water can be taken from the capillary zone. After all drainable water has been removed from the porous body, air must enter the entire surface of the porous body; and, from Eq. 14, the ensuing drainage follows the laws of the steady state. It is suggested that, in such a steady state, the source is the surface of the draining mass, the inflowing material is air, and the process is similar to one analyzed by Mr. Muskat for the rate of advancement of an oil-water interface.[6]

Since this study was made in connection with a specific problem relating to production rather than as a research project, sufficient data to support or refute the suggestions given herein as to the limitations of the analysis were not obtained. This treatment has been included only in the hope that additional information may be available which will better define the range of validity of the analysis.

Conclusions

Ordinarily, when an earth dam is subjected to drawdown of its impounded reservoir, it is assumed that the internal hydrostatic pressures will decrease very slowly, if at all, unless the slopes of the dam are composed of relatively permeable material. Such a slow decrease would materially reduce the stability of the dam. Therefore, substantial sums of money have been spent in securing large quantities of pervious materials for the upstream shoulders of earth dams, or in constructing dams with very flat slopes.

Field observations summarized in this paper indicate that, in materials of relatively low permeability, the hydrostatic pressures may decrease about as rapidly as in pervious materials, with little or no reduction in stability. These observations were in fairly good agreement with hydrostatic pressures computed from analyses similar to those used in problems of heat transmission and consolidation of clays. Such computations also agreed fairly well with observations made in the laboratory on model embankments and on volumes of water drained from sand samples under both gravity and induced pressures. Materials observed included clays, silts, and sands.

The analyses indicate that speed of drainage depends not only on permeability, but also on the volume of water that can be drained. For example, standard Ottawa sand is more permeable than graded Ottawa sand, but requires more time to drain because more water can flow out of the same volume

of sand. The potential rate at which a given material can drain is expressed by a constant designated as "drainability," which is the quotient of the permeability coefficient over the volume of water, per unit head, that can be drained from a unit volume of the material. If this latter quantity should be zero, as it would be in a fine material in which all water is held in the pore spaces by capillarity, the drainability would be infinite, regardless of the magnitude of the permeability coefficient, and the pore pressures would decrease during a drawdown just as fast as they would for a material with a permeability coefficient of infinity. Of course, if the fine material were not well consolidated, so that the capillary forces transmitted to the grain structure resulted in consolidation, the pore pressures would be higher and their rates of decrease would be slower.

Silts and fine sands, which have neither permeability sufficient to permit drainage by a rapid escape of water from the pores, nor yields low enough to offset this drainage, are considered the most difficult materials to drain, and the least desirable materials for the upstream shoulder of a dam.

The data given in this paper indicate that earth slopes subjected to drawdown are more likely to develop local failures from flotation or "piping" action of water draining out of the face of the slope, than to fail by mass sliding. The likelihood of flotation decreases with distance below the surface of the pool, but under certain conditions, it could occur at appreciable distances beneath the surface of the pool, if not protected by an adequate filter.

Although this investigation has not been extended far enough to determine the limits of the analyses, it is tentatively suggested that the analyses will hold as long as the total head inducing drainage does not exceed the head required to remove all drainable water from the material considered. An alternative method of attack for cases beyond this limit has been suggested but not developed. From a practical viewpoint, it is considered that cases beyond this limit would be confined to pervious sands subjected to drawdowns of considerable magnitude.

Acknowledgment

The experimental work described in this paper was done under the auspices of the Tennessee Valley Authority (TVA). The views expressed are those of the writer, and do not necessarily reflect those of the TVA.

APPENDIX I. NOTATION

As far as consistently possible, the following letter symbols conform with "Soil Mechanics Nomenclature," ASCE Manual of Engineering Practice No. 22, and with American Standard Letter Symbols for Hydraulics (Z10.2—1942) and for Heat and Thermodynamics (Z10.4—1943):

B = a simplifying exponent defined by Eq. 29*b*;
b = rate of drawdown;
c_d = drainability analogous to diffusivity or specific heat c'; $c_d = k/w_d$;

D = distance of drawdown at any given time, the total drawdown being designated D';

d = drainage index, expressed as the ratio of the volume drained to a given time to the total volume drained (see Eq. 26):

d_1 = drainage ratio due entirely to gravity;

d_2 = drainage ratio due entirely to pressure;

e = base of Naperian logarithms;

F = force—

F_i = seepage force required for equilibrium, the "actual" or general seepage force being $F'_i = \gamma\, i$;

F_d = a force that promotes drainage;

F_ϕ = internal friction force;

f = any function, as defined in the text; distinction between functions, are designated f_1, f_2 (Eq. 16*b*), or f' (Eqs. 30);

H = total head;

h = head at a given time or section; potential head:

h_c = height of capillary rise;

h_L = head loss due to flow;

h_o = potential head during the initial steady state;

i = hydraulic gradient at the upstream face at a given time;

k = permeability coefficient analogous to the coefficient of heat transmission k';

L = any distance, as defined in the text;

n = an integer having successive values 1, 2, 3, $\cdots$;

q = flow during the initial steady state, between a given point and any convenient fixed datum such as an impervious base;

q_s = quantity of heat required to raise 1 g of transmitting substance 1° C;

q_w = quantity of heat required to raise 1 g of water 1° C;

R = time ratio, t/t_d (Eqs. 30);

r = radius; polar coordinate (see θ);

S = safety factor;

s = length of arc:

s_f = length of arc, measured along a flow line;

s_h = length of arc, measured along a head contour;

T = temperature; T'' = difference in temperature across an element;

t = time; t_d = duration of drawdown;

u_w = pore pressure reading;

V = volume;

v = velocity of flow;

W = weight;

w = volume of water drained:

w_d = specific drainage (Eq. 7); the volume that can be drained from a unit volume of porous material by a unit change of head;

w_y = yield; the volume that is drained, without replacement, from a unit volume of porous material;

x = Cartesian coordinate;

y = Cartesian coordinate;
z = vertical coordinate, or elevation above an indicated base:
  z_d = elevation of drain or outlet;
  z_p = elevation of pore pressure cell;
  z_s = elevation of reservoir surface at any given time;
β = angle with the horizontal, as the slope angle in Fig. 5;
γ = unit weight of water;
θ = polar coordinate of arc (see r);
λ = a substitution factor used to simplify the typography of a complex exponent (see Eq. 23*b*);
ρ = density, in grams per cubic centimeter;
σ_w = surface tension of water;
τ = substitution factor used to simplify the typography of a complex exponent (see Eq. 23*a*);
ϕ = angle of internal friction;
ψ = a parameter equal to q/k; and
∇ = an operator.

APPENDIX II. MATHEMATICAL TREATMENT

Coordinate System.—For a system of any given geometry there is a characteristic flow net; therefore, it would be convenient to consider this flow net as a curvilinear coordinate system, in which the position of any given point is fixed by the intersection of a head contour with a flow line. The coordinates of the point would then be designated by the parameters h_o and ψ, h_o being the numerical value of the head contour during the initial steady state and ψ being equal to q/k—in which q is the flow between the point considered and any convenient datum such as an impervious base (during the initial steady state) and k is the permeability of the medium considered.

The lengths of arc along these curvilinear coordinates are

$$ds_f = dh_o \sqrt{\left(\frac{\delta x}{\delta h_o}\right)^2 + \left(\frac{\delta z}{\delta h_o}\right)^2} = \frac{dh_o}{f_1} \qquad (15a)$$

and

$$ds_h = d\psi \sqrt{\left(\frac{\delta x}{\delta \psi}\right)^2 + \left(\frac{\delta z}{\delta \psi}\right)^2} = \frac{d\psi}{f_2} \qquad (15b)$$

From Darcy's law,

$$d\psi = \frac{dh_o}{ds_f} ds_h \qquad (16a)$$

Therefore:

$$ds_f\, ds_h = \frac{dh_o}{f_1} \frac{d\psi}{f_2} = \frac{(dh_o)^2\, ds_h}{f_1\, f_2\, ds_f} \qquad (16b)$$

and

$$(ds_f)^2 = \frac{(dh_o)^2}{f_1\, f_2} = \frac{(dh_o)^2}{f^2_1}; \qquad \text{and} \qquad f_1 = f_2 \qquad (17)$$

It can be shown[12] that, in a curvilinear coordinate system of two dimensions, the operator ∇^2 becomes

$$\frac{\delta^2}{\delta x^2} + \frac{\delta^2}{\delta z^2} = f_1 f_2 \left(\frac{\delta}{\delta h_o} \frac{f_1}{f_2} \frac{\delta}{\delta h_o} + \frac{\delta}{\delta \psi} \frac{f_2}{f_1} \frac{\delta}{\delta \psi} \right) \ldots\ldots\ldots\ldots (18)$$

or, from Eq. 17: In one dimension—

$$\frac{\delta^2}{\delta x^2} = f_1 \frac{\delta^2}{\delta h^2_o} \ldots\ldots\ldots\ldots (19a)$$

in two dimensions—

$$\frac{\delta^2}{\delta x^2} + \frac{\delta^2}{\delta z^2} = f^2_1 \left(\frac{\delta^2}{\delta h^2_o} + \frac{\delta^2}{\delta \psi^2} \right) \ldots\ldots\ldots\ldots (19b)$$

and, in three dimensions—

$$\frac{\delta^2}{\delta x^2} + \frac{\delta^2}{\delta y^2} + \frac{\delta^2}{\delta z^2} = f^3_1 \left(\frac{\delta^2}{\delta h^2_o} + \frac{\delta^2}{\delta \rho^2} + \frac{\delta^2}{\delta \psi^2} \right) \ldots\ldots\ldots\ldots (19c)$$

Derivation of Differential Equation.—In a rectangular element, $dx\,dy\,dz$, in which v_x, v_y, and v_z are velocity components parallel to the x-axis, y-axis, and z-axis, respectively, the volume of water flowing in time dt is:

Flow	Formula	
Inflow parallel to the x-axis........	v_x	$\times\, dy \times dz \times dt$
Outflow parallel to the x-axis......	$\left(v_x + \frac{\delta v_x}{\delta x}\, dx \right)$	$\times\, dy \times dz \times dt$
Net Flow—		
Parallel to the x-axis............	$\frac{\delta v_x}{\delta x}\, dx$	$\times\, dy \times dz \times dt$
Parallel to the y-axis............	$\frac{\delta v_y}{\delta y}\, dx$	$\times\, dy \times dz \times dt$
Parallel to the z-axis............	$\frac{\delta v_z}{\delta z}\, dx$	$\times\, dy \times dz \times dt$
Total volume of flow.............	$\left(\frac{\delta v_x}{\delta x} + \frac{\delta v_y}{\delta y} + \frac{\delta v_z}{\delta z} \right)\ dx$	$dy\, dz\, dt$

Since Darcy's law may be expressed as

$$v = -\, k\, \nabla\, h \ldots\ldots\ldots\ldots (20a)$$

this total volume can be written as

$$V = -\, k\, \nabla^2\, h\, dx\, dy\, dz\, dt \ldots\ldots\ldots\ldots (20b)$$

From the definition of specific drainage, this volume can also be expressed as

$$V = -\, w_d\, dh\, dx\, dy\, dz \ldots\ldots\ldots\ldots (20c)$$

[12] "Higher Mathematics for Engineers and Physicists," by Ivan S. Sokolnikoff and Elizabeth S. Sokolnikoff, McGraw-Hill Book Co., Inc., New York, N. Y., 1934, pp. 361–363.

Equating the two expressions, Eqs. 20*b* and 20*c*, and assuming $k/w_d = c_d$,

$$c_d \nabla^2 h = \frac{\delta h}{\delta t} \quad \text{(21a)}$$

From Eqs. 19, Eq. 21*a* becomes, in curvilinear coordinates:

$$c_d f^2{}_1 \left(\frac{\delta^2 h}{\delta h^2{}_o} + \frac{\delta^2 h}{\delta \psi^2} \right) = \frac{\delta h}{\delta t} \quad \text{(21b)}$$

Solution for Horizontal Drainage.—Consider a saturated porous body with length much greater than height—that is, $x \gg z$, and allow it to drain at the ends, $x = 0$ and $x = L$. Then $\frac{\delta h}{\delta z} = 0$ and Eq. 21*a* becomes

$$c_d \frac{\delta^2 h}{\delta x^2} = \frac{\delta h}{\delta t} \quad \text{(21c)}$$

The boundary conditions are: $h = 0$ when $x = 0$, $x = L$, $t = \infty$; and $h = H$ when $t = 0$. The solution is analogous to that used for consolidation tests and is

$$h = \frac{4\,H}{\pi} \sum_{n=1}^{n=\infty} \frac{1}{2\,n - 1}\, e^{-\lambda \tau} \sin \frac{(2\,n - 1)\,\pi\,x}{L} \quad \text{(22)}$$

in which, to simplify typography:

$$\tau = \frac{4\,c_d\,t}{L^2} \quad \text{(23a)}$$

and

$$\lambda = \frac{(2\,n - 1)^2\,\pi^2}{4} \quad \text{(23b)}$$

In Eqs. 22 and 23, n is an integer having successive values 1, 2, 3, $\cdots$. The drainage ratio is the ratio of the volume of water removed up to any given time to the total volume of water that can be drained under the existing conditions. For this case, by analogy with settlement computations,

$$d = 1 - \frac{8}{\pi^2} \sum_{n=1}^{n=\infty} \frac{1}{(2\,n - 1)^2}\, e^{-\lambda \tau} \quad \text{(24)}$$

In the solution of Eq. 24, settlement tables may be used to simplify computations.

Solution for Vertical Drainage.—Consider a saturated porous body draining vertically through its base. For this case,

$$d = 1 - \frac{16}{\pi^3} \sum_{n=1}^{n=\infty} \frac{(2\,n - 1)\,\pi + 2\,(-1)^n}{(2\,n - 1)^3}\, e^{-\lambda \tau} \quad \text{(25a)}$$

$$\frac{u_w}{\gamma} = f(t, z) - \frac{1 - d}{d}\, z \quad \text{(25b)}$$

and

$$f(t, z) = \frac{4\,H}{\pi^2} \sum_{n=1}^{n=\infty} \frac{(2\,n - 1)\,\pi + 2\,(-1)^n}{(2\,n - 1)^2}\, e^{-\lambda \tau} \quad \text{(25c)}$$

Now suppose that a constant air pressure is applied at the upper end of the porous body, amounting to a pressure head F_d. Disregarding the effect of gravity, the drainage ratio due to this pressure only can be found from Eq. 24, with z substituted for x. The drainage ratio for the case of gravity drainage alone is given by Eqs. 25. Then, by reasoning analogous to that used in settlement problems, the drainage ratio for the combined pressure and gravity drainage is

$$d = \frac{H\, d_2 + 2\, F_d\, d_1}{H + 2\, F_d} \qquad (26)$$

in which d_1 is the drainage ratio due to gravity alone and d_2 is that due to pressure alone.

Drainage of an Earth Dam.—In the preceding section, all flow is assumed to take place along straight lines. Then the boundary conditions could be expressed in terms of x-coordinates and z-coordinates, so that solutions of Eq. 21a could be expressed as series that would converge to the initial head distribution when the time $t = 0$. In most drainage problems of practical significance, the lines of flow are curved, with curved boundaries, as, for example, the "line of seepage" in an earth dam. Therefore, the coordinate system formed by the resulting flow net is curvilinear. In such a case, f_1, which appears in Eq. 21b and is defined in Eqs. 15, is no longer a constant, but varies with h_o and ψ. Hence, Fourier series solutions will no longer satisfy the differential equation. In heat transmission problems, where there are usually boundaries of elementary geometry, polar or elliptical coordinates can be used to express the boundary conditions. Then series converging to $h = h_o$ when $t = 0$ can be obtained by use of Bessel functions or Lamé functions. Unfortunately, flow nets for most drainage conditions of practical significance cannot be so idealized. Often, they defy analysis, and are determined by successive approximation or graphical estimate. Hence, the following approximation method has been used to compute rates of drainage of earth dams.

Consider the condition:

$$f_1 \sim \frac{\Delta h_o}{\Delta s_f} \qquad (27)$$

in which Δh_o is the head drop between two adjacent equipotential lines in a steady state flow net derived by graphical methods, and Δs_f is the length of a flow line between them. A glance at any of the flow nets in Figs. 2 or 3 will show that, over considerable sections of an earth dam, the ratio is nearly constant. The greatest variations occur near the drain and near the upstream slope, and the greatest errors involved in assuming f_1 as constant will be at these boundaries. However, any equation used to approximate the value of h and conforming to the boundary conditions, $h = 0$ when $h_o = 0$ and $h = H - D$ when $h_o = H$, must approach the same numerical values as these boundaries are approached. Furthermore, the observations described in the text indicate that (at least at appreciable distances below the free surface), $\delta h/\delta\psi = 0$, for earth dams subjected to drawdown. Hence, if the approximate differential equation—

$$c_d \left(\frac{\Delta h_o}{\Delta s_f}\right)^2 \frac{\delta^2 h}{\delta h^2_o} = \frac{\delta h}{\delta t} \qquad (28)$$

—is used to express drainage from an earth dam, the maximum error resulting from the assumption that $f_1 = \Delta h_o/\Delta s_f$ = constant occurs in the boundary regions where the values of h must approach the correct values anyway, as long as the solution satisfies the boundary conditions.

Under these assumptions, the following boundary conditions may be considered: When $t = 0$, $h = h_o$ (initial steady state); when $t = \infty$, $h = \frac{H - D'}{H} h_o$ (final steady state); when $h_o = 0$, $h = 0$; and when $h_o = H$, $h = H - D'$. Considering the drawdown, D', as instantaneous, a solution of Eq. 28 is

$$h = \left(1 - \frac{D'}{H}\right) h_o + \frac{2\,D'}{\pi} \sum_{n=1}^{n=\infty} \frac{(-1)^{n+1}}{n} e^{-n^2 B t} \sin \frac{n\,\pi\,h_o}{H} \quad \text{.....(29a)}$$

in which

$$B = \frac{\pi^2\,c\,(\Delta h_o/\Delta s_f)^2}{H^2} \quad \text{.....(29b)}$$

Actually, of course, the drawdown of a reservoir is never instantaneous, but varies as function of time, $D = f(t)$. Still, it can be imagined as the net result of a series of infinitesimal instantaneous drawdowns which immediately follow one another. The magnitude of each of these drawdowns may be considered as $d(D) = f'(t)\,dt$. If any one of these drawdown increments occurs at time t, if t_d is the time during which all of them occur, and if $R\,t_d$ is the time for which a value of h is desired, the drawdown D' in Eq. 29a can be replaced by $f'(t)\,dt$; and t, by $R\,t_d - t$ (the time interval during which the drawdown increment was effective). Thus, the head due to this increment can be computed. The sum of the heads, due to all such increments occurring up to time t_d (or up to time $R\,t_d$, if $R\,t_d < t_d$), is then the head resulting from the gradual drawdown. Hence, when $R \leqq 1$:

$$h = \left[1 - \frac{f(t)}{H}\right] h_o + \frac{2}{\pi} \sum_{n=1}^{n=\infty} \frac{(-1)^{n+1}}{n} \left(\sin \frac{n\,\pi\,h_o}{H}\right) \times \int_0^{R\,t_d} e^{-n^2 B (R\,t_d - t)} f'(t)\,dt \quad \text{....(30a)}$$

and, when $R \geqq 1$:

$$h = \left[1 - \frac{f(t)}{H}\right] h_o + \frac{2}{\pi} \sum_{n=1}^{n=\infty} \frac{(-1)^{n+1}}{n} \left(\sin \frac{n\,\pi\,h_o}{H}\right) \times \int_0^{t_d} e^{-n^2 B (R\,t_d - t)} f'(t)\,dt \quad \text{....(30b)}$$

Flotation Due to Drawdown.—Assuming that an adequate filter protects the upstream face of an earth dam down to the lowest elevation which the reservoir will reach, then only that part of the face which is always below pool level need be considered. In this region, as suggested by readings of pore pressure cells and as confirmed by watching the flow of dye in models subjected to drawdown, the flow is directed upstream and normal to the face. Therefore, the force polygon is as shown in Fig. 5. The value of the vector F_i in Fig. 5 represents the seepage force at equilibrium. Since the actual seepage force is $\gamma\,i$, in which i is the hydraulic gradient at the upstream face, Eqs. 30 may be used to compare

the seepage force induced by a given drawdown of the reservoir with that required for equilibrium.

For zero time, corresponding to an initial steady state, the distribution of head near the upstream face of an earth dam resting on an impervious base may be computed from a conjugate function transformation.[13] The appropriate solution is

$$h_o = H - \frac{2\,\beta}{\pi}\left(\frac{r \sin \beta}{H}\right)^{(\pi-2\beta)/(2\beta)} \cdot \cos \beta \cos \frac{\pi\,\theta}{2\,\beta} \qquad (31)$$

in which h_o is the potential head referred to the impervious base; H is the maximum potential head; β is the angle made by the upstream face with the horizontal; and r and θ are the polar coordinates of a point referred to the upstream toe as an origin.

The hydraulic gradient along the upstream face is therefore the normal derivative of the head,

$$\text{Gradient } h_o = \left(\frac{r}{H} \sin \beta\right)^{(\pi-2\beta)/(2\beta)} \cos \beta \qquad (32)$$

or, if i is the hydraulic gradient and z is the distance of any point along the upstream face from the impervious base, $r = z \csc \beta$ and

$$i_{t=0} = \left(\frac{z}{H}\right)^{(\pi-2\beta/(2\beta)} \cos \beta \qquad (33)$$

During a drawdown, the hydraulic gradient at the upstream face at any time is gradient $h = \frac{dh}{ds_f} = \frac{\delta h}{\delta h_o}\frac{dh_o}{ds_f}$; or:

$$i = \left(\frac{z}{H}\right)^{(\pi-2\beta)/(2\beta)} (\cos \beta) \frac{\delta h}{\delta h_o} \qquad (34)$$

The value of $\frac{\delta h}{\delta h_o}$ may be obtained from Eqs. 30. If the drawdown proceeds at a constant rate, $D = b\,t$, then $f'(t)\,dt$ in Eqs. 30 may be replaced by $b\,dt$. Integrating as indicated in Eqs. 30 and then differentiating with respect to h_o, for the upstream face (where $h_o = H$):

$$\frac{\delta h}{\delta h_o} = 1 - \frac{b\,t_d}{H} - \frac{2\,b}{B\,H}\sum_{n=1}^{n=\infty} \frac{1}{n^2}(1 - e^{-n^2 B t_d}) \qquad (35)$$

Placing Eq. 35 in Eq. 34, the hydraulic gradient is

$$i = \left(\frac{z}{H}\right)^{(\pi-2\beta)/(2\beta)} (\cos \beta) \left[1 - \frac{b\,t_d}{H} - \frac{2\,b}{B\,H}\sum_{n=1}^{n=\infty}(1 - e^{-n^2 B t_d})\right] \qquad (36)$$

In numerical computations, the hydraulic gradient obtained from Eq. 36 is positive when flow is directed away from the upstream face and negative when directed into the dam. Eq. 36, like Eqs. 30, from which it was derived, is not valid above pool level at any given time.

[13] "Flow of Homogeneous Fluids through Porous Media," by Morris Muskat, McGraw-Hill Book Co., Inc., New York, N. Y., 1st Ed., 1937, p. 343.

AMERICAN SOCIETY OF CIVIL ENGINEERS

Founded November 5, 1852

DISCUSSIONS

MISSISSIPPI RIVER CUTOFFS

Discussion

BY E. J. WILLIAMS, JR., AND EUGENE A. GRAVES

E. J. WILLIAMS, JR.,[18] AND EUGENE A. GRAVES,[19] ASSOC. MEMBERS, ASCE. —An insight into the planning and execution of the cutoffs on the Lower Mississippi River, the results as far as high-water stage reductions are concerned, the technique employed, and the pitfalls to be avoided are all presented in this interesting paper. The main objective of the cutoffs, as stated by the author,

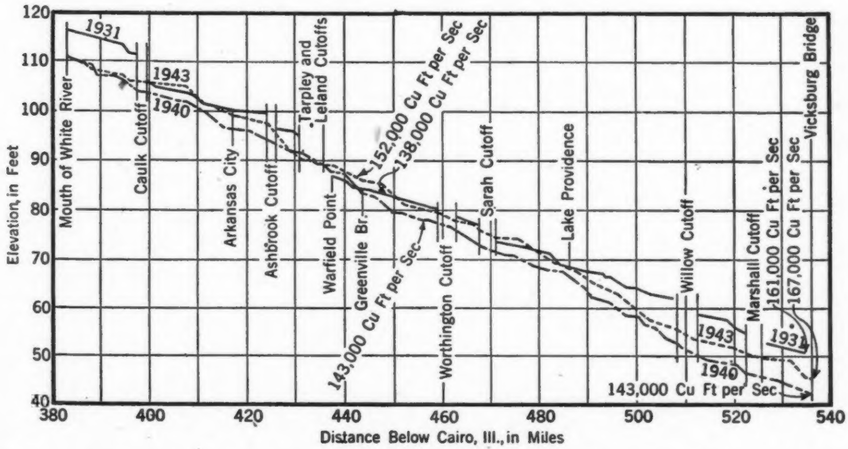

FIG. 7.—COMPARISON OF LOW-WATER PROFILES BEFORE AND AFTER CUTOFFS ON MISSISSIPPI RIVER; MILEAGE BASED ON 1937 SURVEY, BUT MEASURED THROUGH ALL CUTOFFS

was to lower flood heights. In this they have been highly successful. Effects on low-water flow have been slight, but perhaps warrant consideration.

The low-water profile (Fig. 7) is composed of a series of alternately steep and flat slopes, which become more accentuated at lower stages. Steep, low-

NOTE.—This paper by Gerard H. Matthes was published in January, 1947, *Proceedings*. Discussion on this paper has appeared in *Proceedings*, as follows: March, 1947, by W. E. Elam, C. L. Hall, H. D. Vogel, and Harry N. Pharr; and June, 1947, by Lytle Brown, and Anson Marston.

[18] Engr., Mississippi River Comm., Vicksburg, Miss.

[19] Engr., Mississippi River Comm., Vicksburg, Miss.

water slopes generally occur at the foot of shallow crossings, whereas pools between the crossings are generally so deep that very little slope is required to handle the low-water flow. The least depth available varies greatly from year to year, and in a random manner. This is more or less the nature of the river, which normally builds up its crossings during periods of high water and scours them during falling stages and low water in a varying degree, depending on a number of conditions cataloged hereafter. The slopes at the crossings are variable as they depend on: How much the crossings were built up during high stages; the rapidity of the fall; the length of crossing; the toughness of material on the bottom; the amount of dredging; and, possibly, other factors.

The easily erodible crossings are lowered first and a large part of the fall transferred to the ones which do not erode so easily, thus making dredging necessary to assist the natural action of the river at these points. During the low-water periods immediately following the creation of each cutoff, it was necessary to perform more than the normal amount of dredging at the crossings in the upstream reach affected by the cutoff. The excess dredging requirements reduced rapidly from year to year, however, as the local drawdown occasioned by the cutoff was gradually distributed over a considerable reach of the river.

TABLE 5.—LOW-WATER SLOPES OBSERVED BEFORE AND AFTER CUTOFFS

Cutoff designation	Opening date	Distance (mile)[a]	Fall (Feet)				Slope (Foot per Mile)				Discharge[b] (1,000 Cu Ft per Sec)			
			Oct. 2, 1931	Dec. 21, 1937	Oct. 18, 1940	Nov. 11, 1944	Oct. 2, 1931	Dec. 21, 1937	Oct. 18, 1940	Nov. 11, 1944	Oct. 2, 1931	Dec. 21, 1937	Oct. 18, 1940	Nov. 11, 1944
(1)	(2)	(3)	(4)	(5)	(6)	(7)	(8)	(9)	(10)	(11)	(12)	(13)	(14)	(15)
Marshall....	3–12–34	8.4	3.5	3.2	1.8	2.7	0.42	0.38	0.21	0.32	138	135	121	178
Willow......	4– 8–34	37.6	11.7	19.6	18.8	19.8	0.31	0.52	0.50	0.53	138	130	121	177
Sarah.......	3–23–36	4.9	1.8	4.0	2.9	2.3	0.37	0.82	0.59	0.47	138	130	115	179
Worthington.	12–25–33	23.2	6.7	6.2	11.5	9.8	0.29	0.27	0.50	0.42	138	130	115	180
Tarpley.....	4–21–35	4.4	1.0	2.7	1.3	3.2	0.23	0.61	0.30	0.73	138	127	112	181
Ashbrook....	11–19–35	24.2	5.9	9.4	8.7	7.5	0.24	0.39	0.36	0.31	138	127	112	182
Caulk.......	5–13–37	35.0	8.6	....	11.6	12.1	0.25	....	0.33	0.35	138	....	110	182
Average.....	....	....	....	....	....	....	(0.30)	(0.50)	(0.40)	(0.45)	....	....	....	....

[a] Distance from head of cutoff to foot of next cutoff above, measured by 1930 low-water mileage for the 1931 conditions and by 1940 low-water mileage for the 1937 and 1944 conditions. [b] Approximate discharge.

Table 5 shows, by comparison, the changes in slopes in the reaches immediately above the heads of the cutoffs. The slopes above the cutoffs have naturally retained some increase, but there is a tendency for the river to adjust the low-water slope and to improve the steep reaches. This is evident from Fig. 8, which shows the comparison of slopes for 1944 and 1946 for the reach above Hardin Cutoff, which was made in 1942. Just how much adjustment can be expected and how long it will take are not known.

The result of the increase in low-water slopes is an increase in low-water velocities. It does not follow that the maximum low-water velocity is increased but it is possible that such is the case. The low-water velocity seldom exceeds

4 ft or 5 ft per sec, however, and is generally much lower; also dredging can be used to correct any troublesome reach. There has been no noticeable decrease in depths since the opening of the cutoffs. Low-water navigation has been maintained and low-water navigation depths have not been seriously affected. In view of the facts that the river has been materially shortened, and that a number of troublesome reaches have been eliminated in the old bend ways, low-water navigation has definitely been improved by the cutoffs.

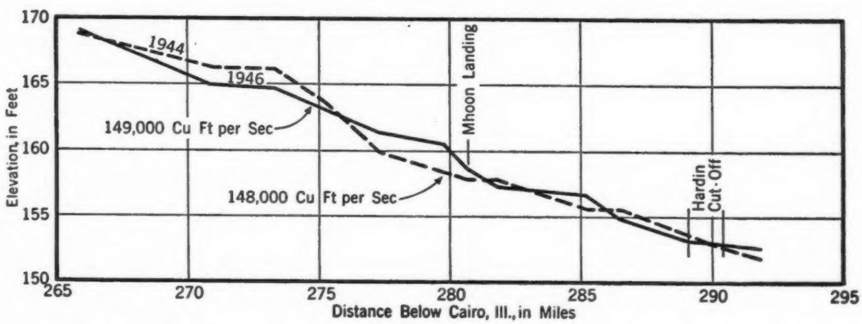

FIG. 8.—LOW-WATER PROFILES ABOVE HARDIN CUTOFF TO SHOW SLOPE ADJUSTMENT AFTER CUTOFF DEVELOPMENT

Loss of valley storage tends to increase flood flows below the cutoffs, as stated by Mr. Matthes. Leaving the old bend ways open saves only a small part of the storage, as lowerings in the backwaters, where large areas have been unwatered, have reduced the available flood storage by a considerable amount. Computations indicate that there is some increase in peak flow as a result of the cutoffs. However, cutoffs below the backwater areas combined with other developments, such as the increased capacity of the Atchafalaya River, in Louisiana, have more than compensated for the increased flow and no resultant stage increase is apparent.

In time of high water the greater depth provides over the wide crossings a large and efficient cross section for flow. The high-water slopes are more uniform than the low-water slopes, being largely independent of those channel features which predominate during low water. For this reason, during high water the lowering effect may extend a considerable distance upstream immediately after the development of the cutoff. To show any progressive changes in high-water slopes, a base year preceding the opening of each cutoff was selected and the slope for this year has been compared with the slopes for years after the opening of the cutoffs.

High-water slope data, in the form of increments of slope over the slope for the base year, are summarized in Table 6 according to the number of years intervening between the opening of the cutoff and the year in question. It will be noted that the increments shown are, in each case, the total increase since the base year and not the annual increase. Practical difficulties have precluded obtaining strictly comparable slope data over a long period of years. This has

resulted in the omission of a number of cutoffs from the tabulation, which shows that the average increase in high-water slope resulting from the cutoffs is about 0.1 ft per mile. The average slope for these reaches before the cutoffs was about 0.3 ft per mile, and after the cutoffs about 0.4 ft per mile.

TABLE 6.—INCREASE IN HIGH-WATER SLOPES IN REACH ABOVE EACH CUTOFF FOLLOWING OPENING OF CUTOFF[a]

Cutoff designation	NUMBER OF YEARS FOLLOWING OPENING OF CUTOFF											
	1	2	3	4	5	6	7	8	9	10	11	12
(1)	(2)	(3)	(4)	(5)	(6)	(7)	(8)	(9)	(10)	(11)	(12)	(13)
Hardin	0.18	0.17	0.11	....	....	....	....	....	....	....	....	....
Jackson	0.04	0.03	0.04	....	....	....	....	....	....	....	....	....
Caulk	....	0.10	....	....	....	0.12	0.11	0.05	....	....	....	....
Ashbrook	0.14	....	0.14	....	....	....	0.19	0.21	0.21	....	....	....
Worthington	....	....	0.04	....	0.07	....	....	....	0.09	0.15	0.12	....
Willow	....	....	0.00	....	0.04	....	....	....	0.09	0.06	0.04	....
Diamond	....	....	....	0.10	....	0.09	....	....	....	0.12	0.11	0.15
Rodney	0.06	....	0.08	....	....	....	0.09	0.07	0.05	....	....	....
Giles	....	....	....	0.05	....	0.08	....	....	....	0.11	0.07	0.07
Average[b]	(0.10)	(0.10)	(0.07)	(0.08)	(0.06)	(0.10)	(0.13)	(0.11)	(0.11)	(0.11)	(0.08)	(0.11)

[a] Increment in slope, in feet per mile, for year shown over slope for base year preceding opening of the particular cutoff. [b] Average total increase to year shown: Average total increase for 12-yr period, 0.096 ft per mile.

AMERICAN SOCIETY OF CIVIL ENGINEERS

Founded November 5, 1852

DISCUSSIONS

DEVELOPMENT AND HYDRAULIC DESIGN, SAINT ANTHONY FALLS STILLING BASIN

Discussion

BY DONALD E. BLOTCKY, M. M. CULP, PAUL BAUMANN, A. J. PETERKA, AND LOUIS M. LAUSHEY

DONALD E. BLOTCKY,[3] ASSOC. M. ASCE.—Criteria for design of the Saint Anthony Falls (SAF) stilling basin (Minneapolis, Minn.) are based on scour conditions considered satisfactory in the movable bed model. Because of the limited knowledge of the mechanics of energy dissipation, empirical equations must be used. However, it is desirable to submit such equations to a rational analysis, thus striving toward the goal of explaining all hydraulic phenomena by rational methods.

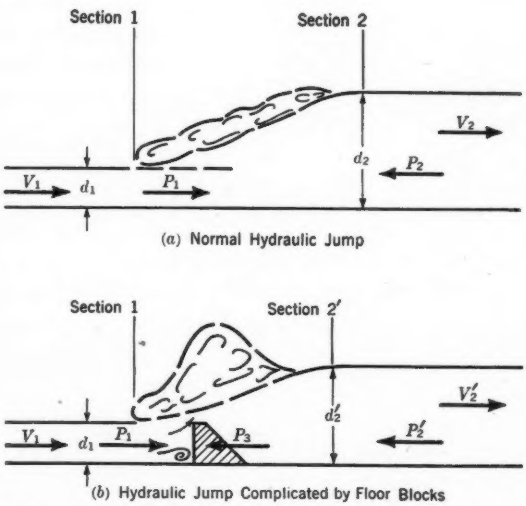

FIG. 18.—VELOCITY, DEPTH, AND PRESSURE RELATIONSHIPS IN HYDRAULIC JUMPS

It is the writer's belief that use of the theoretical equation for the hydraulic jump (Eq. 2) is undesirable where formation of the jump is aided by blocks and sills.

Energy dissipation can be divided into two categories as far as stilling basin action is concerned: First, that in which the energy is dissipated due to impact of water on water; and, second, that in which energy is dissipated due to impact of water on a submerged solid object and the impact of water on water.

NOTE.—This paper by Fred W. Blaisdell was published in February, 1947, *Proceedings*.

[3] Office Engr., T. C. Forrest, Jr., Cons. Engr., Dallas, Tex.

In the first case, exemplified by the hydraulic jump, the degree of energy loss is well known (27).[3a] In the analytical solution of the hydraulic jump (Fig. 18(*a*)), the phenomenon starts at the toe of the jump, at Section 1, and has a theoretical end of jump at Section 2, which is located at the point of maximum d_2. It should be noted that the jump acts from Section 1 to Section 2 without interference. Eq. 2 relates the various parts of the jump as shown in Fig. 18(*a*). The second case (Fig. 18(*b*)) is usually a hydraulic jump with floor blocks added, and will hereinafter be called a "block jump" in distinction to a normal hydraulic jump. The addition of blocks, which cause additional unknown energy losses, invalidates Eq. 2. In place of d_2, the writer suggests that d_c, the critical depth, be used in presenting the design equation for the length of basin. Since the following equalities are true,

$$f(d_c) = \psi(d_2) = \alpha(d_1) = \theta(\mathbf{F}) \quad \ldots\ldots (9)$$

any one of the equal functions can be substituted and the result will be changed in form only. It would, perhaps, be even more desirable to present the equation for L_B as a function of **F** and d'_2. In Table 9, values of d_c are given for various runs as computed from

$$d_c = \sqrt[3]{q^2/g} \quad \ldots\ldots (10)$$

TABLE 9.—SUMMARY OF COMPUTATIONS BASED ON TEST DATA AS APPLIED TO EQ. 10

Test No.	L_B (ft)	d_c (ft)	$\frac{L_B}{d_c}$	**F**
(1)	(2)	(3)	(4)	(5)
C57...	8.50	1.96	4.34	7.52
C75...	15.33	4.07	3.76	8.45
C76...	5.00	1.56	3.20	30.1
C3.....	26.25	3.23	8.13	33.6
C16...	14.00	3.12	4.51	30.5
C28...	8.75	3.08	2.84	29.2
C37...	5.00	3.09	1.62	29.6
F52....	14.02	3.25	4.33	31.0
F51....	14.21	4.10	3.47	40.0
F49....	{16.33, 13.61, 10.88}	4.95	{3.30, 2.75, 2.20}	70.0
F48....	{16.38, 13.10, 9.83}	5.67	{2.89, 2.30, 1.70}	100.0
F46....	{24.22, 20.18, 16.5, 12.11}	6.40	{3.79, 3.20, 2.52, 1.90}	150.0

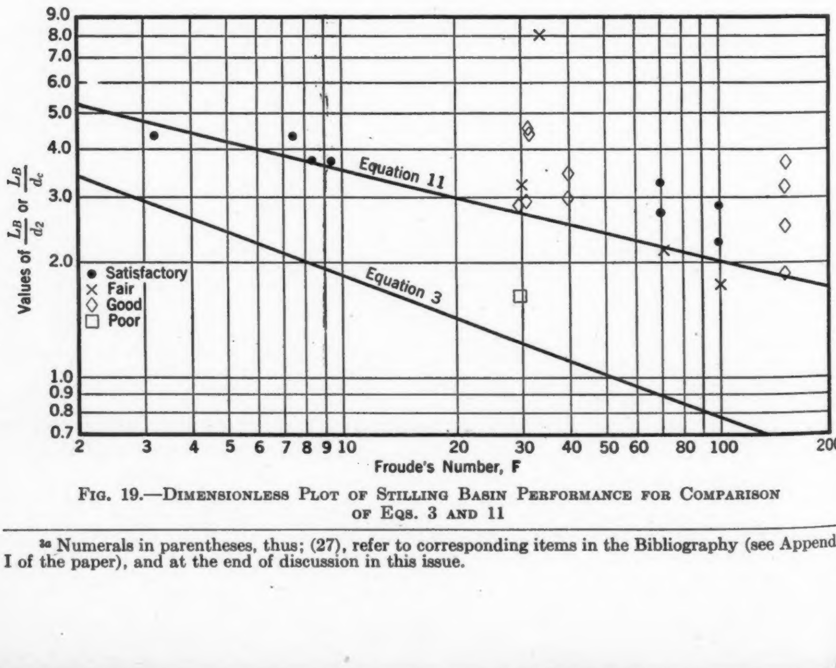

FIG. 19.—DIMENSIONLESS PLOT OF STILLING BASIN PERFORMANCE FOR COMPARISON OF EQS. 3 AND 11

[3a] Numerals in parentheses, thus; (27), refer to corresponding items in the Bibliography (see Appendix I of the paper), and at the end of discussion in this issue.

in which q is the unit discharge and g is the acceleration due to gravity. The ratio L_B/d_c is plotted against $\mathbf{F}$ in Fig. 19, as a result of which

$$L_B/d_c = \frac{6.2}{\mathbf{F}^{0.25}} \qquad (11)$$

is suggested as being more rational than Eq. 3. It is, however, no more exact, inasmuch as both are envelope curves based on the same experimental data.

In an attempt to further analyze the action of the block jump, various runs of the experiment were used as a basis for computation of values shown in Table 10. The equations for the computations are (27*a*):

TABLE 10.—SUMMARY OF BLOCK JUMP ANALYSIS

Test No. (1)	ϵ_j (2)	ϵ_1 (3)	ϵ'_2 (4)	ϵ_2 (5)	ϵ_b (6)	$\frac{\epsilon'_2}{\epsilon_1}$ (7)	$\frac{d'_2}{d_1}$ (8)	$\frac{\epsilon_b}{\epsilon_j}$ (9)	$\mathbf{F}$ (10)
C57	1.03	4.76	3.52	3.73	0.21	0.74	3.15	0.20	7.52
C75	2.53	10.44	6.93	7.91	0.98	0.66	3.00	0.39	8.45
C76	4.25	8.02	3.31	3.77	0.46	0.41	6.24	0.11	30.1
C3	9.80	17.80	6.64	8.00	1.36	0.37	6.21	0.14	33.6
C16	8.62	16.25	6.50	7.63	1.13	0.40	6.09	0.13	30.5
C28	8.14	15.60	6.47	7.46	0.99	0.41	6.07	0.12	29.2
C37	8.28	15.80	6.47	7.52	1.05	0.41	6.06	0.13	29.6
F52	9.12	17.00	6.88	7.88	1.00	0.40	6.28	0.11	31
F51	14.72	25.2	9.10	10.48	1.38	0.36	7.19	0.08	40
F49	29.26	43.2	11.91	13.94	2.03	0.28	9.54	0.07	70
F48	44.49	61.2	14.37	16.70	2.33	0.23	11.60	0.05	100
F46	69.16	91.2	17.60	22.10	4.50	0.19	14.30	0.06	150
T37	1.157	1.66	0.441	0.50	0.059	0.27	10.68	0.05	80.8
T42	2.405	3.340	0.801	0.93	0.129	0.24	11.06	0.05	93.7

TABLE 10.—(*Continued*)

Test No. (1)	$\frac{d'_2}{d_1}$ (8)	$\mathbf{F}$ (10)
T39	15.8	183.1
T46	19.15	274
T44	14.7	161
T35	17.95	247
T53	19.95	288
T50	12.82	121
T17	19.05	261
T8	15.95	190
F103	2.83	5
F107	4.08	10
C63	2.28	3.25

$$\epsilon_j = \frac{(d_2 - d_1)^3}{4\, d_2\, d_1} \qquad (12)$$

$$\epsilon_1 = d_1 \left(1 + \frac{\mathbf{F}_1}{2} \right) \qquad (13)$$

$$\epsilon'_2 = d'_2 + \frac{q^2}{2\, g\, (d'_2)^2} \qquad (14)$$

$$\epsilon_2 = (\epsilon_1 - \epsilon_j) \qquad (15)$$

$$\epsilon_{bj} = (\epsilon_1 - \epsilon'_2) \qquad (16)$$

$$\epsilon_b = (\epsilon_{bj} - \epsilon_j) \qquad (17)$$

In these equations, ϵ_j, ϵ_{bj}, and ϵ_b represent energy loss due to the hydraulic jump, the block jump, and the blocks alone, respectively; d'_2 is the depth of flow at section 2′; ϵ_1, ϵ_2, and ϵ'_2 represent the specific energy at section 1, section 2, and section 2′, respectively; and $\mathbf{F}_1$ is the Froude number at section 1.

The values in Col. 8, Table 10, when plotted (Fig. 20) against the corresponding Froude numbers, result in the equation

$$\frac{d'_2}{d_1} = 1.05\, \mathbf{F}^{0.522} \qquad (18)$$

which is comparable to Eq. 6 and is in a more desirable form.

In the hydraulic jump, $\mathbf{F} = 3$ is the theoretical transition point between the direct jump and the undulated jump. It has been noted (15*a*) that observed values of d_2 within the undulated jump zone are in excess of those computed by Eq. 2. It has also been stated (15*b*) that the actual transition point between the direct jump and the undulated jump is at about $\mathbf{F} = 4$. It is interesting to note that the undular jump also occurs in the block jump. This is evident because the ratio d'_2/d_2 is greater than 1 for small values of **F**, and has occurred for values of **F** as high as 15. For this reason Eq. 18 should not be used for values of **F** less than 15. Further experimentation is necessary to locate the probable range of values for the undulated jump in the block jump.

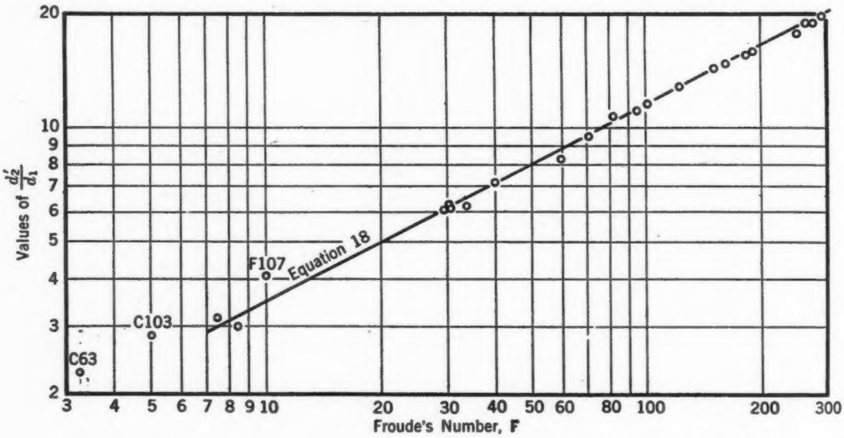

FIG. 20.—RELATION BETWEEN DEPTH RATIO AND FROUDE NUMBER FOR BLOCK JUMP

Col. 6 of Table 10 gives the actual head loss caused by the blocks; Col. 9 gives the ratio of the efficiency of the blocks as compared to that of the hydraulic jump. It should be noted that the blocks are most effective, compared to the hydraulic jump, at low values of **F**.

Fig. 21 is a plot of the values of Cols. 7 and 8, Table 10, against **F**. Study of the manner in which the plotted points follow the curves for the hydraulic jump causes speculation as to the actual nature of the relationship between parts of the block jump. It is apparent that the ratios are comparable to those in a hydraulic jump and thus might be susceptible of an analytical solution based on change of momentum.

A schematic picture of the conditions obtaining in the block jump is given in Fig. 18(*b*). Applying the momentum theorem, P_3 is the only new force involved over that in the solution for the hydraulic jump. Change of momentum may then be expressed by

$$P'_2 + P_3 - P_1 = \frac{Q\,w}{g}\,(V_1 - V'_2)\ldots\ldots\ldots\ldots\ldots(19)$$

in which $P_1 = A_1\,w\,\bar{y}_1$; $P'_2 = A'_2\,w\,\bar{y}'_2$; A is the area at any section; w is the unit weight of water; $\bar{y}$ is the depth to the center of gravity at the section; and

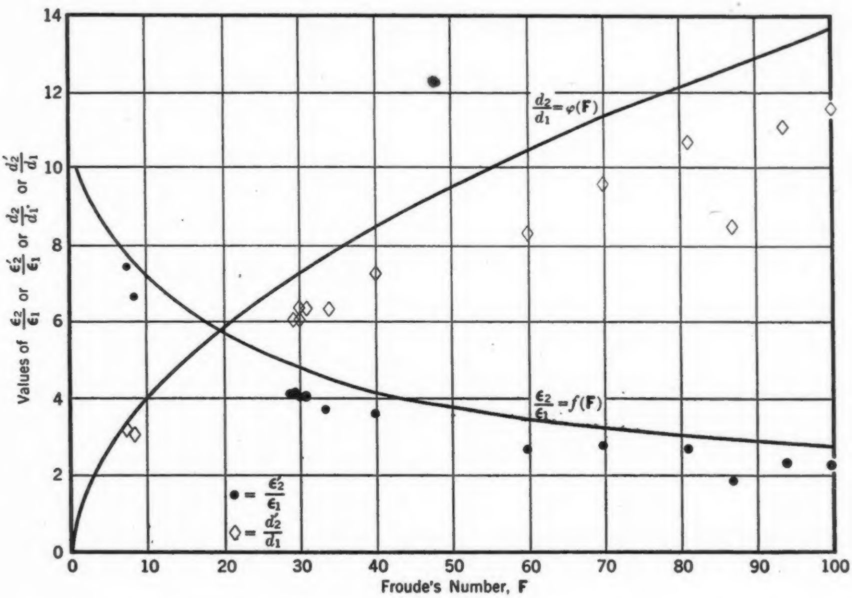

FIG. 21.—RELATION BETWEEN CALCULATED BLOCK JUMP ENERGIES AND DEPTHS AND THOSE OF NORMAL HYDRAULIC JUMP

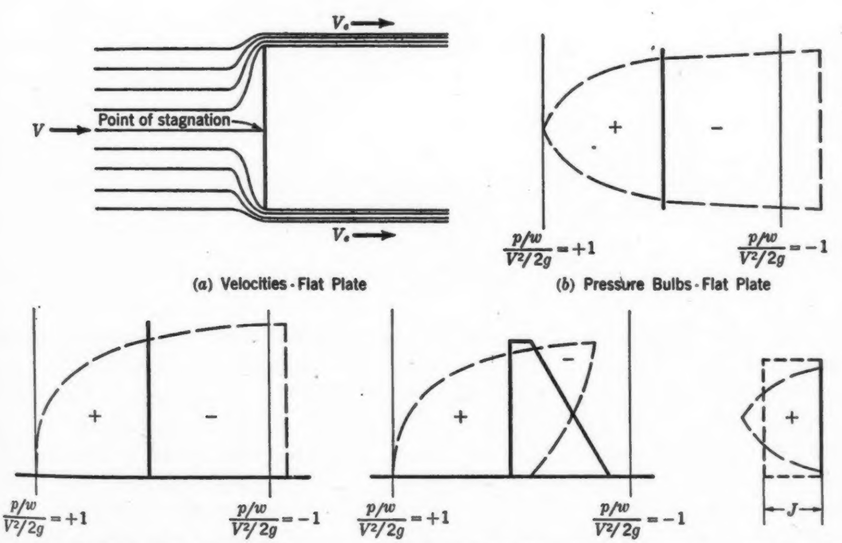

FIG. 22.—RELATIONSHIP OF QUANTITIES IN FLOW AROUND FLAT PLATES AND BLOCKS

V'_2 is the velocity at section 2'. To determine P_3, recourse must be had to the analysis of forces acting on a flat plate perpendicular to flow and completely submerged in the fluid (see Fig. 22(*a*)). It can be shown by dimensional analysis (28)(29) that the force acting on the flat plate is

$$F = \theta(R)\, \rho\, V^2 A_p \qquad (20a)$$

in which $\theta(R) = C_f \frac{1}{2}$; $\rho = \frac{w}{g}$; V is the velocity of approach; A_p is the area of the plate; and C_f is a coefficient of form.

Thus,

$$F = C_f\, w\, A_p \frac{V^2}{2\,g} \qquad (20b)$$

If $F = P_3$ is substituted in Eq. 19,

$$A^1{}_2\, w\, \bar{y}'_2 + C_f\, w\, A_p \frac{V^2}{2\,g} - A_1\, w\, \bar{y}_1 = \frac{Q\,w}{g}(V_1 - V'_2) \qquad (21a)$$

or

$$\frac{(d'_2)^2}{2} + C_f \frac{A_p}{b}\frac{V^2}{2\,g} - \frac{d^2{}_1}{2} = \frac{q}{g}(V_1 - V'_2) \qquad (21b)$$

from which

$$d'_2 = \sqrt{\frac{2\,q}{g}(V_1 - V'_2) + d^2{}_1 - C_f \frac{A_p}{b}\frac{V^2}{g}} \qquad (21c)$$

Eq. 21*c* is dimensionally and dynamically correct; it is only in its application that troubles arise.

If it is assumed that

$$A_p = W\,d \qquad (22a)$$

$$W = k\,b \qquad (22b)$$

and

$$V'_2 = q/d'_2 \qquad (22c)$$

in which W is the width of plate; d, the depth of plate; and k, the percentage of basin width covered by clocks; then Eq. 21*c* may be rewritten

$$d'_2 = \sqrt{\frac{2\,q}{g}\left(V_1 - \frac{q}{d'_2}\right) + d^2{}_1 - C_f \frac{K\,V^2}{g}\,d} \qquad (23)$$

Eq. 23 is an implicit equation which cannot, by any simple means, be solved into an explicit function. For this reason Eq. 23 must be solved by trial and error. As an original valve for d'_2, the value of d_2 can be used. The third solution will generally give the final value of d'_2. In the foregoing analysis it has been assumed that the resistance P_3 is caused by a flat plate. Since this is not true, it must be shown that the general conditions still prevail. Fig. 22(*b*) shows the approximate pressure bulbs on a flat plate under the conditions required by the analysis (30). By bringing the flat plate in contact with a solid boundary (30*a*) the pressure distribution is altered approximately as shown in Fig. 22(*c*). By changing the plate to the form of a floor block the pressure bulbs are again varied to the approximate shapes shown in Fig. 22(*d*). In

analyzing C_f the assumption can be made that the skin friction is negligible and that for all practical purposes

$$C_f = C_d \qquad (24)$$

in which C_d is the coefficient of form drag. Rewriting Eq. 20*b*,

$$\frac{F}{A_p} = p = C_d\, w\, \frac{V^2}{2\,g} \qquad (25a)$$

or

$$\frac{p}{w} = C_d\, \frac{V^2}{2\,g} \qquad (25b)$$

It is noted that the coefficient C_d is actually a nondimensional number, shown to vary with **R**, which, when multiplied by the velocity head of stagnation, gives the pressure head caused by the stagnation of flow. Referring to Fig. 22(*a*), the pressure under ideal circumstances would be the pressure due to stagnation of flow and thus equal to $\frac{V^2}{2\,g}$ or $\frac{V^2_e}{2\,g}$. Since the streamlines of flow are approximately zero in width at the point of separation the velocity V_e must be greater than V, the velocity of approach. For this reason, the negative pressure bulb is greater than the positive pressure bulb; C_d can then be written as

$$C_d = J_+ + J_- \qquad (26)$$

where J_+ is the coefficient in $J_+ \frac{V^2}{2\,g}$ to represent the plus pressure on the front of the plate and J_- is the coefficient in $J_- \frac{V^2}{2\,g}$ to represent the negative pressure on the back of the plate caused by the velocity V_e. The true physical nature of J is shown in Fig. 22(*e*), where it is shown to be the average height of the pressure bulb over the area of the plate.

In two-dimensional flow, J is one side of a plane rectangle; in three-dimensional flow it is the height of a rectangular solid. Thus, by measuring the pressure bulbs on the back and front of a block, the value of C_d is obtainable. Distinction should be made for the C_d of a single block and the C_d for a block group, since interference would cause a change in value. In studies pertaining to cavitation on baffle piers the coefficient J_- was determined to be equal to 0.68 for a single cubical pier (31).

As another approach to C_d, Eq. 23 can be rewritten as

$$C_d = \frac{\frac{2\,q}{g}\left(V_1 - \frac{q}{d'_2}\right) + d^2_1 - (d'_2)^2}{K\,d\,\frac{V^2}{g}} \qquad (27)$$

By assuming K equal to 0.5, d equal to d_1, and V equal to V_1, the value of C_d can be computed for various runs of the experiments. Included in the foregoing assumptions is the inherent fact that the chute blocks will not dissipate any appreciable amount of energy and thus are ignored. The computed values of C_d based on these assumptions are plotted against **R** in Fig. 23.

Up to about $\mathbf{R} = 10^6$, the value of C_d is practically constant, which indicates that C_d is independent of $\mathbf{R}$ for this range. However, one point (T58) with $\mathbf{R} = 1.45 \times 10^6$ and with $\mathbf{F} = 28.2$ is definitely below the values of the other runs. Two possibilities can explain the reason for this change. First,

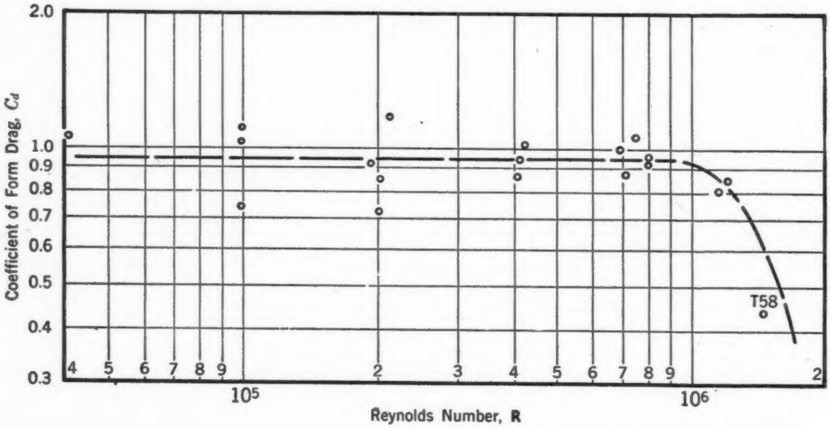

FIG. 23.—PLOT OF C_d VERSUS R FOR BLOCK JUMP

if the range of undulated jumps extends to as high a value of $\mathbf{F}$ as 28.2, then the observed d'_2 would be too high, and consequently the run could not be used in an equation based on change of momentum. Second, the value of $\mathbf{R}_{crit}$ has been reached, in which the boundary layer adjacent to the block has changed from laminar to turbulent flow. Whether a solid, streamlined as slightly as is the block, can exhibit this characteristic is as yet unknown. Other experimenters have made tests to determine C_d for a body similar to the floor block, but so far have given as a result only that C_d was constant and a value. No attempt was made to correlate the value of C_d to $\mathbf{R}$ and no mention is made of the range of $\mathbf{R}$ (32). It is entirely possible for the smooth blocks used in the experiments to exhibit this characteristic, but if so the value computed for C_d cannot be used in application to a prototype. In prototype flow it would be almost impossible for a laminar boundary layer to exist next to a surface as rough as a concrete block.

In a model controlled by the Froude number the value of $\mathbf{R}$ is different for the model and prototype. However, it has been stated that "* * * the Froude number refers to flow with a free surface, and actually has no relationship whatever with the inner mechanism of confined flow * * *" (33). Since the foregoing derivations are based on the premise that the blocks are completely submerged this quotation will hold and $\mathbf{R}$ will be the same, as regards C_d, for model and prototype. The confined flow is between a solid boundary and a streamline which has a pressure greater than zero and which is not affected by surface disturbances. If the submergence is not sufficient to satisfy these conditions the water would be deflected into the air and a free surface of flow would then affect the flow around the blocks.

The author has given aid to designers from two standpoints: (*a*) By presenting design equations the designer has at hand a reasonable method to use; and (*b*) perhaps of more importance, the designer may use a standardized method so that prototype structures may be compared in action after construction.

M. M. CULP,[4] Assoc. M. ASCE.—Early gully control work involving the use of chutes and drop inlet spillways has demonstrated the need for some mechanical device to assist in the dissipation of hydrodynamic energy at the outlet end of such spillways. Erosion damage below several drop inlets and chutes led to field inspections and study of the problem. It seemed that the principal factors involved were:

1. Tailwater elevation;
2. Soil condition in the gully bottom and banks;
3. The stability of the channel grade below the spillway (which affects tailwater);
4. The magnitude, duration, and frequency of discharge through the spillway; and
5. Vegetative growth or other protective cover in the immediate vicinity of the outlet.

Where damage occurred it was obviously the result of eddies produced by a high velocity jet of water emerging from the spillway. Severe damage, requiring extensive repair, has occurred at the outlet of several spillways. For

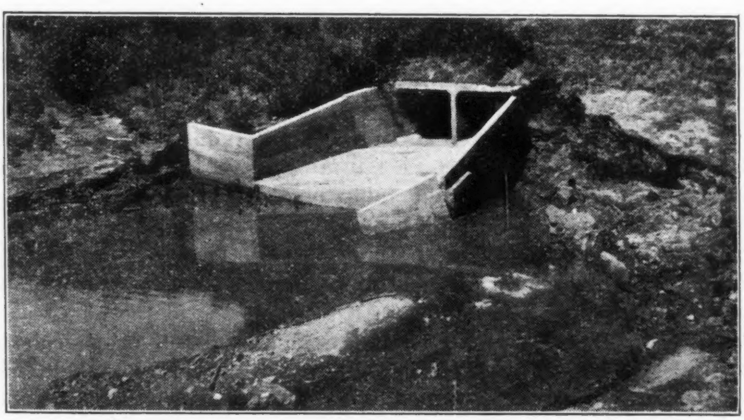

FIG. 24.—FAILURE OF APRON ON TWIN 6-FT BY 6-FT DROP INLET CULVERT DUE TO UNDERMINING AND SCOURING

example, Fig. 24 shows the outlet of a twin 6-ft by 6-ft reinforced concrete drop inlet. The outlet apron had been undermined and so badly cracked that it had to be completely removed during repair operations.

[4] Civ. Engr., Head, Design and Construction Section, Regional Eng. Div., SCS, U. S. Dept. of Agriculture, Milwaukee, Wis.

Several spillways constructed with Saint Anthony Falls (SAF) outlets during the past two years have not been subjected to a real test, as yet, and final conclusions cannot be drawn. However, several flows of less than design capacity have occurred, and the short experience to date indicates that the SAF outlet will function satisfactorily.

The designer of this type of outlet is confronted with the problem of constructing a stage-discharge curve for the natural channel below the spillway. Associated with this problem is the determination of the probable grade and cross section of a stable channel below the spillway. It is a well-recognized fact that natural channels tend to degrade when the bed load is removed by deposition in a reservoir. The problem is complicated further by variations in channel roughness with the stage, and by nonuniform flow conditions that may exist. The problem may be simplified, however, by the construction of a low drop spillway in the channel below the SAF outlet. Such a spillway provides a control from which backwater computations lead to reasonably correct tailwater elevations.

The writer sugggests that Mr. Blaisdell give consideration to the use of the word "chute," in lieu of "flume," to describe the high velocity open spillway shown in Fig. 3. This suggested nomenclature conforms to the definition given in the ASCE *Manual of Engineering Practice No. 11*, "Letter Symbols and Glossary for Hydraulics."

Mr. Blaisdell is to be complimented on a clear presentation of a long, tedious, and difficult program of hydraulic tests of a generalized nature. The writer is confident that the results of his work, as reported in the paper under discussion, will have continued and increasing use, especially in the field of upstream engineering.

PAUL BAUMANN,[5] M. ASCE.—An abundance of information on the model tests of the Saint Anthony Falls (SAF) stilling basin is presented in this paper, and simple empirical formulas are proposed for determination of several critical dimensions. In addition, the design tailwater depth, d'_2, as compared to d_2, the conjugate depth of the hydraulic jump, is expressed in terms of the Froude number, **F**.

Since the primary purpose of a stilling basin is the dissipation of energy, it would have been helpful if information in regard to the configuration of the energy gradient between the upstream (reservoir) side of the outlet and the stilling basin proper had been presented. Such information is particularly desirable in view of the fact that the depth d_1 at the upper end of the basin and of the roller, respectively, is governed by the loss in energy between it and the reservoir surface (assuming the energy line to coincide with the reservoir surface for small velocity of approach). The coefficient ϕ to be applied to the factor $\sqrt{2\,g\,h}$ must be determined experimentally for each problem. Values of ϕ determined on models therefore furnish valuable information for those who must prepare stilling basin designs without the aid of model tests.

In general, it has been found that ϕ does not drop much below 0.9 for supercritical flow of water under rounded gates, although, for water discharging

[5] Asst. Chf. Engr., Los Angeles County Flood Control Dist., Los Angeles, Calif.

over ogee sections of considerable height, ϕ may drop to 0.5 and lower, depending on the smoothness of the surface, the curvature of the ogee section as well as that of the apron, and the transition between the crest and the stilling basin. Such a loss in head, and therefore in energy, is reflected in the depth d_1, which may be considerably in excess of the depth that would be established without such loss. The conjugate depth, d_2, derived from Eq. 2*a*, is necessarily affected correspondingly.

It is an interesting fact in hydraulics that Eq. 2*a*, which is derived from the condition that the sum of the static and dynamic pressure above the jump equals the sum of the static and dynamic pressure below the jump, leads to a loss in energy without the application of any empirical factors. The validity of this equation has been confirmed on models as well as on prototypes. This equation may, with close approximation, be written

$$d_2 = 0.45 \left(v_1 \sqrt{\frac{d_1}{3.28}} - d_1 \right) \ldots\ldots\ldots\ldots\ldots\ldots (28)$$

In contradistinction, the equation for the depth d_1 must always include the empirical factor ϕ and must read

$$d^3_1 - d^2_1 H_0 + \frac{q^2}{\phi^2\, 2\, g} = 0 \ldots\ldots\ldots\ldots\ldots\ldots (29)$$

in which H_0 is the vertical distance from the floor of the stilling basin to the upstream energy line (reservoir surface); and q is the discharge per unit width of stilling basin. Since ϕ appears in the second power, it is readily conceivable that its influence on the value of d_1 is significant.

In discussing the paper, "Baffle-Pier Experiments on Models of Pit River Dams" (34), the writer (34*a*) attempted to determine the most efficient design depth (d'_2) based on the concept that the dissipation of energy (the transformation of kinetic into heat energy) is due to the roller and that the rise in temperature of the roller should be a maximum for the design depth d'_2. The equation for d'_2 so derived is, after simplification and correction,

$$(d'_2)^3 = \frac{q^2}{g} \left(2 - \frac{d'_2}{2\, H} \right) \ldots\ldots\ldots\ldots\ldots\ldots (30)$$

in which H is the vertical distance between the upstream energy line (reservoir surface) and the stilling basin water surface for design depth d'_2. In arriving at this equation, the empirical formula—

$$V_E = \alpha\, Q \sqrt{\frac{H}{g}} \ldots\ldots\ldots\ldots\ldots\ldots (31)$$

—was used for the volume of the roller. In Eq. 31, V_E is the volume of the roller; α is a coefficient; and Q is the total discharge ($= q\, b$).

The difference between the conjugate depth d_2 and the values for d'_2 resulting from Eq. 30 is demonstrated by Fig. 25, which indicates that d_2 is considerably in excess of d'_2. This is particularly noticeable with an increase

in head. The values, however, would tend to become reconciled if d_2 were determined by the use of a proper coefficient ϕ with the value of d_1 as previously discussed.

To demonstrate the relation between values for d'_2 determined by Eq. 30 and by the author, respectively, Fig. 12, an important part of the paper, is

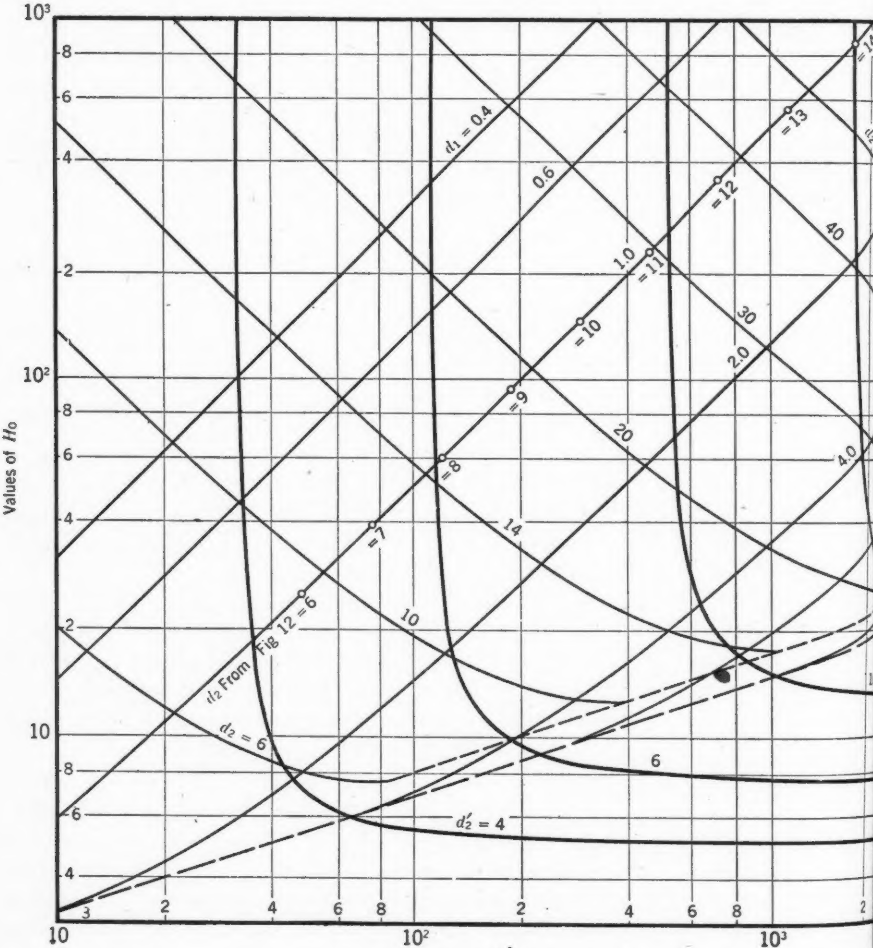

FIG. 25.—COMPARI[...]DEPTHS

used. It was derived from the series of culvert outlet tests which are not shown in the paper.

For $d_1 = 1$ ft and $b_1 = 9$ ft, Eq. 29 may be rewritten

$$H_0 = 1 + \frac{q^2}{\phi^2\, 2\, g} \quad \text{(32)}$$

in which $q = \frac{Q}{b_1}$.

The curves shown in Fig. 12 plot as straight lines on semilogarithmic paper. They may, therefore, be extrapolated so as to cover depths d'_2 considerably in excess of 7 ft, as shown in Fig. 26. The two curves intersect and therefore have a common point, whose approximate coordinates are: $Q = 540$ cu ft per sec and $d'_2 = 7.9$ ft. The two curves would be expected to merge into one be-

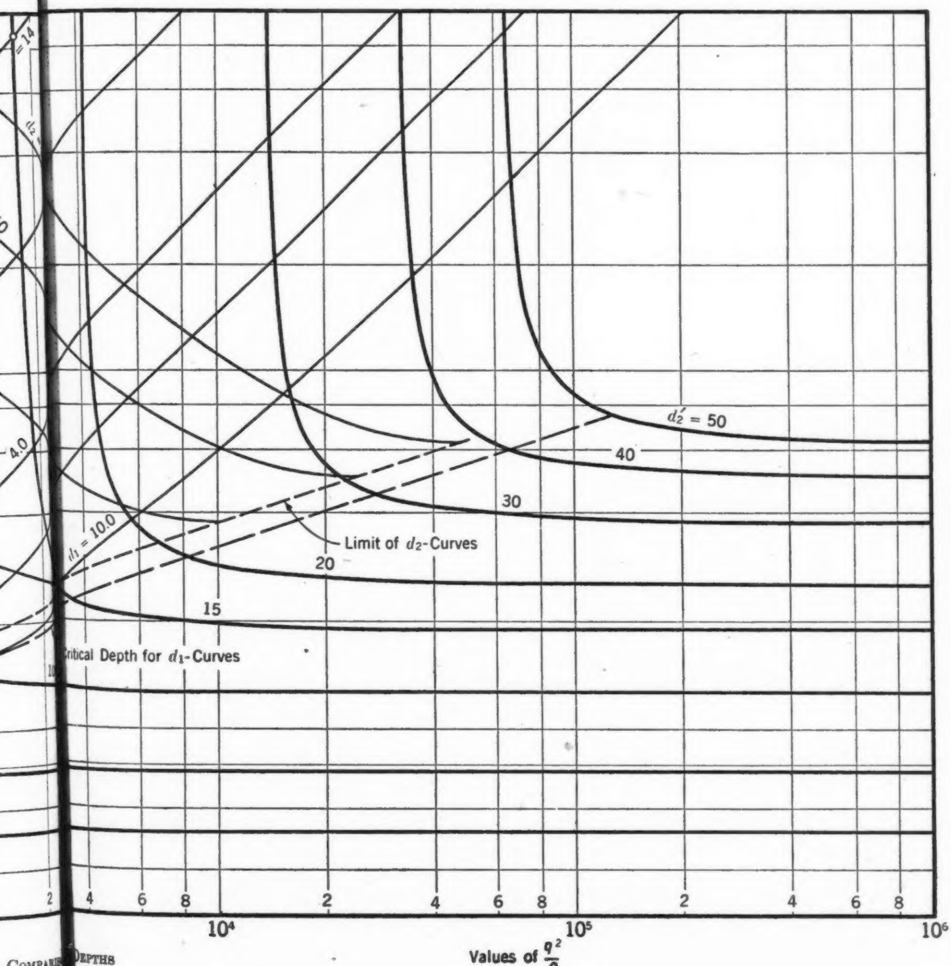

—COMPARI DEPTHS

yond this point. Hence, this point would coincide with a break in the curves. Only the curve through points at which the roller was washed out of the basin for increasing flow is used. Points for d'_2-values, as plotted in Fig. 25, naturally fall on the curve for $d_1 = 1$ ft for a unit value of ϕ. It may be noted that, despite the d'_2-values so determined being considerably at variance with the d'_2-values from Eq. 30 for small values of Q $\left(\text{that is, } \frac{q^2}{g} \text{ and } H_0\right)$, they ap-

proach each other with an increase in Q and H_0, and coincide for $d'_2 = 13$ ft±. Below this point the model tests indicate that a greater design depth is necessary; above this point a design depth equal to or smaller than that resulting from Eq. 30 is required.

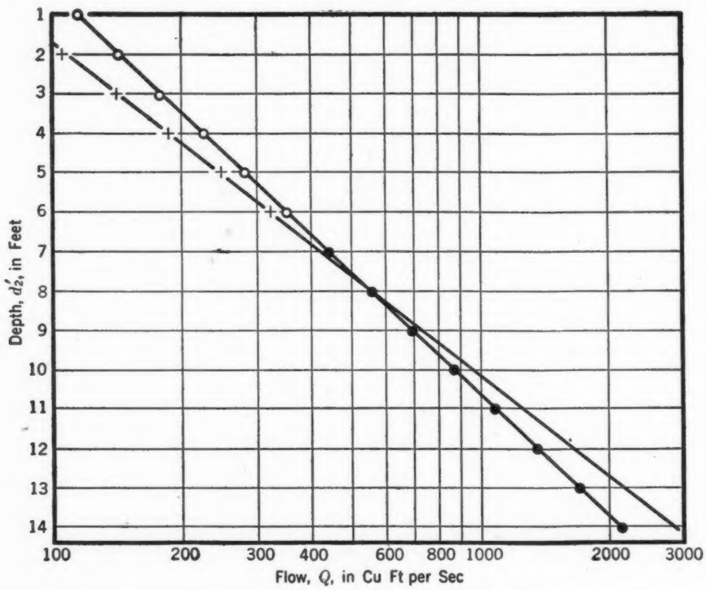

FIG. 26.—SEMILOGARITHMIC PLOT OF CURVES FROM FIG. 12

It is realized that the extrapolation of the curves in Fig. 12 is somewhat of a liberty in view of the author's statement that the roller could not be washed out of the stilling basin after the depth d'_2 had been increased to 7.20 ft, even for a discharge of nearly 600 cu ft per sec. For such a discharge ($Q = 598$ cu ft per sec; $\frac{q^2}{g} = 138$; and $H_0 = 70$ for $\phi = 1$), $d_2 = 16.1$ ft with close approximation, which is 223% of the depth d'_2 found necessary to maintain a roller. The total residual energy due to d_2 amounts to 16.37 ft; it amounts to 8.53 ft due to $d'_2 = 7.20$ ft. The initial total energy in both cases amounts to 70 ft.

The minimum residual energy would be due to the critical depth—

$$d_c = \sqrt[3]{\frac{q^2}{g}} \qquad (10)$$

—which establishes itself for $d'_2 = 2\,H$ in Eq. 30. However, the critical depth in the stilling basin is not compatible with its purpose, which is stilling action to minimize downstream scour.

A. J. PETERKA,[6] Assoc. M. ASCE.—General studies of the type reported in this paper have been needed for some time. Designers in particular have

[6] Hydr. Engr., Bureau of Reclamation, U. S. Dept. of Interior, Denver, Colo.

seized every available scrap of information that would ease the problem of designing small stilling basins that will operate for the first time as prototype structures, or larger basins that will be submitted to a laboratory for refinement of features. Unfortunately, in most hydraulic laboratory investigations, it is not possible to concentrate on general solutions since funds are usually available only to solve the problems for a specific installation. Because of this situation only a limited amount of information is available for general solutions.

The author is to be complimented for his approach to a problem that is difficult in many ways. His results, no doubt, will serve the purpose for which they were intended. However, there will be a tendency for designers to use this material for purposes beyond its range of reliability and the intent of this discussion is to indicate some of these limiting factors rather than to criticize, adversely, the excellent treatment given by the author.

The stilling basin operation, indicated by Fig. 6, appears to be greatly dependent on the chute blocks, baffle blocks, and end sill. It also appears that the configuration of the movable bed downstream from the apron had some effect in determining the length of the basin. Since at the start of each test the bed was molded above the elevation of the apron, there was probably some resistance offered to the flow that could favorably affect the performance of a short apron. Without a high bed, somewhat different action might take place, as the result of a different distribution of velocities.

The stilling basin profiles indicate that for L_B less than about 2 d_2 very little energy is dissipated on the apron. Thus, the basin becomes a distributor rather than a dissipator. The high-velocity flow entering the basin is deflected upward toward the surface, and the hydraulic jump acts merely to distribute the energy over a greater area with most of the dissipation occurring in the channel downstream from the apron. If the energy is not to be dissipated on the apron, the writer feels that it would be more economical to dispense with the apron accessories, consisting of chute blocks and baffle piers, and to adopt a curved deflector bucket to "throw" the water away from the structure. This method has been used successfully by others. A special application of this type of energy distributor was used successfully on the Fontana Dam spillway in the Tennessee Valley (35).

The advisability of relying primarily on such relatively fragile structures as chute blocks and baffle piers for satisfactory apron performance is questioned by the writer. If the prototype apron is submerged, as many of them are, underwater inspection and repair of blocks and piers are difficult. If the apron accessories should become damaged or lost, for any reason, the safety of the entire structure is endangered. As a precaution against undermining the apron, it might prove enlightening in future tests to determine the necessary depth of cutoff wall with some or all of the apron accessories removed. The resulting erosion pattern would also indicate the importance of keeping close watch on the condition of these same accessories if a deep cutoff wall is not used.

The main criterion for evaluating apron efficiency, during the author's tests, was the extent of the erosion in the model, and no mention of wave action below the apron is made. From Figs. 2(a) and 6, it appears that considerable wave action and resulting surface roughness occurred. The destructive effect of these

waves is often as important as the scour of the channel bottom. If the basin discharged into an unlined canal or steep banked stream with soft or overhanging sides, some type of bank protection would be necessary. The prevalence of high surface velocities below the apron, if they existed, might also be of concern.

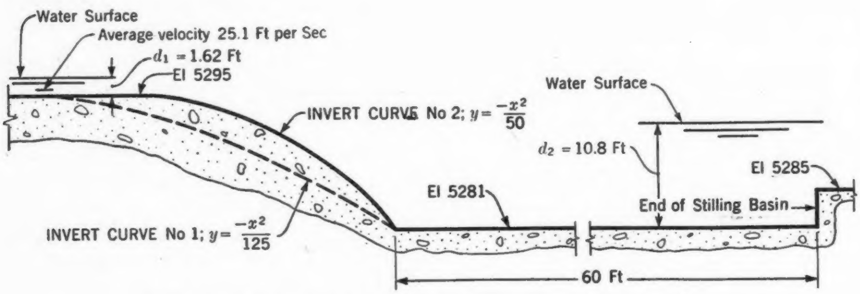

FIG. 27.—STILLING BASIN PROFILE, HORSETOOTH OUTLET WORKS

No mention was made by the author of any changes in the transition parabola during the tests and it is assumed that the same parabola was used throughout. During hydraulic model studies for Horsetooth Dam outlet works, in Colorado (Fig. 27), made in the Hydraulic Laboratory of the Bureau of Reclamation under the writer's supervision, it was found that the shape of the parabola had considerable effect on the stability of the hydraulic jump. Steeper

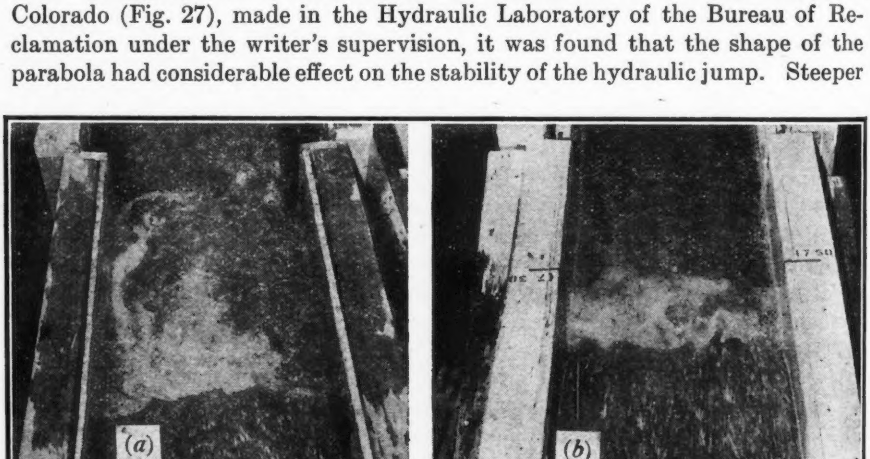

FIG. 28.—STILLING BASIN, HORSETOOTH OUTLET WORKS (SEE CURVES IN FIG. 27)

(a) Unsymmetrical Jump with Trajectory Curve No. 1
(b) Symmetrical Jump with Trajectory Curve No. 2

slopes at the point of entry into the basin resulted in improved basin efficiency, lower waves in the downstream canal, and more uniform velocity distribution at the end of the basin as shown in Fig. 28. Apron accessories were not used in this stilling basin.

During tests, supervised by the writer, on the Enders Dam spillway, in Nebraska, which also makes use of a transition parabola (Fig. 29), the value of

the proposed chute blocks, d_1 in height, was not readily apparent. Subsequent tests, and check tests, both with and without chute blocks indicated that, in this case at least, erosion was greater with the blocks in place. Removal of the blocks decreased the extent and depth of the erosion of the sand bed below the apron, as shown in Fig. 30. Furthermore, observations indicated no change in

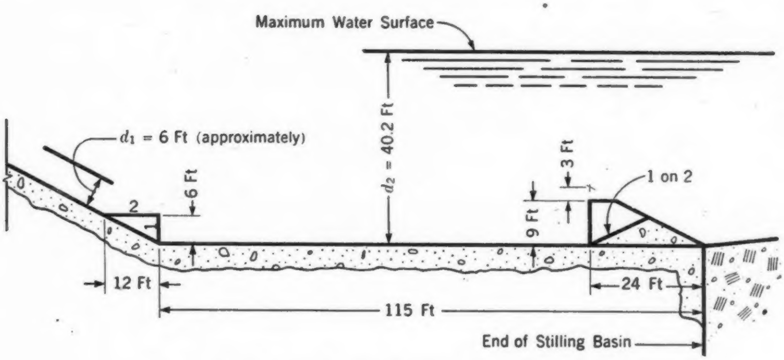

FIG. 29.—STILLING BASIN PROFILE, ENDERS SPILLWAY

the appearance of the operation when the blocks were removed. Use of the blocks, however, did increase the amount that the tailwater elevation could be reduced without causing the jump to wash out of the apron. Finally, it was shown that the same range of useful tailwater could be produced by increasing the height of the dentated end sill from 9 ft to 12 ft, as shown in Fig. 29.

The explanation of the action of these particular chute blocks, offered by the writer, is pure conjecture but may be of some value. Although the Enders spillway chute blocks were equal in height to d_1, as proposed by the author, they were not sufficiently tall. Because of the steep transition profile, the top length of the chute blocks was relatively short. Thus, the directional effect given to the water leaving the top surfaces was negligible, and the flow continued downward much as if the chute blocks were not in place. Had the stilling basin approach been flatter, the top length of the chute blocks would have been proportionately longer, giving greater directional effect to the water and inducing energy dissipating eddies to form. It appears that, if the transition profile is to be varied from one structure to another, the top length of the blocks is of greater importance than the block height.

The author's conclusions regarding the lateral spacing of the floor blocks are in good agreement with results of tests made by the writer on Kentucky Dam in the Tennessee Valley, and on some of the larger structures of the Bureau of Reclamation. A good over-all estimate for design purposes is 50%. Model tests of certain specific installations may show a need for increasing the block area more than 50% to provide flow stability on the apron, but this increase also produces a more concentrated boil. Reducing the block area substantially below 50% results in less turbulence but does not take full advantage of the possibilities.

The 45° wing wall shown by the author has also proved a satisfactory solution to a vexing problem. In most stilling basins the erosion below the downstream corners of the basin is somewhat greater than at any other location,

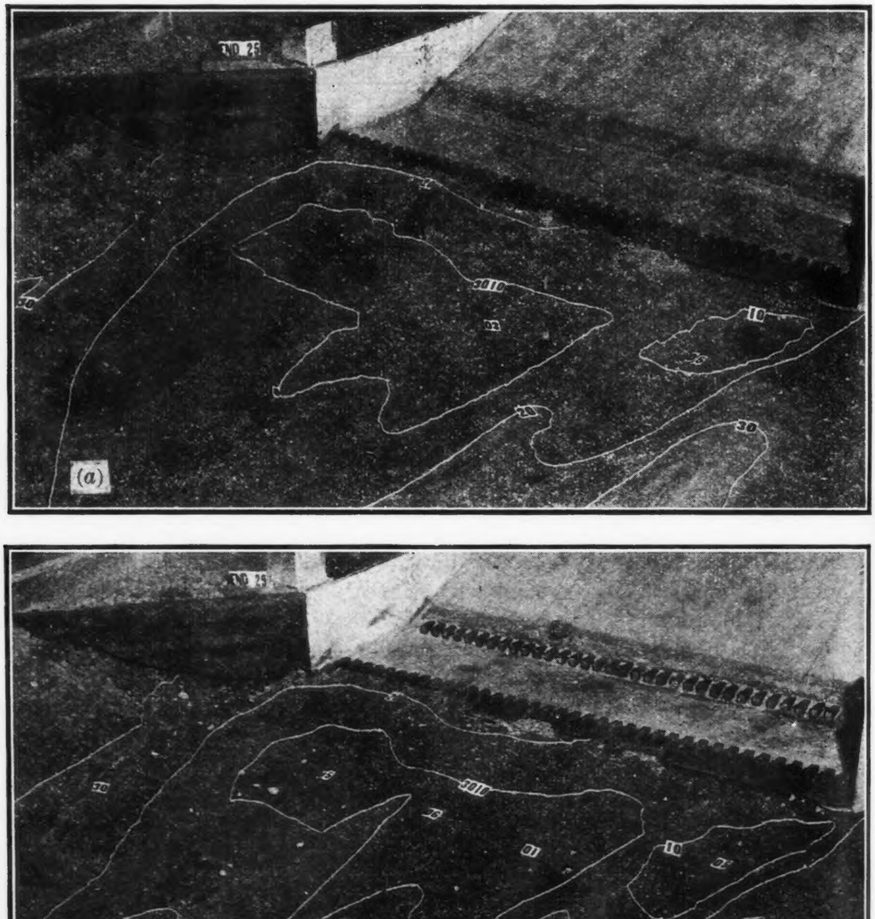

FIG. 30.—EFFECT OF CHUTE BLOCKS ON THE SCOURING BELOW THE SPILLWAY BASIN, ENDERS DAM (45° WING WALL)

(a) Blocks Removed
(b) Blocks Installed

because the downstream channel is wider than the stilling basin, creating a deadwater area at each side of the basin just beyond the end sill. The water leaving the end sill is directed upward, inducing a current from the dead-water area to

flow laterally under the main flow as it leaves the end sill. This circulation results in excessive erosion at the apron corners even if surface velocities appear to be low. Addition of the 45° wing wall reduces the amount of circulation and

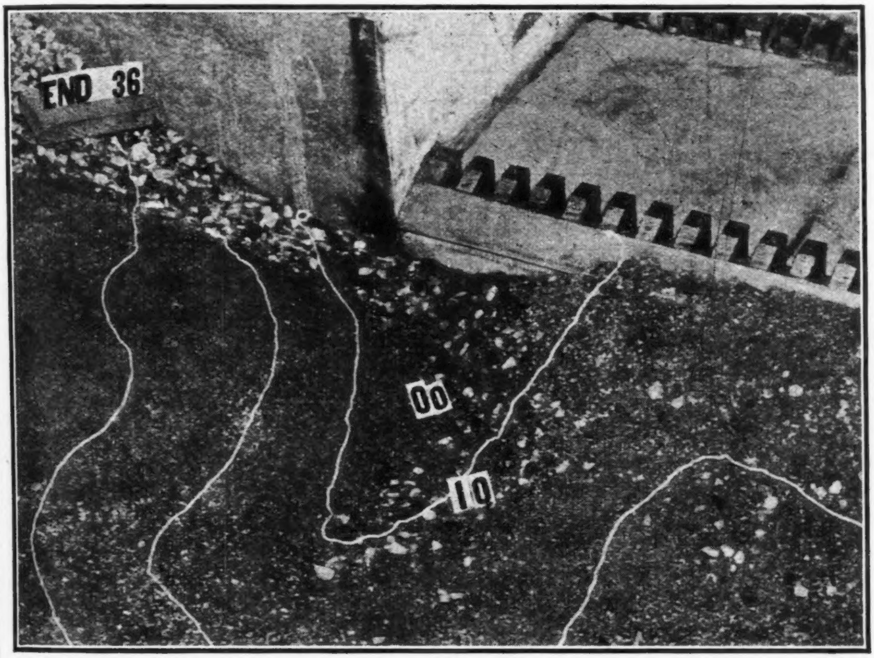

FIG. 31.—EROSION AT APRON CORNER WITH 90° WING WALL

the resulting erosion considerably, as shown by comparison of Figs. 30(*b*) and 31. If the dead-water area is large, or if it extends behind the wing wall, special treatment at the corners of the apron may be necessary.

LOUIS M. LAUSHEY,[7] JUN. ASCE.—The results reported in this paper lead one step closer to the economical design of stilling basins. During 1946 and 1947 the writer conducted somewhat similar tests to determine the effects of a rectangular end sill on the hydraulic jump in a level, rectangular channel. Emphasis was concentrated on the tailwater depth required to form a jump, the proportioning of the height of sill, and the length of the basin required to accommodate the jump. It is interesting to compare the results of these tests with a rectangular end sill in a rectangular basin to those obtained on the Saint Anthony Falls (SAF) basin which uses both a sill and an array of blocks to dissipate the kinetic energy.

The tests on end sills of various heights were conducted in a level, steel flume 12 in. wide and 40 ft long. Water was circulated by a centrifugal pump, and was measured by a calibrated venturi meter. The depth of flow was con-

[7] Instr., Civ. Eng. Dept., Carnegie Inst. of Technology, Pittsburgh, Pa.

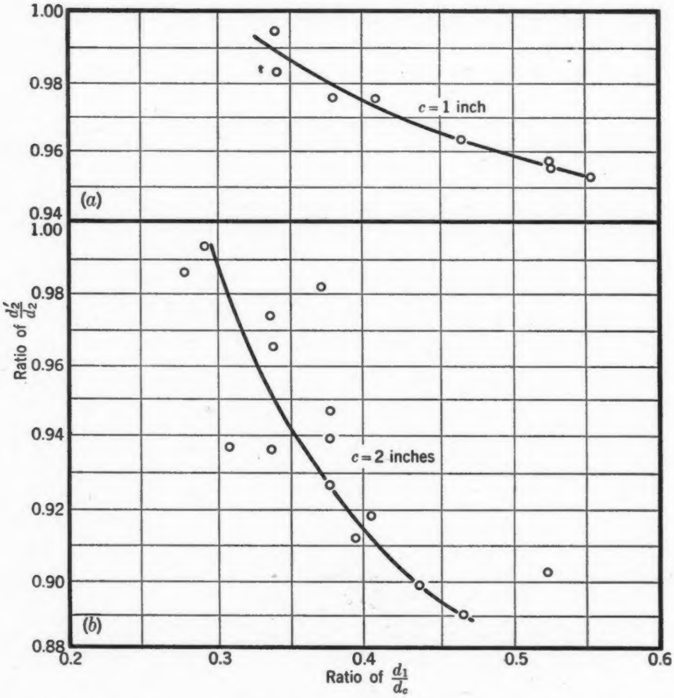

FIG. 32.—DIMENSIONLESS PLOT SHOWING TAILWATER DEPTH RATIOS AS A FUNCTION OF THE RATIO d_1/d_c FOR TYPICAL SILLS

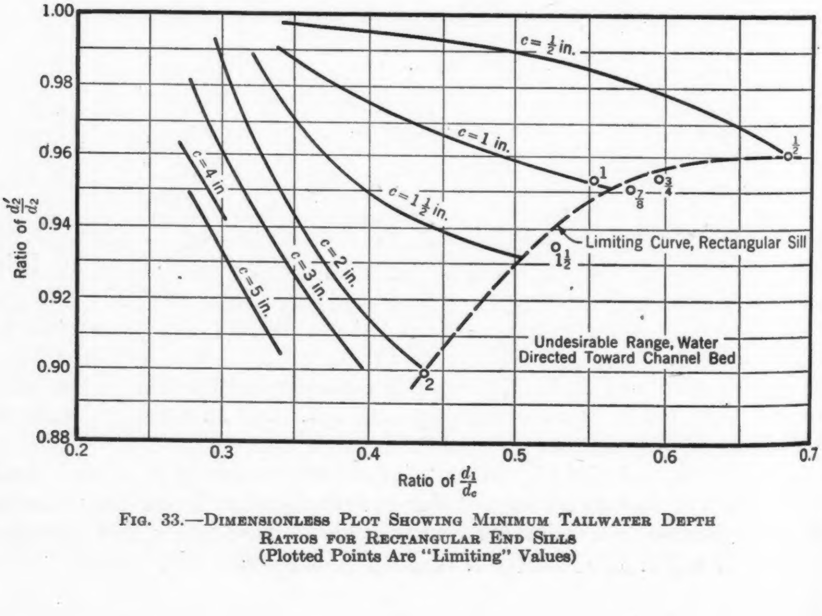

FIG. 33.—DIMENSIONLESS PLOT SHOWING MINIMUM TAILWATER DEPTH RATIOS FOR RECTANGULAR END SILLS
(Plotted Points Are "Limiting" Values)

trolled at the upper end of the flume by raising or lowering a sluice gate hinged to a horizontal steel plate, 6 ft long, to guide the water parallel to the channel bottom. The jump was formed on the test section representing the apron, the downstream end of which was 8 ft from the outfall end of the flume. Sills were introduced at the end of the apron. Depths of flow were controlled by an adjustable tail gate at the end of the flume, and were measured in open manometers. Seven pressure openings were drilled at 2-ft intervals along the center line of the channel; four openings were on the apron, and three were downstream. The sills were made of $\frac{1}{4}$-in. steel plate, 12 in. long, with heights varying from $\frac{1}{2}$ in. to 5 in. The maximum dimensions of the flume in the reach below the jump were 12 in. wide, 20 in. deep, and 8 ft long.

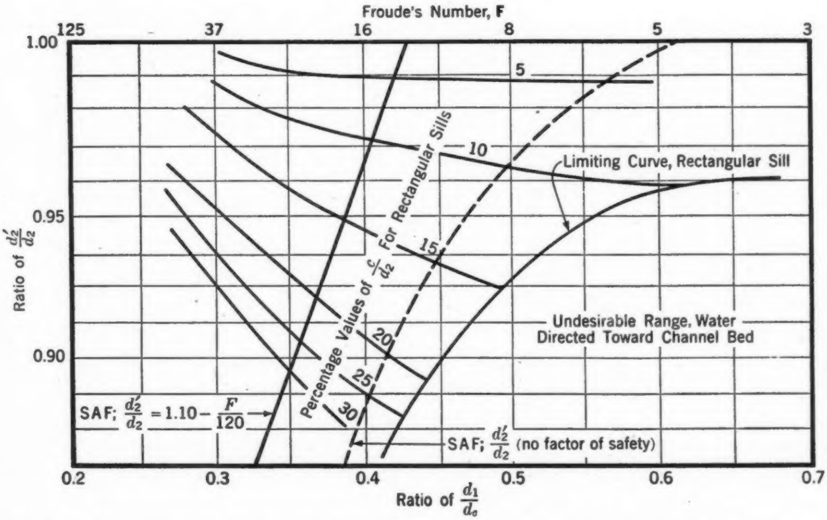

FIG. 34.—COMPARISON OF TAILWATER DEPTH RATIOS FOR THE SAF BASIN AND END SILL BASIN

Comparison of Tailwater Depths Required.—Results of the tests to determine the tailwater depth required for a jump in a basin with an end sill are shown in Figs. 32, 33, and 34. The curves in Fig. 32 are typical curves for sills 1 in. and 2 in. high, the points having been plotted to show the precision attained. The ordinates, values of $\frac{d'_2}{d_2}$, are the same ratios as those used in the SAF analysis, but the dimensionless ratio $\frac{d_1}{d_c}$ was chosen for the abscissa. This is the ratio of initial depth to critical depth before the jump, and it is helpful in visualizing the flow characteristics at the toe of the spillway. It is a function of the head on the dam and the height of the dam above the water surface on the apron. For example:

$$\frac{d_1}{d_c} = \frac{\dfrac{Q}{V_1}}{\dfrac{Q^{\frac{2}{3}}}{g^{\frac{1}{3}}}} = \frac{Q^{\frac{1}{3}}\, g^{\frac{1}{3}}}{V_1} = \frac{(32.2)^{\frac{1}{3}}\, C^{\frac{1}{3}}\, (H^{\frac{3}{2}})^{\frac{1}{3}}}{(64.4)^{\frac{1}{2}}\, (H + h)^{\frac{1}{2}}} = 0.396\, C^{\frac{1}{3}} \left(\frac{H}{h + H}\right)^{\frac{1}{2}} \quad \ldots\ldots(33)$$

In Eq. 33, C is the spillway coefficient of discharge; H is the head on the dam, in feet; and h is the height of crest above water surface on the apron, in feet. Eq. 33 has the following significance: (*a*) When $\frac{d_1}{d_c} \doteq 1.0$, the flow is at critical depth and the height of the jump is zero; (*b*) when $\frac{d_1}{d_c} > 1.0$, flow is tranquil and no jump can form; and (*c*) when $\frac{d_1}{d_c}$ approaches zero, the height of the jump approaches infinity. However, it can be shown that $\frac{d_1}{d_c}$ is a function of the Froude number, which was used in the SAF tests, and is equal to:

$$\frac{d_1}{d_c} = \frac{d_1}{\frac{Q^{\frac{2}{3}}}{g^{\frac{1}{3}}}} = \frac{g^{\frac{1}{3}}\, d_1}{V^{\frac{2}{3}}_1\, d^{\frac{2}{3}}_1} = \left(\frac{g\, d_1}{V^2_1}\right)^{\frac{1}{3}} = \frac{1}{\mathbf{F}^{\frac{2}{3}}} \qquad (34)$$

The method of analyzing the test data was therefore similar, except that an attempt was made to find the effect on the tailwater depth of varying the sill height with the ratio $\frac{d_1}{d_c}$ (or **F**) maintained constant. Results shown in Fig. 33 indicate that increasing the sill height or increasing the ratio $\frac{d_1}{d_c}$ permits a reduction in the tailwater depth ratio. The minimum depth ratios with maximum height sills, and depth ratios for lower sills, were obtained during runs conducted as follows: With no sill in place, the inlet valve was opened and the inlet plate adjusted to produce a jet of the required initial depth, free from undulations and spray. The end of the jump was moved to the end of the apron by adjusting the tailwater control gate, and the "placing" was checked visually and by inspection of the depths recorded in the manometer tubes on and below the apron. The initial depth and discharge were measured and used to compute a theoretical depth d_2 which had to check the observed depth at the end of the jump. Without changing the discharge and initial depth, sills of increasing height were placed, successively, at the end of the apron. The most accurate values of d'_2 were obtained by starting with too low a tailwater depth, and raising it slowly. When the water was too shallow, a frothy fringe of water formed just below the sill. This fringe moved upstream as the tailwater was raised, and disappeared when all depths downstream from the sill were the same. When the tail gate was raised too far, the jump moved upstream on the apron.

Fig. 34 shows the comparison of the limiting curve of tailwater depth ratios to that proposed for the SAF basin. The variable ratio $\frac{c}{d_2}$ is the parameter linking the main variables $\frac{d'_2}{d_2}$ and $\frac{d_1}{d_c}$, whereas this parameter has been made equal to 0.07 in the SAF basin. The ratios $\frac{c}{d_2 - d_1}$, $\frac{c}{d'_2 - d_1}$, $\frac{c}{\frac{V^2_1}{2g}}$, and $\frac{c}{d'_2}$ were also tried

to reduce the scatter resulting in the plot, but without profit. To obtain a comparison, the actual test points (without a factor of safety) from the SAF data in Fig. 11 were plotted as well as Eq. 6*b*. Results are in close agreement for the two basins, although the height of the rectangular sill for a given value of **F** would produce variable results.

Comparison of Height of End Sill.—Fig. 34 shows that, as the Froude number is increased, sills larger than 0.07 d_2 can be used safely without blocks in a rectangular basin. From Table 4 of the SAF tests, best results were obtained at $\mathbf{F} = 40$ with $\frac{c}{d_2} = 0.15$. The ratio of $\frac{d'_2}{d_2}$ for this sill height would be about 0.97 in the end sill basin, which is much higher than the value of 0.85 recommended for the SAF basin. However, the difference might be explained by the effectiveness of the blocks at the higher Froude numbers.

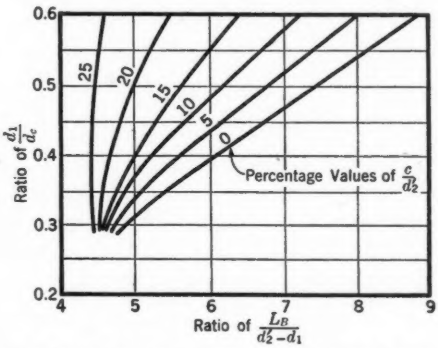

Fig. 35.—Length of Jump to Height of Jump Ratios for Rectangular End Sills

The maximum height of end sill that could be used safely was obtained by increasing the height of sill, with the discharge and initial depth constant, until sufficient height was reached to make the sill begin to act as a control. The limit was reached when all depths downstream could not be made the same because of the drop down curve, which indicated water was directed toward the bottom.

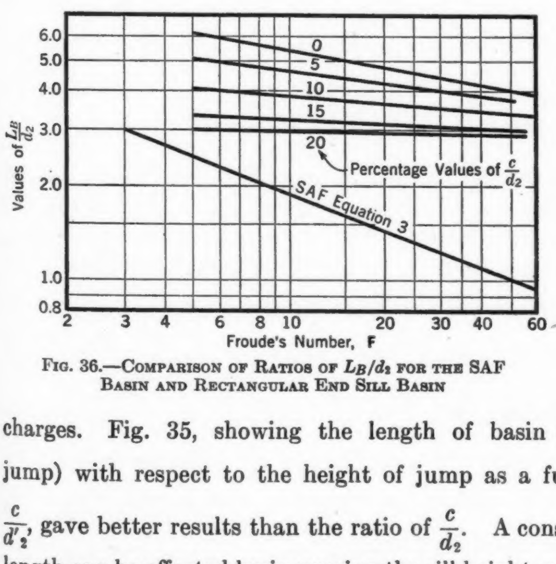

Fig. 36.—Comparison of Ratios of L_B/d_2 for the SAF Basin and Rectangular End Sill Basin

Comparison of Length of Basin.—The difficulty of expressing the basin length as a function of d_2 for all values of **F** was mentioned by the author when $L_B = 1.25$ d_2 gave results too short for small discharges and too long for higher discharges. Fig. 35, showing the length of basin (taken equal to length of jump) with respect to the height of jump as a function of $\frac{d_1}{d_c}$ (and **F**) and $\frac{c}{d'_2}$, gave better results than the ratio of $\frac{c}{d_2}$. A considerable reduction in basin length can be effected by increasing the sill height, using Figs. 35 and 36. This condition is especially true at the low Froude numbers where an almost 50%

reduction is possible because of the sill. Referring to Fig. 36, the SAF basin requires considerably less length, although with high rectangular end sills the lengths become more nearly the same. Floor and chute blocks therefore appear to be effective devices in reducing the length of jump.

Other Comparisons.—It was noted during the rectangular end sill tests that a boil formed over the sill for ratios of $\frac{d_1}{d_c} \leqq 0.32$ (equivalent to $\mathbf{F} \geqq 30$). This is interesting because in the SAF basin the roller was washed out of the stilling basin when **F** was less than about 30. The solution was to increase the tailwater depth. Practically the same procedure had to be followed for the rectangular end sill basin. Inspection of Fig. 34 shows that, with values of **F** in this range, the ratio of $\frac{d'_2}{d_2}$ had to be increased to almost unity to create sufficient depth to reduce and to absorb the downward velocity components so that they would not erode the bottom.

An attempt was made to determine the head loss created by the sill. The total head (velocity head plus depth) at the initial and final depths was computed for several tests with the rectangular sill. The head loss in the jump when no sill was used was measured and checked by the Stevens equation (36)(37),

$$i = \frac{6.25\,(\sqrt{1 + 16\,r} - 3)^3}{(1 + r)\,(\sqrt{1 + 16\,r} - 1)} \qquad (35)$$

in which i is the percentage of original head lost in the jump; and r is the ratio of velocity head to depth before the jump. The difference between the measured loss with a sill and that without a sill was expressed as a ratio of the original total head. It was found that the loss increased when the sill height was increased and when $\frac{d'_2}{d_2}$ was decreased. The head loss due to the sill was small, and was never more than 6% of the original head. This maximum loss was obtained when $\frac{c}{d'_2} = 0.25$ and $\frac{d'_2}{d_2} = 0.89$.

Calculation of the pressure-plus-momentum force at the end of the jump from the measured initial depth and discharge, neglecting the force on the sill, will give a smaller value than would be calculated at a section before the jump. The difference results from the back pressure of the sill. Tests indicated that the ratio of the force on the sill to the total force was increased when $\frac{c}{d'_2}$ was increased and $\frac{d'_2}{d_2}$ decreased. When the sill was 20% of the depth d'_2, the apparent force on the sill was about 10% of the total force, and $\frac{d'_2}{d_2}$ was equal to 0.90. Analysis of the other data indicates that for the range of sills up to $\frac{c}{d'_2} = 0.25$ the force on the sill, representing the error in using the momentum equation without correction, would be roughly

$$(P + M)_c = \left(1 - \frac{d'_2}{d_2}\right)(P + M)_1 \qquad (36)$$

in which $(P + M)_c$ is the force on the sill, in pounds; and $(P + M)_1$ is the pressure plus momentum force before the jump, in pounds.

The author is correct in stating that the SAF basin can be built shorter than the rectangular end sill type. For values of Froude numbers up to $\mathbf{F} = 30$, little difference seems to exist in the tailwater depth required for a jump. The indication is, however, that for the higher Froude numbers and the low tailwater depths, with a height of sill that would ordinarily be used, the rectangular basin would be inferior to one designed according to the SAF dimensions.

Bibliography.—

(15) **"The Hydraulic Jump in Terms of Dynamic Similarity,"** by B. A. Bakhmeteff and A. E. Matzke, *Transactions*, ASCE, Vol. 101, 1936, p. 630. (*a*) p. 676. (*b*) p. 643.

(27) **"Hydraulics of Open Channels,"** by Boris A. Bakhmeteff, McGraw-Hill Book Co., Inc., New York, N. Y., 1932, p. 241. (*a*) Chapter 18.

(28) **"Aerodynamics of the Airplane,"** by Clark B. Millikan, John Wiley & Sons, Inc., New York, N. Y., 1941, pp. 3–8.

(29) **"Principles of Naval Architecture,"** edited by Henry E. Rossell and Lawrence B. Chapman, Soc. of Naval Architects and Marine Engrs., Vol. 2, 1939, pp. 52–59.

(30) **"Fluid Mechanics for Hydraulic Engineers,"** by Hunter Rouse, Eng. Societies Monographs, 1938, Fig. 109. (*a*) p. 230.

(31) **"Engineering for Dams,"** by William P. Creager, Joel D. Justin, and Julian Hinds, John Wiley & Sons, Inc., New York, N. Y., 1944, Vol. 1, p. 84.

(32) **"Aerodynamics of the Perisphere and Trylon at World's Fair,"** by Alexander Klemin, Everett B. Schaefer, and J. G. Beerer, Jr., *Transactions*, ASCE, Vol. 104, 1939, p. 1449.

(33) **"Modern Conceptions of the Mechanics of Fluid Turbulence,"** by Hunter Rouse, *ibid.*, Vol. 102, 1937, p. 468.

(34) **"Baffle-Pier Experiments on Models of Pit River Dams,"** by I. C. Steele and R. A. Monroe, *Transactions*, ASCE, Vol. 93, 1929, pp. 451–546. (*a*) p. 518.

(35) **"Model and Prototype Studies on Unique Spillway: Part III of Symposium on Fontana Dam Spillway,"** by A. J. Peterka, *Civil Engineering*, June, 1946, p. 250.

(36) **"Determining the Energy Lost in the Hydraulic Jump,"** by J. C. Stevens, *Engineering News-Record*, June 4, 1925, p. 928–929.

(37) *Ibid.*, May 20, 1943, p. 58.

Corrections for *Transactions*: In February, 1947, *Proceedings*, on page 125, in Fig. 1(*a*) the dimension "$n_2 @ \frac{3}{4} d \frac{b_2}{b_1} \pm$," change "$d$" to "$d_1$"; on page 134, below the caption for Fig. 7, add "(Correction: Add a point at $\mathbf{F} = 3.18$ and $L_B/d_2 = 2.11$)"; in Fig. 9(*c*), the elevation of the point at the end of the wing wall is "− 0.02" instead of "0.02"; in Fig. 15(*a*), the elevation of the contour at

the end of the wing wall is "-0.2" instead of "0.2"; in Figs. 9, 15, and 16 change the ordinate caption to read "Distance" instead of "Elevation"; on page 145, in the key to Fig. 9 change "$\mathbf{R} \times 10^{3}$" to "$\mathbf{R} \times 10^{-3}$" and at subcaption (*i*) change "T17" to "T13"; on page 148, after line 18, add "(In Fig. 11, the plotted points are identified as follows: The triangles refer to tests of the flume outlet series, the circles to the turbine room series, and the numbers to the test numbers.)"; on page 154, in line 35, change the sentence to read "* * * sill which deflects the jet upward as it leaves the basin"; and, below the caption for Fig. 17, add "(Correction: In caption (*a*) **R** should be **R**, denoting the Reynolds number)."

AMERICAN SOCIETY OF CIVIL ENGINEERS

Founded November 5, 1852

DISCUSSIONS

STABILITY OF SOIL SLOPES

Discussion

BY K. B. HIRASHIMA

K. B. HIRASHIMA,[37] ESQ.—This paper, which is a valuable contribution to the literature on slope stability in that it provides an insight into the mechanics of slope failure, should be of interest to all engineers dealing with earth structures, such as highway cuts and embankments, earth dams, etc. In spite of considerable literature on the subject, cited by the author in the "Introduction," it is a phase of engineering science to which most engineers pay altogether too little attention. The subject of slope stability is one of great complexity involving many factors that are indeterminate and not fully understood. One needs only to observe the number of slope failures that actually occur to realize the truly complex nature of slope stability.

The stability of slopes in cohesionless soil is easy to understand. Slope failure in such cases is, as the author concludes, purely a superficial phenomenon. Hence, for a mass of cohesionless soil to be stable, it is only necessary that the side slopes be less than the angle of repose. It is noteworthy that Table 1 gives two values of the angle of repose, a maximum and a minimum, whereas most textbooks give but a single value. In regions subject to earthquakes and other such disturbances, important earth structures should perhaps have slopes not exceeding the minimum angle of repose, thus decreasing the tendency to slide.

In a cohesive soil, the cohesion is sometimes defined[38] by

$$c = P_i \tan \phi \qquad (27)$$

in which P_i is the hypothetical internal pressure and $\tan \phi$ is the coefficient of internal friction. The internal pressure P_i acts uniformly in all directions.

In his model test, the author uses an ingenious arrangement to impart an "equivalent cohesion" to a sandy mass by applying a uniform atmospheric pressure to the side slopes and top. This externally applied force gives rise to a

NOTE.—This paper by Ek-Khoo Tan was published in January, 1947, *Proceedings*. Discussion on this paper has appeared in *Proceedings*, as follows: May, 1947, by Paul Baumann, and Gregory P. Tschebotarioff; and June, 1947, by Jacob Feld, and Earl M. Buckingham.

[37] Testing Engr., Territorial Highway Dept., Honolulu, Hawaii.

[38] "Soil Mechanics," by Dimitri Krynine, McGraw-Hill Book Co., Inc., New York and London, 1st Ed., 1941.

stress system within the mass which can be resolved, at any given point, into a uniform direct stress, the same in all directions, and a shear stress. Theoretically, if this shear stress is of any consequence, it should affect the stress distribution due to the gravitational forces.

In the present model study it is not possible to reproduce all the conditions that exist in the prototype. An actual earth structure, such as a highway embankment, is bonded to the foundation soil—that is, there is a certain continuity to the soil mass. In a model, the soil mass is necessarily discontinous because of the model's rigid base. The change in boundary conditions affects the stress distribution; for instance, it is possible for the circle of sliding failure to undercut the toe of the slope, the so-called "Swedish break." For an embankment built on solid rock, that is, a rigid base, the failure line must necessarily pass through or above the toe of the slope.

In Fig. 6 is given the maximum height at which an unsupported bank of cohesive soil will stand vertically. It would have been interesting if the author had given additional data so as to make possible a comparison with the usual theoretical formula:[39]

$$H = \frac{2\,c}{w} \tan\left(45 + \frac{\phi}{2}\right) \qquad (28)$$

in which H is the maximum height of unsupported bank of cohesive soil; c is the cohesion; w is the unit weight of soil; and ϕ is the angle of internal friction. The paper presents a comparison of three methods of slope analysis: The photoelastic analysis, the Swedish circular arc method, and the theoretical plasticity analysis. For routine use, the Swedish circular arc method is the only practical one. This method deals essentially with averages. Thus, if the shearing stress tending to cause sliding failure is less than the shearing strength of the soil along the assumed arc of failure, the soil mass is assumed to be safe according to the usual rule. However, a careful study of the author's analysis will show that a dangerous condition may, nevertheless, exist—that is, certain regions within the soil mass may be so highly stressed that a condition of plasticity prevails. The gradual spreading of the plastic zone may lead to eventual failure, and it is well to remember in this connection that the spreading of a plastic zone within a large mass of earth is an extremely slow process that may require weeks, months, or even years.

In actual engineering earth structures, the pore water pressure[40, 41] must be known. The author does not give any data as to moisture content in any of his experiments. Apparently, it was necessary to use the sandy material in a dry state in order to control the "equivalent cohesion" within narrow limits.

The writer is familiar with a soil which has a natural moisture content of more than 200%, based on the dry weight of the soil, in its undisturbed state. A vertical bank from 8 ft to 10 ft high can be cut through this material. The slope will be stable and there will be no drainage of water from the sides, in

[39] "Present Status of Soils Investigations," by C. A. Hogentogler and E. S. Barber, *Proceedings*, 19th Annual Meeting, Highway Research Board, National Research Council, Washington, D. C., 1939, p. 377.

[40] "Factors of Safety to be Applied in the Utilization of Shear Test Data," by D. M. Burmister, *ibid.*, p. 439.

[41] "Theoretical Soil Mechanics," by Karl Terzaghi, John Wiley & Sons, Inc., New York, N. Y., 1943.

spite of the tremendous water content. On the other hand, building a highway embankment of any great height with such a soil is quite a problem, in view of the fact that rainfall conditions in the region where this particular soil is found are such that drying out the soil is impractical. Plastic zones will readily form within such a mass because of the high water content. The progressive creep of these plastic zones which may take years, has given rise to sudden settlements. However, it is the pore water pressure that is the basic cause of these difficulties, and the designer must have some idea of how this pressure acts in order to arrive at a safe design. Incidentally, in this particular soil a type of failure occurs that has not been mentioned thus far. If for any reason the moisture content of this soil drops below a certain critical value, as, for example, in times of drought, it turns irreversibly into a granular sandy mass, and the side slopes will fail in chunks along the surfaces separating the dry mass from the wet mass.

AMERICAN SOCIETY OF CIVIL ENGINEERS

Founded November 5, 1852

DISCUSSIONS

FRICTION COEFFICIENTS IN A LARGE TUNNEL

Discussion

BY W. R. BARROWS, HUNTER ROUSE, KARL R. KENNISON, E. J. K. CHAPMAN, JULIAN HINDS, AND WILLIAM P. CREAGER AND STEPHEN H. HAYBROOK

W. R. BARROWS,[17] Assoc. M. ASCE.—A part of the Apalachia tunnel was left unlined after an economic investigation had indicated that such a move would be wise. During the course of this investigation, it became necessary to estimate the probable friction loss in the unlined part. A search of the literature produced very little information. To make matters worse, the published data reported widely varying coefficients of friction for apparently similar conditions and gave no clue as to the probable value for the problem at hand. At this point the Aluminum Company of America made available data on the unlined tunnel of its Nantahala project. From these data the value of n in the Manning formula was estimated to be 0.037 for the unlined tunnel. This value compares favorably with the values determined by precise measurements in the Apalachia tunnel and was computed for velocities ranging from 2.18 to 4.28 ft per sec.

The Nantahala tunnel had been recently completed in a rock formation similar to the rock in which the Apalachia tunnel was driven. When it was unwatered after completion of the unit test, it was inspected by a party of engineers familiar with the Apalachia tunnel, who agreed that, in so far as could be observed, there was no difference in either the surface roughness or the manner the rock broke out in the two tunnels. The estimated coefficient for the Nantahala tunnel is slightly lower than that determined for the Apalachia tunnel. The difference could easily have resulted from the fact that the minor losses in the Nantahala tunnel had to be estimated.

Unlined parts of the Nantahala tunnel were driven to three different sections with nominal dimensions of 12 ft wide by 12 ft high, 14 ft wide by 13 ft high, and 13 ft wide by 14 ft high, the theoretical section in each case having an arched roof with a radius equal to half the width and a flat floor connected

NOTE.—This paper by G. H. Hickox, A. J. Peterka, and R. A. Elder was published in April, 1947, *Proceedings*. Discussion on this paper has appeared in *Proceedings*, as follows: June, 1947, by Weston Gavett.

[17] Civ. Engr., Albuquerque, N. Mex.

to the spring line of the arch by vertical sides. Cross sections of the completed tunnel were available and from them the average area and wetted perimeter of the different sections were determined. The discharge was determined from unit efficiency tests, and the head loss between the forebay and the surge tank was measured.

The experimental values for the coefficient of friction of an unlined rock tunnel presented by Messrs. Hickox, Peterka, and Elder are based on the measured properties of the actual section "adjusted to equivalent circular sections." This point deserves emphasis. The engineer when considering reported values of n for excavations which may deviate considerably from the desired dimensions should assure himself that the values were determined in such a way as to make them applicable to his problem. For instance, assume that the coefficient of friction of an unlined tunnel 12 ft in diameter was determined using the theoretical properties of the section instead of the actual. Such a value applied to a tunnel 30 ft in diameter would result in an estimated head loss equal to approximately two thirds of the actual head loss, assuming equal overbreak. However, the values reported by the authors should be applicable in similar rock tunnels over a wide range of sections.

HUNTER ROUSE,[18] M. ASCE.—Test results that extend the existing range of measured data are welcome in any field of engineering. To the best knowledge of the writer, the resistance measurements presented by the authors of this factual paper go well beyond the available information in two respects. First, the Reynolds numbers are nearly a full logarithmic cycle higher than those of all but a few isolated measurements on large conduits. Second, the absolute roughness of one series far exceeds that of boundary surfaces generally considered in the roughness category. With this apparent two-directional enlargement of the resistance field, several checks upon the matter at once suggest themselves. Are the new results in accord with present knowledge of this problem? If not, do these results indicate errors in present knowledge, or is such knowledge sufficiently sound to disclose inaccuracies in either the data or the authors' analysis?

In 1942 the writer showed[19] that the best available resistance measurements for a wide variety of new and old commercial pipe approximated the transition curve of C. F. Colebrook:[20]

$$\frac{1}{\sqrt{f}} - 2 \log \frac{r}{k} = 1.74 - 2 \log \left(1 + 18.7 \frac{r/k}{\mathbf{R} \sqrt{f}} \right) \qquad (7)$$

On the basis of this analysis, the writer prepared a general resistance diagram[19,21] permitting solution for either V or h_f for (presumably) the flow of any fluid at any speed through any size of conduit having a surface comparable to any one of those for which data were analyzed. In this diagram an asphalted surface

[18] Director, Iowa Inst. of Hydr. Research, State Univ. of Iowa, Iowa City, Iowa.

[19] "Evaluation of Boundary Roughness," by Hunter Rouse, *Proceedings*, 2d Hydraulics Conference, Studies in Eng., *Bulletin No. 27*, Univ. of Iowa, Iowa City, 1943.

[20] "Turbulent Flow in Pipes, with Particular Reference to the Transition Region Between the Smooth and Rough Pipe Laws," by C. F. Colebrook, *Journal*, Inst. C. E., London, February, 1939.

[21] "Elementary Mechanics of Fluids," by Hunter Rouse, John Wiley & Sons, Inc., New York, N. Y., 1946, p. 211.

was listed as having an equivalent sand roughness of $k = 0.005$ in.; a concrete surface, of $k = 0.1$ to 0.01 in. The authors' values for the asphalted and concrete linings were 0.0035 in. and 0.04 in., respectively. The writer's diagram included no relative roughness values higher than $k/r = 1/10$, however, for two reasons: First, the effective diameter of a very rough conduit is difficult to define, both practically and theoretically; second, boundary irregularities having a greater relative magnitude than approximately one tenth of the radius begin to represent cross-sectional constrictions rather than surface roughness and cannot significantly be discussed in the same terms. The maximum value listed in this paper is about one sixth.

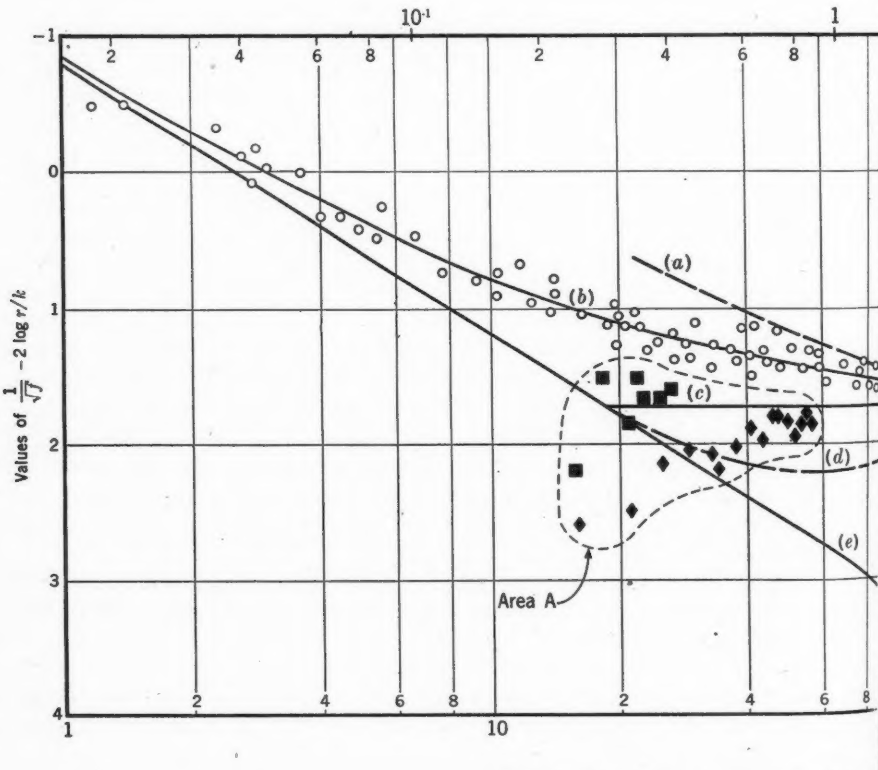

Fig. 13.—Comparison of Apalachia Tunnel

The authors restrict their interpretation of the surface-resistance measurements to two primary features—the variation of f with $\mathbf{R}$, and the variation of n with $\mathbf{R}$. The former, with Fig. 10 the corresponding exhibit, shows little of the actual relationship of the three series to existing generalized treatments; nevertheless, the resulting values of k for the assumed limits of the apparent transition curves are tabulated. Portrayal of n as a function of $\mathbf{R}$, furthermore,

is hardly consistent with either the true significance of n as a roughness parameter or with the authors' evaluation of k, for most assuredly showing how k (neither more nor less a roughness parameter than n) varied with **R** was not considered.

As has long appeared evident,[22] whether the resistance of a conduit boundary is dependent on or independent of **R** is governed by whether the zone of laminar flow at the boundary (that is, the laminar sublayer, for which the nominal thickness δ' is equal to $65.6\, r/\mathbf{R}\, \sqrt{f}$) encloses and thus renders the surface irregularities ineffective, or is itself disrupted and thus rendered ineffective by the irregularities. In a word, whether the wall behavior is smooth or

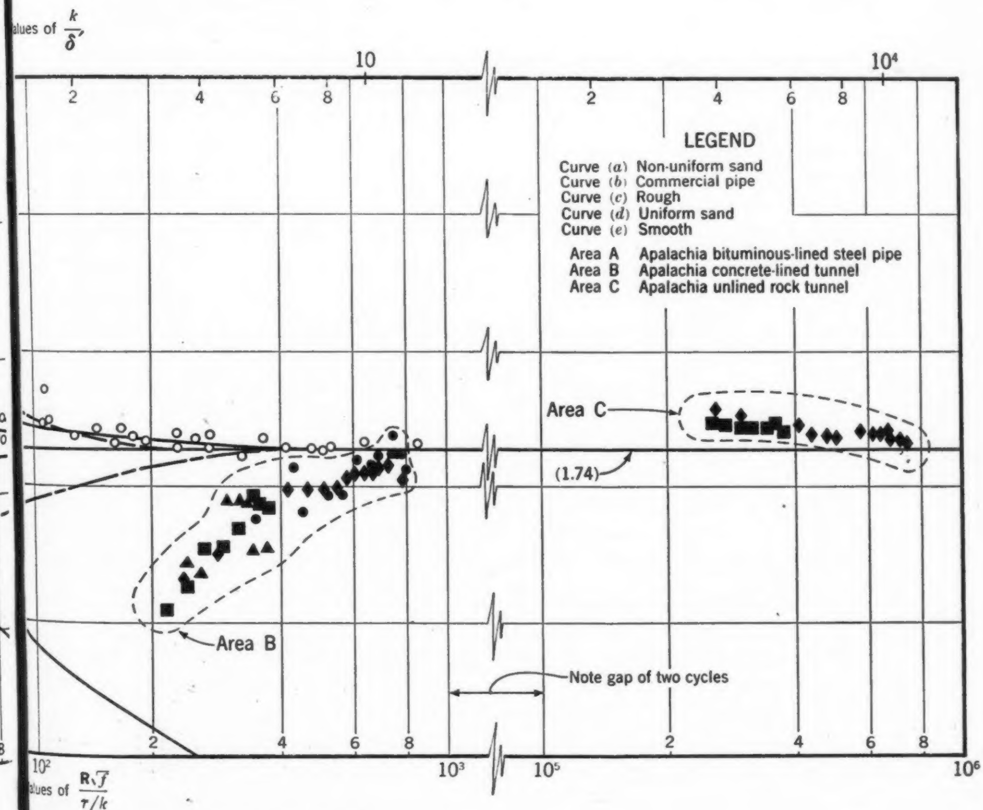

TA WITH PREVIOUS EXPERIMENTAL RESULTS

rough depends on whether the ratio k/δ' is, respectively, much less or much greater than unity. This ratio is evidently proportional to the quantity $(\mathbf{R}\, \sqrt{f})/(r/k)$. A plot using this parameter for the abscissa scale and the quantity $1/\sqrt{f} - 2 \log r/k$ for the ordinate scale in effect reduces all resistance data to the same common denominator of relative viscosity-versus-roughness

[22] "Modern Conceptions of the Mechanics of Fluid Turbulence," by Hunter Rouse, *Transactions*, ASCE, Vol. 102, 1937, p. 463.

action. J. Nikuradse[12] first used this method in correlating his tests on uniform sand roughness, which resulted in the single function for all his data shown by curve (*d*) of Fig. 13. Extending this study to the conditions of nonuniform sanded surfaces, C. F. Colebrook and C. M. White[23] obtained a gradual displacement of the transition function with increasing nonuniformity; curve (*a*), Fig. 13, represents the limiting one of their series. Since most natural roughnesses are essentially nonuniform, it is reasonable that the transition curve for such surfaces should lie between these limits and yet begin at a far lower value of k/δ' than that for uniform surface irregularities; this condition is satisfied by C. F. Colebrook's function shown in Fig. 13 by curve (*b*).

Data previously analyzed by the writer[19] and reproduced in Fig. 13 include new and old pipes varying from 2 in. to $72\frac{1}{2}$ in. in diameter and fabricated of such materials as galvanized iron, wrought iron, cast iron, tarred cast iron, spiral-riveted steel, and wood stave. The three series of the authors' data are likewise reproduced, using the values of r/k given in Tables 4, 7, and 8. It is at once evident that the zone covered by any one series is very small compared with that encompassed by all three; also evident is the departure of the data from the trend of the general transition between smooth and rough boundary behavior. In fact, the data for the bituminous-coated steel pipe (area A), when reduced to the proportions of this plot, no longer indicate a significant trend, and the centroid of this area is well below the general function. A trend of the data for the concrete-lined tunnel (area B) is more apparent, but is not in agreement with any of the earlier functions; the centroid is likewise low. Finally, the data for the unlined rock tunnel (area C) are so far beyond the range of viscous action (note that k is some six thousand times the computed magnitude of δ') that the slight downward trend probably has no significance.

From this comparison it may be concluded that the authors' method of evaluating the relative and absolute roughness is generally unreliable. If the centroid of the unlined tunnel data, with a value of $f = 0.099$, is used to determine the relative roughness from the limiting ordinate 1.74 of the roughness function (curve (*c*), Fig. 13), this will be found to be $r/k = 5.3$, for which $k = 26$ in., as compared with the authors' values of $r/k = 6.17$ and $k = 22$ in. If the centroid of the concrete lining data ($f = 0.0123$) is likewise used, it will be found that $r/k = 4{,}300$ and $k = 0.025$ in., in distinction to the authors' values of $r/k = 2{,}690$ and $k = 0.04$ in. Since the bituminous lining data, on the other hand, lie well within the zone of viscous influence, it is necessary either to locate the centroid on a general resistance diagram (such as that prepared by the writer from the Colebrook function[19,21]) and read r/k directly thereon, or to solve Eq. 7 for the same conditions by the process of trial and error. The result will be $r/k = 170{,}000$, for which $k = 0.00063$ in. These values differ considerably from the authors' selection of $r/k = 30{,}900$ and $k = 0.0035$ in. There is a comparable difference between this value of 0.00063 in. for the 18-ft bituminous-lined steel pipe and the average of 0.005 in. previously determined[20]

[12] "Stromungsgesetze in rauhen Rohren," by J. Nikuradse, *Forschungsheft*, Verein Deutscher Ingenieure, Heft 361, 1933.

[23] "Experiments with Fluid-Friction in Roughened Pipes," by C. F. Colebrook and C. M. White, *Proceedings*, Royal Soc. of London, Vol. 161, 1937.

for asphalted cast-iron pipe varying from 4 in. to 5 ft in diameter, which may be attributable to the effect of pipe joints and methods of surface application.

Although the discrepancies between the authors' and the writer's calculations are small in two of the three cases, it is the general method rather than the numerical results which the writer seeks to emphasize. In no way, however, is it sought to disparage contributions of this nature. Variations such as those indicated by the authors' data have been the rule rather than the exception, even in apparently well-controlled laboratory experiments. Although one cannot expect to duplicate laboratory results under field conditions with respect to either accuracy or over-all range of Reynolds numbers, field corroboration of laboratory analyses are fully as essential as are final acceptance tests for any hydraulic design. The authors are therefore to be heartily commended for their effort to provide several links in the necessary chain of field evidence. The particular merit of the paper as a whole is twofold: First, it gives a clear indication of the desirability of preparing for prototype tests of this nature during the design of every large installation. Second, it gives an equally clear indication of the degree of accuracy which may be expected in predicting the performance of a conduit; surely the use of more than two significant digits is still quite futile.

KARL R. KENNISON,[24] M. ASCE.—Much valuable information on coefficients of flow in large diameter tunnels has been assembled in this paper. It occurs to the writer that it will be interesting and instructive to compare this information with that obtained in actual operation over a period of years on the Quabbin Aqueduct tunnel built by the Metropolitan District Water Supply Commission,[25,26,27,28] in Massachusetts. The great length of this tunnel, 24.6 miles, and the uniformity of operating conditions over long intervals of time obviously contribute much to the accuracy of the data and the precision with which the results can be computed. For example, since the filling of Quabbin Reservoir was started late in 1939, the aqueduct has been used for free discharge into Wachusett Reservoir in the following quantities:

Period	Million gal
September 17 to October 28, 1941	20,426
August 6 to September 7, 1943	17,020
June 13 to September 11, 1944	25,425
June 27 to September 22, 1945	22,008
August 26 to September 13, 1946	10,745
January 27 to February 11, 1947	9,660

The tunnel is operated as a pressure tunnel. It was constructed as a horseshoe-shaped grade tunnel, since the internal water pressure is less than

[24] Chf. Engr., Construction Div., Met. Dist. Comm., Commonwealth of Massachusetts, Boston, Mass.

[25] "The Metropolitan District Water Supply Tunnel from the Ware River to the Wachusett Reservoir," by Frank E. Winsor, *Journal*, Boston Soc. of Civ. Engrs., November, 1932, p. 461.

[26] "Boston's New Metropolitan Water Supply," by Frank E. Winsor, *Civil Engineering*, June, 1934, p. 283.

[27] "Boston Metropolitan Water Supply Extension," by Karl R. Kennison, *Journal*, New England Water Works Assn., June, 1934, p. 147.

[28] "Ware River Intake Shaft and Diversion Works," by Karl R. Kennison, *Civil Engineering*, August, 1934, p. 388.

the external pressure resulting from the normal ground-water level. This is not strictly true for a short distance at the Wachusett Reservoir end, where a length of 500 ft next to uptake shaft 1 was constructed as a circular pressure tunnel 12 ft 9 in. in diameter, with the lining grouted against the ledge to prevent leakage from the tunnel under the full head of Quabbin Reservoir. This head is effective throughout the entire length of the tunnel as far as the outlet control gates at the top of shaft 1. Another section, 200 ft long at the extreme westerly end next to the Quabbin intake shaft (shaft 12), was similarly constructed as a circular pressure tunnel to prevent excessive leakage from the reservoir into the tunnel whenever the latter is unwatered for inspection purposes by inserting stop logs at shaft 12. With these two exceptions, the horseshoe section is maintained throughout the entire length of 129,413 ft between downtake shaft 12 and uptake shaft 1. These lengths of circular tunnel represent a small percentage of the total and furthermore have the same cross-sectional area. Hence, the fact that these end sections have a slightly greater hydraulic radius can be neglected.

The width of the tunnel is 11 ft 0 in. between vertical side walls; the height is 12 ft 9 in. from invert to crown. The cross-sectional area is 127.6 sq ft, and the hydraulic radius is 3.03 ft. Flow is unobstructed except as follows:

(*a*) The downtake waterway in shaft 12 is about 115 ft deep and is crossed by numerous struts spanning the openings in which stop logs and screens are placed. Ordinarily water is drawn from the upper intake, which permits free entrance from the reservoir for a depth of nearly 50 ft from the surface. Water drawn from the lower intake must rise through an uptake shaft before turning to drop into the downtake shaft.

(*b*) Shaft 11-A is an uptake shaft for diverting flood flows from the Ware River into Quabbin Reservoir; hence, there is a large opening in the crown.

(*c*) At the bottom of construction shafts 11, 10, 7, 6, 5, and 3 there is a sizable rectangular opening in the crown and a large sump in the invert.

(*d*) At the bottom of shaft 9 there is a central pier 18 in. wide, in addition to large openings in the crown for access and for placing emergency stop logs in the two 4-ft 9-in. bays, and in addition to the invert sump. There are also two low racks 4 ft 6 in. high in each of the two bays for the purpose of catching any debris that may roll along the invert. These racks are constructed of $\frac{1}{4}$-in. flats, 3 in. on centers. They are placed there merely because the access to this point is convenient because of gravity drainage into Wachusett Reservoir. The net cross-sectional area may well be taken as from about 110 to 115 sq ft.

(*e*) At a point between shaft 9 and shaft 8, there is a 2-ft-wide central pier, which was left after the removal of a heavy steel bulkhead behind which the Quabbin end of the tunnel was constructed while the Wachusett end was first operated for diversions from the Ware River directly to Wachusett Reservoir. The net waterway area is 102.1 sq ft.

(*f*) At shaft 8, a downtake shaft for Ware River floods, there is a considerable enlargement in the area as well as a large sump in the invert crossed by a narrow footbridge.

(*g*) At the bottom of shaft 4, there is a central pier 18 in. wide and the shaft otherwise resembles shaft 9. The net waterway area is 108.5 sq ft. No racks are placed there.

(*h*) At shaft 2, an uptake shaft leading to a spillway at the surface, there is a large opening in the crown as well as the sump in the invert.

(*i*) Shaft 1, the uptake shaft to Wachusett Reservoir, contains a 144-in. by 90-in. venturi meter, by which all the flows are measured. At the top, a branch extends horizontally through two 6-ft control valves in series and discharges under water into a stilling pool through a 5-ft $5\frac{1}{2}$-in.-diameter end nozzle with a waterway area of 23.4 sq ft. The nozzle crown is several feet beneath the surface. Under all the high velocity conditions considered in this discussion, the water is pushed ahead in large eddies, which flow back around the nozzle in such a manner that the static head is practically zero at the nozzle crown (El. 388.2).

By the summer of 1943, Quabbin Reservoir had filled to within 30 ft of the flow line and a continuous draft was made for about a month under conditions of steady uniform flow. On September 3 of that year, fifteen readings were taken, at 1-min intervals, of the water level in a well connected to the bottom of shaft 12. The average level was El. 494.16; the maximum departure from the mean was 0.35 ft. It was estimated that 0.72 ft should be added to this pressure gradient to obtain the true energy gradient, allowing for velocity head and some downstream loss on account of the bend.

On the same day, about 1 hour earlier, ten readings were taken, at 1-min intervals, of the water level in shaft 9. The average level was El. 466.29, and the maximum departure from the mean was 0.09 ft. It was estimated that the true energy gradient, including velocity head, was 467.29. Hence, the loss of head in the 47,098 ft between shafts 12 and 9 was 27.59 ft, which is estimated to be reduced to about 27.3 ft by miscellaneous minor losses occurring at the previously described shaft bottoms en route. Hence, the slope of the hydraulic gradient was 0.580 per thousand.

Four hours earlier on the same day fifteen readings were taken, at 1-min intervals, of the water level in shaft 2. The average level was El. 423.57, and the maximum departure from the mean was 0.20 ft. It was estimated that the true energy gradient, including velocity head, was 424.29. Hence, the loss of head in the 72,413 ft between shafts 9 and 2 was 43.00 ft, which is estimated to be reduced to about 42.0 ft by miscellaneous minor losses occurring past the pier between shafts 9 and 8, and at the other shaft bottoms, including somewhat less than full recovery of velocity head at the downstream end of the piers at shafts 9 and 4. Hence, the slope of the hydraulic gradient was 0.580 per thousand, the same as that in the other stretch upstream. Continuing this same slope for the remaining 9,902 ft to the bottom of uptake shaft 1, the computed energy gradient at that point was El. 418.54, and the difference or loss from this point to the crown of the nozzle in the stilling chamber, El. 388.2, was 30.3 ft. Of this total, 21.4 ft represented velocity head at the discharge end, leaving about 8.9 ft for all the miscellaneous losses in the uptake shaft, including those of the meter and valves. This loss, in feet, equals 0.0000282

TABLE 12.—OPERATING DATA FOR QUABBIN AQUEDUCT TUNNEL

Line No.	Date	Average reservoir elevation[a]	Total head available[b] (ft)	HEAD LOSSES (FT)			Hydraulic slope (ft per thousand ft)	AVERAGE FLOW		Average velocity (ft per sec)	Temperature (°C)	Kutter's n	Hazen-Williams' C
				Velocity head at exit	Miscellaneous	Friction		Mgd	Cu ft per sec				
(1)	(2)	(3)	(4)	(5)	(6)	(7)	(8)	(9)	(10)	(11)	(12)	(13)	(14)
1	September 3, 1943		As described for this day				0.580	561.9	869.9	6.81	17	0.0111	144
2	July 13 to 26, 1944	507.64	119.4	24.2	15.1	80.1	0.619	597.2	925	7.25	17	0.0109	148
3	September 1 to 9, 1944	505.97	117.8	23.8	16.9	77.1	0.596	591.8	916	7.18	16	0.0108	150
4	June 28 to July 20, 1945	519.60	131.4	25.6	18.3	87.5	0.677	614.7	951	7.46	15	0.0110	146
5	September 11 to 21, 1945	519.58	131.4	25.9	18.5	87.0	0.673	617.7	956	7.49	17	0.0109	147
6	September 1 to 12, 1946	528.97	140.8	28.1	17.5	95.2	0.736	643.5	996	7.81	20.5	0.0110	146
7	January 30 to February 10, 1947	528.64	140.4	28.1	17.5	94.8	0.733	643.5	996	7.81	1.0	0.0110	146

[a] Average surface elevation of Quabbin Reservoir. [b] Difference in elevation between Quabbin Reservoir surface and outlet (388.2).

mgd², which has been checked by the writer on a number of other occasions as entirely reasonable.

In writing a convenient expression of the loss as a function of the rate of flow, the use of the exponent 2 is justified because of the narrow range within which the rate fluctuates. The loss in getting into the tunnel from Quabbin Reservoir and in the downtake to the bottom of shaft 12 is estimated from excellent data to be 0.0000100 mgd² with draft from the upper intake (0.0000160 mgd² with draft from the lower intake). The losses are summarized as follows:

Type of head loss	Head, in ft/mgd²
Reservoir to bottom of shaft 12	0.0000100
Past shaft bottoms and piers	0.0000041
Bottom of shaft 1 to exit	0.0000282
Total miscellaneous	0.0000423
Velocity head at exit	0.0000680
	0.0001103
Friction	0.000235
	0.000345

In confirmation of the previous reference to the inherent accuracy and precision caused by the great length of the tunnel, note that it takes as much as 11% uncertainty in the determination of miscellaneous losses to correspond to 1% difference in the rate of flow. Based on this fairly accurate determination of these miscellaneous losses in terms of the rate of flow, the data for all the long runs have been tabulated and used to determine the probable coefficient, as shown in Table 12. The change in reservoir elevation during any run is so small and at so uniform a rate that no appreciable error is introduced in observing it. The same is true of the

steadiness of the rate of flow. Although infiltration of as much as 3 mgd has been noted just after unwatering of the tunnel, leakage under actual operating conditions at full head is considered negligible.

The losses in Col. 6, Table 12, are for drafts from the upper intake in the case of the last two runs, in 1946 and 1947, and from the lower intake in the previous years. In the case of run 2, however, the upper intake was also open providing free access and approximately the same head loss conditions as normal draft from the upper intake at the later high reservoir levels. Col. 12 is based on depth observations in the reservoir in front of the intake.

For convenience, the data in Col. 13 were read from the writer's diagram and those in Col. 14 from the Hazen-Williams slide rule.

The writer has noted, in studying these data, that there appears to be a slight improvement in the coefficient immediately following a long period of flushing out at these high velocities. It should also be pointed out that there is a tendency for air to enter aqueducts of this type and to be carried along the crown. This results in an appreciable lubricating effect, the actual hydraulic radius being somewhat greater than the theoretical and the roughness being actually somewhat greater than indicated by using the theoretical radius. Such differences, however, are very slight.

E. J. K. CHAPMAN,[29] Assoc. M. ASCE.—The results published in this paper are of considerable value and the authors are to be commended for their careful and analytical presentation of the facts. One set of results is of particular interest in that it discloses certain surprising features which would not normally have been expecteed. These are the data given for the 18-ft-diameter concrete-lined tunnel. In the section between the Apalachia Dam adit and the Apalachia adit, the results indicate a variation in Manning's n from 0.0122 to 0.0136 as the velocities increase from 3.8 ft per sec to 12.6 ft per sec. This variation in n is large and seems much greater than could have been anticipated, especially in view of the careful manner in which the tests were conducted. Manning's formula has been well tested in the past in many large tunnels and has proved reliable, and the values of n determined for any given tunnel are usually more consistent. In addition to the variations of n, the top value of 0.0136 is considerably higher than would have been expected from the descriptions of the concrete surfaces given in the paper. In fact, in the section between Turtletown Creek and McFarland adit, a value of 0.0138 was reached and maintained over a fair range of velocity.

It is interesting to note that the value taken for a design basis[30] was 0.0130 and it might well have been hoped that a better value than this would be obtained, especially before the tunnel had seen any service.

The writer is closely associated with James Williamson, who has done much work on the underlying causes of frictional resistance created by turbulent flow in pipes.[31] In the manuscript of an unpublished paper, Mr. Williamson

[29] Cons. Engr., Glasgow, Scotland.

[30] "The Design of Recent TVA Projects: VIII. Apalachia and Ocoee No. 3," by H. W. Goodhue, R. L. Smart, and A. A. Meyer, *Civil Engineering*, October, 1943, p. 465.

[31] "Considerations on Flow in Large Pipes, Conduits, Tunnels, Bends, and Siphons," by James Williamson, *Journal*, Inst. C. E., London, April, 1939, p. 451.

touches on the special conditions occurring in very large pipes with very high R/k-ratios. He shows how pipes with R/k-ratios greater than 2,000 can be expected to develop spiral flow which may be of the stable or continuing form, where the pitch is independent of the velocity. In such cases the frictional resistance is expected to be higher than that given by calculations based on normal axial flow.

The Apalachia 18-ft-diameter concrete-lined tunnel has an R/k-ratio of 2,690, or possibly higher. This ratio brings the tunnel into the spiral flow region, and a further unusual feature of the tunnel is that the section is circular, which would allow spiral flow to develop and continue, whereas the more usual horseshoe shape would tend to maintain axial flow.

From these considerations, the writer feels that the probable explanation of the surprisingly high value of Manning's n is due to the fact that spiral flow has developed, especially at the higher velocities.

It is noted from the description of the design of the project[30] that the associated Ocoee No. 3 project included a horseshoe-shaped tunnel of somewhat smaller diameter than the Apalachia tunnel. Presumably the workmanship and finish of the concrete surfaces were similar in the two projects. If so, the Ocoee tunnel, in view of its smaller R/k-ratio in conjunction with its horseshoe section, would probably not present conditions for spiral flow. Thus, frictional loss would be expected to give a more constant and generally lower value of Manning's n.

The authors do not publish any data on Ocoee No. 3 in their paper, but possibly some tests were made even if these consisted only of recording the surge tank water levels at steady flows, from which, with suitable allowances, a calculation could be made of the whole loss from reservoir to surge tank and a value of n could be determined. If so, it would be extremely interesting to discover if the writer's supposition is borne out by an apparently lower value of n.

Probably the only positive method of determining whether spiral flow does occur at Apalachia would be to make pitometer traverses on two or more diameters of the 18-ft pipe and plot the velocity distribution. The velocity contours would clearly indicate whether flow is symmetrical across the whole diameter or not. A suitable place to install appliances for taking these traverses appears to be at the 16-ft-diameter steel pipe crossing over Turtletown Creek. Unfortunately the contraction from 18-ft to 16-ft diameter a short distance upstream will apply an energy effort causing reversion toward uniform velocity, and one could expect at this place only a slight residual indication of spiral flow. Better results would be obtained if it were possible to make the measurements on an 18-ft-diameter section.

It is not often that an opportunity occurs to check a large-scale effect which cannot be determined by laboratory experiment, but the writer feels that such an opportunity exists in the two tunnels referred to and strongly urges that, in the interest of hydraulics, the hydraulic engineers of the Tennessee Valley Authority should re-examine the test results for the two tunnels and make further experiments, if practicable, to determine the effect of spiral flow on resistance to flow.

The pertinent points are:

(1) Does Ocoee No. 3 tunnel, with presumably similar surface conditions to those in the Apalachia tunnel, show a lower coefficient n by the Manning formula?

(2) Does spiral flow occur in the Apalachia tunnel and not in the Ocoee No. 3 tunnel?

JULIAN HINDS,[32] M. ASCE.—In this carefully conducted series of experiments, the authors have invaded a size range for circular conduits flowing full on which very little research has been done previously. The results deserve careful study and frank discussion by all engineers interested in the development of better pipe flow data.

Because of the complexity of the layout, the precise allocation of losses to particular reaches of line is not simple, but the complexities are fully presented and the method of allocation is explained in detail. The considerable lengths of the various reaches contributed to dependability.

It is noted that the reduced data are compared both with a "conventional" formula (Manning) and the more recent Reynolds number formulas. This comparison is particularly appropriate because of the efforts being made to unify practice and theory in pipe line design.

The earliest and most fundamental of the formulas used for computing resistance to flow in pipe lines are those proposed by Chézy and Darcy. These formulas are not independent, but are transposable, either into the other. Any table or diagram for finding the coefficients in one of them can be made to yield the coefficients for the other simultaneously. Any difference in regard to convenience of use is inconsequential. The Darcy equation has the esthetic virtue of being nondimensional, for which reason it is preferred in mathematical discussions. Auxiliary methods are required for finding the coefficients in each of these equations.

Supplementing these two basic equations are the conventional Kutter, Manning, Williams-Hazen, Scobey, and other formulas. The Kutter formula is used for finding the Chézy coefficients; and, although it is primarily adapted to open channels, at times it is applied to pipes. The Williams-Hazen and the Scobey formulas are exponential in form and are considered applicable only to pipes. The Manning formula also is exponential and usually is so employed, but is occasionally used for determining the Chézy coefficient—for both open and closed conduits.

All these formulas are empirical, applicable to water only, and may be confidently adopted only within the range of experimental verification. Much work has been done on the development of rational flow formulas for the flow of all fluids in all pipes. Definite progress has been made, but complete coordination between laboratory and field experiments as well as between theory and designing office practice has not been accomplished.[33] If the new formulas are to be applicable to all kinds of fluids, it is essential that they take into

[32] Gen. Mgr. and Chf. Engr., The Met. Water Dist. of Southern California, Los Angeles, Calif.

[33] "Comparison of Formulas for Pipe Flow," by Julian Hinds, *Journal*, A.W.W.A., November, 1946, p. 1226.

account the effect of viscosity. This effect is introduced through the Reynolds number, **R**. (All nomenclature is identical with that used by the authors unless otherwise noted.) The dimensionless factor, f, in the Darcy formula (Eq. 1) is used as the other variable; hence, these new equations will be referred to as the $(f-\mathbf{R})$-equations or formulas.

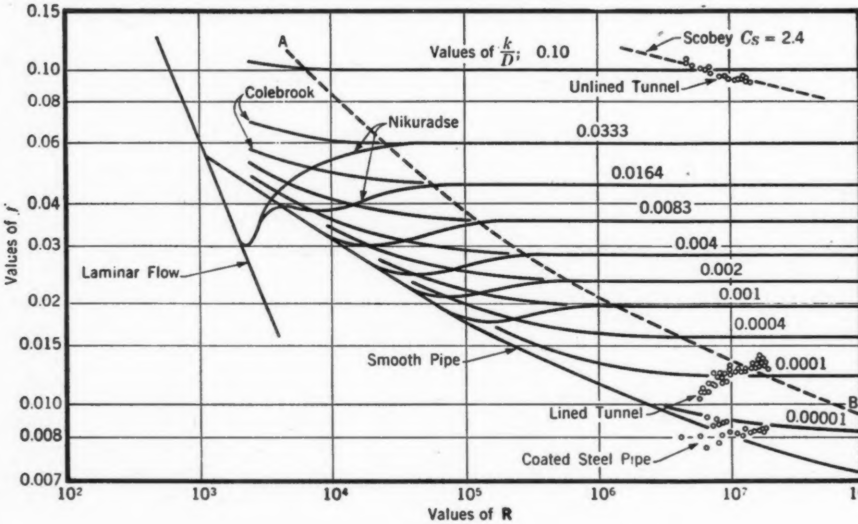

FIG. 14

The relation of these equations to each other, to the authors' data, and to one important collection of previously published data, is illustrated in Fig. 14. This group of curves covers the full range of pipe flow conditions up to $\mathbf{R} = 100,000,000$, passing from laminar flow on the left through a transition zone to a zone of complete turbulence in the upper right-hand part of Fig. 14. Laminar flow has no connection with the data reported in this paper and need not be discussed.

There are at present three $(f-\mathbf{R})$-equations within the turbulent range bidding for acceptance, each in its particular field. The most thoroughly substantiated of these is the smooth pipe formula credited by the authors to Theodor von Kármán, M. ASCE, and Ludwig Prandtl:

$$\frac{1}{\sqrt{f}} = 2.0 \log \mathbf{R} \sqrt{f} - 0.80 \qquad (8)$$

The accuracy of Eq. 8 for the flow of water or air through glass or drawn brass pipe was experimentally substantiated by T. D. Stanton and T. F. Pannell for values of **R** up to 500,000.[34] Its conformity to flow in larger pipes and in other types of surfaces has been reasonably well substantiated by others. In 1939 C. F. Colebrook published a diagram showing the applicability of this equation

[34] "Similarity of Motion in Relation to Surface Friction of Fluids," by T. D. Stanton and T. F. Pannell, *Transactions*, Royal Soc. of London A, Vol. 214, 1914, p. 199.

to cast-iron pipe from 4 in. to 60 in. in diameter, provided with spun cement and bituminous linings; he also showed its applicability to an 18-ft concrete-lined tunnel.[20]

Eq. 8 is presumed to apply to all fluids and is doubtless accurate for actually smooth surfaces beyond all practical requirements. As will subsequently appear, flow in even moderately roughened pipes seems to follow this curve for limited values of **R**.

The smooth pipe curve, Eq. 8, plats as a single line in Fig. 14. It thus serves merely as a boundary for an unlimited multitude of possible flow conditions for which other formulas are required. Eq. 6, likewise reasonably well established, is applicable to flow conditions in the zone of complete turbulence, the upper right-hand part of Fig. 14.

Data substantiating the applicability of this equation to smooth pipes roughened by uniform sand grains glued to the interior surface were published by J. Nikuradse in 1933.[35,36] The results of these experiments classified as to the ratio of sand grain size (k) to pipe diameter (D) are shown in Fig. 14. (The Nikuradse data were transferred to Fig. 14 photostatically. The results are accurate enough for present purposes, but not necessarily exact.) It will be noted that the plotted points follow the smooth pipe curve for varying distances, depending on the relative roughness (k/D), then pull away, continuing downward for a distance and finally rising to a constant value of f. Beyond this point the ($f-\mathbf{R}$)-curve for any specific value of k/D is horizontal. Eq. 6 gives the vertical distribution of the horizontal parts of these lines.

The points at which the platted data assume horizontal directions are not sharply defined, but are approximately delineated by curve A–B, Fig. 14, the equation of which is

$$\frac{1}{\sqrt{f}} = \frac{\mathbf{R}}{200} \times \frac{k}{D} \qquad (9)$$

The region to the right of, and above, this line constitutes the zone of complete turbulence. Within this zone, viscosity has no effect on flow and, for a given pipe, values of Darcy's f and Chézy's C are constant; they are the same for gas, water, gasoline, hot or cold crude oil, or any other fluid. Within the range of applicability of Eq. 6, a diagram of the complicated form of Fig. 14 is unnecessary. Values of both f and C can be taken from a simple diagram or table.

Unfortunately, a large percentage of the flow problems encountered in practice do not fall within this range, but lie in the transition zone. If it could be shown that all rough pipe flows follow the form of Mr. Nikuradse's experimental data, it would be on the side of safety (although not necessarily economical) to ignore the dip shown by him in the transition zone. All rough pipe for all purposes then could be designed in accordance with Eq. 6, except for small values of **R** for which the smooth pipe formula, Eq. 8, controls.

[35] "Gesetzmässigkeiten der turbulenten Strömung in glatten Röhren," by J. Nikuradse, *Zeitschrift*, Vereines Deutscher Ingenieure, Band 77, 1933, p. 48.

[36] "The Mechanics of Turbulent Flow," by Boris A. Bahkmeteff, Princeton Univ. Press, Princeton, N. J., 1941, p. 32.

However, other experimenters have found that pipes with natural roughness follow a different law in the transition zone. There appears to be a continuous upcurve toward the left, rather than the dip found for the sand-roughened pipe. After analyzing available data, Mr. Colebook proposed a formula covering flow both in the transition zone and in the zone of complete turbulence:[20]

$$\frac{1}{\sqrt{f}} = -2 \log \left(\frac{k/D}{3.7} + \frac{2.51}{\mathbf{R}\sqrt{f}} \right) \ldots\ldots\ldots\ldots\ldots\ldots (10)$$

Eq. 10 is asymptotic to the smooth pipe curve on the left (in Fig. 14) and to the Nikuradse curves on the right, and is offered by its proponents as a universal rough-pipe flow formula. It is not as formidable as it appears to be. In fact, it is readily adaptable to presentation by diagrams.[37] The chief difficulties with Eq. 10 are lack of final assurance of correctness within the transition zone and lack of an established set of values for k. The relation of the Colebrook curve to the Nikuradse data is shown in Fig. 14. It is not convenient to show data supporting the Colebook equation on this diagram.

The $(f-\mathbf{R})$-equations purport to be at least partly rational and are supported by laboratory experiments. The conventional formulas are empirical and depend for support largely on field tests. Field tests cannot be made with laboratory precision, but a multiplicity of comparisons should show a common trend. To date this has not been demonstrated to be true. Curves based on field experiments frequently cut sharply across theoretical curves, a fact that needs explanation.

The authors' data are platted in Fig. 14 to show their general relation to the $(f-\mathbf{R})$-equations. This platting does not replace, but supplements, the original platting in Fig. 10. Points for the tar-lined steel pipe conform to the smooth pipe curve out to $\mathbf{R}$ = 10,000,000. These points lie too far from the zone of complete turbulence to give a definite indication of the final value of k. If it is assumed that an extension of these experiments would follow the Colebrook trend, then a value of k/D somewhat less than 0.00001 might be anticipated or, say, a value of k less than 0.0002 ft. On the other hand, if it is anticipated that these points will follow the Nikuradse trend, rising to a maximum of 0.00002 or 0.00003 in the vicinity of the line A–B, the value of k would be about 0.0004 ft. The authors arrived at a value of 0.0035 in. or about 0.0003 ft.

These data do not justify the drawing of a conclusion as to the precise value of k for this type of pipe, but they do illustrate the necessity for determining whether flow in such pipe follows the Nikuradse or the Colebrook trend.

The points for the cement-lined tunnel are more consistent within themselves than those for the steel pipe. They cross the curve A–B and appear to level off at about k/D = 0.0002 or, say, at a value of k somewhat less than 0.004 ft, which conforms to the authors' value of k = 0.04 in. It will be noted that these data definitely follow the Nikuradse rather than the Colebrook trend. If repeatedly confirmed by other field experiments, this fact may have a profound influence on the final selection of a flow formula. However, it will

[37] "Friction Factors for Pipe Flow," by Lewis F. Moody, *Transactions*, A.S.M.E., Vol. 66, 1944, p. 671.

be noted from Fig. 11 that these data also are at distinct variance with the Manning formula, which suggests that a critical review of why these points fall as they do may add something to the over-all understanding of the problem.

The points for the unlined tunnel are more consistent among themselves than would be expected under the circumstances. They are platted in the upper right-hand corner of Fig. 14 and are far within the zone of complete turbulence. Consequently, they might be expected to lie on a horizontal line; actually, they are distinctly inclined. Their combined center of gravity lies slightly below the $k/D = 0.10$ line as determined by Eq. 10 or 6. The corresponding value of k approximates the authors' estimated value of 22 in. Also, as revealed by Fig. 12, these points show a definite trend away from a constant Manning's n. Strangely, they conform excellently to the Scobey steel pipe formula for a coefficient $C_s = 2.4$. Of course, this value of C_s is entirely outside the range for which Mr. Scobey's formula was proposed and tested and the Scobey formula has no analytical correlation with the rough pipe law; hence, this conformity contributes nothing to the solution of the general problem. Again, a critical examination of why these platted points fail to follow the expected trend should add to the general understanding of the resistance to flow in pipes.

It is hoped that the ideas expressed herein may help in the ultimate evaluation of the results of these and future tests.

WILLIAM P. CREAGER,[38] M. ASCE, AND STEPHEN H. HAYBROOK,[39] JUN. ASCE.—Some excellent experiments to determine the friction loss coefficients in several types of conduits have been described by the authors. The writers desire to discuss the test results as applied to rock-lined tunnels, about which there is, relatively, a dearth of information.

The writers have advocated that, for consistency of records, tests on open conduit losses be tabulated by the Kutter formula and tests on closed conduit losses by the Hazen-Williams formula for general use where special formulas, such as the Scobey formula, have not been devised for special types of conduits.

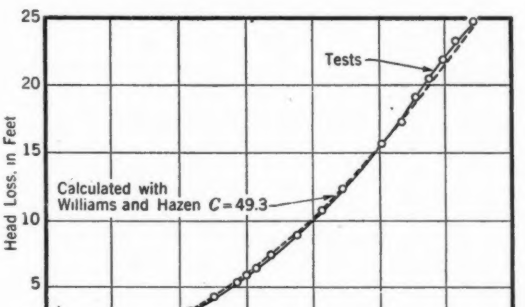

FIG. 15.—HEAD LOSSES IN UNLINED ROCK TUNNEL

With this in mind, the writers have tabulated in Fig. 15, by a full line, the relation between discharge and losses determined by tests for the Apalachia

[38] Cons. Engr., Buffalo, N. Y.

[39] Engr., Justin and Courtney, Philadelphia, Pa.

unlined rock tunnel; and also, by a dotted line, the same data calculated from the Hazen-Williams formula:

$$v = 1.32\, C\, R^{0.63}\, S^{0.54} \qquad (11)$$

using a C-value of 49.3.

The deviation in loss is only 2.5% and the corresponding deviation in C is only about 1.5%. Based on similar comparisons for other unlined rock tunnels, the rock surface trimming in the Apalachia tunnel was well done, it being the opinion of the writers that a Hazen-Williams $C = 50$ is about the best which can be expected and that $C = 45$ is a safe value for average conditions.

Correction for *Transactions:* In April, 1947, *Proceedings*, on page 464, change the heading over Cols. 8 and 9 from "Coefficient CB" to "Coefficient C_B."

AMERICAN SOCIETY OF CIVIL ENGINEERS

Founded November 5, 1852

DISCUSSIONS

CONTINUOUS FRAME ANALYSIS BY ELASTIC SUPPORT ACTION

Discussion

By L. J. Mensch, Frederick S. Merritt, I. Oesterblom, Thomas C. Kavanagh, A. Floris, and Tao King

L. J. Mensch,[7] M. ASCE.—The method of balancing fixed-end moments—connected with the name of Hardy Cross,[8] M. ASCE,—has had an immense success with teachers and students in the analysis of framed structures. Such members were formerly designed by the conventional moment formulas $\left(\frac{w\,L^2}{10}, \frac{w\,L^2}{12},\right.$ and $\left.\frac{PL}{6}\right)$ as first adopted by the Hennebique firm of Paris, France, before the turn of the century, and as since adopted by many building codes, except for the cases of very long spans, for which engineers of mathematical ability used Clapeyron's theorem, or a more or less complicated variation of it.

Professor Cross's method did not require deep studies or high mathematical skill, which explains its immediate success, but, at best, it is only a trial-and-error method requiring considerable time. Shorter methods have been known ever since Saint-Venant demonstrated that distant members have no appreciable effect on the member under investigation. For example, referring to Fig. 8, in the analysis of girder CE, the restraint of members AC, CD, EF, and EG only have to be taken into account.

The authors have shown Clapeyron's so-called exact method with new nomenclature simplified by previous calculation of certain elastic constants. However, even this simplified method requires too much effort for everyday use. Elsewhere[9,10,11,12] the writer has shown that a great deal more time and effort may be saved by the same theorem if Saint-Venant's principle is used. For

Note.—This paper by J. Charles Rathbun and C. W. Cunningham was published in April, 1947, *Proceedings*.

[7] Gen. Contractor, Evanston, Ill.

[8] "Analysis of Continuous Frames by Distributing Fixed-End Moments," by Hardy Cross, *Transactions*, ASCE, Vol. 96, 1932, p. 1.

[9] *Ibid.*, Vol. 83, 1919–1920, p. 1682.

[10] *Ibid.*, Vol. 102, 1937, p. 1050.

[11] *Ibid.*, p. 897 and p. 438.

[12] *Journal*, ACI, February, 1932, p. 387.

girder CE in Fig. 8, the primary moments[10] are given by:

$$M_{CE} = \frac{3\,P\,L}{8}\,\frac{1 + 2\,N_E}{4\,(1 + N_C)\,(1 + N_E) - 1} \qquad (33a)$$

$$M_{EC} = \frac{3\,P\,L}{8}\,\frac{1 + 2\,N_C}{4\,(1 + N_C)\,(1 + N_E) - 1} \qquad (33b)$$

when

$$N_E = \frac{3\,K}{\Sigma m\,K_E} \qquad (34a)$$

and

$$N_C = \frac{3\,K}{\Sigma m\,K_C} \qquad (34b)$$

In these equations m is an elastic factor depending on the restraint of each adjacent member at the far end. When the end is hinged, $m = 3$; when the end is fixed, $m = 4$; when the restraint lies between these two conditions, $m = 3.6$ is a good guess.

For girders, $K = I/L$; for columns, $K = I/h$. For girder CE, $K = 15/24$; $K'_C = 15/24$; $K''_C = 6/12$; $K'_E = 15/24$; $K''_E = 4/12$;

$$N_C = \frac{3 \times 15/24}{3.6 \times 15/24 + 4 \times 6/12} = 0.442;$$

and

$$N_E = \frac{3 \times 15/24}{3.6 \times 15/24 + 4 \times 4/12} = 0.522.$$

These values, when introduced in Eqs. 33*a* and 33*b* with those for $P = 4{,}000$ and $L = 24$, give $M_{CE} = 9{,}615$ ft-lb and $M_{EC} = 8{,}660$ ft-lb, which agree within 1% with the values given in Table 5. These moments will be modified by the action of the 8,000-lb uniform load on span EG.

The moments in EG are found from the formulas:

$$M_{EG} = \frac{W\,L}{4}\,\frac{1 + 2\,N_G}{4\,(1 + N_E)\,(1 + N_G) - 1} \qquad (35a)$$

$$M_{GE} = \frac{W\,L}{4}\,\frac{1 + 2\,N_E}{4\,(1 + N_E)\,(1 + N_G) - 1} \qquad (35b)$$

It is easily found that $N_E = 0.522$ and $N_G = 0.422$, so that

$$M_{EG} = \frac{8{,}000 \times 24}{4}\,\frac{1 + 2 \times 0.422}{4 \times 1.422 \times 1{,}522 - 1} = 11{,}550 \text{ ft-lb}$$

and

$$M_{GE} = \frac{8{,}000 \times 24}{4}\,\frac{1 + 2 \times 0.522}{4 \times 1.422 \times 1.522 - 1} = 12{,}820 \text{ ft-lb},$$

which again closely agree with the tabulated results. Moment M_{EG} must be distributed to EC and EF in relation to stiffness, thus, $M'_{EC}:M'_{EF} = 3.6 \times 15/24:4 \times 4/12$, from which $M'_{EC} = 7{,}250$ ft-lb and $M'_{EF} = 4{,}300$ ft-lb. The maximum moment is $M_{EC} = 8{,}660 + 7{,}250 = 15{,}910$ ft-lb, as compared with 16,067 ft-lb given in the table.

The maximum value of M_{EG} is found by a similar distribution of the moment of M_{EC}, and is $M_{EG} = 11{,}550 + 8{,}660 \times 54/86 = 16{,}990$ ft-lb, as compared with 17,145 ft-lb in Table 5.

If the value of $m = 4$ for the columns be replaced by $m = 3.6$, there is a slight modification of the value of the moments, usable for Example 6, Fig. 12.

To show a short cut for analyzing sidesway, Example 2, Fig. 7, is chosen. Then,

$$M_{AC} = \frac{3\,P\,L}{8}\,\frac{1 + 2\,N_C}{4\,(1 + N_A)\,(1 + N_C) - 1} \qquad (36a)$$

$$M_{CA} = \frac{3\,P\,L}{8}\,\frac{1 + 2\,N_A}{4\,(1 + N_A)\,(1 + N_C) - 1} \qquad (36b)$$

In this problem $N_C = \frac{3 \times 15/24}{4 \times 4/12} = 1.408$ and $N_A = \frac{3 \times 15/24}{4 \times 6/12} = 0.938$, so that $M_{AC} = 7{,}720$ ft-lb and $M_{CA} = 5{,}830$ ft-lb when no sidesway is possible. Then the shears acting in the columns will be: In AB $(7{,}720 + 7{,}720/2)/12 = 965$ lb; in CD $(5{,}830 + 5{,}830/2)/12 = 729$ lb. These shears should be equal. They can be made so if an imaginary force of $965 - 729 = 236$ lb be assumed as acting in a horizontal direction (AC) at the top of the column. The problem is to find the proportionate parts to be assigned to each column, and, furthermore, how these shears modify the moments at the top and bottom of the columns.

By figuring a number of multicolumn bents the writer found that the proportionate part taken by column AB closely equals $\frac{K_{AB} + K_{AC}}{K_{AB} + 2\,K_{AC} + K_{CD}} = \frac{6/12 + 15/24}{6/12 + 2 \times 15/24 + 4/12} = 0.54$, and that the shear in AB equals $236 \times 0.54 = 127$ lb, and, in CD $= 238 - 127 = 111$ lb. The zero point of moments produced in the fixed-ended columns by these shears is located between $0.4\,h$ and $0.5\,h$ from the column top. In many cases a good average for this distance is $0.45\,h$. Hence, the moment at the top of column AB is diminished by $127 \times 0.45 \times 12 = 686$ ft-lb, and the moment at the top of column CD is increased by $111 \times 0.45 \times 12 = 600$ ft-lb, which values closely agree with those in Table 3.

As another example for finding the shear, it is proposed to find the proportionate part of the shear for columns CD and AB of Fig. 8. For column CD, it is

$$\frac{K_{CA} + K_{CE} + K_{CD}}{\Sigma K \text{ of columns} + 2\,\Sigma K \text{ of all girders}} = \frac{15/24 + 15/24 + 6/12}{2 \times 9/12 + 2 \times 6/12 + 4/12 + 2 \times 4 \times 15/24} = 0.223,$$

and, for column AB, it is $\frac{K_{AC} + K_{AB}}{\Sigma K \text{ of columns} + 2\,\Sigma K \text{ of girders}} = 0.176.$

The authors deserve great credit for having shown clearly the influence of sidesway in their examples. They have, however, side-stepped the issue of the influence of the width of the columns and the depth of the girders on the calculated moments.

Tests to near destruction of properly designed frames have consistently shown reserve strengths from 30% to more than 100% greater than those predicted by the classical "exact" theories. This was partly because the clear spans were smaller than the center-to-center distances, and partly because the plasticity of materials of construction under high stresses and long time loading made the negative moments considerably smaller. This discrepancy has long been known, but the use of the center-to-center distances and the use of a constant modulus of elasticity is still preached; it seems to have become an article of faith.

The writer cannot refrain from emphasizing that the deluge of literature on the analysis of framed structures since World War I has drowned the works of the few true thinking pioneers and the investigators of genius. In addition, this mass of literature has so dazzled students that they have lost their heads in the belief that everything old was wrong and everything new was right, and that a study of these new methods will lead them to an advanced standing in their profession, and to prosperity. The fact is that they are being robbed not only of their time, and their chance of acquiring useful knowledge, but also of their money.

Frederick S. Merritt,[13] Assoc. M. ASCE.—Several papers such as this one have been published in recent years demonstrating the feasibility of one-cycle moment distribution. They are proof that open-minded designers recognize that multicycle distribution has many shortcomings in both theoretical and practical applications. Although it can be proved that, in general, one-cycle distribution is a more powerful tool than multicycle distribution, most of these papers, including this one, do not conclusively show superiority over the multicycle method in solving practical problems. The reasons are quite evident:

Either method can be used to analyze statically indeterminate structures, and the papers on one-cycle distribution published in the past in *Proceedings* have been unable to prove that the method is simpler, quicker, or easier to visualize—because too many extraneous concepts are introduced, requiring much preliminary computation. For example, in this paper "elastic length" is an unnecessary concept, as far as practical problems in general are concerned; results in extra computations when evaluating elastic properties of every span; and increases the number of required formulas, as well as complicating them. Thus, the superiority of one-cycle distribution will not be conclusive until the preliminary computations are reduced to a minimum and then by comparison it is shown that less work is involved than in, say, two cycles of fixed-end distribution.

The first step in streamlining one-cycle moment distribution is to base the method on the fewest necessary and sufficient fundamental terms for evaluating the elastic properties of each span, independent of the rest of the structure. Experience shows that the least number of terms required is three. Although these may be selected in many ways, the best ones are those that yield the simplest and fewest formulas.

[13] Asst. Editor, *Engineering News-Record*, New York, N. Y.

A group that satisfies this criterion is $C^F{}_L$, $C^F{}_R$, and K. The first two are the "moment ratios" to left and right, respectively, for fixed ends—the ratio of the moment applied at one end of a beam to the moment carried over or induced at the other end when rotation is completely prevented. The third term is the moment to be applied at one end of the beam, considering it simply supported, to produce a unit rotation at the other end. These terms apply to beams of variable moment of inertia as well as to prismatic sections.

For beams of constant moment of inertia, $C^F{}_L = C^F{}_R = 2$ and $K = 6\,E\,I/L$. Since relative values of K are used in most cases, the coefficient 6 may often be disregarded.

Secondary terms needed to solve specific problems may be evaluated using the fundamental terms. For example, the moment to be applied at the left end of a beam, considering it simply supported, to produce unit rotation there is $K/C^E{}_L$.

The second streamlining step is to evaluate the end restraints due to the rest of the structure in the least number of terms. Instead of using "flexibility" for distribution of moments at a joint, requiring manipulation of reciprocal relationships, as the authors did, it is preferable to use stiffness. The stiffness S of the end of an unloaded span is defined as the moment producing a rotation of unity at the end where it is applied when the other end of the beam is restrained against rotation by other members of the structure.

Simpler formulas result if they are expressed in terms of "moment ratios." [14] The moment ratio C is defined for an unloaded member of a continuous structure as the ratio of the moment introduced at one end of the span to the moment carried over to the other end. Thus, moment ratio is the reciprocal of the authors' carry-over factor.

Equivalent to "combined flexibility," restraint R at the end of an unloaded beam at a joint is the moment applied at that end to produce a unit rotation in all the members at the joint. By definition of continuity, R is equal to the sum of the stiffnesses of the adjacent ends of the other members at the joint. Furthermore, the moment induced in any of these other members bears the same ratio to the applied moment as the stiffness of the member does to the restraint. Consequently, end moments are distributed at a joint in proportion to the stiffnesses of the members.

Stiffness can be expressed in terms of C as follows:

$$S_L = \frac{K}{C^F{}_L - 1/C_R} \qquad \text{(37a)}$$

$$S_R = \frac{K}{C^F{}_R - 1/C_L} \qquad \text{(37b)}$$

For beams of constant moment of inertia,

$$S_L = \frac{K}{2 - 1/C_R}; \qquad S_R = \frac{K}{2 - 1/C_L} \qquad \text{(37c)}$$

---

[14] "Moment Ratios Simplify Continuity Analysis," by Frederick S. Merritt, *Engineering News-Record*, November 1, 1945, p. 112, and November 15, 1945, p. 102.

In turn, moment ratios can be computed in terms of the stiffnesses of adjacent spans:

$$C_L = C^F{}_L + \frac{K}{R_L} \qquad (38a)$$

$$C_R = C^F{}_R + \frac{K}{R_R} \qquad (38b)$$

Toward hinged supports, for which $R = 0$, C is infinitely large; toward fixed ends, for which R is infinitely large, $C = C^F$. For beams of constant moment of inertia,

$$C_L = 2 + \frac{K}{R_L}; \qquad C_R = 2 + \frac{K}{R_R} \qquad (38c)$$

A physical interpretation of moment ratios, in addition to the carry-over concept, can be obtained in terms of fixity, defined as the ratio C^F/C, which varies from zero for simple supports to 100% for fixed ends. If θ_P is the rotation of a beam at a hinged support and θ is the rotation when restraint is present, it can be shown that fixity is equal to $1 - \frac{\theta}{\theta_P}$ and, consequently, is a straight-line function of the angular rotation. For example, if a column footing rotates 0.4 as much as it would if it were unrestrained by the soil, the fixity is $1 - 0.4$, or 0.6. Also, assuming $C^F = 2$, the moment ratio for the column in the direction of the footing may be taken as 2/0.6, or 3.33. In addition, this concept can be used in the case of flexible connections.

Corresponding to Eqs. 16 for prismatic beams, the following formulas apply for end moments in loaded spans of variable moment of inertia (clockwise end moments and rotations being assumed positive):

$$M_L = -\frac{K(C_R\,\phi_L + \phi_R)}{C_R\,C_L - 1} \qquad (39a)$$

$$M_R = -\frac{K(C_L\,\phi_R + \phi_L)}{C_R\,C_L - 1} \qquad (39b)$$

in which ϕ represents the simple beam end rotation due to the load on the span. However, it is generally easier to begin distribution with fixed-end moments.

To indicate how this streamlined version works, Example 1(*a*) is recalculated. Referring to Fig. 6 and noting that the relative value of K is unity for all spans:

Step (*a*).—Same as the authors.

Step (*b*).—$S_{BA} = \frac{1}{2 - 1/2} = 0.667$; $C_{CB} = 2 + \frac{1}{0.667} = 3.5$. Similarly, $S_{DE} = \frac{1}{2 - 1/\infty} = 0.5$; $C_{CD} = 2 + \frac{1}{0.5} = 4$; $S_{CD} = \frac{1}{2 - 1/4} = 0.571$; and $C_{BC} = 2 + \frac{1}{0.571} = 3.75$.

Step (*d*).—For a concentrated load at the center of a simply supported span, $\phi = \pm \frac{3\,P\,L}{8\,K}$. Therefore, $M_{BC} = -\frac{3.75 \times 0.375 - 0.375}{3.75 \times 3.5 - 1} \times 4 \times 24$

$= -8.16$; and $M_{CB} = \dfrac{3.5 \times 0.375 - 0.375}{3.75 \times 3.5 - 1} \times 4 \times 24 = 7.42$. Then, $M_{AB} = \dfrac{8.16}{2} = 4.08$ and $M_{DC} = \dfrac{-7.42}{4} = -1.86$.

Example 4 (Fig. 9) is also solved to illustrate a more general technique.

Step (a).—For prismatic beams, the moment ratio can be estimated from

$$C = 2 + \frac{\gamma K_1}{\Sigma K} \qquad (40)$$

in which K_1 is the K-value of the member whose C-value is to be assumed; ΣK is the sum of the K-values of the other members of the joint toward which the ratio is directed; and γ is a constant varying from 1.5 for full restraint to 2.0 for no restraint at the far ends of these other members. Since γ varies between such narrow limits, it has only a very small effect on C.

From Fig. 9, the relative values of K are: $K_{AB} = 6$; $K_{CD} = 4$; $K_{AC} = 7.5$; and $K_{BD} = 6$. Assume $C_{AB} = 2 + \dfrac{1.75 \times 6}{6} = 3.75$ and $C_{CD} = 2 + \dfrac{1.75 \times 4}{6} = 3.17$.

Step (b).—Through the use of these assumed moment ratios, the distribution constants for the other members may be found. $S_{AB} = \dfrac{6}{2 - \dfrac{1}{3.75}} = 3.46$; $C_{CA} = 2 + \dfrac{7.5}{3.46} = 4.17$; $S_{CA} = \dfrac{7.5}{2 - \dfrac{1}{4.17}} = 4.26$; $C_{DC} = 2 + \dfrac{4}{4.26} = 2.94$; $S_{DC} = \dfrac{4}{2 - \dfrac{1}{2.94}} = 2.41$; $C_{BD} = 2 + \dfrac{6}{2.41} = 4.49$; and $S_{BD} = \dfrac{6}{2 - \dfrac{1}{4.49}} = 3.38$.

The corrected $C_{AB} = 2 + \dfrac{6}{3.38} = 3.77$ and S_{AB} is practically unchanged.

Similarly, $S_{CD} = \dfrac{4}{2 - \dfrac{1}{3.17}} = 2.37$; $C_{AC} = 2 + \dfrac{7.5}{2.37} = 5.16$; $S_{AC} = \dfrac{7.5}{2 - \dfrac{1}{5.16}} = 4.15$; $C_{BA} = 2 + \dfrac{6}{4.15} = 3.45$; $S_{BA} = \dfrac{6}{2 - \dfrac{1}{3.45}} = 3.51$; $C_{DB} = 2 + \dfrac{6}{3.51} = 3.71$; and $S_{DB} = \dfrac{6}{2 - \dfrac{1}{3.71}} = 3.47$. The corrected $C_{CD} = 2 + \dfrac{4}{3.47} = 3.15$ and S_{CD} is practically unchanged.

Next, a moment of + 1,000 is applied at each joint separately, and distributed. For example, for a moment of 1,000 at joint A, $M_{AB} = \dfrac{3.46}{3.46 + 4.15} \times 1{,}000 = 455$; $M_{BA} = \dfrac{455}{3.77} = 121$; $M_{BD} = -121$; $M_{DB} = -\dfrac{121}{4.49} = -27$;

$M_{DC} = 27; M_{CD} = \frac{27}{2.94} = 9; M_{CA} = -9; M_{AC} = -\frac{9}{4.17} = -2$. Moments thus determined are given in Table 16.

Step (*d*).—From Example 1(*a*), ϕ for the 4-kip load is $\pm \frac{3\,P\,L}{8\,K}$, and the fixed-end moments are numerically equal to $\frac{2 \times 0.375 - 0.375}{4 - 1} \times 4 \times 24 = 12$. These moments are then distributed by multiplying the values in Col. 2, Table 16, by 0.012, and those in Col. 4 by -0.012. Moments for the 4-kip load with sidesway prevented are shown in Table 17(*a*).

TABLE 16.—INFLUENCE FACTORS FOR MOMENT OF 1,000 APPLIED AT EACH JOINT, EXAMPLE 4

Member	Point of Moment Application			
	Joint A	Joint B	Joint C	Joint D
(1)	(2)	(3)	(4)	(5)
AC....	546	−139	145	13
AB....	454	139	−145	−13
BA....	112	510	−11	−150
BD....	−112	490	11	150
DB....	6	100	−104	591
DC....	−6	−100	104	409
CD....	−97	−8	357	130
CA....	+97	8	643	−130

Step (*g*).—Under sidesway, joints A and C deflect equal amounts horizontally. Hence, the fixed-end moments in AB and CD caused by a horizontal movement, being proportional to the *K*-values, are in the ratio of 6 to 4. To eliminate the forces that were assumed to prevent sidesway to permit distribution of moments for the 4-kip load, apply fixed-end moments of $-1{,}000\,M$ at the top and bottom of CD and of $-1{,}500\,M$ at the top and bottom of AB.

TABLE 17.—TABULATION AND DISTRIBUTION OF MOMENTS, EXAMPLE 4

Line	Description	Member							
		AC	AB	BA	BD	DB	DC	CD	CA
	(*a*) STEP (*d*) (4-KIP LOAD, NO SIDESWAY)								
1	Fixed-end moment........	−12.0	....	....	....	....	....	....	+12.0
2	Distribution of A moment[a].	+ 6.55	+5.45	+1.35	−1.35	+0.07	−0.07	−1.16	+ 1.16
3	Distribution of C moment[a].	− 1.74	+1.74	+0.13	−0.13	+1.25	−1.25	−4.28	− 7.72
4	Total....................	− 7.19	+7.19	+1.48	−1.48	+1.32	−1.32	−5.44	+ 5.44
	(*b*) STEP (*g*) (SIDESWAY DISTRIBUTION)								
5	Fixed-end moment........	....	−1,500	−1,500	....	....	−1,000	−1,000	....
6	Distribution of *A* moment[a].	+ 819	+ 681	+ 168	− 168	+ 9	− 9	− 145	+ 145
7	Distribution of *B* moment[a].	− 208	+ 208	+ 765	+ 735	+ 150	− 150	− 12	+ 12
8	Distribution of *C* moment[a].	+ 145	− 145	− 11	+ 11	− 104	+ 104	+ 357	+ 643
9	Distribution of *D* moment[a].	+ 13	− 13	− 150	+ 150	+ 591	+ 409	+ 130	− 130
10	Total....................	+ 769	− 769	− 728	+ 728	+ 646	− 646	− 670	+ 670
	(*c*) STEP (*i*) (SIDESWAY CORRECTIONS AND FINAL MOMENTS)								
11	Sidesway corrections......	+ 0.52	−0.52	−0.49	+0.49	+0.44	−0.44	−0.46	+ 0.46
12	Final moments...........	− 6.67	+6.67	+0.99	−0.99	+1.76	−1.76	−5.90	+ 5.90

[a] Distribution of moment applied at the joint designated.

Then, using Table 16, distribute the moments and assemble the results as in Table 17(*b*).

Step (*h*).—The shear in AB and CD due to these moments plus the moments previously obtained for the 4-kip load must be zero.

$$\begin{aligned} +7.19 - 769\,M + 1.48 - 728\,M - 5.44 - 670\,M - 1.32 - 646\,M &= 0 \\ 2{,}813\,M &= 1.91 \\ M &= 0.00068 \end{aligned}$$

Step (*i*).—Multiplication of the values in line 10, Table 17(*b*), by this value of M gives the sidesway correction for the 4-kip load (line 11, Table 17(*c*)), and the final moments (line 12) are obtained by addition of these corrections to the moments for sidesway prevented (line 4).

I. OESTERBLOM,[15] M. ASCE.—For some years structural frames have been analyzed by the relaxation method so as to avoid the innumerable equations involved in the energy methods, with their attendant confusion and labor. In other words, the classical methods were dead when it came to the matter of analyzing frames. In the face of this trend, the authors have resurrected the classical treatment of frames—with a modification.

The first few pages set up a foundation by borrowing, chiefly from the classics, but also from the modern "relaxationists." A new element, the "elasticity factor," L, is introduced. There follow two pages of real substance and twenty-seven pages of illustrative examples. The first pages can be passed over quickly after they have been recognized as mostly old acquaintances. So also can the last pages, when it is found how simple the problems are; for any method will solve a primitive problem fairly and with little labor.

As to the real substance of the paper, it is claimed that the new method provides very well for "flexible connections," meaning such as have a small but limited rotation; and that it is applicable to Vierendeel type trusses and frames (see heading, "Summary"). In a sense this is true; but the same may be claimed for the relaxation method when used intelligently; seemingly the latter can be adapted more simply and with less labor. The elaborate calculations shown for the easy problems in this paper are thus not at all inviting.

Among the many who have tried to improve upon the relaxation method, or to overcome the discouraging algorithms of the classics in the solution of frames, it has become the custom to illustrate with primitive examples. This is not said in a derogatory sense because such exploration is essential to progress. A few simple problems are in order. In a classroom, no doubt, all the examples had better be primitive, for young minds should not be burdened too heavily; but the larger audience of practicing engineers, will ask of any new method: "Does the method 'work' for an extensive and irregular framework, for short and long spans or columns mixed, for an offset layout, or for an irregular footing plan?" "Will it 'work' with a mixture of all kinds of loads—point loads, spread loads, sway loads, with loads sometimes off and sometimes on?"

[15] Engr., Carbide and Carbon Chemicals Corp., South Charleston, W. Va.

With one exception the illustrations are not convincing. Even in the exception the authors offer no solution; they merely present an outline of how the method should be applied. In a practical sense, the exception, Example 7, is not a realistic problem. It does not have the usual complications, but consists of four equal spans in a four-story frame, in which all stories are the same. Loading is confined to two point loads and two spread loads only; no wind is involved. The loads are on the inner spans and are alternating; the point loads are at midspan. The layout is a simple one never found in real life.

Even so, the authors have not presented an answer. Possibly, the elasticity factors L (which should be formulated from all the restraining elements of the frame and not approximated roughly from only those most adjacent) are so complicated that they are entirely beyond human ken, and thus in the same class as the multiple equations in the original classical methods. Perhaps no practical solution is possible; or the answer would be a loose approximation at best. This is thus a challenge to the authors: Can they complete the analysis they have outlined and obtain true answers? If they can they should do so and thus prove that the method has practical value. If they win, their service to the profession is real and they are to be highly honored.

In expressing himself thus forcefully on this subject the writer has had in mind not only the present paper but several others—all erring in the sense that they outline the technique without exploring the underlying philosophy. In a philosophic sense the modern methods are far removed from the classic methods of analyzing elastic frames. Any investigator, pioneering in new ideas as to frames, must therefore anchor his promises to either of the two—unless he is able to offer an entirely new philosophic approach—for there can be no such thing as a mixture of, or an average between, "energy" and "relaxation" methods; to state the question in more practical terms: Do the current explorers in this field realize the stupendous task they set themselves? The vastly superior relaxation method has its roots in the work of master mathematicians and philosophers, who discovered and developed it under the stress of urgent necessity during World War I; and the development has continued ever since.

When an author therefore makes a claim for a new and better method there must be (and this is a check on his own work) at least one critical and outstanding departure from known and accepted forms. He should analyze and describe this departure and submit a rigorous mathematical proof—either by explicit detail in the text or by tying his thesis by reference to authoritative and readily available sources. If this cannot be done the method is not ready for publication.

A technical paper is a record of constructive thoughts designed for continuing and recurrent study in future time; and it should be sufficiently inclusive to be definitely conclusive both when written and for all time to come. It should be as nearly perfect as possible.

These parenthetical observations, while suggested by this topic, are not aimed exclusively or even primarily at the present paper. They apply to all treatments of statically indeterminate frames, for which claims of complete originality or novelty are advanced.

THOMAS C. KAVANAGH,[16] Assoc. M. ASCE.—This method of frame analysis is of considerable interest in connection with the calculation of buckling restraints of axially loaded bars in a rigid jointed framework. Methods employing restraint coefficients similar to the authors' "elastic factors" have been employed for this purpose in various forms since the beginning of the twentieth century. All such methods involve solution of the problem of an indeterminate framework wherein the various elastic properties of the members are modified by the presence of axial loads. For the special cases wherein the axial loads are small, their effect may be disregarded as is the custom in ordinary methods of indeterminate analysis.

One of the earliest and most comprehensive uses of restraint coefficients was by H. Zimmermann, who developed the properties of these coefficients (*Spannziffer*) in a long series of publications dating from 1906, summarized in his book[17] on the buckling of frameworks. Eq. 11 is but a slightly different form of the general equation for an axially unloaded bar with rotational end restraints; for on substitution of Eq. 8 it may be rewritten:

$$1 + \frac{L}{3\,E\,I}\left(\frac{1}{Z_B} - \frac{1}{Z_A}\right) - \frac{3}{4}\left(\frac{L}{3\,E\,I}\right)^2 \frac{1}{Z_A}\,\frac{1}{Z_B} = 0 \qquad (41)$$

or, by substitution of Mr. Zimmermann's definitions, modified in accordance with the authors' sign convention,

$$m' = -\frac{1}{Z_A}; \qquad m'' = \frac{1}{Z_B} \qquad (42)$$

Eq. 41 takes the basic form,

$$1 + A\,(m' + m'') + \tfrac{3}{4}\,A^2\,m'\,m'' = 0 \qquad (43)$$

in which

$$A = \frac{L}{3\,E\,I} \qquad (44)$$

In the case of the axially loaded member, the coefficients are modified, but the form remains the same, and the equation will be found repeated in most literature pertaining to elastic stability of bars. It is significant to note that Eq. 43 can be rewritten in the form,

$$(A\,m' + 4/3)\,(A\,m'' + 4/3) = (\tfrac{2}{3})^2 \qquad (45)$$

which is an equilateral hyperbola, whose properties and physical interpretation were investigated at length by Mr. Zimmermann. Special cases like Eqs. 3 and 5, or others such as equal end restraints, are readily obtainable from these equations.

In 1935–1936, N. J. Hoff[18,19] developed along different lines the concept of the "relative stiffness factor," defined by:

$$\Omega = \frac{E\,I}{L}\,\frac{\theta}{M} \qquad (46)$$

---

[16] Instr. in Civ. Eng., New York Univ., New York, N. Y.

[17] "Knickfestigkeit der Stabverbindungen," by H. Zimmermann, Wilhelm Ernst & Son, Berlin, 1925.

[18] "Transversely Loaded Framework Members," by N. J. Hoff, *Journal*, Royal Aeronautical Soc., August, 1935, p. 718.

[19] "Elastically Encastred Struts," by N. J. Hoff, *ibid.*, September, 1936, p. 663.

and used it for both axially loaded or axially unloaded members. The symbols on the right are as defined in the authors' paper.

In 1938, the moment distribution approach was utilized by Eugene E. Lundquist,[20] Assoc. M. ASCE, using the concepts of stiffness (elastic factor) and carry-over factor. That the approach is expressible in terms of Eq. 39 was demonstrated by W. R. Osgood, M. ASCE, in a discussion[21] of the same paper. It might be noted here that since the elastic factor is simply the summation of the stiffnesses of the restraining members, it would seem preferable to retain the widely understood term "stiffness" in place of the new term "elastic factor."

In all the above problems, as related to elastic stability analysis, one is faced with the problem of selecting joints with known or assumed restraints (stiffnesses), after which the remaining joints are resolved in a step-by-step process.

The authors are to be commended upon their clear presentation and the systematic procedure outlined, particularly as related to the problems of flexible connections and joint translation. Although the approach considering joint translation has been solved[22] for axially loaded members, it has never been systematically exploited.

A. Floris,[23] Esq.—Introducing a method of analysis of hyperstatic structures, the authors claim that the theory presented in this paper is classical, or exact, requiring the solution of very few, if any, simultaneous elastic equations. This statement needs a close examination.

Classical methods are those which do not require successive or final corrections. The redundant quantities (that is, forces, moments, displacements, and rotations) of the hyperstatic structure are determined by the aid of an algorism in a systematic and unequivocal manner leading always to simple but troublesome linear simultaneous equations. It follows that the classical methods, although tedious and time consuming, are direct and the results obtained are final.

The authors' analysis, on the other hand, is preeminently a relaxation method. In certain cases, relaxation methods require also the solution of simultaneous equations. It is true, that by introducing the elastic moment area (conjugate beam), the authors side-step the iteration process of the moment-distribution method. Nevertheless, their analysis is an indirect one.

In accordance with the usage of American technical literature, the authors call Mohr's elastic moment-area method, the conjugate beam theory. Mohr in his writings[24, 25] never mentioned it, and it is not known in German technical literature by this name. It belongs, instead, to the elastic weights methods. Furthermore, this terminology is mathematically incorrect; for to be called conjugate there must be two paired quantities equal but differing in sign. The

[20] "Principles of Moment Distribution Applied to Stability of Structural Members," by E. E. Lundquist, *Proceedings*, 5th International Cong. for Applied Mechanics, 1938, p. 145.

[21] *Ibid.*, p. 149.

[22] "Elastic Stability of Plane Frameworks," by W. Prager, *Journal of the Aeronautical Sciences*, September, 1936, p. 388.

[23] Asst. to Structural Engr., Pacific Elec. Ry. Co., Los Angeles, Calif.

[24] "Beitrag zur Theorie der Holz-und Eisenkonstruktionen," by Otto Mohr, *Zeitschrift des Architekten-und-Ingenieur-Vereins zu Hannover*, 1868, p. 19.

[25] "Abhandlungen aus dem Gebiete der Technischen Mechanik," by Otto Mohr, Wilhelm Ernst & Sohn, Berlin, 1914, p. 342.

moment and the elastic moment areas are unequal and both of the same sign, positive or negative as the case may be. It is perhaps better to call this method the associate beam theory.

In the moment-distribution method the base system is a beam fixed at both ends. By releasing joints one at a time, the carry-over stiffness factors, fixed-end moments, and final moments are determined. By analogy, the base system of the authors' method is a beam elastically supported at both ends. By releasing the fixed points, after the carry-over and elastic factors have been determined, the moments of the elastic moment area, and, finally, the actual moments are found. As in the relaxation methods, the sidesway produced by unbalanced moments and shears is corrected to satisfy the equilibrium of the structure.

In the moment-distribution method the fixed-end moments can be taken from reference books, and are independent of the elasticity of the structure. The bending moments of the authors' base system (Eqs. 16) depend on the elasticity of the whole structure and cannot be determined in advance.

An attentive reader will search in vain for a proof of the analysis developed in this paper; he must be satisfied with heuristic reasoning. Only comparing them with the solutions reached by other well-known methods can the validity of the results obtained by the authors' method be established.

In Fig. 2 and Fig. 3 the beams and moments are not drawn properly, and the interaction of forces and moments is not clear. Support B is fixed in Fig. 2 and elastic in Fig. 3. In both cases, point A is hinged but vertically restrained. This is not mentioned explicitly. In end B of the fixed and elastically supported beams, the moment produced by M_{AB} is a rectangle; the moment area of the vertical reaction at A is a triangle with opposite sign. By superimposing the two moment areas, Figs. 2(a) and 3(a) are obtained.

In addition, the formulas are presented in a rather unsatisfactory and impractical manner. The general expression (Eq. 10b), for instance, can be written in the more convenient form—

$$\theta_A = M_{AB}\left(\frac{L}{3\,E\,I} - \frac{L^2}{12\,E\,I\,L_{AB}}\right) \qquad (47)$$

—in which the influence of support B is clearly indicated. The first term within the parentheses is the elastic factor at end A when end B can rotate freely, which is the basic case. The second term is the elastic factor that shows the influence of the degree of fixity at end B on the rotation of the beam at support A. If B is fixed, then $Z_B = 0$ and, from Eq. 8, $L_{AB} = L$. Thus the expression within the parentheses becomes equal to Eq. 3. On the other hand, if B is hinged, then $Z_B = \infty$, hence $L_{AB} = \infty$ and the second term within the parentheses vanishes, as it should, to agree with Eq. 4.

In conclusion, the proposed method offers no real advantages over the moment-distribution method, although it can be of some value in cases involving only sidesway. It is more tedious, more complicated, and certainly more difficult to remember and apply than the classical methods. The claim that iteration (cycles of distribution) is avoided and that the method is thus rendered briefer is rather illusory.

Tao King,[26] M. ASCE.—The "classical" method of analyzing continuous frames, presented in this paper, is at least of theoretical interest. Compared with the Hardy Cross method of moment distribution,[27] the authors claim the advantage of avoiding repeated cycles (but the solution of a "few" simultaneous equations is still required), and express the belief that the method is particularly adapted to the solution of frames such as the Vierendeel truss.

All examples given in the paper can be solved readily by the Cross method of distributing fixed-end moments with the application of proper "correction moments" where required. For practical purposes, only three or four cycles are necessary. If convergency is rather slow, five or six cycles may be required. Another advantage of the Cross method lies in the fact that the

TABLE 18.—Solution of Example 6 by the

Line[a]	Joint B		Joint A		Joint C			Joint E
	BD	BA	AB	AC	CA	CD	CE	EC
								(a) Customary Cycles of
1	2/5	3/5	6/11	5/11	5/14	4/14	5/14	15/38
2	....	....	....	....	....	....	−12.000	+12.000
3	−29.333	....	....	−36.667	−36.667	....	−23.333	−23.333
4	+11.733	+17.600	+20.000	+16.667	+25.714	+20.572	+25.714	+ 4.210
5	+ 8.000	+10.000	+ 8.800	+12.857	+ 8.333	+ 8.000	+ 2.105	+12.857
6	−23.371	....	....	−29.214	−29.214	....	−19.968	−19.968
7	+ 2.148	+ 3.223	+ 4.122	+ 3.435	+10.980	+ 8.784	+10.980	+ 1.826
8	+ 3.699	+ 2.061	+ 1.611	+ 5.490	+ 1.717	+ 3.699	+ 0.913	+ 5.490
9	− 7.987	....	....	− 9.983	− 9.984	....	− 8.815	− 8.815
10	+ 0.891	+ 1.336	+ 1.572	+ 1.310	+ 4.454	+ 3.563	+ 4.453	+ 0.860
11	+ 1.516	+ 0.786	+ 0.668	+ 2.227	+ 0.655	+ 1.516	+ 0.430	+ 2.227
12	− 3.229	....	....	− 4.037	− 4.036	....	− 3.665	− 3.666
13	+ 0.371	+ 0.556	+ 0.623	+ 0.519	+ 1.821	+ 1.457	+ 1.822	+ 0.424
14	+ 0.618	+ 0.311	+ 0.278	+ 0.910	+ 0.259	+ 0.618	+ 0.212	+ 0.911
15	− 1.316	....	....	− 1.644	− 1.644	....	− 1.549	− 1.548
16	+ 0.155	+ 0.232	+ 0.249	+ 0.207	+ 0.752	+ 0.601	+ 0.751	+ 0.220
17	+ 0.254	+ 0.124	+ 0.116	+ 0.376	+ 0.103	+ 0.254	+ 0.110	+ 0.375
18	− 0.540	....	....	− 0.675	− 0.676	....	− 0.668	− 0.669
19	+ 0.065	+ 0.097	+ 0.100	+ 0.083	+ 0.313	+ 0.251	+ 0.313	+ 0.118
20	−36.326	+36.326	+38.139	−38.139	−27.120	+49.315	−22.195	−16.481
								(b) Adjustments for
m_1	−17.600	+17.600	+20.000	−20.000	−10.953	+20.572	− 9.619	− 7.123
m_2	−13.223	+13.223	+12.922	−12.922	− 9.901	+16.784	− 6.883	− 5.285
m_3	− 3.397	+ 3.397	+ 3.183	− 3.183	− 3.813	+ 7.262	− 3.449	− 2.465
m_4	− 1.342	+ 1.342	+ 1.291	− 1.291	− 1.560	+ 2.973	− 1.413	− 1.015
m_5	− 0.543	+ 0.543	+ 0.527	− 0.527	− 0.633	+ 1.219	− 0.586	− 0.417
m_6	− 0.221	+ 0.221	+ 0.216	− 0.216	− 0.260	+ 0.505	− 0.245	− 0.176
m_7	− 0.152	+ 0.152	+ 0.149	− 0.149	− 0.184	+ 0.357	− 0.173	− 0.128
Σ	−36.478	+36.478	+38.288	−38.288	−27.304	+49.672	−22.368	−16.609

[a] The lines m_1, m_2, etc., are the algebraic sums of carried-over moments, correction moments, and distributed

[26] Head Prof., Civ. Eng., Peiping Polytechnic College, Peiyang Univ., Peiping, China.

[27] *Transactions*, ASCE, Vol. 96, 1932, p. 1.

angles of joint rotations, $E\,\theta$, and those of bar rotations, $E\,R = \frac{E\,\Delta}{L}$, may easily be calculated from the table of moment distribution. These values, when known, will help one in visualizing the deformed structure under the external loads.

The Vierendeel trusses in Examples 4 to 7 have rectangular panels and can be solved best by the Cross method. Example 6 is perhaps the most complicated one given by the authors. The writer has solved it by fixed-end moment distribution, as shown in Table 18.

HARDY CROSS METHOD OF CONVERGING APPROXIMATIONS

JOINT E		JOINT G			JOINT I		JOINT J	Line[a]
EF	EG	GE	GH	GI	IG	IJ	JI	
MOMENT DISTRIBUTION								
8/38	15/38	5/14	4/14	5/14	5/11	6/11	3/5	1
....	−16.000	+16.000	....	....	....	....	....	2
....	+16.667	+16.667	....	+43.333	+43.333	....	....	3
+2.246	+ 4.210	−27.143	−21.714	−27.143	−19.697	−23.636	−20.800	4
+0.667	−13.571	+ 2.105	− 8.000	− 9.848	−13.571	−10.400	−11.818	5
....	+15.388	+15.389	....	+31.961	+31.961	....	....	6
+0.974	+ 1.827	−11.288	− 9.031	−11.288	− 3.632	− 4.358	− 3.450	7
+0.317	− 5.644	+ 0.913	− 3.515	− 1.816	− 5.644	− 1.725	− 2.179	8
....	+ 6.475	+ 6.474	....	+10.104	+10.104	....	....	9
+0.458	+ 0.859	− 4.343	− 3.474	− 4.343	− 1.243	− 1.492	− 1.434	10
+0.150	− 2.171	+ 0.429	− 1.346	− 0.621	− 2.171	− 0.717	− 0.746	11
....	+ 2.385	+ 2.385	....	+ 3.847	+ 3.846	....	....	12
+0.226	+ 0.425	− 1.677	− 1.341	− 1.676	− 0.435	− 0.523	− 0.592	13
+0.078	− 0.838	+ 0.212	− 0.499	− 0.217	− 0.838	− 0.296	− 0.261	14
....	+ 0.840	+ 0.841	....	+ 1.460	+ 1.460	....	....	15
+0.117	+ 0.220	− 0.642	− 0.513	− 0.642	− 0.148	− 0.178	− 0.245	16
+0.042	− 0.321	+ 0.110	− 0.181	− 0.074	− 0.321	− 0.122	− 0.089	17
....	+ 0.275	+ 0.275	....	+ 0.548	+ 0.548	....	....	18
+0.063	+ 0.117	− 0.242	− 0.194	− 0.242	− 0.048	− 0.057	− 0.101	19
+5.338	+11.143	+16.465	−49.808	+33.343	+43.504	−43.504	−41.715	20
MORE EXACT SOLUTION								
+2.246	+ 4.877	+ 5.524	−21.714	+16.190	+23.636	−23.636	−20.800	m_1
+1.641	+ 3.644	+ 6.206	−17.031	+10.825	+14.758	−14.758	−15.268	m_2
+0.775	+ 1.690	+ 3.044	− 6.989	+ 3.945	+ 3.217	− 3.217	− 3.613	m_3
+0.376	+ 0.639	+ 1.137	− 2.687	+ 1.550	+ 1.240	− 1.240	− 1.338	m_4
+0.195	+ 0.222	+ 0.411	− 1.012	+ 0.601	+ 0.474	− 0.474	− 0.506	m_5
+0.105	+ 0.071	+ 0.143	− 0.375	+ 0.232	+ 0.179	− 0.179	− 0.190	m_6
+0.076	+ 0.052	+ 0.084	− 0.220	+ 0.136	+ 0.109	− 0.109	− 0.114	m_7
+5.414	+11.195	+16.549	−50.028	+33.479	+43.613	−43.613	−41.829	Σ

moments in cycles 1, 2, etc.; m_7 is obtained by multiplying m_6 by $\frac{r}{1-r}$, in which $r = \frac{m_6}{m_5}$.

In Table 18 (a), line 1 gives the distributing factors, and line 2 shows the fixed-end moments resulting from the loads applied on the top chords CE and EG, Fig. 12. In lines 3, 6, 9, etc., are given the correction moments to be applied so as to balance the unbalanced moments in the panels, resulting from the ex-

TABLE 18.—(*Continued*)

Line[a]	Joint J	Joint H			Joint F			Joint D		
	JH	HJ	HG	HF	FH	FE	FD	DF	DC	DB
					(a)—(Continued)					
1	2/5	1/3	1/3	1/3	3/8	2/8	3/8	1/3	1/3	1/3
2	....	....	....	....	....	....	....	....	....	....
3	+34.667	+34.667	....	+13.333	+13.333	....	−18.667	−18.667	....	−29.333
4	−13.867	−16.000	−16.000	−16.000	+ 2.000	+1.334	+ 2.000	+16.000	+16.000	+16.000
5	− 8.000	− 6.933	−10.857	+ 1.000	− 8.000	+1.123	+ 8.000	+ 1.000	+10.286	+ 5.866
6	+25.568	+25.569	....	+12.311	+12.311	....	−15.975	−15.975	....	−23.371
7	− 2.300	− 7.030	− 7.030	− 7.030	+ 0.953	+0.635	+ 0.953	+ 7.398	+ 7.398	+ 7.398
8	− 3.515	− 1.150	− 4.515	+ 0.476	− 3.515	+0.487	+ 3.699	+ 0.476	+ 4.392	+ 1.074
9	+ 8.084	+ 8.083	....	+ 5.180	+ 5.179	....	− 7.052	− 7.053	....	− 7.987
10	− 0.956	− 2.691	− 2.692	− 2.691	+ 0.451	+0.300	+ 0.451	+ 3.033	+ 3.032	+ 3.033
11	− 1.345	− 0.478	− 1.737	+ 0.225	− 1.345	+0.229	+ 1.516	+ 0.225	+ 1.781	+ 0.445
12	+ 3.077	+ 3.078	....	+ 1.908	+ 1.908	....	− 2.932	− 2.932	....	− 3.229
13	− 0.394	− 0.999	− 0.998	− 0.999	+ 0.234	+0.156	+ 0.234	+ 1.237	+ 1.237	+ 1.236
14	− 0.499	− 0.197	− 0.670	+ 0.117	− 0.499	+0.113	+ 0.618	+ 0.117	+ 0.728	+ 0.185
15	+ 1.168	+ 1.167	....	+ 0.672	+ 0.672	....	− 1.239	− 1.239	....	− 1.315
16	− 0.163	− 0.363	− 0.363	− 0.363	+ 0.125	+0.084	+ 0.126	+ 0.508	+ 0.508	+ 0.508
17	− 0.181	− 0.081	− 0.256	+ 0.062	− 0.181	+0.058	+ 0.254	+ 0.063	+ 0.300	+ 0.077
18	+ 0.438	+ 0.439	....	+ 0.220	+ 0.220	....	− 0.535	− 0.535	....	− 0.541
19	− 0.067	− 0.128	− 0.128	− 0.128	+ 0.069	+0.046	+ 0.069	+ 0.212	+ 0.212	+ 0.212
20	+41.715	+36.953	−45.246	+ 8.293	+23.915	+4.565	−28.480	−16.132	+45.874	−29.742
					(b)—(Continued)					
m_1	+20.800	+18.667	−16.000	− 2.667	+15.333	+1.334	−16.667	− 2.667	+16.000	−13.333
m_2	+15.268	+11.606	−17.887	+ 6.281	+ 5.264	+1.758	− 7.022	− 7.577	+17.684	−10.107
m_3	+ 3.613	+ 4.242	− 7.207	+ 2.965	+ 2.115	+0.787	− 2.902	− 3.544	+ 7.424	− 3.880
m_4	+ 1.338	+ 1.601	− 2.735	+ 1.134	+ 0.797	+0.385	− 1.182	− 1.470	+ 3.018	− 1.548
m_5	+ 0.506	+ 0.607	− 1.033	+ 0.426	+ 0.298	+0.197	− 0.495	− 0.614	+ 1.236	− 0.622
m_6	+ 0.190	+ 0.230	− 0.384	+ 0.154	+ 0.108	+0.104	− 0.212	− 0.260	+ 0.512	− 0.252
m_7	+ 0.114	+ 0.136	− 0.227	+ 0.091	+ 0.081	+0.078	− 0.159	− 0.184	+ 0.362	− 0.178
Σ	+41.829	+37.089	−45.473	+ 8.384	+23.996	+4.643	−28.639	−16.316	+46.236	−29.920

[a] The lines m_1, m_2, etc., are the algebraic sums of carried-over moments, correction moments, and distributed moments in cycles 1, 2, etc.; m_7 is obtained by multiplying m_6 by $\frac{r}{1-r}$, in which $r = \frac{m_6}{m_5}$.

ternal loads or reactions, or from the newly introduced hypothetical moments after each cycle of distribution and carry-over. The balancing moments in each panel are divided between the top and bottom chords in proportion to their stiffness factors. Lines 4, 7, 10, etc., show the distributed moments, and lines 5, 8, 11, etc., give the carried-over moments. Final moments are indicated in line 20, which sums up all the moments in each column. For practical results, one might have stopped at the end of the fourth cycle.

No attempt has been made to balance the shears in the verticals; it can be proved easily that, when the moments around all the joints are balanced and when the proper "correction moments" are applied after each cycle, the final shears in the verticals must necessarily be balanced.

If one wishes to obtain still more "exact" values for the final end moments, Table 18(*b*) may be prepared. The values given in the last horizontal line of Table 18(*b*) agree almost exactly with those in line 25, Table 13. The signs of the moments as used by the writer are exactly opposite to those used by the authors.

The products $E\,\theta$ for each joint and $E\,R$ for each member can be readily computed from Table 18. In Example 6, it is evident that: (1) The ($E\,R$)-value for the top chord in any panel should be the same as that for the bottom chord in the same panel; (2) the ($E\,R$)-value for all the verticals should be the same; and (3) the sum of the ($E\,R$)-values for all the bottom chords should be zero, since the supports B and J are unyielding.

Let $E\,R_1$, $E\,R_2$, $E\,R_3$, and $E\,R_4$ be the angles of bar rotation for top and bottom chords in the first, second, third, and fourth panels (see Fig. 12), and let $E\,R_5$ be the angle of bar rotation for each and every vertical. The tentative values of $E\,R_1$, $E\,R_2$, $E\,R_3$, and $E\,R_4$ are computed as follows:

$$E\,R_{BD} = \frac{\text{sum of correction moments}}{-\,6 \times K_{BD}}$$

$$= \frac{-\,29.333 - 23.371 - 7.987 - 3.229 - 1.315 - 0.541 - 0.379}{-\,6 \times \frac{1}{2}} = +\,22.052.$$

(In the foregoing, the value $-\,0.379$ is the last correction moment, 0.541, multiplied by the ratio $\frac{r}{1 - r}$ for member BD.) Similarly, $E\,R_{DF} = +\,15.592$; $E\,R_{FH} = -\,11.257$; and $E\,R_{HJ} = -\,24.422$.

The sum of these ($E\,R$)-values, being equal to $+\,1.965$, is not zero. This discrepancy of $+\,1.965$ must be divided equally among the four panels, since the latter are of equal lengths. In other words, all the verticals must rotate through an angle $E\,R_5$ of $-\,0.491$, which is equal to one fourth of this discrepancy with the sign changed. All the tentative ($E\,R$)-values must be combined with this value of $E\,R_5$ in order to obtain the true values of $E\,R_1$, $E\,R_2$, $E\,R_3$, and $E\,R_4$, thus: $+\,21.561$, $+\,15.101$, $-\,11.748$, and $-\,24.913$, respectively. The ($E\,\theta$)-value for any joint may now be computed from:

$$E\,\theta = \frac{\text{sum of distributed moments at the joint}}{\text{four times the sum of stiffness factors around the joint}} + E\,R_5 \quad \text{..(48)}$$

Thus, $E\,\theta_B$ is found as follows:

$$\begin{aligned} E\,\theta_B = {} & +\,11.733 + 17.600 + 2.148 + 3.223 + 0.891 + 1.336 + 0.371 \\ & + 0.556 + 0.155 + 0.232 + 0.065 + 0.097 \\ & + 0.113/4\,(1/2 + 3/4) - 0.491 = +\,7.213 \end{aligned}$$

(In the foregoing the value $+\,0.113$ is $(+\,0.065 + 0.097) \times \frac{r}{1 - r}$ for the members around that joint.) Similarly: $E\,\theta_D = +\,13.733$; $E\,\theta_F = +\,1.451$;

$E\,\theta_H = -\,14.135$; $E\,\theta_J = -\,9.385$; $E\,\theta_A = +\,8.420$; $E\,\theta_C = +\,17.211$; $E\,\theta_E = +\,2.606$; $E\,\theta_G = -\,18.682$; and $E\,\theta_I = -\,10.584$.

Corrections for *Transactions.*—In April, 1947, *Proceedings*, on page 417, change line 22 to read: "* * * a free body and subjected to an external positive moment M_R. The thrust and shear have been omitted from the sketch for simplicity. Since the sum * * *." The first sentence of Section 6, page 421, should read: "If the frame is one in which there is no joint translation * * *."

AMERICAN SOCIETY OF CIVIL ENGINEERS

Founded November 5, 1852

DISCUSSIONS

BEAM DEFLECTIONS BY SECOND AND THIRD MOMENTS

Discussion

BY A. FLORIS, ROBERT B. B. MOORMAN, AND FRANK J. MCCORMICK

A. FLORIS,[2] ESQ.—By means of his second-moment and third-moment concepts, the author derives formulas for the determination of slopes and deflections, which are used afterward in the analysis of hyperstatic structures. It is stated in the "Synopsis" of this paper that "The various methods for computing beam deflections may be classified into two main groups—the double-integration method and the moment-area method."

The application of the author's second and third moments to statical problems is facilitated by the aid of seven theorems. From these theorems the last two are admittedly similar in nature to those of the moment-area method. The labor involved in these computations is by no means less than the work required by other methods.

In enumerating the various methods for determining slopes and deflections, the author overlooks the principle of virtual displacements and the Castigliano theorems related to it. By the use of this general principle, and with the Müller-Breslau formulas for quick integration involving algebra only,[3] the most rapid results can be obtained in a direct manner.

The slopes and deflections (and hence the hyperstatic quantities) can be determined also by means of a fourth-order differential equation of the elastic curve.[4,5] By using Laplace transforms the tedious process of determining the four constants of integration is eliminated, and the differential equation is transformed into an algebraic equation.[6] Even without the use of the Laplace transformation the problem can be arranged in a manner suitable for practical solution.[7]

NOTE.—This paper by Hsu Shih-Chang was published in March, 1947, *Proceedings*.

[2] Asst. to Structural Engr., Pacific Elec. Ry. Co., Los Angeles, Calif.

[3] "Graphische Statik der Baukonstruktionen," by H. F. B. Müller-Breslau, Alfred Kröner, Stuttgart, Vol. III, Pt. II, 1908, p. 90.

[4] "Applied Elasticity," by John Prescott, Dover Publications, New York, N. Y., 1946, p. 52.

[5] "An Introduction to the Theory of Elasticity for Engineers and Physicists," by R. V. Southwell, Clarendon Press, Oxford, 1936, p. 172.

[6] "Applied Mathematics for Engineers and Physicists," by Louis A. Pipes, McGraw-Hill Book Co., Inc., New York and London, 1946, p. 217.

[7] "On the Theory of the Elastic Curve of the Deflected Beam," by P. C. Khoudiakoff, *Bulletin*, Polytechnic Soc., Imperial Technical School, Moscow, 1909, p. 213 (in Russian).

The second moment as defined by the author has a physical meaning that he has not utilized. If W is taken as the mass of the system, the second moment is only the moment of inertia of this mass with respect to an axis normal to the center line of the beam. Using the author's notation, M''_O is then the moment of inertia of the system with respect to the normal through point O, the

TABLE 1.—SECOND MOMENTS OR MOMENTS OF INERTIA

Loading	Mass	Area	Axis	Moment of Inertia: Notation	Moment of Inertia: Mass	Moment of Inertia: Area
(a) RECTANGULAR						
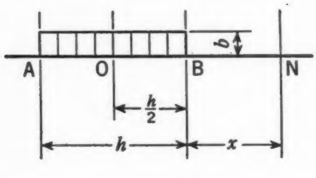	m	$b\,h$	A	I_a	$\frac{m\,h^2}{3}$	$\frac{b\,h^3}{3}$
			O	I_o	$\frac{m\,h^2}{12}$	$\frac{b\,h^3}{12}$
			B	I_b	$\frac{m\,h^2}{3}$	$\frac{b\,h^3}{3}$
			N	I_n	$\frac{m\,h^2}{12}+m\left(\frac{h}{2}+x\right)^2$	$\frac{b\,h^3}{12}+b\,h\left(\frac{h}{2}+x\right)^2$
(b) TRIANGULAR						
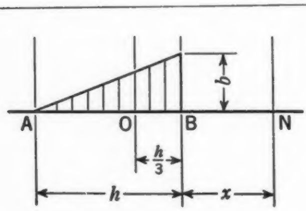	m	$\frac{b\,h}{2}$	A	I_a	$\frac{m\,h^2}{2}$	$\frac{b\,h^3}{4}$
			O	I_o	$\frac{m\,h^2}{18}$	$\frac{b\,h^3}{36}$
			B	I_b	$\frac{m\,h^2}{6}$	$\frac{b\,h^3}{12}$
			N	I_n	$\frac{m\,h^2}{18}+m\left(\frac{h}{3}+x\right)^2$	$\frac{b\,h^3}{36}+\frac{b\,h}{2}\left(\frac{h}{3}+x\right)^2$
(c) TRIANGULAR						
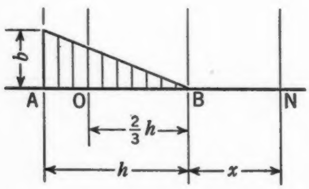	m	$\frac{b\,h}{2}$	A	I_a	$\frac{m\,h^2}{6}$	$\frac{b\,h^3}{12}$
			O	I_o	$\frac{m\,h^2}{18}$	$\frac{b\,h^3}{36}$
			B	I_b	$\frac{m\,h^2}{2}$	$\frac{b\,h^3}{4}$
			N	I_n	$\frac{m\,h^2}{18}+m\left(\frac{2}{3}h+x\right)^2$	$\frac{b\,h^3}{36}+\frac{b\,h}{2}\left(\frac{2}{3}h+x\right)^2$

center of gravity of the mass, M''_N is the moment of inertia of the mass with respect to the normal through point N, etc. Some of these values for masses of various shapes are given in reference books.[8]

If the mass is replaced by the loading area, the moment of inertia for area is obtained, which is more familiar to the structural engineer. Conversely, the

[8] "Hütte, des Ingenieurs Taschenbuch," Wilhelm Ernst & Son, Berlin, Pt. I, 1908, p. 219.

moments of inertia for mass are derived from the moments of inertia for areas. Mass here is taken as equivalent to load. Of all the moments of inertia, only M''_O needs to be determined by integration. The moments with respect to axes A, B, and N can be found by means of the well-known formula for moments of inertia at points other than the center of gravity. From the values of moments of inertia for few basic loadings, the values of the moment of inertia for a variety of loadings can be obtained by superposition. Table 1 is a sample of second moments for three loadings given by the author.

Considerable originality is displayed by Mr. Hsu and his interesting paper deserves careful study.

ROBERT B. B. MOORMAN,[9] M. ASCE.—Although the author is to be commended for his efforts to simplify computations for the deflections of beams, the writer feels that the simplification, by introducing second and third moments of the loads, is manifest only in some special cases and cannot be said to be general. The author contends that the use of second and third moments of the loads to compute deflections is a more direct method than that of considering the deflection to be a function of the bending moment. With this the writer cannot agree. Actually the angle changes that occur along the axis of

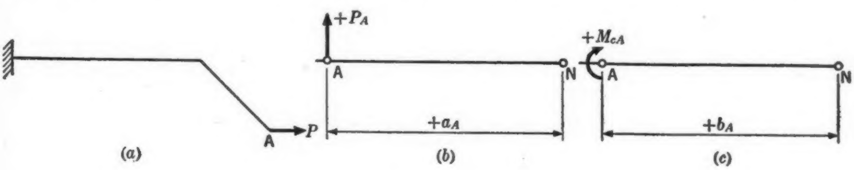

FIG. 20

a structure are used in computing the deflections. For beams, columns, or curved members the usual procedure is to assume the angle change equal to the bending moment divided by $E\,I$.

A direct method of computing deflections should not be limited to straight beams but should also be applicable to a simple arrangement as shown in Fig. 20(*a*). Point O of theorem III should be specified as the point at which the resultant is located on the reference line and not as "any other point (O)." The same is probably true for theorem IV.

TABLE 2.—SUMMARY OF MOMENT FORMULAS

Loading	First moment	Second moment	Third moment
Load (see Fig. 20 (*b*))	$M_N = P_A\,a_A$	$M''_N = P_A\,a^2_A$	$M'''_N = P_A\,a^3_A$
Couple (see Fig. 20 (*c*))	$M_N = M_{cA}$	$M''_N = 2\,M_{cA}\,b_A$	$M'''_N = 3\,M_{cA}\,b^2{}_A$
Balanced force system	....	$M'' =$ constant	$M'''_N = M'''_O + 3\,M''\,x$
Unbalanced force system (point O at resultant)	....	$M''_N = M''_O + M''_{O.N}$	$M'''_N = M'''_O + 3\,M''_O\,x + M'''_{O.N}$
Force system symmetrical about point O	....	....	$M'''_O = 0$

[9] Prof., Civ. Eng., Univ. of Missouri, Columbia, Mo.

The usefulness of the paper would probably be enhanced if the information were summarized somewhat as demonstrated in Table 2. Likewise it would be helpful to have the information contained in the section entitled "Second and Third Moments of Force Systems Acting on Straight Beams" extended and tabulated.

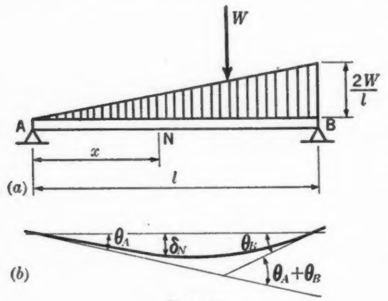

FIG. 21

That the proposed method can be applied expeditiously to certain deflection problems is illustrated by the following example. Let it be required to determine the equation for the deflection and the equation for the slope at any point for the beam shown in Fig. 21. The deflection at end B is zero, or

$$\delta_B = \theta_A\, l + \frac{1}{6\,E\,I} M'''_{AB,\,B} = 0 \qquad (73)$$

Substituting for $M'''_{AB,\,B}$ in Eq. 73:

$$\theta_A\, l + \frac{1}{6\,E\,I}\left(- \frac{W\,l^3}{10} + \frac{W\,l^3}{3} \right) = 0 \qquad (74)$$

from which

$$\theta_A = - \frac{7}{180\,E\,I} W\,l^2 \qquad (75)$$

The deflection at any point N is

$$\delta_N = \theta_A\, x + \frac{1}{6\,E\,I} M'''_{AN,\,N}$$

$$= - \frac{7}{180\,E\,I} W\,l^2\,x + \frac{1}{6\,E\,I}\left(\frac{W}{3} x^3 - \frac{W\,x^2}{l^2} \times \frac{x^3}{10} \right)$$

$$= \frac{W\,x}{180\,E\,I\,l^2}(-\,3\,x^4 + 10\,x^2\,l^2 - 7\,l^4) \qquad (76)$$

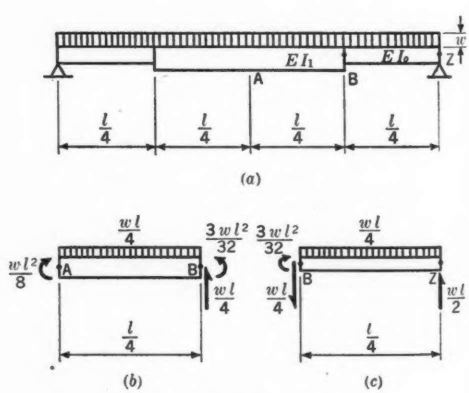

FIG. 22

The slope at any point N is

$$\theta_N = \theta_A + \frac{1}{2\,E\,I} M''_{AN} = - \frac{7}{180\,E\,I} W\,l^2 + \frac{1}{2\,E\,I}\left(\frac{W}{3} x^2 - \frac{W\,x^2}{l^2} \times \frac{x^2}{6} \right)$$

$$= \frac{W}{180\,E\,I\,l^2}(-\,15\,x^4 + 30\,x^2\,l^2 - 7\,l^4) \qquad (77)$$

To illustrate a case in which the computations for deflection are about the same whether or not the proposed method or the moment-area method is used, consider the beam shown in Fig. 22. Let it be required to determine the deflec-

tion at point A, which may be expressed as

$$\delta_A = y_{ZA} = \frac{1}{6\,E\,I_1} M'''_{AB,\,Z} + \frac{1}{6\,E\,I_0} M'''_{BZ,\,Z}$$

$$= \frac{1}{6\,E\,I_1}\left[3\left(\frac{w\,l^2}{8}\right)\left(\frac{l}{2}\right)^2 - \frac{1}{4}\left(\frac{w\,l}{4}\right)\left(\frac{l}{4}\right)^2\left(\frac{3\,l}{8}\right) - \left(\frac{w\,l}{4}\right)\left(\frac{3\,l}{8}\right)^3\right.$$

$$\left. + \left(\frac{w\,l}{4}\right)\left(\frac{l}{4}\right)^3 - 3\left(\frac{3\,w\,l^2}{32}\right)\left(\frac{l}{4}\right)^2\right] + \frac{1}{6\,E\,I_0}\left[3\left(\frac{3\,w\,l^2}{32}\right)\left(\frac{l}{4}\right)^2\right.$$

$$\left. - \left(\frac{w\,l}{4}\right)\left(\frac{l}{4}\right)^3 - \frac{1}{4}\left(\frac{w\,l}{4}\right)\left(\frac{l}{4}\right)^2\left(\frac{l}{8}\right) - \left(\frac{w\,l}{4}\right)\left(\frac{l}{8}\right)^3\right]$$

$$= \frac{w\,l^4}{6\,(32)^2\,E}\left(\frac{67}{I_1} + \frac{13}{I_0}\right) \qquad (78)$$

It is probable that the proposed method will be found useful in simplifying those analyses[10] which involve the moment of the $\frac{M}{E\,I}$-diagram about the support. In a case of this kind the loads can be used in place of the bending moments.

FRANK J. McCORMICK,[11] Assoc. M. ASCE.—A study of this paper reveals that, as defined by the author, the second moment (M'') is equal to twice the area of the bending moment diagram, and the third moment (M''') is equal to six times the moment of that area with respect to one end.

This ingenious substitution of these analytical expressions for the geometrical concepts used in the moment-area and conjugate beam methods is not likely to seem advantageous to most readers, for the invention of these latter methods was an attempt to avoid the mathematical abstractions of the double-integration process in favor of the concreteness of geometrical or physical concepts. In fact, the advantage of being able to visualize the operations involved has led to the invention of many similar substitution methods. Among these are the elastic weight, moment distribution, and column analogy methods in structural analysis, and the membrane, electrical, and hydrodynamical analogies in the field of elasticity. All these represent an effort to simplify the problem, either by replacing the quantities involved by more familiar ones, or by replacing relatively abstract mathematical quantities by analogous concrete physical ones.

Where the conjugate beam method refers the student back to the familiar concepts of shear and bending moment, the method proposed by the author requires the student to learn the new concepts of second and third moments of forces and couples. This could be defended if by so doing less actual labor need be applied for a solution. However, the author has not shown this to be true in the examples presented.

---

[10] "Continuous Frame Analysis by Elastic Support Action," by J. Charles Rathbun and C. W. Cunningham, *Proceedings*, ASCE, April, 1947, p. 419, Eqs. 16.

[11] Associate Prof. of Applied Mechanics, Kansas State College, Manhattan, Kans.

Corrections for *Transactions:* In March, 1947, *Proceedings,* on page 292, Eq. 6, change "$M_N = M_{cA}$" to "$M_N = M_c$." On page 294, line 6, change "Eq. 8" to "Eq. 12"; line 29, change "M_{cO}" to "M'_{cO}"; line 30, change "N''_N" to "M''_N"; and line 33, change "P'_O" to "P_O." On page 297, line 31, insert "to" after "equal." On page 298, Eq. 26*c*, change "M_B" to "M_b"; and Eq. 27, line 1, change the last quantity in parentheses to read "$\sum_1^m M_m \int_{l-b_m}^{l} dx$." On page 300, Eq. 32*a*, change "$M''_{O,N}$" to "M''_{ON}." On page 304, Eq. 54, line 2, change "$\approx$" to "$=$". On page 305, line 11, change "Eqs. 48, 52, and 55" to "Eqs. 48, 52, and 54"; and Eq. 57*a*, line 3, change "$-\frac{P\,l^3}{8}$" to "$-\frac{P\,l^2}{8}$." On page 306, line 17, change "displayed" to "displaced." On page 307, line 1, change "Eqs. 62" to "Eqs. 63." On page 308, Eq. 69*a*, insert "24" before "V_d." On page 309, Eq. 72, line 2, the first quantity in parentheses should read "$l_1\, M_{\overline{AB},A}$."

AMERICAN SOCIETY OF CIVIL ENGINEERS
Founded November 5, 1852

DISCUSSIONS

MISSISSIPPI RIVER BRIDGE AT DUBUQUE, IOWA

Discussion

BY JONATHAN JONES

JONATHAN JONES,[5] M. ASCE.—This paper well exemplifies the type of descriptive account of current work which the Society should seek always to secure for its *Transactions*. Granted that current news accounts of structures in general may better be presented elsewhere, it is important that *Transactions* serve as a complete reference work for the continuing development in structure types, including their history, the advantages and disadvantages claimed, and the methods of design and execution. It is to be regretted that, in the particular field of long span bridges, *Transactions* does not now constitute such a reference work. Many of the most important bridges, which showed developments in type, extensions of span, etc., are to be found in its pages; but many others are not. The writer feels that one of the great services the Society can perform for its members would be to adopt a policy in each Division which would ensure the procurement and publication in *Transactions* of the papers necessary to constitute such a history of progress in executed works.

The authors are to be commended for having selected for this written record the features that will be of greatest benefit to a structural engineer desiring to perform analogous work.

Referring to the authors' "Conclusions," the writer is quite in agreement that the bridge possesses a pleasing form. The relative importance of aesthetic success in any given case must depend, to some extent, upon the question of whether large numbers of people will find themselves in such a position as to behold the structure in the aspect which has concerned the designer. For possibly a majority of highway bridges this condition does not hold, as they are beheld by the public from the decks only and not in elevation. In such cases as that of a highway bridge visible to railway passengers on a parallel structure, the writer has noted that a surprising number of nonengineers do note and comment upon this matter of appearance. The present structure

NOTE.—This paper by R. N. Bergendoff and Josef Sorkin was published in June, 1947, *Proceedings*.

[5] Chf. Engr., Fabricated Steel Constr., Bethlehem Steel Co., Inc., Bethlehem, Pa.

being located adjacent to a city of some size, probably the question of appearance should be given more than ordinary weight.

The other general conclusion of the authors, however—that the type is fundamentally economical as compared with a cantilever—is not joined in by the writer. Unfortunately, no data can be assembled quickly to prove or disprove a contention of this type. There is no point in attempting to obtain approximate weights and costs of alternative types from a consideration of the recorded weights and costs of other structures. It is impossible for a designing engineer to weight the unit costs of structures of alternative types as a contractor will weight them in estimating. In recent years several important highway bridges have been built that are of a special continuous type (not that of the Dubuque Bridge), the proponents of which were able to prove by careful estimates that it would show definite economy over more conventional types. When at last one purchaser took the logical step of preparing two sets of plans with equal care and equal conservatism in all regards, and issuing them for alternative bids, the prices for the conventional type were well under those for the special type.

The writer mentions this as a "hedge" to his opinion that economy is not an advantage of the bridge type used at Dubuque; nor does he feel that the authors, although they state a basis for their conclusion, have pursued their argument to its end.

In the second paragraph under "Design Procedure," and in later description, the authors explain the three phases essential to the erection procedure: (1) The erection of the arch by cantilevering; (2) the manipulation of the end reactions and the erection and stressing of the center span tie; and (3) completion of erection of the floor steel and appurtenant details. Now with erection labor costs what they are, there is clearly no economy inherent in the taking of "three bites at the same cherry." That these three phases were necessary is true, of course, and that the separation into these phases decreased the amount of weight to be supported during the first phase is equally true; but it is very doubtful in the writer's mind that such a three-phase procedure, with the greater time required for the performance, could cost as little as the one-phase procedure required for conventional cantilever erection.

In the second paragraph under "Design Procedure," also, the authors state:

> "The form of the trusses of the central span lends itself to an economical arrangement for cantilever erection with maximum depth over intermediate supports tapering to a minimum depth at the center of the span."

This statement, however, overlooks the fact that in a conventional cantilever the depth of the main trusses over the intermediate supports would be fairly close to twice the 70-ft depth of the present structure. The depths of the arch structure were favorable for the erection of the arches, but unfavorable for the erection of the bridge as a whole. In Table 4, for instance, comparing Col. 8 with Col. 5, it will be noted that, for chords L4-L6, L6-L8, L8-L9; and U5-U7, U7-U9, and U9-U11, the total stresses under erection plus erection wind are from two to four times as great as the stresses for dead, live, and impact loading. The authors partly met this situation by increasing erection

stresses 50% over the stresses of normal design. This increase was the occasion for considerable worry, and the writer would not care to erect such a structure under that assumption again. It must be remembered that erection wind is not a figment of the imagination. Wind on a loaded structure in service may be considered a hypothetical load, on the ground that during a hurricane vehicles do not travel; but nothing can stop the wind from blowing at any stage—even the most unfavorable stage—of erection, and the provision for ample wind stress at a reasonable unit is essential. Despite this increase in temporary unit stress, however, the fact remains that there is permanently built into the chords of this bridge, over the intermediate piers, a great deal of steel which will never serve any useful purpose again. It is difficult for the writer to understand how economy can necessarily be inherent in a design of which that is true.

During the erection of a typical cantilever bridge, or of a three-span continuous bridge of the same general outline as the cantilever, there is no great excess of stress over that which will be developed by dead, live, and impact loading; the exceptions being particularly one top-chord and one bottom-chord member per truss in each half span, lying between the cantilever arm and suspended span. These "wasted" members carry the moment from cantilevering only the half length of the suspended span; instead of half the length of the main span, as at Dubuque. As the erection of the typical cantilever or continuous span proceeds, all the necessary material for support of live load is put in place. After the two halves of the bridge meet at midspan, one day spent in adjusting the juncture between cantilever and suspended spans of the cantilever type, or adjusting the end reactions of the continuous type, completes the erection of the steel. Economy, and safety of erection, both seem to inhere in these types.

It would be a real contribution if an owner would some day do what was described herein—issue, for bidding, alternative plans of a continuous-tied-arch structure and a more conventional cantilever type.

AMERICAN SOCIETY OF CIVIL ENGINEERS

Founded November 5, 1852

DISCUSSIONS

CLASSIFICATION AND IDENTIFICATION OF SOILS

Discussion

BY RALPH E. FADUM

RALPH E. FADUM,[3] ASSOC. M. ASCE.—The critical review of the soil classification systems used in civil engineering, as presented by the author, is a worthy contribution to the literature of soil mechanics. The author is to be commended for directing attention to the inadequacies of the much used textural classification systems according to which all soils are distinguished on the basis of grain-size composition. He has submitted ample evidence to support his thesis that the grain-size composition does not, by itself, reflect the significant physical properties of fine-grained soils.

In the proposed Airfield Classification (AC) System the author distinguishes between two primary soil groups—the so-called coarse-grained group and the fine-grained group. Sands and gravels comprise the first group and silts and clays the latter group. Soils of the coarse-grained group are distinguished primarily on the basis of grain-size composition. In general, a visual examination will suffice to differentiate the eight soil types included in this group. The six soil types included in the fine-grained group, on the other hand, are distinguished primarily by the degree of plasticity that they exhibit as measured by the simple, manual tests described by the author. It is noteworthy that in accordance with this system fourteen soil types, which have significantly different physical properties, can, with experience, be recognized by simple visual and manual tests that can be made without the aid of laboratory facilities.

The proposed system is flexible and, accordingly, suitable for classifying soils with respect to performance characteristics under a wide variety of conditions. The author has referred to the AC system as the Airfield Classification System. This name connotes a restrictive meaning that does not do justice to its general applicability.

The author recommends (see heading, "12. Fine-Grained Soil Groups of AC System") that 0.1 mm be used as the boundary size between the coarse-grained

NOTE.—This paper by Arthur Casagrande appeared in June, 1947, *Proceedings*.

[3] Prof. of Soil Mechanics, School of Civ. Eng. and Eng. Mechanics, Purdue Univ., Lafayette, Ind.

and fine-grained groups—

> "* * * usually those soils containing more than 50% of material smaller than 0.1 mm in size (passing No. 150 mesh) are classified as fine-grained soils (ML or CL); and soils containing less than 50% smaller than 0.1 mm in size are classified as coarse grained (SF or SC)."

This arbitrary limit provides a convenient method of separating a soil into its component fractions for detailed laboratory analysis. If a soil is dispersed in water, the particles larger than approximately 0.1 mm will settle out very quickly; those smaller than this size will remain in suspension. Thus, the coarse-grained and fine-grained fractions can be separated conveniently by a process of successive washing and decanting. After drying, the coarse fraction is suitably prepared for a dry sieve analysis. The wash water containing the fines can be used for hydrometer analysis (if the gradation of this fraction is considered significant), or the fines can be recovered from the wash water and subjected to other tests that may be prescribed for the so-called binder fraction.

The binder fraction is usually defined (22)[3a] as that fraction of a soil the constituents of which pass a standard No. 40 sieve. The writer is of the opinion that the results of the physical tests such as the Atterberg limit tests as determined from the binder fraction, consisting of the fraction of a soil smaller in size than 0.1 mm, would be more significant than the results obtained from the same tests performed on a binder fraction consisting of all material passing the No. 40 sieve.

In his discussion of the various methods of classifying soils the author includes one that he refers to as descriptive soil classification (see heading, "15. Descriptive Soil Classification"). This method, which is used extensively, consists in "Describing a soil in detail on the basis of a careful visual and manual inspection, utilizing more or less generally accepted nomenclature * * *." The author states (see heading, "15. Descripture Soil Classification") that: "The disadvantage of the descriptive classification lies in a lack of uniformity of soil terminology." The following remarks are directed particularly toward the soil terminology used in a descriptive soil classification system.

Confusion in terminology has arisen from the practice of differentiating soil types quantitatively on the basis of grain size composition, from the use of provincial names such as Boston Blue Clay, Chicago Blue Clay, etc., and from the use of terms such as marl and loam that do not convey sufficiently specific meanings. To be acceptable and useful, terminology used in a descriptive soil classification system should:

1. Consist of terms with which a boring foreman, an earthwork engineer, and a soil mechanician are equally conversant;
2. Describe the significant characteristics that can be determined quickly without the aid of laboratory facilities;
3. Be discriminating; and
4. Convey a well-defined meaning.

[3a] Numerals in parentheses, thus: (22), refer to corresponding items in the Bibliography (see Appendix of the paper), and at the end of discussion in this issue.

For purposes of soil identification and descriptive classification it is suggested that the following three size fractions be recognized as significant in describing the grain-size composition of a soil—the gravel fraction, the sand fraction, and the fine-grained fraction (composed of particles smaller than 0.1 mm in size). The composition in terms of these fractions can be expressed conveniently by a number system, as follows: 50–10–40 designates a soil composed 50% by weight of gravel, 10% by weight of sand, and 40% by weight of fines; and 0–20–80 designates 20% by weight of sand and 80% by weight of fines. If graphical representation is preferred, a triangular chart similar to those shown in Fig. 3 could be used. Reasonable estimates of composition according to these fractions suitable for identification purposes can be made without the aid of laboratory facilities.

As stated, sands and gravels are distinguished solely on the basis of the size of their constituent particles. Factors other than grain size, however, must be considered in distinguishing between silts and clays. The author has directed attention to the fact that the grain-size composition of two fine-grained soils may be identical; yet, the physical properties can be significantly different. The effect of mineralogical composition, which is reflected by the shape of the soil particles, dominates the effect of grain size on the properties of a fine-grained soil. Soils composed essentially of "clay-size" minerals, as defined by the various classification scales in current use, may exhibit either silt-like or clay-like properties. According to engineering concepts a fine-grained soil or fraction is identified on the basis of the degree of plasticity and dry strength that it exhibits. A clay-like soil can be made to exhibit plastic properties by an adjustment of its water content and it has considerable strength when air-dried. (The term plastic is used, herein, to describe that property of a material which enables it to be deformed quickly without exhibiting a noticeable elastic rebound or volume change and without cracking or crumbling.) A silt-like soil cannot be made plastic and it exhibits little or no strength when air-dried. There are no simple, direct methods suitable for routine identification and classification purposes by which the clay-like constituents of the fine-grained fraction can be separated quantitatively from the silt-like constituents. It is suggested, therefore, that the terms silt and clay be used in a qualitative rather than in a quantitative sense.

In light of the foregoing remarks and in the interest of promoting agreement on soil terminology to be used in a descriptive soil classification system, the following summarized recommendations are proposed:

1. The terms "gravel," "sand," "silt," and "clay," used singly or in combination, shall form the basic elements of a soil name. The name shall be qualified by the use of carefully selected adjectives so as to make the description of a soil complete and discriminating.
2. Distinction between silts and clays shall not be based upon the size of the constituent particles.
3. The terms "silt" and "clay" shall be used in a qualitative rather than in a quantitative sense.

4. The gravel fraction, the sand fraction, and the fine-grained fraction shall be recognized as the significant fractions in describing the grain-size composition of a soil.

5. The fine-grained fraction (or binder fraction) shall be defined as that fraction of a soil the constituents of which are smaller than 0.1 mm in size.

6. The fine-grained fraction shall be designated "silt" if it cannot be made plastic and if it exhibits little or no strength when air-dried. (Careful distinction must be made between inorganic and organic silts (23).)

7. The fine-grained fraction shall be designated "clay" if it can be made plastic by an adjustment of its water content and if it exhibits considerable strength when air-dried.

The foregoing recommendations were submitted by the writer to the American Society for Engineering Education for use in formulating a set of standard definitions (24).

Bibliography.—

(22) **"Preparation of Soil Samples for Mechanical Analysis and Determination of Subgrade Constants,"** Designation D 421–39, *A.S.T.M. Standards*, 1944, pp. 614–615.

(23) **"Exploration of Soil Conditions and Sampling Operations,"** by H. A. Mohr, *Publication No. 376*, Graduate School of Eng., Harvard Univ., Cambridge, Mass., 3d Ed., November, 1943, pp. 9–12.

(24) **"Definitions of Soil Components,"** Rept. of the Foundations and Soil Mechanics Committee, *Civil Engineering Bulletin*, Civ. Eng. Div., Am. Soc. for Eng. Education, March, 1947.